TUM

Lehrstuhl für Akustik Mobiler Systeme

Sound and vibration in a mixed frame
- Applications in aeroacoustics and rotor dynamics -

Marcus Mäder

If I have seen further
it is by standing on ye sholders of Giants

Isaac Newton

(1643–1727)

Kurzfassung

Aeroakustik und Rotordynamik sind zwei verschiedene Themen, wenn es um technische Anwendungen sowie die Formulierung der damit verbundenen Probleme geht. Dieser Umstand ergibt sich nach dem Verständnis des Autors aus den ursprünglich unterschiedlichen Betrachtungsweisen, in denen die Probleme der einzelnen Themengebiete formuliert wurden und immer noch beschrieben werden. In der Aeroakustik wird in der Regel eine eulerscher Betrachtungsweise gewählt, in der die fundamentalen Gleichungen, die als die Bilanzgleichungen der Kontinuumsmechanik bekannt sind, eingebettet sind. Diese Sichtweise wird traditionell von Ingenieuren der Fluiddynamik bevorzugt, da die Verfolgung der Bewegung jedes einzelnen Fluidteilchens nicht von besonderem Interesse ist. Stattdessen erlaubt die Beobachtung der Feldgrößen an festen Positionen im Raum eine effektive Analyse fluiddynamischer Probleme. Im Gegensatz dazu sind Probleme der Rotordynamik historisch gesehen ein Thema der Strukturmechanik, wofür üblicherweise eine lagrangesche Betrachtungsweise bevorzugt wird. Hier ist die Verfolgung der Bewegung von materiellen Teilchen von allgemeinem Interesse. Da für die meisten ingenieurwissenschaftlichen Problemen der Strukturdynamik die Annahme kleiner Deformationen gültig ist, ist die Verwendung einer lagrangeschen Betrachtungsweise ohne zusätzliche Herausforderungen möglich. Darüber hinaus ist die Beschreibung wesentlicher Randbedingungen in diesem Rahmen viel einfacher realisiert, da die Gebietsgrenzen wohldefiniert sind.

Müssen beide Themen parallel berücksichtigt werden, wie z. B. bei der Entwicklung von Strahltriebwerken, ist die Entscheidung für die eine oder die andere Betrachtungsweise mit dem Umstand verbunden, dass einige Nachteile unabwendbar sind. Aus diesem Grund entwickelten die Forscher eine verallgemeinerte Beschreibung, die im Englischen als „Arbitrary Lagrangian Eulerian Frame" bezeichnet und in der auf eine willkürlich gewählte Referenz bezogen wird. Die Beschreibung von Störungen basiert folglich in Bezug auf diese Referenz. Offensichtlich ist eine derartige Betrachtungsweise in der Lage, Störungen sowohl in der Aeroakustik als auch in der Rotordynamik abzubilden.

In dieser Arbeit werden beide Forschungsgebiete, d. h. die Aeroakustik und die Rotordynamik, im Frequenzbereich auf der Grundlage einer willkürlichen lagrange-eulerianischen Betrachtungsweise analysiert, die im ersteren Fall in der Untersuchung der weniger bekannten Galbrun-Gleichung besteht. Mit Blick auf die Literatur sieht man, dass Themen der Rotordynamik mit dieser Betrachtungsweise ausführlicher untersucht worden. Im Detail kommen sowohl die Modalanalyse als auch die harmonische Analyse als Teil der Modellreduktion und der modalen Superposition in verschiedenen Fällen zum Einsatz. Die Ergebnisse zeigen, dass ähnliche physikalische Verhal-

tensweisen, wie z. B. Modenaufspaltung, in beiden Anwendungen vorhanden sind. Folglich ist es beabsichtigt, dem Leser die grundlegende gemeinsame Betrachtungsweise näherzubringen, die auf beide Anwendungen angewendet werden kann, um zukünftige Entwicklungen hin zu einer einheitlichen Theorie zu erleichtern. Mit diesem deduktiven Ansatz wird der Leser in eine höhere Abstraktionsebene eingeführt, von der aus mehrere Aspekte zu verschiedenen Bereichen der zugrunde liegenden Forschung beigetragen werden. Diese Bereiche sind das Kennen der „Literatur", das Verstehen der „Physik", das Entwickeln von „numerischen Methoden" und schließlich das Finden von „Anwendungen", da dies alles Teil der Forschung im Allgemeinen ist. Daher dient diese Arbeit als Vorbereitung, zukünftig die beiden Themengebiete mittels einer gemeinsamen Betrachtungsweise zu beschreiben, um somit die Themengebiete der Aeroakustik und Rotordynamik einander anzunähern. Indem beide Forschungsbereiche mittels einer Betrachtungsweise formuliert werden, ist ein einheitliches Verständnis zu erreichen. Aus der Sicht des Autors ist eine vollständige Kopplung beider Anwendungen eine natürliche Entwicklung der zukünftigen Forschung, liegt allerdings außerhalb des Rahmens dieser Arbeit.

Abstract

Aeroacoustics and rotor dynamics are two different subjects when it comes to engineering applications as well as the formulation of associated problems. This circumstance, as understood by the author, stems from the originally different frameworks in which problems of the individual subjects have been formulated and still are described. In aeroacoustics, usually a Eulerian frame is chosen in which the fundamental equations, known as the balance equations of continuum mechanics, are embedded. This frame is traditionally preferred by engineers of fluid dynamics, since tracking the motion of each fluid particle is not of particular interest. Instead, the variation of the field quantities at fixed positions in space allows to effectively analyze problems of fluid dynamics. In contrast, problems of rotor dynamics are historically a subject of structural mechanics for which a Lagrangian framework is usually preferred, where tracing the motion of material particles is of general interest. Since for most engineering cases of structural dynamics, a small deformation assumption is valid, utilizing a Lagrangian frame comes without additional challenges. In addition, applying essential boundary conditions is realized much easier in this frame, as domain interfaces are well defined.

For problems, where both subjects have to be considered such as in turbofan engineering, the decision for one or the other framework comes with the burden of accepting some disadvantages. For this reason, researchers came up with a generalized framework known as Arbitrary Lagrangian Eulerian frame, in which "arbitrary" refers to an arbitrarily chosen reference frame from which perturbations are measured. Evidently, such a frame is capable of mapping perturbations in both aeroacoustics as well as rotor dynamics.

In this work, both research fields, namely aeroacoustics and rotor dynamics are analyzed in the frequency domain based on an Arbitrary Lagrangian Eulerian point of view, which in the former case consists of studying the less-known Galbrun equation. Looking at the literature, the latter case has been studied more extensively. In detail, the modal analysis as well as the harmonic analysis as part of model reduction and modal superposition scheme are applied in distinct cases. The results show that similar physical behaviors, such as mode splitting, are present in both applications. Consequently, it is intended to provide the reader with a fundamental understanding of the common framework that can be applied to both applications in order to facilitate future developments towards a unified theory. With this deductive approach, the reader is introduced to a higher abstraction level, from which several aspects to distinct fields of the underlying research are contributed. These fields are knowing the "Literature", understanding "Physics", developing "Numerical Methods", and finally finding "Applications", as this is all part of research in general.

Therefore, this thesis serves as a preparation to describe the two research fields in one single frame in order to bring the topics of aeroacoustics and rotor dynamics closer together. By viewing both research fields in one frame, a unified understanding is on its way and, as seen by the author, a full coupling of both applications, will be a natural development of future research, but is beyond the scope of this work.

Acknowledgment

Recalling the years that I have spent working on the content of this thesis, I can say with a clear conscience that this work has been one of the greatest challenges I have faced so far. Now, I want to take the opportunity to give credit to the people who took my hand and helped me to finish this work. Without their help, this work certainly still would be only a fleeting thought of a young student.

I dedicate the greatest thanks to my supervisor Prof. Dr.-Ing. Steffen Marburg. Your untiring patience and the freedom you gave me to expand and explore my research in a wide variety of areas enable me to look back with inestimable gratitude. Thank you, Steffen. I also greatly want to thank Prof. Manfred Kaltenbacher for reviewing this thesis and the fruitful discussions. Thank you Prof. Wolfgang Polifke for taking the chair of the examination committee. Many many thanks go to my mentor and friend Dr. phil. Monika Gatt. Your open ears, the introduction to philosophy, and the valuable discussions helped me to organize and structure my thoughts. I would also like to express my thanks to Martina Sommer and Elke Reichardt, who helped me doing daily administrative tasks – especially Martina's patience deserves much gratitude. Man sieht wirklich nur mit dem Herzen gut. Among all the colleagues I was able to get to know and spend time with, I especially want to thank Patrick Langer, Lennart Moheit, Johannes Henneberg, Anton Melnikov, Theo Kiesel, Christian Geweth, Stefanie Retka, Kheirollah Sephavand, and the whole team of the chair as well as all colleagues around the world. What an unforgettable time I was able to experience together with you all – especially the off activities after a long day of attending a conference.

Der abschließende Dank gehört zum Einen meinen Freunden und zum Anderen – und dieser Dank lässt sich kaum in angemessene Worte fassen – meiner Familie. Eure Kraft und die unermüdliche Unterstützung in meine Arbeit haben mich in einer Art und Weise vorangetrieben, wie es kaum zu beschreiben ist. Ich danke einem ganz besonderen Freund, Martin Stache. Danke für alles und die großartiken Momente. Des Weiteren danke ich meiner besten Freundin Maria Krieger sowie Tom Keller, Daniel Pantic, Marcel Wiesenberg, Oliver Bornhak, Marion Sedlmeir und Wolfgang Löffler sowie der Familie Chen und meinen Freunden und Freundinnen. Danke, dass ihr mir immer wieder eine Auszeit vom Doktorandendasein ermöglicht und mir unendlich Kraft gegeben habt.

Ganz besonderer Dank gebührt meiner Partnerin Marlene Buchart – danke für deine Liebe, Zuneigung und deine Geduld. Ebenso danke ich meiner Schwester Domenica, meinem Bruder Julius und meiner Nichte Mia. Ihr seid alle eine wahrer Sonnenschein, und ich bin unheimlich dankbar, euch an meiner Seite zu wissen.

Der größte und wichtigste Dank geht an dieser Stelle an drei ganz besondere Menschen, ohne die ich diese Worte in der Form nicht schreiben könnte. Euch allein gebührt diese Seite dieser Arbeit, mit der Hoffnung, meinem Dank ansatzweise Ausdruck verleihen zu können. Es sind unbeschreibliche Emotionen, die mit diesen Worten verbunden sind. Ich liebe euch.

Ich widme diese Arbeit von ganzem Herzen euch drei –

meiner Oma Renate Mäder, meinem Vater Istvan Pali und meiner Mutter Edda Mäder-Pali.

Appended Publications

A M. Maeder, G. Gabard, and S. Marburg. 90 years of Galbrun's equation: An unusual formulation for aeroacoustics and hydroacoustics in terms of the Lagrangian displacement. *Journal of Theoretical and Computational Acoustics*, 2050017 (39 pages), 2020.

Author contribution statement:

Maeder, Marcus: Conceptualization (85 %), Methodology, Formal analysis, Investigation, Data Curation, Writing – Original Draft, Writing – Review & Editing (65 %), Visualization, Project administration. **Gabard, Gwénaël:** Conceptualization (15 %), Writing – Review & Editing (10 %). **Marburg, Steffen:** Resources, Writing – Review & Editing (25 %), Supervision.

B M. Maeder, A. Peplow, M. Meindl, and S. Marburg. Solving Galbrun's equation with a discontinuous Galerkin finite element method. *Acta Acustica united with Acustica*, 105(6):1149–1163, 2019.

Author contribution statement:

Maeder, Marcus: Conceptualization, Methodology (65 %), Software (75 %), Validation, Formal analysis (65 %), Investigation (75 %), Data Curation, Writing – Original Draft, Writing – Review & Editing (65 %), Visualization, Project administration. **Peplow, Andrew:** Formal analysis (35 %), Investigation (25 %), Writing – Review & Editing (15 %). **Meindl, Maximilian:** Methodology (35 %), Software (25 %), Writing – Review & Editing (10 %). **Marburg, Steffen:** Resources, Writing – Review & Editing (10 %), Supervision.

C M. Maeder, R. D´Auria, E. Grasso, G. Petrone, S. De Rosa, M. Klaerner, L. Kroll, and S. Marburg. Numerical analysis of sound radiation from rotating discs. *Journal of Sound and Vibration*, 468:115085, 2020.

Author contribution statement:

Maeder, Marcus: Conceptualization (85 %), Methodology (65 %), Software (65 %), Validation, Formal analysis, Investigation (75 %), Data Curation, Writing – Original Draft (55 %), Writing – Review & Editing (55 %), Visualization, Project administration. **D´Auria, Roberto:** Methodology (25 %), Software (10 %), Investigation (15 %), Writing – Original Draft (40 %), Writing – Review & Editing (5 %). **Grasso, Ettore:** Conceptualization (15 %), Methodology (10 %), Software (10 %), Investigation (10 %), Writing – Original Draft (5 %), Writing – Review & Editing (5 %). **Petrone, Giuseppe:** Writing – Review & Editing (5 %). **De Rosa, Sergio:** Writing – Review & Editing (5 %), Supervision (10 %). **Klaerner, Matthias:** Software (15 %), Writing – Review & Editing (10 %). **Kroll, Lothar:** Supervision (5 %). **Marburg, Steffen:** Resources, Writing – Review & Editing (15 %), Supervision (85 %).

D M. Maeder and Technical University of Munich. Double cutting disc with curved deformation lines. Publication date: 27 December 2018, International Publication Number WO 2018/234547 A1, 2018. Author contribution statement:

Maeder, Marcus: Invention, Conceptualization, Methodology, Software, Validation, Formal analysis, Investigation, Data Curation, Writing-Original Draft, Writing – Review & Editing, Visualization, Project administration.

Publications not appended to this work

All publications until the year 2017 have been published under name "Guettler" and afterwards under the name of birth "Maeder".

- M. Maeder and S. Marburg. Changing perspectives in aeroacoustics. In J. Peissig and S. C. Langer, editors, DAGA: 46. Jahrestagung der Deutschen Arbeitsgemeinschaft für Akustik, Hannover, Germany, 2020

- M. Maeder, R. D'Auria, E. Grasso, G. Petrone, S. De Rosa, M. Klaerner, L. Kroll, S. Marburg: Utilizing a lumped parameter model for analyzing the sound radiation of a spinning plate. In S. De Rosa, F. Franco, M. Guida, F. Marulo and G. Petrone, editors, MEDYNA2020: Proceedings of MEDYNA2020, 3rd Euro-Mediterranean Conference on Structural Dynamics and Vibroacoustics, 17–19 February 2020, Napoli, Italy, 2020

- M. Maeder, A. Peplow, S. Marburg. Numerical analysis of the augmented Galbrun equation using discontinuous Galerkin finite elements. In M. Kaltenbacher, J. M. Melenk, L. Nannen, and F. Toth, editors, Waves2019: 14th International Conference on Mathematical and Numerical Aspects of Wave Propagation. Book of Abstracts. 25.–30. August 2019, Vienna, Austria, pages 158–159. TU Wien, 2019

- M. Maeder, S. Marburg: A method for filtering Galbrun's equation to identify acoustically relevant modes in complex flows, GAMM 2018: 89th Annual Meeting of the International Association of Applied Mathematics and Mechanics, Munich, Germany, 2018

- M. Maeder, S. Marburg: Methode zur Trennung der akustisch relevanten Moden in komplexen Strömungen durch Filterung der Galbrun-Gleichung. In B. Seeber, editor, DAGA: 44. Jahrestagung der Deutschen Arbeitsgemeinschaft für Akustik, Munich, Germany, 2018

- M. Maeder, S. Marburg: Utilizing a discontinuous Galerkin method for solving Galbrun's equation in the frame of aeroacoustics, *Proceedings of Meetings on Acoustics*, Proceedings of Meetings on Acoustics 173EAA 30 (1), 045005, 2017

- M. Guettler, C. Jelich, S. Marburg, E. Grasso, S. De Rosa: A vibroacoustic analysis of prestressed saw blades to identify instabilities considering gyroscopic effects and centrifugal forces utilizing the finite element method, The Journal of the Acoustical Society of America 141 (5), 3576–3576, 2017

- M. Guettler, S. Marburg: Randbedingungen der Galbrun-Gleichung in komplexen Strömungen. In B. Nolte, G. Schmidt, editors, DAGA: 43. Jahrestagung der Deutschen Arbeitsgemeinschaft für Akustik, Kiel, Germany, 2017

- M. Guettler, S. Marburg: Comparing different aero-acoustic formulations in terms of results of an eigenvalue problem, *INTERNOISE 2016 - 45th International Congress on Noise Control Engineering: Improving the World Through Noise Control*, 2016

- M. Guettler, S. Marburg: The nonlinear inhomogeneous Galbrun-Equation: Derivation and possible Ways to solve numerically, *INTERNOISE 2014 - 43rd International Congress on Noise Control Engineering: Improving the World Through Noise Control*, 2014

- M. Guettler, S. Marburg: Die inhomogene Galbrun-Gleichung: Herleitung und Ansätze zur numerischen Lösung. In B. Kollmeier, editor, DAGA: 40. Jahrestagung der Deutschen Arbeitsgemeinschaft für Akustik, Oldenburg, Germany, 2014

List of Acronyms

ALE   Arbitrary Lagrangian Eulerian

APE   Acoustic Perturbation Equation

ASC   Aeroacoustics Specialists Committee

BEM   Boundary Element Method

CAA   Computational AeroAcoustics

CAE   Computer Aided Engineering

CEAS   Council of European Aerospace Societies

DG   Discontinuous Galerkin

DG-FEM   Discontinuous Galerkin Finite Element Method

ERP   Equivalent Radiated Power

FDM   Finite Difference Method

FE   Finite Element

FEM   Finite Element Method

FVM   Finite Volume Method

FSI   Fluid Structure Interaction

LEE   Linearized Euler Equation

LES   Large Eddy Simulation

LNSE   Linearized Navier-Stokes Equation

LPM   Lumped Parameter Model

PML   Perfectly Matched Layer

List of Figures

List of Tables

Contents

Part I

Summary and Overview

Chapter 1

Introduction

Sound and vibration in a mixed frame, as the title of this work already indicates, deals with wave propagation both in fluids and in structures. Since the two phenomena already have been extensively studied in the past, the focus quickly shifts to the rest of the title. "In a mixed frame" might leave the reader with some questions. However, the very tricky part arises from the word "and". Since both sound in fluids and vibration in structures are seemingly very different in their nature, the unification encompasses many challenges.

But before going into detail, some effort is taken to explain why the presented line of thought is relevant. The simplest way of highlighting the importance is by looking at two very different research fields that belong to the above mentioned classification, namely, on the one hand, aeroacoustics as a research field in which wave generation and propagation in flow is analyzed, and on the other hand, rotor dynamics, where rotating elastic structures can vibrate, due to external loading or unbalanced masses.

Apparently, when it comes to technical applications, the two very different research fields come close together. As an example, Sutliff [178] as well as Kurtz and Marte [112] highlighted the interaction between aeroacoustics and rotor dynamics when dealing with turbofan engines, which are nowadays commonly used in most commercial airplanes. Furthermore, wind turbines are very attractive electric energy producers. Unfortunately, the interaction between rotor dynamics and flow [36] can cause amplitude modulation of sound waves that lead to health issues [169]. Only the knowledge of the complete physical process that is involved could lead to a minimization of aeroacoustic sound emission through structural optimization [125]. A third category belongs to the automotive industry, where because of extensively used electric motors, other sound sources become prominent, such as break squeal [150], tire noise and aeroacoustic sound from cooling machines [160]. The latter are also used in buildings, where their noise emission can influence the

ability to concentrate [145]. As can be seen, in most cases the interaction between aeroacoustics and rotor dynamics is often present in industrial applications and possibly leads to annoyance or even health-related issues. Therefore, noise reduction is a major concern of research and the industry [6].

This work is dedicated to the general understanding of aeroacoustic and rotor dynamics as seen from a common unified framework, known as the "Arbitrary Lagrangian Eulerian" frame within the frequency domain. This higher level of abstraction allows the reader to identify common aspects between the two rather different research fields. It is believed by the author that this work will contribute to the development of a unified theory, where both physics can be expressed in a more elegant way, leading to a more effective coupling and eventually powerful schemes for solving problems in more complex systems.

Outline of this work

In the first part of this work, a discussion on the state of the art towards sound and vibration is given, followed by a summary that gives insight into the contributions of this work, which closes the introductory chapter. In chapter 2, the applied methods are discussed, followed by a description of the utilized models in chapter 3. A summary of the appended publications is the content of chapter 4, after which the results are discussed among the available literature in chapter 5. This work finishes with a conclusion in chapter 6. All the appended publications are found in the second part of this work.

1.1 State of the art

When it comes to understanding sound and vibrations in a mixed frame, as indicated by the title of this work, it is essentially necessary to understand all parts of the title before a picture of the whole can be drawn. To get familiar with the incredibly broad scientific field, recently Pierce [155] published a comprehensive textbook on acoustics, which certainly summarizes the state of the art to a reasonable extent. Furthermore, Mechel [131] and Rossing [165] provide a very good overview on acoustics. For deeper insight on how to use numerical methods for solving acoustic problems, the reader is referred to Marburg and Nolte [128] and Kaltenbacher [104].

However, by concentrating on aeroacoustics as well as rotor dynamics, which will be discussed in more detail in the subsequent outlines, the two topics seem to be quite different in their nature and yet show many similarities, if an appropriate level of abstraction is accepted. Usually, dealing

with both research fields involves dealing with complicated mathematical expressions and complex problems at the same time, making analytical solutions almost impossible to find. For this reason, a number of numerical schemes have been developed in the last decades to provide the user with a tool that allows deeper understanding of complex processes. One numerical method broadly accepted within the scientific and industrial community is the finite element method (FEM), where a tremendous amount of research activities have been carried out. This is reflected by the number of textbooks dedicated to this research field [12, 17, 53, 192]. Furthermore, the so-called discontinuous Galerkin finite element method (DG-FEM) can be seen as a generalized form of the standard FEM that allows to adequately resolve convection phenomena [16, 43, 45, 88], which becomes especially relevant in the field of aeroacoustics [47, 81, 93, 172] and rotor dynamics [64, 75]. Since both fields have a common nature in continuum mechanics, a few references are suggested for studying these fundamentals [1, 2, 17, 77, 130, 166, 175, 181].

Generally speaking, when viewing aeroacoustics and rotor dynamics in a common frame, the interaction between the two domains can be of essential interest. If fluids and structures are part of this interaction, it is called fluid structure interaction (FSI). The reason for emphasizing this in such a way is due to the large number of available publications related to this stand-alone research topic, see for instance the small selection [13, 14, 19, 40, 84, 91, 92, 134, 177, 189, 191].

Another important aspect that needs to be considered in the context of wave propagation deals with waves traveling into the far field, which usually is considered as an unbounded domain. However, in terms of utilizing numerical tools, discretizing an unbounded domain is not possible. Therefore, a suitable truncation must be conducted, which artificially maps the properties of the unbounded domain to the truncated domain. For this reason, so-called perfectly matched layer (PML) absorbing boundaries [23] as well as infinite finite elements [5, 133] have been developed and applied among other methods [63, 78–80]. Under certain circumstances, structure-born sound [46] can be modeled utilizing approximation methods, such as the equivalent radiated power (ERP) [66, 111] or a lumped parameter model (LPM) [58, 59], which have been applied in optimization procedures [129].

In the following outlines, the discussion is focused on reviewing the state of the art with respect to an arbitrary Lagrangian Eulerian frame, aeroacoustics, and finally rotor dynamics.

1.1.1 The Arbitrary Lagrangian Eulerian description

The Arbitrary Lagrangian Eulerian (ALE) frame is a generalized combination of both fundamental frames of continuum mechanics, namely the Lagrangian frame and the Eulerian frame [1, 2]. The

former is characterized by the fact that a mesh of grid points is attached to the underlying medium and moves with it. In contrast, the Eulerian frame pictures a stationary frame, i.e. the mesh is fixed in space, and the medium is moving relatively to it. Both distinct frameworks have their own advantages and disadvantages. However, because of the shortcomings, as discussed in section 2.2 in more detail, of a purely Lagrangian frame and a purely Eulerian frame, a possible generalized unification is the ALE framework, as pointed out by Donea and Belytschko [52]. In fact, since this publication is a review that covers also the application towards numerical methods, it is a good starting point for researchers who are interested in this topic. Furthermore, the ALE concept made its first appearance within the finite difference method (FDM) in the 1960s and further within the finite element method in the late 1970s. For a comprehensive insight, see Belytschko et al. [17] and references within.

With respect to the application within the FEM scheme, the reader should consult Donea et al. [54], Hetzler [89], Huerta and Casadei [97], and Nackenhorst [140].

1.1.2 Aeroacoustics

The term aeroacoustics refers to the research field of wave generation and propagation, where the elastic medium in which the waves propagate is moving with respect to a stationary observer or an initial reference system, respectively. Historically, this research field arose in the 1950s when Lighthill published his famous work on sound generated aerodynamically [123, 124]. Lighthill reformulated the well-known Navier-Stokes equation into a wave-type equation with sources. His work was further developed by Curle, who considered the influence of rigid solid boundaries [48], or Ffowcs Williams and Hawkings, who pictured the sound generation by turbulence and arbitrary moving surfaces in an original frame by utilizing generalized functions such as the Heaviside function to distinguish between surfaces and fluid in order to arrive at an integral equation. A generalized version of an acoustic analogy has been presented by Goldstein [82] and was mathematically analyzed [20] and successfully applied together with using large eddy simulations (LES) [106].

Since the earlier years of aeroacoustics, extensive research has been conducted towards understanding sound in moving media, which can be seen by the list of textbooks available on this topic [47, 81, 93, 104]. In addition, a number of review articles summarize the available literature (i) towards compressible, viscous fluid dynamics [83], (ii) which model to use and when – for predicting aerodynamic noise [139], (iii) with respect to issues and methods of computational aeroacoustics (CAA) [3, 122, 179], (iv) towards the application in turbofan liner optimization [7], and (v) on PML absorbing boundary conditions for CAA [94, 103]. But there also has been criti-

cism on the use and abuse of acoustic analogies [51].

To get an insight into recent developments of aeroacoustics research in Europe, the reader is referred to the annual CEAS-ASC report, see for instance Gély and Bennett [74].

Historically, many applications are linked to the turbofan engineering, since Lighthill's first contribution examined the acoustic radiation of free stream, see for instance the noise prediction of a mixing jet, where experiments validated the applied theory [99]. Ultimately, combustion noise together with thermoacoustic instability has been investigated too. Also the case of a cylinder being placed in a cross flow has been studied [105], as well as eigenvalue problems in lined ducts with flow [4]. This fundamental research together with the increase in computational power enabled researchers to investigate even more complicated problems such as cooling fans [90] or the human voice production process [158, 193]. Besides the usual separation in hydrodynamics and aeroacoustics, direct simulations have also been conducted [29].

In the following outlines, a closer look will be given towards methods that have been developed using a Eulerian frame and a mixed or ALE frame, respectively. Traditionally the former framework is favored by researchers in the field of fluid dynamics. However, the utilizing of an ALE frame to describe aeroacoustic phenomena has numerous advantages as will be discussed below.

Conventional Eulerian frame

When deriving the fundamental equations of fluid dynamics and aeroacoustics, respectively, most scholars in the field of fluid dynamics choose a Eulerian frame to describe the balance equations of fluid dynamics. The reason is that in the Eulerian frame, tracing single particles is not of particular interest, since in most cases of fluid dynamics this circumstance involves large displacements associated with flow motion. Therefore, instead of following each particles' trajectory, as done by using a Lagrangian frame, it is more convenient to analyze the variation of the field quantities at certain positions in space [1, 2].

Dealing with aeroacoustics often involves a separation of quantities since the hydrodynamics quantities are usually much larger than the associated perturbations [47, 104, 128]. Since this approach is common in the community of aeroacoustics, it comes natural that a number of different methods for describing sound in moving media have been developed, due to a different definition within the separation process and assumption towards the fluid flow behavior [56, 85, 152, 154, 159, 171, 173].

A number of hybrid CAA methods that are well-known in the aeroacoustic community should be mentioned at this point. First, the linearized Euler equations (LEE) [10, 28], which are usually

applicable to inviscid flows. Second, the linearized Navier-Stokes equation (LNSE) [107], which essentially drops the assumption of an inviscid flow and even can be used to investigate aeroacoustic phenomena involving viscothermal losses, and finally the acoustic perturbation equations (APE) [56, 57, 138]. Since this topic is extensively investigated by many scholars, the reader is referred to the publication of Schoder and Kaltenbacher [170] for a review on the state of the art of hybrid aeroacoustic computations. In terms of numerical methods that have been developed and successfully applied, please see Gabard et al. [70], Gabard et al. [68], Gabard et al. [69], and Hüppe and Kaltenbacher [98].

ALE frame – Galbrun's equation

A very different way was taken by Galbrun, who formulated the basic equations of aeroacoustics in a mixed Lagrangian/Eulerian frame as early as 1931 [73]. By that time, the wording ALE was not common within the scientific community. However, the proposed formulation of Galbrun is indeed an ALE frame applied to the basic equations of fluid dynamics. At first sight, deriving such a more complex theory seems to be unnecessary, unless distinct advantages are identified that outshine the disadvantages. A listing of these aspects follows as the advantages are that (i) the coupling condition at interfaces with continuity of normal acoustic displacement can be directly treated, (ii) even for homentropic rotational flow, an exact conservation law as well as a definition of acoustic intensity exists, and (iii) stable and efficient finite element formulations in the frequency domain have been developed [146]. On the contrary, there also exist a number of disadvantages such as: (I) the underlying ALE framework is more complicated, (II) spurious solutions can pollute solutions when utilizing standard Lagrange elements, and (III) boundary conditions of in- and outflow regions are complicated to formulate [50, 67, 72, 146, 156, 162, 183]. For more information on spurious solutions the reader is referred to Donea and Belytschko [52], Wang and Bathe [185], and Bathe et al. [13]. A comparison to analytical solutions and LEE formulations can be found in Brazier [37].

Despite the possible difficulties that arise by applying Galbrun's equation, a number of scholars have done extensive research in this field [21, 24, 67, 119, 161]. For general derivations and possible extensions to a non-linear theory, see the literature [38, 132, 156]. As already pointed out, since Galbrun's equation is a second-order vector wave equation, some mathematical difficulties come along, known as spurious modes that can possibly lead to a pollution of the sought solution, when standard FEM schemes are applied. To overcome this drawback, various approaches have been proposed throughout the years. On the one hand, a mixed formulation proved to be a stable scheme for which good numerical results are achieved [50, 72, 146, 183]. On the other hand, a

regularization of Galbrun's equation, as proposed by Bonnet-Ben Dhia and her co-workers [30, 31, 33–35], enables one to use the original pure displacement-based form of Galbrun's equation, where no pressure degrees of freedom are present, as it is in the mixed formulation.

Furthermore, when dealing with aeroacoustics by using an ALE frame, some considerations must be taken into account and essentially unbounded domains need to be considered. Since in practical cases computational costs need to be minimized, unbounded domains represent a major conflict in this context, unless appropriate boundary conditions are stated on the surface of the truncated domain. For this reason, two powerful methods are brought up. The first one using infinite finite elements, see Retka and Marburg [163], and the second one relies on PML absorbing boundary conditions [8, 15, 18, 61]. This way originally unbounded domains can be truncated and efficiently solved using numerical methods.

In terms of sources of Galbrun's equation only a few publications consider this aspect [67, 71]. However, a major field of applications is concerned with analyzing the sound propagation within ducts that can have lined walls [9, 22, 147, 153, 182, 183], where the majority of problems are considered in a time-harmonic regime, see Berriri et al. [25] as well as Rodríguez and Santama-rina [164] for an analysis of the time dependent Galbrun equation. This circumstance, as under-stood by the author, stems from the existence of spurious solutions. Consequently, in a transient analysis, these spurious modes are excited and lead to unstable solutions, if no stabilization mea-sures are taken.

Recently, Galbrun's equation has been applied to helioseismology in order to study the wave prop-agation in an arbitrary flow [41], which seems to be a very interesting research field for the future.

1.1.3 Rotor dynamics

Rotor dynamics is a very broad research field among mechanical engineers with many associated topics. Since it is out of the scope of this work to review all aspects of rotor dynamics, the reader is referred to literature [102, 108, 109] and references within and especially the textbooks [64, 75], to get an introduction to the interesting research field. Among the many types of rotors that are possible to think of, in this context only rotating elastic disks are investigated, where the axis of rotation remains stable. Such disks under no rotation can adequately be described by the Kirchhoff plate theory [2].

Keeping in mind that the elastic structures are rotating, evidently applying an ALE frame for de-scribing the rotor dynamics motion is an attractive approach. To clarify this, rotor dynamics, as it should be understood in this work, means that an elastic body is rotating with constant speed

around its main symmetry axis and deflections are measured with respect to an undeformed reference frame. Consequently, if the rotating disk is considered rigid and the axis of rotation remains fixed in space, then no deflection as seen from an ALE point of view would be recognizable, even though the disk is rotating relative to the reference frame. From this starting point, several applications can be analyzed, namely, general rotor dynamic investigations on disks [55, 76, 113], rings [26, 27, 96] and more specific rolling contact mechanisms of tires [126, 140, 141, 190], railway wheelsets [60, 180, 184], or break disk [186, 187] and even sound radiation of such systems [39, 42, 117, 118].

As can be seen from the above stated examples, the use of numerical methods, such as FEM, are state-of-the-art tools [110, 143, 144, 149, 174]. Furthermore, it is apparent that the rotation induces a sort of asymmetry, which disturbs the double symmetry and leads to a so-called mode splitting, which, from a stationary point of view, i.e. in an ALE frame, leads to a forward and backward traveling wave. Even in the non-rotating case, disturbances such as cracks or geometrical deviations of actual double symmetric structures, e.g. beams with circular cross section, can lead to mode splitting [176]. However, if a rotational speed is present, the dynamic analysis must include effects that are linked to the rotation, in order to capture the effect on the surrounding domain correctly [39].

Another application that has been skipped above are saw blades. Here, the structural dynamics are especially relevant. This circumstance is explained by looking at the resulting frequency of the backward traveling wave. It can be seen that once the rotational speed increases, the associated frequency of a backward traveling wave decreases, which turns to zero for a critical speed [62, 136, 168]. This instability can result in a harmful environment for workers in the vicinity of such rotors, since the kinetic energy stored in the rotor is usually quite high for such cases and the associated deflection shape of the disk is quasi stationary for a stationary observer. For this reason, a number of techniques have been developed to influence the stability of the saw blade in the ultimately critical speed. See for example [11, 86, 87, 120, 121, 135, 142, 148, 151, 167] and the review of Mote and Szymani [137].

1.2 Contribution of this work

The main contribution of this work is dedicated towards understanding and analyzing sound and vibration in a mixed frame, where two applications are in focus – the first application from the research field of aeroacoustics and the second from the field of rotor dynamics. These research fields, as understood by the author, can be divided into four classes. Note that due to the engineering background of the author, the following classification is biased and does not claim general validity.

The first class is named "Literature" and includes the research on available publications, the most in-depth knowledge and understanding of the state of the art. The second class is dedicated to "Physics" and encompasses the fundamental understanding of physical processes as well as the mathematical tools to describe them. The third class deals with "Numerical Methods". In this class, computer-aided engineering is utilized for the numerical treatment of complex equations, specifically partial differential equations describing the physical processes mentioned above. Last but not least, the fourth class "Application" deals with the derivation of useful solutions for solving relevant problems. These classes build on each other and can be seen as an engineering guide for dealing with problems and finding suitable solutions.

In the sense of understanding sound and vibration in an arbitrary Lagrangian Eulerian frame as a superordinated umbrella applied to aeroacoustics and rotor dynamics, four publications are appended to this work contributing to each class defined above. Each contribution can briefly be summarized as follows.

Publication A summarizes available publications that can be linked to Galbrun's equation, which describes aeroacoustic wave propagation in the frame of a Lagrangian perturbation of a Eulerian quantity. This review paper is the first attempt, to the best of the author's knowledge, to summarize contributions to this particular research topic and to place Galbrun's equation comprehensively in relation to other approaches and methods of aeroacoustics. Therefore, on the one hand, the contribution can be seen as a possible starting point for interested researchers and, on the other hand, it helps to understand how Galbrun's equation is classified and where it derives from. In addition, the cited publications are sorted with respect to superordinate research topics. The author's intention is to facilitate orientation in the large number of publications. Furthermore, the general derivation of Galbrun's equation is recalled and possible ways of further development are highlighted. Therefore, the main contribution of this publication can be associated with the class "Literature", as mentioned above.

Publication B recalls the numerical instabilities that occur when Galbrun's equation in its pure displacement-based formulation is solved utilizing a standard finite element method in the context of a numerical modal analysis. To remedy this problem, a discontinuous Galerkin finite element method is applied to the pure displacement-based form of Galbrun's equation. Furthermore, a convergence analysis highlights the stability of the method and a parameter analysis provides details for the selection of adequate flux parameters. For the case of a duct with uniform flow and an annulus with a rotating shear flow, numerous investigations on the eigenvectors were carried out, in which an appropriate classification strategy was proposed to distinguish acoustically dominated modes from non-acoustically dominated modes, such as vortical modes or spurious modes. As shown, this also can be realized by applying adequate constraints through a Lagrange multiplier strategy on the weak form level of Galbun's equation. The main contribution of this publication can be associated with the class "Numerical Method".

Publication C contributes to the physical understanding of sound radiation from a rotating elastic disk where a lumped parameter model was applied as an appropriate strategy for quantifying the sound power emission. As highlighted in the publication, the numerical model accounts for effects such as Coriolis forces and the resulting deflection of the disk is seen from an arbitrary Lagrangian Eulerian frame. The possibility of applying a modal super position strategy for computing the harmonic response considerably saves computational cost. Furthermore, the effect was identified that deflection shapes forming acoustic short circuits at low rotational speeds contribute to the sound radiation at higher speeds. Last but not least, mode splitting that is associated with elastic deforming disks under rotation is audible but only away from the rotational axis. Therefore, the main contribution of this publication can be associated with the class "Physics".

Publication D presents an improved version of a rotating disk which can be applied as a saw plate in industrial branches such as the wood industry or medicine. The key contribution is associated with the use of a pre-deformed plate configuration and additional tensioning lines in a spiral configuration. Compared to standard versions of such a disk, i.e. a single monolithic disk with circular tensioning lines, the critical speed of the proposed disk is improved by 33%. If kinetic energy is considered as a measure of productivity, an improvement of 75% is achieved. At this point, the patent is in its nationalization and regionalization stage in the European Union, the United States of America as well as the Republic of China. This contribution falls under the last class "Application".

A more detailed summary can be found in Chapter 4. Overall, the contributions of this work can be assigned to the four classes defined above with respect to the research of an arbitrary Lagrangian Eulerian framework applied to aeroacoustics as well as rotor dynamics.

Chapter 2

Applied Methods

This chapter is dedicated to the basic methods used in this work. First, a general notation is introduced to provide the mathematical definitions for this thesis. Second, the ALE framework is discussed and finally applied to aeroacoustics and rotor dynamics.

2.1 General notation

The following notations are recalled from Publication A. For the remainder of this work, a Euclidean space $\Omega \subset \mathbb{R}^3$ with a Cartesian coordinate system is considered, defined by orthonormal basis tuple $\mathscr{B} = (\vec{e}_1, \vec{e}_2, \vec{e}_3)$, unless specified differently. In order to describe physical processes, tensors of n-th order are defined as follows:

- ρ, θ - Tensor of zeroth order or scalar,

- $\vec{v}$, $\vec{f}$, $\vec{q}$ - Tensor of first order or vector with components v_k,

- $\vec{\vec{\sigma}}$, $\vec{\vec{\tau}}$, $\vec{\vec{\Pi}}$ - Tensor of second or higher order with components σ_{kl}.

Furthermore, time and spatial derivative operators acting on tensors help to describe physical processes. For the spatial derivatives, the Nabla operator $(\nabla(\cdot) = (\frac{\partial(\cdot)}{\partial x_1}, \frac{\partial(\cdot)}{\partial x_2}, \frac{\partial(\cdot)}{\partial x_3})^T)$ is introduced. In addition, $(\cdot)_{,i}$, where $i = 1, 2, 3$, is equivalently used for partial derivative with respect to the corresponding spatial coordinate. Together with the Einstein summation convention, this description is particularly useful because of its explicit character. However, the use of the well-known Nabla calculus reveals its advantage when changing the underlying coordinate system. The following mathematical rules apply and are given in the Nabla calculus and a component formulation to avoid confusion or misunderstanding.

- $\vec{q} = \nabla \rho = \text{grad } \rho = q_i \vec{e}_i = \rho_{,i} \vec{e}_i,$

- $\vec{\vec{\sigma}} = \nabla \vec{v} = \text{grad } \vec{v} = \sigma_{kl} \vec{e}_k \otimes \vec{e}_l = v_{k,l} \vec{e}_k \otimes \vec{e}_l,$

- $\vec{\vec{\tau}} = \nabla^T \vec{v} = \text{grad}^T \vec{v} = \tau_{kl} \vec{e}_k \otimes \vec{e}_l = v_{l,k} \vec{e}_k \otimes \vec{e}_l,$

- $\rho = \nabla \cdot \vec{v} = \text{div } \vec{v} = v_{k,l} \vec{e}_k \cdot \vec{e}_l = v_{k,l} \delta_{kl} = v_{k,k},$

- $\vec{q} = \nabla \cdot \vec{\vec{\sigma}} = \text{div } \vec{\vec{\sigma}} = q_k \vec{e}_k = \sigma_{kl,i} \vec{e}_k \otimes \vec{e}_l \cdot \vec{e}_i = \sigma_{kl,i} \delta_{li} \vec{e}_k = \sigma_{kl,l} \vec{e}_k,$

- $\vec{q} = \nabla \times \vec{v} = \text{rot } \vec{v} = q_k \vec{e}_k = e_{kmn} v_{m,n} \vec{e}_k.$

Here, $(\cdot)$ represents the scalar product, $\delta_{ij} = \vec{e}_i \cdot \vec{e}_j$ is the Kronecker symbol with $\delta_{ij} = 1$ if $i = j$ and $\delta_{ij} = 0$ if $i \neq j$, $\otimes$ the dyadic product and e_{lmn} the Levi-Civita symbol, defined as

$$e_{lmn} = \begin{cases} 1 & \text{if} \quad l,m,n = 1,2,3 \quad \text{and cyclic,} \\ -1 & \text{if} \quad l,m,n = 3,2,1 \quad \text{and cyclic,} \\ 0 & \text{else.} \end{cases} \tag{2.1}$$

In the above stated rules, the divergence operator applied to a second-order tensor acts on the second component of this tensor. This form is known as *right divergence operator*, see Belytschko et al. [17]. This definition has a significant consequence on the definition of this tensor, especially in the case where $\vec{\vec{\sigma}}$ represents the Cauchy stress tensor. Consequently, this stress tensor with
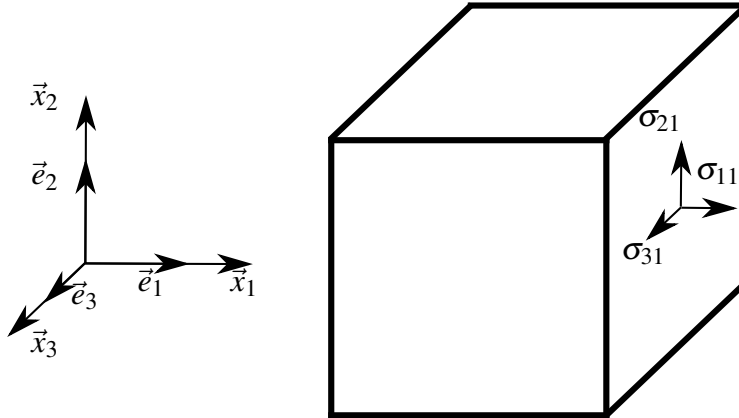

Figure 1: The Cauchy stress tensor in a Cartesian coordinate system, see Publication A

its components σ_{kl} is defined such that the first component k is dedicated to the direction of the principle force, which in turn is assigned to the principle plane with its normal in x_l-direction, see Figure 1. This definition becomes especially relevant when considering the balance equations of nonlinear continuum mechanics where the stress tensor can be unsymmetrical. Textbooks where the definition is vise versa, i.e. the *left divergence operator* applies, are also available, see for

example [1, 2, 17, 130]. The reason for stressing the precise definition is due to the negligent treatment in numerous publications, which can result in confusion or even inconsistencies when studying literature.

Upon these basic notations, the derivation of the ALE formulations follows in the subsequent section, where the basic frameworks of continuum mechanics are recalled in order to provide a general description.

2.2 ALE framework

In this section, the fundamentals for understanding the ALE framework are discussed. As a start, a brief account is given of the classical concepts of Lagrangian and Eulerian descriptions. Both are considered as the fundamental frames of continuum mechanics and, consequently, their application depends on the advantages and disadvantages which accompany them. The ALE formulation takes the main advantages of both frames as a unified formulation from which the Lagrangian as well as the Eulerian frame can be deducted through simplifications. Therefore, the ALE description can be seen as a generalized form. With great respect to the authors, the following outlines are based
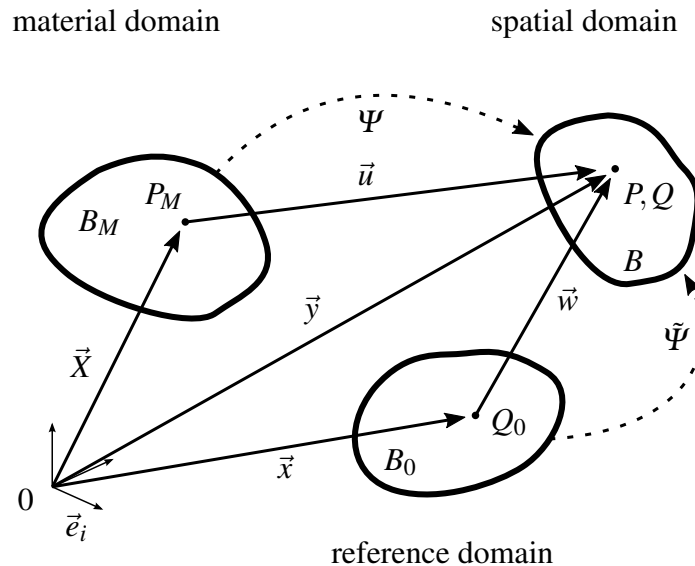

Figure 2: Mapping of frames for ALE definition, after Donea and Belytschko [52]

on the well-written work of Donea and Belytschko [52] as well as Belytschko et al. [17], which serve as fabulous reviews of the topic. For a deeper insight, the reader is referred to the literature, see [17, 52, 53, 140] and citations within.

Figure 2 serves as a guide for deriving the main concept of the ALE description. Consider a continuum Ω in the three-dimensional vector space $\mathbb{R}^3$ with $\vec{e}_i$ being its basis for an open time interval $\langle 0, T \rangle \in \mathbb{R}$. Furthermore, an infinitesimal volume element of this continuum shall be named *particle*. The motion of all particles within space along the time axis can be followed or described by their distinctive trajectories. The position of a particle occupying a point P_M is defined by its spatial coordinates $\vec{X}$ at the initial time T_0. This initial configuration or initial domain is named *material domain* and denoted by B_M. As the continuum evolves in time and space, its configuration may change even though the number of particles remain unchanged. The configuration at the present time t is denoted by B and called *spatial domain*. The particle in this configuration occupies the point P with its vector position $\vec{y}$.

Consequently, the behavior of the continuum can be described by a mapping Ψ such that

$$\Psi : B_M \times \langle 0, T \rangle \to \mathbb{R}^N \quad \text{with} \quad N = 3, \tag{2.2}$$

$$\vec{X}, t \to \vec{y}. \tag{2.3}$$

From this mapping, the system of equations can be deducted as

$$y_i = \Psi_i(X_j, t) \tag{2.4}$$

that forms the relation between the domain B and the domain B_M. It is assumed that this mapping is unique, continuous with continuous derivatives, and reversible. These assumptions yield that the Jacobian J_M with respect to the material domain does not vanish. Therefore, the relation

$$J_M = |\frac{\partial y_i}{\partial X_j}| \neq 0 \tag{2.5}$$

must be fulfilled. With this condition, an inverse calculation exists as

$$X_i = \Xi_i(y_j, t). \tag{2.6}$$

Furthermore, the displacement vector u is simply calculated by the following formula

$$\vec{u} = \vec{y} - \vec{X}. \tag{2.7}$$

In the case that the components of the displacement vector are expressed in terms of the material coordinates of $\vec{X}$ as

$$\vec{u} = u_i(X_j, t)\vec{e}_i, \tag{2.8}$$

the representation is named *Lagrangian representation*. In contrast, if the components of $\vec{u}$ are expressed by the components of the spatial coordinates, i.e. taking equation (2.6) into account, the displacement vector is expressed by

$$\vec{u} = U_i(y_l, t)\vec{e}_i \tag{2.9}$$

and named *Eulerian representation*. In anticipation of the use of the FEM as a domain discretization procedure, one can understand the Lagrangian description in such a way that the mesh is fixed to the associated material particles and that the mesh deforms from its initial configuration to the present configuration together with the underlying continuum. This is in contrast to the Eulerian description where the mesh is fixed in space and the particles move across with a relative velocity. Table 1 provides a comparison of advantages and disadvantages of the two frames discussed above. Note that this assessment is biased by personal opinion as well as by the limited number of publications that have been studied.

Framework	Advantages	Disadvantages
Lagrangian	Clear demarcation of interfaces	Inability to cope with large distortion
	Good resolution of details	Adaptive remeshing complicated
	No convective terms from material time derivative	
Eulerian	Good handling of strong distortion	Precise interface definition necessary
		Weak resolution of details

Table 1: Comparison between the Lagrangian and the Eulerian framework

The original concept of deriving an ALE formulation is primarily driven by the will to combine the advantages of both fundamental frameworks. This goal is achieved by introducing a new domain B_0 called *reference domain*, which in this sense is arbitrary. As will be seen in the subsequent outlines, this form of framework provides a generalization, and through simplifications the Lagrangian and the Eulerian description can be deducted from there.

In the ALE framework, a reference point Q_0 is chosen, which is neither necessarily connected to any material point nor possesses a fixed position in space. The position of the reference point in its initial configuration is defined by the vector $\vec{x}$. It follows that the motion of the continuum of

interest is defined by the application of

$$\tilde{\Psi} : B_0 \times \langle 0, T \rangle \to \mathbb{R}^N \quad \text{with} \quad N = 3, \tag{2.10}$$

$$\vec{x}, t \to \vec{y} \tag{2.11}$$

through the reference domain. Consequently, the components of the spatial vector $\vec{y}$ result from

$$y_i = \tilde{\Psi}_i(x_j, t), \tag{2.12}$$

where again it is assumed that continuity of the function $\tilde{\Psi}$ and its derivatives up to a sufficient order are guaranteed as well as that an inverse exists and

$$J = |\frac{\partial y_i}{\partial x_j}| \neq 0 \tag{2.13}$$

immediately follows. From the above stated arguments and the vector notation in Figure 2, one can see that for any present position $\vec{y}$ one configuration in the material domain as well as one configuration in the reference domain can be assigned as

$$\vec{y} = \vec{\Psi}(\vec{X}, t) = \vec{X} + \vec{u}, \tag{2.14}$$

$$= \vec{\tilde{\Psi}}(\vec{x}, t) = \vec{x} + \vec{w}. \tag{2.15}$$

So far, the key features of the ALE framework are presented. However, for understanding its application to the well-known balance equations of continuum mechanics, the definition of appropriate time derivatives is missing. With these definitions, the corresponding velocity vectors together with the rate of change of physical quantities evolve as will be discussed in the following.

For each material point, the velocity vector $\vec{v}_M$ is defined by the partial time derivative of the position vector as

$$\vec{v}_M = \frac{\partial \vec{y}(X_j, t)}{\partial t}\bigg|_{\vec{X}} = \frac{\partial \vec{u}(X_j, t)}{\partial t}\bigg|_{\vec{X}}, \tag{2.16}$$

which is the Lagrangian representation of the velocity. Here, $\vec{X}$ is kept constant during differentiation. Note that $\vec{X}$ identifies an initial configuration and therefore is not a function of time. For the reference point, the same procedure yields

$$\vec{v}_R = \frac{\partial \vec{y}(x_l, t)}{\partial t}\bigg|_{\vec{x}} = \frac{\partial \vec{w}(x_l, t)}{\partial t}\bigg|_{\vec{x}}. \tag{2.17}$$

At this point, it is important to note that both the Lagrangian and the Eulerian description can

be recovered. In the case of a Lagrangian frame, setting $B_0 = B_M$, $\tilde{\Phi} = \Phi$, and considering equations (2.14) and (2.15) yields

$$\vec{w} = \vec{y} - \vec{X} = \vec{u}, \tag{2.18}$$

$$\vec{v}_R = \vec{v}_M. \tag{2.19}$$

On the contrary, in a Eulerian frame the reference domain becomes the spatial domain as $B_0 = B$ and $\tilde{\Phi}$ can be seen as an identity transformation. This yields $w = y$ and similarly from equations (2.14) and (2.15)

$$\vec{w} = 0, \tag{2.20}$$

$$\vec{v}_R = 0 \tag{2.21}$$

follows. By summarizing the above stated arguments, three different situations are identified:

1. $\vec{v}_R = 0$; mesh is fixed in space; Eulerian description,

2. $\vec{v}_R = \vec{v}_M$; mesh is fixed to material; Lagrangian description,

3. $\vec{v}_R \neq \vec{v}_M \neq 0$; mesh is independent of material; ALE description.

As a next step, the rate of change of physical quantities depending on the different frames is presented. The physical quantity of interest shall be named Φ hereafter. It is important to note that when Φ is a function of $\vec{X}$, $\vec{y}$, or $\vec{x}$, the representation is called material, spatial, or mixed representation, respectively. Furthermore, three different time derivatives exist which are denoted by spatial, material, and mixed derivatives. Note that to prevent insufficient clarity in the subsequent outlines, the component notation is preferred for improved readability whenever confusion might arise. Table 2 lists the various derivatives with adequate notation and individual interpretations. Next, it is important to investigate how the material time derivative is constructed if Φ is formulated in three possible representations, as stated above. If the physical quantity is defined in its material representation, the material time derivative follows in a straightforward manner as

$$\frac{\mathrm{D}\Phi(\vec{X},t)}{\mathrm{D}t} = \left. \frac{\partial \Phi(\vec{X},t)}{\partial t} \right|_{\vec{X}}. \tag{2.22}$$

In the case that Φ is defined in its spatial representation, the material time derivative becomes more

Designation	Formula	Interpretation
Material time derivative	$\frac{\mathrm{D}\Phi}{\mathrm{D}t}$	Variation per unit time felt by observer moving with material
Spatial time derivative	$\left.\frac{\partial\Phi}{\partial t}\right\|_{\vec{y}}$	Variation per unit time at fixed position in space
Mixed time derivative	$\left.\frac{\partial\Phi}{\partial t}\right\|_{\vec{x}}$	Variation per unit time felt by observer moving with the reference

Table 2: Definition of different time derivatives, see Donea and Belytschko [52]

complex, since $\vec{y}$ is a function of time and therefore the chain rule applies, which yields

$$
\frac{\mathrm{D}\Phi(y_l,t)}{\mathrm{D}t} = \left.\frac{\partial\Phi(y_l,t)}{\partial t}\right|_{y_l} + \left.\frac{\partial\Phi(y_l,t)}{\partial y_i}\right|_t \left.\frac{\partial y_i(t)}{\partial t}\right|_{X_l}, \tag{2.23}
$$

$$
= \left.\frac{\partial\Phi(y_l,t)}{\partial t}\right|_{y_l} + v_{Mi}(y_l,t)\left.\frac{\partial\Phi(y_l,t)}{\partial y_i}\right|_t. \tag{2.24}
$$

Equation (2.24) can be interpreted as follows: An observer looking at a position $\vec{y}$ in space is noticing two contributions for the rate of change of the quantity Φ. First, the field of the quantity is changing with time, which is expressed by the spatial time derivative of Φ, see the first term in equation (2.24). Second, the field Φ itself possesses a velocity with which it is moving relative to the observer. Together with the non-vanishing spatial gradient of Φ, a second contribution is added, known as convective term, cf. the second term in equation (2.24).

Eventually, if Φ is defined in its reference representation, the material time derivative is obtained in a similar fashion as

$$
\frac{\mathrm{D}\Phi(x_l,t)}{\mathrm{D}t} = \left.\frac{\partial\Phi(x_l,t)}{\partial t}\right|_{x_l} + \left.\frac{\partial\Phi(x_l,t)}{\partial x_i}\right|_t \left.\frac{\partial x_i(t)}{\partial t}\right|_{X_l}, \tag{2.25}
$$

where the first term on the right-hand side is referred to the mixed time derivative of Φ. For the convection term, an appropriate velocity has to be identified. For this purpose, the partial time derivative of equations (2.14) and (2.15) for a fixed $\vec{X}$ yields

$$
\left.\frac{\partial y_i(X_l,t)}{\partial t}\right|_{X_l} = \left.\frac{\partial \Psi_i(X_l,t)}{\partial t}\right|_{X_l} = \left.\frac{\partial \tilde{\Psi}_i(x_l,t)}{\partial t}\right|_{x_l} + \left.\frac{\partial \tilde{\Psi}_i(x_l,t)}{\partial x_j}\right|_t \left.\frac{\partial x_j(t)}{\partial t}\right|_{X_l}. \tag{2.26}
$$

Considering again equations (2.14) and (2.15) and inserting equation (2.16) and (2.17) into (2.26)

yields

$$v_{Mi} = v_{Ri} + \left.\frac{\partial y_i(x_l,t)}{\partial x_j}\right|_t \left.\frac{\partial x_j(t)}{\partial t}\right|_{X_l}. \tag{2.27}$$

Furthermore, equation (2.27) can be used to isolate the partial time derivative of $\vec{x}$ for a fixed position $\vec{X}$ such as

$$\left.\frac{\partial x_j(t)}{\partial t}\right|_{X_l} = \left.\frac{\partial x_j(y_l,t)}{\partial y_i}\right|_t \left(v_{Mi} - v_{Ri}\right). \tag{2.28}$$

Now, equation (2.25) can be reformulated as

$$\frac{\mathrm{D}\Phi(x_l,t)}{\mathrm{D}t} = \left.\frac{\partial \Phi(x_l,t)}{\partial t}\right|_{x_l} + \left.\frac{\partial \Phi(x_l,t)}{\partial x_i}\right|_t \left.\frac{\partial x_i(y_l,t)}{\partial y_j}\right|_t \left(v_{Mj} - v_{Rj}\right), \tag{2.29}$$

or further simplified as

$$\frac{\mathrm{D}\Phi(x_l,t)}{\mathrm{D}t} = \left.\frac{\partial \Phi(x_l,t)}{\partial t}\right|_{x_l} + \bar{c}_i \left.\frac{\partial \Phi(y_l,t)}{\partial y_i}\right|_t. \tag{2.30}$$

where

$$\bar{c}_i = \left(v_{Mi} - v_{Ri}\right). \tag{2.31}$$

Essentially, equation (2.30) can be seen as the fundamental derivative for transforming the conservation equations of continuum mechanics into the ALE frame. In the following sections, these concepts are applied to fluid dynamics and rotor dynamics to derive suitable equations of motion.

2.3 Application to fluid dynamics

In this section, the above stated concepts are applied to the conservation equations of fluid dynamics. The main goal of this approach lies in a rather unusual definition of perturbations of physical quantities, which then can be seen as reference quantities and their fluctuations. This approach leads to a formulation of aeroacoustics known as Galbrun's equation, in which fluctuations are expressed as a function of a Lagrangian displacement with respect to a Eulerian quantity. This is in contrast to the common procedure that is being followed by scholars in the field of aeroacoustics, where traditionally the fluctuations as well as the reference quantities are formulated in a pure Eulerian framework. However, some interesting advantages can be identified when using Galbrun's equation. Perhaps the most important one arises when interfaces are considered. As has been discussed above, the Lagrangian frame allows a precise definition and formulation of such interfaces. Therefore, considering fluid fluctuations in a Lagrangian frame allows one to easily couple

the fluid domain to other domains involving jumps in the physical properties, see Brazier [38]. However, to arrive at the mentioned perturbation formulation some additional considerations are needed, which are primarily recalled from Publication A and citations within.

Preliminary remarks

To shed more light upon this method and how the ALE framework is adopted, Figure 3 illustrates the relation between the reference state and the perturbed state. These two states can be understood as trajectories of a fluid flow, where the reference flow is free of perturbations. In this context,
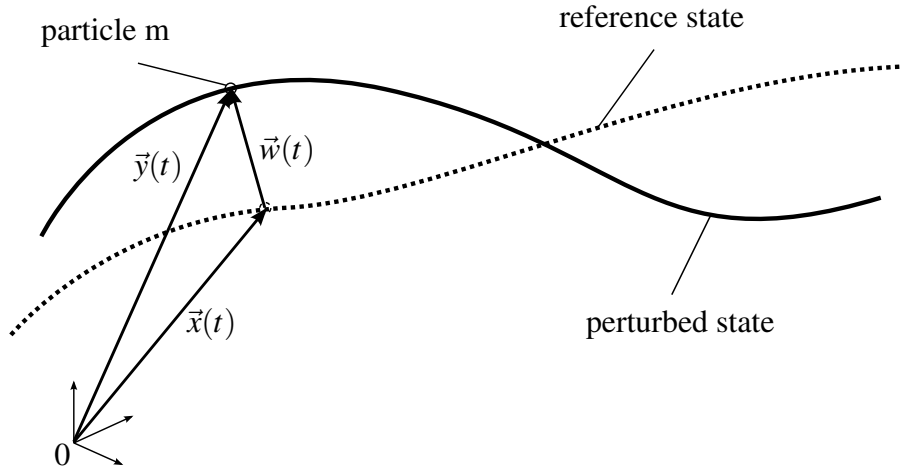

Figure 3: Frame of reference state and perturbed state, see Publication B

a given particle m takes the position $\vec{y}$ for time instance t, where perturbations are present. If perturbations are absent, the particle is located at $\vec{x}$. This way, the perturbation can be described as a function of $\vec{w}$ which has a Lagrangian character.

To highlight the differences of the perturbation description, the three frames are briefly acknowledged. The Eulerian perturbation of a physical quantity Φ reads

$$\Phi'(\vec{y},t) = \Phi(\vec{y},t) - \Phi_0(\vec{y},t).$$

(2.32)

In a pure Lagrangian frame, the perturbations are denoted by

$$\bar{\Phi}(\vec{X},t) = \Phi(\vec{X},t) - \Phi_0(\vec{X},t).$$

(2.33)

Now in the mixed framework, the perturbations are defined as follows:

$$\tilde{\Phi}(\vec{x},t) = \Phi(\vec{y},t) - \Phi_0(\vec{x},t). \tag{2.34}$$

From equation (2.34), it can be seen that the reference quantity as well as its perturbation are referred to a position $\vec{x}$ and that the associated sum results in the Eulerian quantity $\Phi(\vec{y},t)$. Furthermore, it is possible to combine the Eulerian perturbation with the mixed perturbation using equations (2.32) and (2.34), which yields

$$\Phi'(\vec{y},t) = \tilde{\Phi}(\vec{x},t) - (\Phi_0(\vec{y},t) - \Phi_0(\vec{x},t)). \tag{2.35}$$

One relevant conclusion can be drawn at this point. When investigating equation (2.35), it follows that the Eulerian perturbation and the mixed perturbation are equivalent, if the gradient of the reference field vanishes. In addition, if a small perturbation restriction is applicable and the reference field has smoothly varying gradients, equation (2.35) can be reformulated as

$$\Phi'(\vec{y},t) = \tilde{\Phi}(\vec{x},t) - \vec{w}^T \cdot \nabla \Phi_0(\vec{x},t), \tag{2.36}$$

where (2.15) has been used, see references [37, 67, 71, 156] for more detail. Before deriving the Galbrun's equation, an appropriate formalism must be discussed which allows the conversion of the gradient and divergence operator from the Eulerian frame to the mixed frame. This will be the focus of the briefly presented subsequent outlines. For deeper insight, the reader is referred to Minotti et al. [132] as well as Publication A, attached to this work.

As already indicated in equation (2.13), the Jacobian of the mixed frame is calculated by taking the determinant of the deformation gradient $\vec{\vec{F}}$ as

$$J = \det \vec{\vec{F}} \quad \text{or} \quad J = \frac{1}{6} e_{lmn} e_{pqr} F_{lp} F_{mq} F_{nr}, \tag{2.37}$$

where the deformation gradient stems from

$$\mathrm{d}\vec{y} = \vec{\vec{F}} \cdot \mathrm{d}\vec{x} \quad \text{with} \quad \mathrm{d}y_i = F_{ij} \mathrm{d}x_j. \tag{2.38}$$

If the Lagrangian deformation $\vec{w}$, see equation (2.13), is included, equation (2.38) yields

$$\vec{\vec{F}} = \vec{\vec{I}} + \nabla \vec{w} \quad \text{with} \quad F_{ij} = \delta_{ij} + w_{i,j}, \tag{2.39}$$

23

where $\vec{\vec{I}}$ represents the second order identity tensor. Furthermore, the inverse of $\vec{\vec{F}}$ is given by

$$\vec{\vec{G}} = \vec{\vec{F}}^{-1} = \frac{1}{J}\vec{\vec{T}}^{T} \quad \text{with} \quad G_{ij} = F_{ij}^{-1} = \frac{1}{J}T_{ji}. \tag{2.40}$$

In equation (2.40), the tensor $\vec{\vec{T}}$ represents the cofactor matrix [77] of $\vec{\vec{F}}$ as

$$\vec{\vec{T}} = (1 + \nabla \cdot \vec{w})\vec{\vec{I}} - \nabla^{T}\vec{w} + \vec{\vec{N}} \quad \text{with} \quad T_{ij} = (1 + w_{l,l})\delta_{ij} - w_{j,i} + N_{ij}. \tag{2.41}$$

Last but not least, the tensor $\vec{\vec{N}}$ is stated as

$$\begin{aligned} \vec{\vec{N}} &= \frac{1}{2}\left((\nabla \cdot \vec{w})^2 - \nabla\vec{w} : \nabla\vec{w}\right)\vec{\vec{I}} - (\nabla \cdot \vec{w})\nabla^{T}\vec{w} + (\nabla\vec{w} \cdot \nabla\vec{w})^{T}, \\ N_{ij} &= \frac{1}{2}\left(w_{l,l}^2 - w_{m,n}w_{n,m}\right)\delta_{ij} - w_{l,l}w_{j,i} + w_{j,l}w_{l,i}. \end{aligned} \tag{2.42}$$

As can be seen, the double dots (:) refer to the double contradicting vector product. Finally, the spatial derivative of an arbitrary tensor $\vec{P}$ in the perturbed field in conjunction with the Green-Ostrogradsky theorem reads as

$$P_{,j}(y_l,t) = \left(P_0(x_l,t) + \tilde{P}(x_l,t)\right)_{,i} G_{ij}(x_l,t), \tag{2.43}$$

and the divergence of $\vec{P}$ with sufficient order yields

$$P_{j,j}(y_l,t) = \frac{1}{J(x_l,t)}\left[\left(P_{0i}(x_l,t) + \tilde{P}_i(x_l,t)\right)T_{ij}(x_l,t)\right]_{,j}. \tag{2.44}$$

For additional information on the derivation, see Minotti et al. [132]. All information necessary to develop Galbrun's equation is available at this point. In the subsequent steps, the transformation formalism and the mixed time derivative are applied to the conservation equations of fluid dynamics.

Application to conservation equations and equations of state

For deriving Galbrun's equation, it is necessary to discuss the basic equations of the underlying physics, which include the conservation equations of continuum mechanics as well as constitutive equations of the associated material model together with thermodynamic relations, see references [51, 67, 92, 128, 155].

The conservation equations of fluid dynamics, known as balance of mass, momentum and energy,

are stated in Eulerian quantities as

$$\frac{D\rho}{Dt} = -\rho\, v_{l,l}, \tag{2.45}$$

$$\rho\frac{Dv_j}{Dt} = \sigma_{ji,i} + f_j, \tag{2.46}$$

$$\rho\frac{De}{Dt} = \sigma_{kl}v_{k,l} - q_{j,j} + \dot{\vartheta}, \tag{2.47}$$

where ρ denotes the fluid density, $\vec{v}$ the vector of fluid velocity, $\vec{\vec{\sigma}}$ the Cauchy stress tensor, $\vec{f}$ body forces, e the internal energy, $\vec{q}$ the heat convection vector, and $\dot{\vartheta}$ any additional heat sources. Furthermore, the Cauchy stress tensor reads

$$\sigma_{ij} = -p_{ij} + \tau_{ij}. \tag{2.48}$$

Here, the components of the hydrodynamic pressure are

$$p_{ij} = \frac{1}{3}\sigma_{ll}\delta_{ij} = p\delta_{ij}. \tag{2.49}$$

Typically, for a Newtonian fluid under Stoke's hypothesis, the shear stress tensor $\vec{\vec{\tau}}$ is a function of the velocity and the dynamic viscosity $\mu(T)$, which is a function of temperature T. It follows that

$$\tau_{ij}(v_l,\mu) = \mu\left(v_{i,j} + v_{j,i} - \frac{2}{3}v_{k,k}\delta_{ij}\right). \tag{2.50}$$

Note that the Cauchy stress tensor is symmetric, which solves the conservation equation of angular momentum. Strictly speaking, this conservation equation belongs to the set of fundamental equations of continuum mechanics, but since the result only proves the symmetry of the Cauchy stress tensor, an explicit treatment is omitted. Furthermore, by using Fourier's law, the heat flux vector is formulated as

$$\vec{q} = -k\nabla T \quad \text{with} \quad q_i = -kT_{,i}. \tag{2.51}$$

The parameter k denotes the heat conductivity for homogeneous and isotropic behavior. The fluid is considered being in local thermodynamic equilibrium, i.e. that the density ρ and the internal energy e can be expressed by a potential depending only on two other variables such as

$$\text{thermal: } \rho = \rho(T,p) \quad \text{and} \quad \text{calorical: } e = e(T,p). \tag{2.52}$$

For further derivations, the total differentials read as follows:

$$\delta\rho = \left.\frac{\partial\rho}{\partial T}\right|_p \delta T + \left.\frac{\partial\rho}{\partial p}\right|_T \delta p, \tag{2.53}$$

and

$$\delta e = \left.\frac{\partial e}{\partial T}\right|_p \delta T + \left.\frac{\partial e}{\partial p}\right|_T \delta p. \tag{2.54}$$

Next, Gibbs law is introduces as

$$T\delta s = \delta e - \delta\left(\frac{p}{\rho^2}\right) = \delta h - \frac{1}{\rho}\delta p, \tag{2.55}$$

where s denotes the entropy and h the enthalpy. Note that the assumption of a local existing thermodynamic equilibrium yields that the differentials within the flow can be converted by utilizing the relation $\delta() = \frac{\mathrm{D}()}{\mathrm{D}t}\delta t$. Thus, using equation (2.55) together with the above stated differentials of the thermodynamic and caloric potentials, cf. equations (2.53) and (2.54), the conservation equation of the inner energy, i.e. equation (2.47), is replaced by the entropy as

$$\rho\frac{\mathrm{D}s}{\mathrm{D}t} = \frac{1}{T}\left[\tau_{kl}v_{k,l} - q_{j,j} + \dot{\vartheta}\right]. \tag{2.56}$$

Note that up to this point, nothing has been said about the thermodynamic relations of the fluid. This lack is resolved by considering the equation of state. For this purpose, an additional potential is established such that the pressure is a function of density and entropy only as

$$\text{state: } p = p(\rho, s). \tag{2.57}$$

The total differential follows in a straightforward manner, which yields

$$\delta p = \underbrace{\left.\frac{\partial p}{\partial\rho}\right|_s}_{c^2} \delta\rho + \underbrace{\left.\frac{\partial p}{\partial s}\right|_\rho}_{\alpha} \delta s. \tag{2.58}$$

Since this relation must also hold for any moving particle, again by utilizing $\delta() = \frac{\mathrm{D}()}{\mathrm{D}t}\delta t$,

$$\frac{\mathrm{D}p}{\mathrm{D}t} = c^2\frac{\mathrm{D}\rho}{\mathrm{D}t} + \alpha\frac{\mathrm{D}s}{\mathrm{D}t} \tag{2.59}$$

follows, where the time differentials have been omitted, as they are common in all terms. Equation (2.59) can be understood as an equation of state for moving fluids, where pressure variations are

related to density as well as entropy variations. At this point, the preliminary discussions about the basic concepts of fluid dynamics have been conducted and the presented transformations can be applied as follows.

First, an expression for the density perturbations is derived. For this purpose, one takes the simple thought experiment that an infinitesimal small mass element dm remains constant no matter whether present in the perturbed or reference state. Therefore, it follows that

$$\mathrm{d}m = \rho_0 \mathrm{d}V_0 = \rho \mathrm{d}V = \text{const.} \tag{2.60}$$

The infinitesimal volume element dV can be converted using the Jacobian, which yields

$$\mathrm{d}V = J\mathrm{d}V_0. \tag{2.61}$$

Furthermore, the density can be separated in reference and perturbation as

$$\rho = \rho_0 + \tilde{\rho}. \tag{2.62}$$

From equations (2.60), (2.61), and (2.62), the density perturbation follows in a straightforward manner as

$$\tilde{\rho} = \rho_0 \left(\frac{1-J}{J} \right), \tag{2.63}$$

which is in agreement with the literature, see Minotti et al. [132] as well as Publication A.

Second, the transformation rules are applied to the conservation equation of momentum. To do this, equations (2.34), (2.43), (2.44), (2.48), and (2.49) are used to transform equation (2.46) into the mixed frame, which yields

$$(\rho_0 + \tilde{\rho}) \left(\frac{\mathrm{D}v_{0k}}{\mathrm{D}t} + \frac{\mathrm{D}\tilde{v}_k}{\mathrm{D}t} \right) - \frac{1}{J} \left((-p_0 \delta_{ki} - \tilde{p}\delta_{ki} + \tau_{0ki} + \tilde{\tau}_{ki}) T_{ij} \right)_{,j} = f_{0k} + \tilde{f}_k. \tag{2.64}$$

Third, the same procedure applies to the conservation of entropy such that

$$(\rho_0 + \tilde{\rho}) \left(\frac{\mathrm{D}s_0}{\mathrm{D}t} + \frac{\mathrm{D}\tilde{s}}{\mathrm{D}t} \right) = \frac{1}{T_0 + \tilde{T}} \left(\tau_{0kl} + \tilde{\tau}_{kl} (v_{0k} + \tilde{v}_k)_{,i} G_{il} - \cdots \right.$$
$$\left. - \frac{1}{J} \left((q_{0i} + \tilde{q}_i) T_{ij} \right)_{,j} + \dot{\vartheta}_0 + \tilde{\dot{\vartheta}} \right) \tag{2.65}$$

follows. Last but not least, in this concept, the equation of state (2.59) is transformed accordingly

and reads

$$\frac{\mathrm{D}p_0}{\mathrm{D}t} + \frac{\mathrm{D}\tilde{p}}{\mathrm{D}t} = c^2 \left(\frac{\mathrm{D}\rho_0}{\mathrm{D}t} + \frac{\mathrm{D}\tilde{\rho}}{\mathrm{D}t} \right) + \alpha \left(\frac{\mathrm{D}s_0}{\mathrm{D}t} + \frac{\mathrm{D}\tilde{s}}{\mathrm{D}t} \right). \tag{2.66}$$

Note that in all foregoing equations, the (x_l, t) dependencies have been omitted for better readability. For deriving Galbrun's equation, some simplifications have to be stated, which will be the content of the subsequent discussion.

Derivation of Galbrun's equation

Galbrun's equation describes a linearized form of wave propagation in terms of a Lagrangian displacement $\vec{w}$. Based on the above stated equations, the way for deriving Galbrun's equations is discussed in the subsequent part. In linear acoustics, only small perturbations are considered and, respectively, the goal is to find adequate equations for all perturbations. With respect to hitherto presented equations, a small perturbation assumption is understood in such a way that a parameter $\varepsilon \ll 1$ exists, which scales perturbations as

$$\Phi = \varepsilon^0 \Phi_0 + \varepsilon^1 \tilde{\Phi} + \mathcal{O}(\varepsilon^2). \tag{2.67}$$

Furthermore, spatial derivatives of the Lagrangian displacement $\vec{w}$ scale with ε^1, i.e. the Euclidean distance follows the relation $||\nabla \vec{w}||_2 \sim \varepsilon^1$. Taking these considerations into account, the Jacobian and the transformation tensor $\vec{\vec{T}}$ read

$$J = 1 + w_{l,l} + \mathcal{O}(\varepsilon^2), \tag{2.68}$$

$$T_{ij} = \delta_{ij} - w_{j,i} + w_{l,l}\delta_{ij} + \mathcal{O}(\varepsilon^2), \tag{2.69}$$

and all second-order terms are neglected. From equation (2.62), the small perturbation assumption leads to the rather simple relation

$$\tilde{\rho} = -w_{l,l}\rho_0. \tag{2.70}$$

From a physical point of view, this relation implies that if the divergence of the displacement field is positive within a fluid particle, the density fluctuation is negative. A similar discussion can be conducted by analyzing the conservation equation of mass, see equation (2.45). Furthermore, the assumption of small perturbations is applied to the transformed balance equation of momentum (2.64) and the transformed balance equation of entropy (2.65), while acknowledging the linearized density perturbation from equation (2.70). After some cumbersome calculations, the balance equa-

tion of momentum yields

$$\mathscr{G}\{w\} + \mathscr{G}_{\tau f}\{w\} + \mathscr{G}_{NL}\{w\} = \mathscr{S}_0 + \mathscr{S}_1, \tag{2.71}$$

where

$$\mathscr{G}\{w\} = \rho_0 \frac{\mathrm{D}^2 w_k}{\mathrm{D}t^2} + p_{0,k} w_{q,q} - p_{0,l} w_{l,k} + \tilde{p}_{,k} - \tilde{\tau}_{kj,j}, \tag{2.72}$$

$$\mathscr{G}_{\tau f}\{w\} = \tau_{0ki,j} w_{j,i} + \tau_{0ki} w_{j,ij} - \tau_{0kj,j} w_{l,l} - \tau_{0kj} w_{l,lj} - f_{0k} w_{l,l} - \tilde{f}_k w_{l,l}, \tag{2.73}$$

$$\mathscr{G}_{NL}\{w\} = -\tilde{p}_{,j} w_{j,k} + \tilde{\tau}_{ki,j} w_{j,i} + \tilde{p}_{,k} w_{l,l} - \tilde{\tau}_{kj,j} w_{l,l} - \tilde{\tau}_{kj} w_{l,lj}, \tag{2.74}$$

$$\mathscr{S}_0 = -\rho_0 \frac{\mathrm{D}v_{0k}}{\mathrm{D}t} - p_{0,k} + \tau_{0kl,l} + f_{0k}, \tag{2.75}$$

$$\mathscr{S}_1 = \tilde{f}_k. \tag{2.76}$$

Note that the velocity fluctuation $\vec{v}$ has been replaced by the material time derivative of the displacement $\vec{w}$ as

$$\tilde{v}_k = \frac{\mathrm{D}w_k}{\mathrm{D}t} \tag{2.77}$$

In the above stated equation (2.71), $\mathscr{G}\{w\}$ denotes an extended Galbrun operator where viscous effects are taken into account. Furthermore, $\mathscr{G}_{\tau f}\{w\}$ represents wave propagation effects due to viscosity and body forces that interact with the flow quantities Φ_0. To remain consistent, $\mathscr{G}_{NL}\{w\}$ retains all nonlinear components arising from the mathematical derivation, which can be neglected, since only small perturbations are considered. In a similar approach carried out to derive well-known aeroacoustic analogies [82, 123], these nonlinear terms could be shifted to the right hand side of equation (2.71). Such an equation could be useful to derive source terms in a certain source region, where precise flow computations are adequate as part of a hybrid flow/acoustic analysis [170]. These terms, if possibly known, would represent sources of a new equation as

$$\mathscr{G}\{w\} + \mathscr{G}_{\tau f}\{w\} = \mathscr{S}, \tag{2.78}$$

which can be understood as an acoustic analogy based on Galbrun's equation where viscous effects and body forces are taken into account and sources can be computed in a limited source region.

Note that on the source side of equation (2.71), two different source contributions exist. The first source $\mathscr{S}_0$ contains all possible source components with respect to the reference flow. The second source $\mathscr{S}_1$ contains sources due to body force fluctuations. Therefore, neglecting nonlinear terms, equation (2.71) reads

$$\mathscr{M}\{w\} = \mathscr{G}\{w\} + \mathscr{G}_{\tau f}\{w\} = \mathscr{S}_0 + \mathscr{S}_1. \tag{2.79}$$

Until now, nothing has been declared, neither with respect to the constitutive equations nor to the reference flow. Thus, equation (2.79) can be seen as a generalized form of Galbrun's equation for small perturbations and be applied to flow acoustics or even underwater acoustics. Note that so far all flow quantities Φ_0 are functions in space and time. It is convenient to separate these terms in time-averaged mean values and incompressible hydrodynamic fluctuations, cf. Seo and Moon [173], as

$$\Phi_0(x,t) = \bar{\Phi}(y) + \Phi^{inc}(y,t). \tag{2.80}$$

By doing so, the pressure fluctuation $\tilde{p}$ can be understood as acoustic perturbations commonly known as sound. In the case when the fluid takes the properties of a perfect gas and heat conduction as well as heat sources are neglected, a similar approach applied to equation (2.56) yields

$$\rho_0 \frac{\mathrm{D}\tilde{s}}{\mathrm{D}t} = \mathscr{E}_0 + \mathscr{E}_1, \tag{2.81}$$

where

$$\mathscr{E}_0 = -\rho_0 \frac{\mathrm{D}s_0}{\mathrm{D}t} + \frac{1}{T_0} \tau_{0kl} v_{0k,l}, \tag{2.82}$$

$$\mathscr{E}_1 = \frac{1}{T_0} \left(\tau_{0kl} \tilde{v}_{k,l} - \tau_{0kl} v_{0k,i} w_{i,l} + \tilde{\tau}_{kl} v_{0k,l} \right). \tag{2.83}$$

Note for this case, the temperature perturbation $\tilde{T}$ has been set to zero and again nonlinear terms have been dropped. In addition, if heat flux needs to be taken into account, the presented approach can easily be adopted to further develop Galbrun's equation so that viscothermal acoustics can be analyzed.

Boundary and initial conditions

To close the system of equations making the problem well-posed, appropriate boundary conditions as well as initial conditions need to be defined. These conditions are especially relevant when considering fluid structure interactions. Typically, in acoustically hard wall bounded domains the condition

$$w_j n_j = 0 \qquad \text{on} \quad \Gamma, \tag{2.84}$$

serves as an adequate boundary condition. In cases where the boundary is moving, typically in vibroacoustics, the major advantage of Galbrun's equation can be easily seen, since the boundary condition is a natural condition between two Lagrangian displacements, namely the structural displacement and the fluid displacement, respectively. Similarly, the initial conditions can be stated

for the displacement and the associated velocity as

$$\vec{w}(\vec{x},0) = \vec{w}_{(0)}(\vec{x}) \qquad \text{in} \quad \Omega, \tag{2.85}$$

$$\frac{\partial \vec{w}(\vec{x},0)}{\partial t} = \vec{v}_{(0)}(\vec{x}) \qquad \text{in} \quad \Omega. \tag{2.86}$$

Finally, a more detailed discussion on how to adopt the well-known Robin boundary condition for time harmonic cases and which constitutive equations can be used for aeroacoustics and hydroacoustics are found in Publication A, Publication B and citations within. For completeness, the proposed version of the Robin boundary condition for Galbrun's equation reads

$$\left(-\mathrm{j}\omega w_l + v_{0k} w_{l,k} - w_k v_{0l,k}\right) n_l = Y \left(-c_0^2 \rho_0 w_{l,l} - w_l p_{0,l}\right), \tag{2.87}$$

where c_0 denotes the speed of sound in the fluids reference configuration and Y the boundary admittance. Note that a time dependency in the form of $e^{-\mathrm{j}\omega t}$ has been assumed.

2.4 Application to rotor dynamics

In this section, the application of the aforementioned concept of the ALE approach to rotor dynamics is discussed. Since some of the outlines will be similar to the ones stated before, only the major differences will be highlighted.
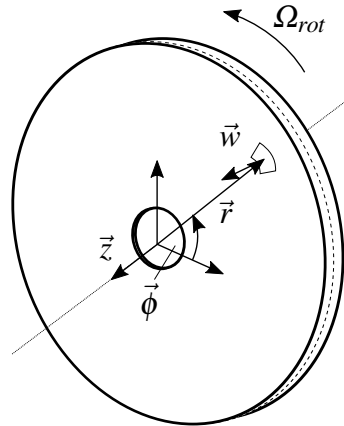

Figure 4: Rotor dynamics model of disk with rotational axis and natural plane (dashed line)

Figure 4 presents the object of interest, which can be seen as a thin elastic disk (Kirchhoff plate) with two orthogonal planes of symmetry, with the intersection of the two planes forming the axis of

rotation. The latter is considered to be spatially fixed and aligned with the $\vec{z}$-axis despite the movement of the body during rotation and the elastic deformation. In addition, the rotational speed Ω_{rot} is kept constant during the structural dynamic analysis. When applying the ALE concept to rotor dynamics, the main principle, as it is understood in this context, can be seen in such that the initially undeformed body is rotating relative to an envelope that spans around the outer surface of the disk. In the case where the disk behaves like a rigid rotating body, the deformation of the envelope with respect to its initial configuration is zero. Only elastic deformations of the disk, which in turn are influenced by the rotation, result in a deformation of the envelope. In a different perspective, the envelope only presents deformations that are effectively felt by the surrounding fluid. Note that in this thought experiment, the shear boundary layer that exists due to the general non-slip boundary condition of the fluid in the vicinity of the surface of the rotating body is neglected, which consequently can be understood as a slip boundary condition. To arrive at appropriate models that allow investigations, e.g. in the frequency domain, some simplifications must be conducted which are adequate for the models discussed in Publication C and Publication D. These simplifications include (i) the rotor has a well-defined axis of rotation, (ii) the rotational speed remains constant, (iii) only small deformations are considered, except for the motion around the axis of rotation, (iv) the imbalance of the rotor is small, (v) either the rotor or the supports show isotropic stiffness behavior, and (vi) in the inertial reference frame, the rotor needs to be axial-symmetric, see Kiesel [108]. Furthermore, the derivation of an adequate system of equations for axisymmetric elastic rotors with constant rotational speeds has been widely discussed in the literature [64, 75, 89, 110] and references within. Therefore, only the main concepts are presented at this point. This includes the main principle of deriving the system dynamics, appropriate contributions due to non-potential loads as well as the link to the ALE framework as follows.

In rotor dynamics, a common approach for calculating the equation of motion is based on Hamilton's principle. Since it offers direct access to a weak formulation, this approach is especially well-suited if approximate solutions schemes are utilized to solve the system of equations by means of numerical methods. According to Hetzler [89], whose work is greatly acknowledged for the subsequent outlines, the system dynamics are expressed as

$$\delta \int_t L \, \mathrm{d}t + \int_t \delta W_q \, \mathrm{d}t = 0 \tag{2.88}$$

together with essential boundary conditions on Γ. In equation (2.88), L represents the difference of the kinetic energy T and the potential energy U and therefore simply reads $L = T - U$. In addition, δW_q denotes the virtual work done by all non-potential forces. Note that in this case, it is assumed that the momentum fluxes across the boundaries are zero as well as all contributions

due to possible contact mechanisms are neglected, see Hetzler [89] if these contributions or fluxes must be acknowledged. The kinetic energy follows in a straightforward manner as

$$T = \frac{1}{2}\int_\Omega \dot{y}_k \rho_s \dot{y}_k \, \mathrm{d}\Omega,\tag{2.89}$$

where ρ_s denotes the mass density of the structure. For linear elastic material behavior, the contribution to the potential energy reads

$$U = U^{(el)} = \frac{1}{2}\int_\Omega \varepsilon_{kl} C_{klmn} \varepsilon_{mn} \, \mathrm{d}\Omega,\tag{2.90}$$

where additional contributions can be added if needed. Note that $\vec{\vec{C}}^{(4)}$ denotes the fourth-order elasticity tensor and $\vec{\vec{\varepsilon}}$ the second-order strain tensor. Furthermore, the virtual work done by non-potential forces can be decomposed into contributions due to material damping and other contributions as

$$\delta W_q = \delta W_d + \delta W_f.\tag{2.91}$$

If Rayleigh damping, commonly used in structural dynamics, with the two damping parameters $\alpha^{(d)}$ and $\beta^{(d)}$ is assumed, δW_d yields

$$\delta W_d = -\int_\Omega \delta y_i \alpha^{(d)} \rho \dot{y}_i \, \mathrm{d}\Omega - \int_\Omega \delta \varepsilon_{kl} \beta^{(d)} C_{klmn} \dot{\varepsilon}_{mn} \, \mathrm{d}\Omega.\tag{2.92}$$

Furthermore, when external forces act on the structure, the virtual work contribution can accordingly be calculated as

$$\delta W_f = \sum_i \delta y_{(i)k} F_{(i)k},\tag{2.93}$$

where the sum is taken over all forces $\vec{F}_{(i)}$ acting on the structure together with the associated virtual displacements $\delta\vec{y}_{(i)}$.

In accordance with the ALE framework, the actual motion of each material particle is not of particular interest, since the rotation of the body results in a large displacement with respect to the initial configuration. Instead, it is useful to decompose the motion of the elastic structure into a prescribed transport motion plus deformations. Here, the configuration after the rigid body motion can be seen as a reference from which deformations are measured, which again is suitable to the main idea of the ALE framework. Before deriving the final weak formulation, the ALE transformation rules must be applied. First, in the reference frame the material velocity reads

$$\dot{y}_k = \frac{\mathrm{D}y_k(x_l,t)}{\mathrm{D}t} = \frac{\partial x_k(x_l,t)}{\partial t} + \frac{\partial w_k(x_l,t)}{\partial t} + \frac{\partial w_k(x_l,t)}{\partial x_j}\frac{\partial x_j(x_l,t)}{\partial t}\tag{2.94}$$

where equation (2.15) has been used. Furthermore, $\partial \vec{x}(x_l,t)/\partial t = \vec{v}_T$, which can be understood as transport velocity but in this sense is not a physical vector quantity. Finally, by considering only small perturbations, the linearized strain tensor reads

$$\varepsilon_{kl} = \frac{1}{2}(w_{k,l} + w_{l,k}). \tag{2.95}$$

The above stated outlines are briefly recalled from Hetzler [89] to provide the reader with a fundamental frame for deriving the equation of motion in the ALE framework, which, applied to the case of a Kirchhoff plate as shown in Figure 4, yields the final equation of motion in the weak formulation as

$$\int_0^{2\pi} \int_{r_i}^{r_a} \delta \vec{w} \left(\ddot{\vec{w}} + 2\Omega_{rot} \frac{\partial \dot{\vec{w}}}{\partial \phi} + \Omega_{rot}^2 \frac{\partial^2 \vec{w}}{\partial \phi^2} \right) \rho_s h r \, \mathrm{d}r \mathrm{d}\phi + \delta U_K = 0, \tag{2.96}$$

where r_i and r_a are the inner and the outer radius, h the thickness, and U_K the elastic potential of the Kirchhoff plate. Note that the displacement field is defined in cylindrical coordinates $\vec{w} = \vec{w}(r,\phi,z)$. Finally, appropriate geometrical boundary conditions are set in the form

$$\vec{w}(r = r_i, \phi, z) = 0 \qquad \forall \phi = [0, 2\pi], \quad \forall z = [-h/2, h/2], \tag{2.97}$$

$$\frac{\partial \vec{w}}{\partial r}(r = r_i, \phi, z) = 0 \qquad \forall \phi = [0, 2\pi], \quad \forall z = [-h/2, h/2], \tag{2.98}$$

which is understood as a fixed-fixed boundary condition of the inner disk surface. For additional information on the derivation and the concepts of rotor dynamics, the reader is referred to the literature [60, 64, 75, 89, 101, 102, 110, 141, 186, 187].

At this point, equation (2.96) provides a basic formulation well-suited for the treatment with numerical methods such as the finite element method or others. As discussed in Publication C, the sound radiation of such rotating disks can be of great interest. Therefore, the so-called structure-born sound is dealt with in the following.

Structure-born sound

In a majority of technical applications, vibrating structures are surrounded by fluid being either stationary or moving in space relative to the vibrating structure. To investigate the sound radiation into a far field domain, several theoretical methods have been developed. In the simplified case where the fluid is at rest, the well-known Kirchhoff-Helmholtz integral was established using generalized solutions of the wave equation, known as Green's functions. If the radiating structure is enclosed

by a rigid baffle, the Kirchhoff-Helmholtz integral simplifies to the Rayleigh integral [155], which is recalled at this point:

$$p'(\vec{y}, t) = \frac{\rho_0}{2\pi} \iint \frac{\dot{v}_n(x_1, x_2, t - R/c)}{R} \mathrm{d}x_1 \mathrm{d}x_2. \tag{2.99}$$

Here, $\dot{v}_n$ denotes the surface normal acceleration which is integrated over the flat radiator surface defined by (x_1, x_2) at the retarded time $t - R/c$ and, additionally, R being the distance between the field point $\vec{y}$ and the source point $\vec{x}$ on the radiator surface. With respect to the above stated concepts of the ALE framework applied to rotor dynamics and taking equation (2.17) into account, the surface normal velocity reads

$$\vec{v}_n = \vec{v}_R \cdot \vec{n}. \tag{2.100}$$

Note that this relation only holds where momentum fluxes across the boundaries are zero. At this point other physical interface relations are possible to include, but are beyond this work.

However, the Rayleigh integral as stated above is rarely used for engineering applications such as optimization tasks involving the reduction of the sound power. In these kinds of tasks, a large number of objective functions must often be evaluated and if the computation of the integral is part of that process, the computational cost can easily exceed reasonable values [65, 128]. Therefore, simplified models such as the lumped parameter model [58] or the equivalent radiated power were developed to estimate the sound power and both models have been successfully applied [66, 111]. Similarly to the mentioned references, the LPM and the ERP have been effectively applied to rotating structures in Publication C.

These simplified models are especially handy when numerical methods are used for the computation, since they are easy to implement and in some cases can even be utilized when model reduction methods allow a tremendous reduction in computational cost. For a deeper insight, the interested reader is referred to the literature [46, 66, 104, 111, 128, 155].

2.5 Numerical methods

In this section, the basic numerical methods are introduced, which are utilized throughout this work and to achieve the results in Publication B, Publication C, and Publication D. Since the computational tools discussed in the subsequent outlines are state of the art and are successfully applied in many fields of engineering research as well as in industrial applications, it is not intended to recall all aspects in every detail. Instead, the main focus remains on the general concepts and appropriate references are provided for the reader interested in greater detail.

Three well-known methods are considered, namely the standard finite element method, the discontinuous Galerkin finite element method, and, last but not least, the boundary element method. In each subsection, the main ideas are presented and some advantages and disadvantages are discussed. However, generally speaking, the three mentioned methods exhibited a tremendous development since their first appearance, are versatile in their application and are continuously further improved.

Standard Finite Element Method

The standard finite element method (FEM) has been successfully applied in Publication C and Publication D, where the structural dynamics of rotating disks were analyzed. In these investigations, the numerical method showed its capabilities and its usefulness when dealing with multiphysical problems such as static deformation under external loading, plastic deformation due to exceeding yield stresses, eigenvalue estimations within a numerical modal analysis, and a subsequent investigation where rotational effects are considered. With this versatile application, it is no wonder why FEM has been such a success story throughout several engineering fields.

In abbreviated form, the way to derive a FEM formulation starts by defining a suitable set of equations that describe the physical behavior in an appropriate fashion, i.e. to an extent where an acceptable accuracy is achieved. This set of equations usually consists of the local balance equations of continuum mechanics, constitutive equations, and, depending on the field of unknowns, additional kinematic relations that correlate deformation with strain. Note that closed solutions to these sets of equations only exist for a limited number of cases. Since, in general, it is hard to find solutions that fulfill the local balance equations over the whole domain Ω, the groundbreaking idea of FEM is to test the balance equations with a suitable test function and integrate the whole test over Ω to find approximate solutions. This integral formulation is also known as weak formulation. Exemplarily, the following mixed boundary value problem is assumed

$$\rho \ddot{u}_j = \sigma_{ji,i} + f_j \qquad \text{in} \quad \Omega, \tag{2.101}$$

$$u_j = u_{(d)j} \qquad \text{on} \quad \Gamma_d, \tag{2.102}$$

$$t_j = \sigma_{ji} n_i = t_{(n)j} \qquad \text{on} \quad \Gamma_n, \tag{2.103}$$

which recasts the momentum equation for vanishing reference velocities with the additional prescribed Dirichlet boundary conditions $u_{(d)j}$ on Γ_d and the Neumann boundary conditions $t_{(n)j}$ on Γ_n, respectively. The weak formulation of equation (2.101) reads as follows:

Find $\vec{u} \in V := \{\vec{v} \in \mathrm{H}^1(\Omega) : \vec{v} = \vec{u}_{(d)} \text{ on } \Gamma_d\}$ such that

$$\int_\Omega \rho \ddot{u}_j v_j \, \mathrm{d}\Omega = \int_\Omega \sigma_{ji,i} v_j \, \mathrm{d}\Omega + \int_\Omega f_j v_j \, \mathrm{d}\Omega \tag{2.104}$$

for all test functions $\vec{v} \in V_0 := \{\vec{v} \in \mathrm{H}^1(\Omega) : \vec{v} = 0 \text{ on } \Gamma_d\}$. Here, the Sobolev $\mathrm{W}_2^1(\Omega)$ space is defined as $\mathrm{H}^1(\Omega) = \{\vec{v} \in \mathrm{L}_2(\Omega), \nabla \vec{v} \in \mathrm{L}_2(\Omega)\}$, which is equipped with a norm of square integrable functions, see Kaltenbacher [104] for further details. The first integral on the RHS of equation (2.104) can be transformed by means of integration by parts which yields

$$\int_\Omega \rho \ddot{u}_j v_j \, \mathrm{d}\Omega = \int_\Gamma v_j \sigma_{ji} n_i \, \mathrm{d}\Gamma - \int_\Omega \sigma_{ji} v_{j,i} \, \mathrm{d}\Omega + \int_\Omega f_j v_j \, \mathrm{d}\Omega, \tag{2.105}$$

where the boundary conditions can be applied and appropriate discretization procedures can be utilized to form a system of equations in the form of

$$\mathrm{A}u = f. \tag{2.106}$$

For further details and how an implementation can be realized, the reader is referred to the references [17, 49, 60, 76, 104, 110, 128, 140, 143, 144, 149, 174] and the discussion in Publication C.

Discontinuous Galerkin Finite Element Method

Based on the discussion about the discontinuous Galerkin finite element method presented in Publication B, some of the key features are recalled to provide the reader with basic concepts and to get familiar with the main idea of using DG-FEM. Generally speaking, the use of DG-FEM combines advantages of standard FEM formulations as well as finite volume methods (FVM), i.e. that high-order schemes, common in FEM, and the locally defined schemes from FVM can be combined to achieve a more efficient and more flexible numerical frame. This way, DG-FEM is especially useful when analyzing flow problems.

Similar to standard FEM formulations, the fundamental steps for deriving a DG-FEM formulation consist of (i) deriving the general equations, usually in the form of partial differential equations, (ii) defining suitable functional spaces for the unknowns and the test functions, and (iii) multiplying the basic equations with the test functions and integrating over the domain to find the weak form with the help of integration by parts. In contrast to standard FEM, in the DG-FEM the integral is not taken over the whole domain but only over a number of sub-domains, which then are the single elements of the numerical scheme. From this argument it is clear that neighboring elements can share the same geometrical nodes, but the solution differs, i.e. each element owns its own set of

degrees of freedom, which are not condensed when building the global system matrices as done in standard FEM schemes. Consequently, the question arises whether the single elements interact with each other, so that the global physical behavior can be accurately resolved [88].

The crucial aspect lies in the inter-elemental communication, which is realized by formulating appropriate fluxes that stem from the integration-by-parts method when deriving the weak formulation. In standard FEM schemes, these terms are usually zero on the domain boundaries and therefore are not necessarily accounted for. In DG-FEM schemes, these fluxes establish the relation between the elements and in this way map the global physical behavior of the problem at hand. To explain this in more detail, Figure 5 is recalled from Publication B and shows two DG elements that share two nodes and one element edge. As can be seen, at each node in space at po-
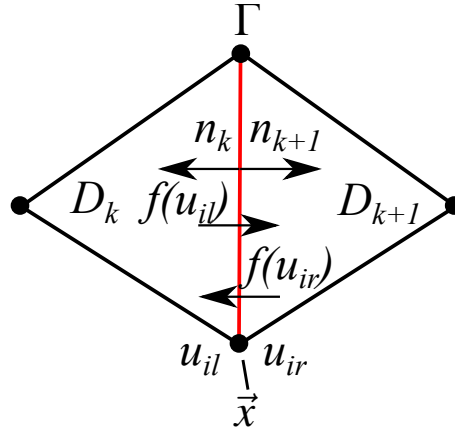
Figure 5: Two DG elements with common surface Γ, see Publication B

sition $\vec{x}$ there exist two solutions denoted by $u_{il}(\vec{x})$ and $u_{ir}(\vec{x})$ that belong to a left element D_k and a right element D_{k+1}, respectively. To enforce the relation between the two elements, the so-called Lax-Friedrich flux, which blends between a central and an upwind flux, proved to be a suitable choice for flow-related problems [43, 53, 88].

The general numerical scheme can be outlined as follows. An inner product is defined as

$$(\vec{u}, \vec{v})_\Omega = \int_\Omega \vec{u}\vec{v}\,\mathrm{d}\Omega \qquad (2.107)$$

in the functional space of $L^2(\Omega)$, where all functions are square integrable over the domain Ω. For the weak formulation this inner product is reformulated as a local inner product as

$$(\vec{u}, \vec{v})_{D^k} = \int_{D^k} \vec{u}\vec{v}\,\mathrm{d}D^k \quad \text{and} \quad ||\vec{u}||^2_{D^k} = (\vec{u}, \vec{u})_{D^k}, \qquad (2.108)$$

where the unification of all elements resolves the computational or in other words the discretized

domain Ω_h such that

$$\Omega \simeq \Omega_h = \bigcup_{k=1}^{K} D^k. \tag{2.109}$$

Furthermore, the Lax-Friedrichs flux is recalled as

$$f_{LF}(u_{il}, u_{ir}) = \frac{f(u_{il}) + f(u_{ir})}{2} + \frac{\alpha_{LF}}{2} n \cdot (u_{il} - u_{ir}), \tag{2.110}$$

with the flux constant α_{LF} which needs to be chosen according to the problem at hand [88].

The application of the DG-FEM scheme for solving Galbrun's equation is discussed in more detail in Publication B. Further details can be found in the references [45, 88].

Boundary Element Method

The boundary element method (BEM) is another numerical method suitable for analyzing wave propagation especially in large domains, which was one part in Publication C. The main advantage of this method is that the initial boundary value problem can be reformulated through two steps of integration by parts when deriving the weak formulation, such that only boundary contributions remain. When deriving the basic equations of a BEM formulation of the Helmholtz equation, the Kirchhoff–Helmholtz boundary integral

$$c(\vec{y})p'(\vec{y}) + \int_{\Gamma} \frac{\partial G(\vec{x},\vec{y})}{\partial n(\vec{x})} p'(\vec{x}) d\Gamma(\vec{x}) = \int_{\Gamma} G(\vec{x},\vec{y}) a v_f'(\vec{x}) d\Gamma(\vec{x}) \tag{2.111}$$

is recast if the sources are placed on the boundary, i.e. $\vec{y} \in \Gamma$ and $0 < c(\vec{y}) < 1$, and from there a suitable weak formulation is derived. In equation (2.111), $c(\vec{y})$ denotes a specific parameter of the boundary topology, $G(\vec{x},\vec{y})$ represents the free space Green's function, $\partial()/\partial n(\vec{x})$ is the spatial derivative in normal direction, $a = j\omega t$ due to the time harmonic dependency of $e^{-j\omega t}$ that has been assumed, and last but not least $v_f'(\vec{x})$ denotes the fluid particle velocity in normal direction, see Marburg and Nolte [128] for a deeper insight.

By introducing an appropriate test function χ, the weak formulation of equation (2.111) yields

$$\int_{\Gamma} \chi(\vec{y}) c(\vec{y}) p'(\vec{y}) d\Gamma(\vec{y}) + \cdots$$
$$+ \int_{\Gamma} \chi(\vec{y}) \left(\int_{\Gamma} \left[\frac{\partial G(\vec{x},\vec{y})}{\partial n(\vec{x})} - sk G(\vec{x},\vec{y}) Y(\vec{x}) \right] p'(\vec{x}) d\Gamma(\vec{x}) \right) d\Gamma(\vec{y}) = \tag{2.112}$$
$$sk \int_{\Gamma} \chi(\vec{y}) \left(\int_{\Gamma} G(\vec{x},\vec{y}) v_s'(\vec{x}) d\Gamma(\vec{x}) \right) d\Gamma(\vec{y}).$$

where the Robin boundary condition

$$v_f'(\vec{x}) - v_s'(\vec{x}) = Y(\vec{x})p'(\vec{x}) \tag{2.113}$$

has been applied and $s = \mathrm{j}\rho_0 c$ and $k = \omega/c$, where c denotes the speed of sound, and k the wave number. After the discretization process, where a Collocation or Galerkin method can be used, the system of equations takes the form of

$$A(\omega)P(\omega) = B(\omega)V_s'(\omega). \tag{2.114}$$

In general, the system matrices A and B are fully populated and a function of ω. This makes the BEM formulation rather unsuitable for harmonic analysis procedures if no further measures are taken. However, since only the boundary needs to be discretized and not the entire domain, as with FEM, the resulting reduced number of degrees of freedom makes BEM an interesting method for analyzing wave propagation in large domains. For deeper insight the reader is referred to the list of references [40, 47, 100, 104, 128, 171] and references within.

Chapter 3

Models

In this chapter, the utilized models are presented which have been used to achieve the results in Publication B, Publication C, and Publication D. Starting with the discussion about the general numerical models used within the frame of the finite element method, this also includes DG-FEM as well as the boundary element methods. However, the outlines are restricted to the basics for the models that have been involved in Publication B and Publication C to avoid repetitions of the content in the corresponding publications. In contrast, the models of Publication D are discussed in more detail, in order to provide the reader with a deeper insight into the main ideas, which facilitates the interpretation of the results. In a second part of this chapter, the material models of the applied solids and fluids are explained in further detail. Note that all the discussed problems are investigated in the frequency domain.

3.1 Numerical models

Since the implementation of a new numerical scheme is not part of this work, commercially available solutions have been utilized for setting up the numerical models, solving the system of equation, and visualizing the computed results. On the one hand, for all problems involving aeroacoustics, Comsol Multiphysics$^{®}$* allowed the implementation of the weak form of Galbrun's equation. On the other hand, the software tools Abaqus/CAE and Abaqus/Standard† allowed solving problems of rotor dynamics and the associated acoustic radiation. In addition, the in-house BEM code "Akusta" [129] provided the necessary infrastructure to compute reference solutions based on models created with Abaqus/CAE within Publication C.

---

*COMSOL Multiphysics$^{®}$ v. 5.4., www.comsol.com., COMSOL AB, Stockholm, Sweden.

†Abaqus v. 6.14-2, www.3ds.com, Dassault Systèmes Corp., Providence, RI, USA, 2017

As suggested by Langer et al. [115], for all finite element models, elements with a second-order basis function have been utilized to achieve a reasonable solution quality on behalf of a justifiable amount of computational cost.

A simple duct

In Figure 6 a simple duct model from Publication B is recalled, which can be seen as a simplified two-dimensional problem. Furthermore, a uniform mean flow in one direction is assumed, which is indicated by the component of $\vec{v}_0$ and the Mach-number reads $Ma = \frac{v_{01}}{c_0}$. The general dimensions

(a) Geometry and flow direction

(b) Finite element mesh
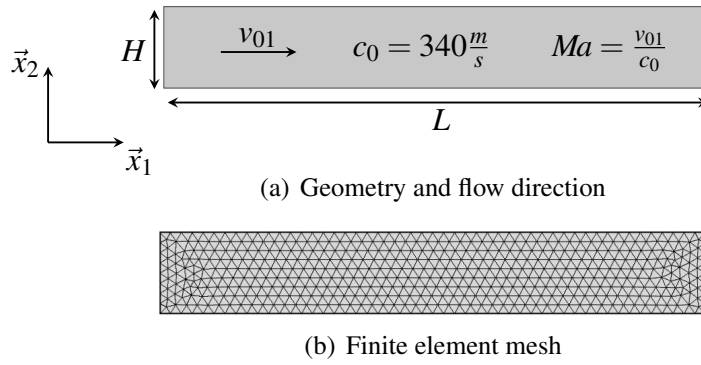
Figure 6: Duct model, see Publication B

of the duct are the height of $H = 0.5\,\text{m}$ and a length of $L = 3.4\,\text{m}$. As discussed in Publication B, this model is well-suited for a numerical modal analysis, where the influence of the flow velocity on the eigenvalues and eigenvectors of the problem can be studied and compared to analytical solutions. Figure 6(b) depicts a mesh of 930 triangular elements which has been used for the DG-FEM scheme. For the latter, after discretization and applying the boundary conditions, the formal system of equations

$$\left(-\omega^2[M] - j\omega[D] + [C]\right)[w] = 0 \tag{3.1}$$

are solved, where ω are the unknowns of the associated eigenvalue problem. Here, $[M]$ denotes the mass matrix, $[D]$ the damping matrix, and $[C]$ the stiffness matrix, respectively. All unknowns are stacked in the column matrix $[w]$. Note that additional restrictions can be imposed by well-studied approaches using Lagrange multipliers. As an example, such a restriction can be that the rotation of the displacement field is enforced to vanish, i.e.

$$\nabla \times \vec{w} = 0, \tag{3.2}$$

which can be used to investigate to what extent the solutions of the eigenvalue analysis are characterized by either the rotation or the divergence of the displacement field. This in turn allows one to estimate whether the investigated mode is acoustically relevant, see Publication B.

The presented model serves as a basis for a number of numerical investigations, namely a comparison study with respect to well-established methods such as LEE and LNSE and between standard FEM and DG-FEM schemes in order to highlight the benefits of using Galbrun's equation together with DG-FEM. In addition, investigating different boundary conditions and their effect on the eigenvalues and eigenvectors was part of the analysis. Furthermore, a convergence study has been conducted to show the stability behavior of the scheme.

The annulus

As can be clearly seen, the above discussed model of a two-dimensional duct covers a rather academic case. Therefore, the duct is enlarged and closed to an annulus where a prescribed swirling flow can be introduced. Such a configuration could be seen as a simplified two-dimensional approximation of a turbofan engine. Figure 7 shows the general geometry and an associated DG-FEM

(a) Geometry and flow direction   (b) Finite element mesh
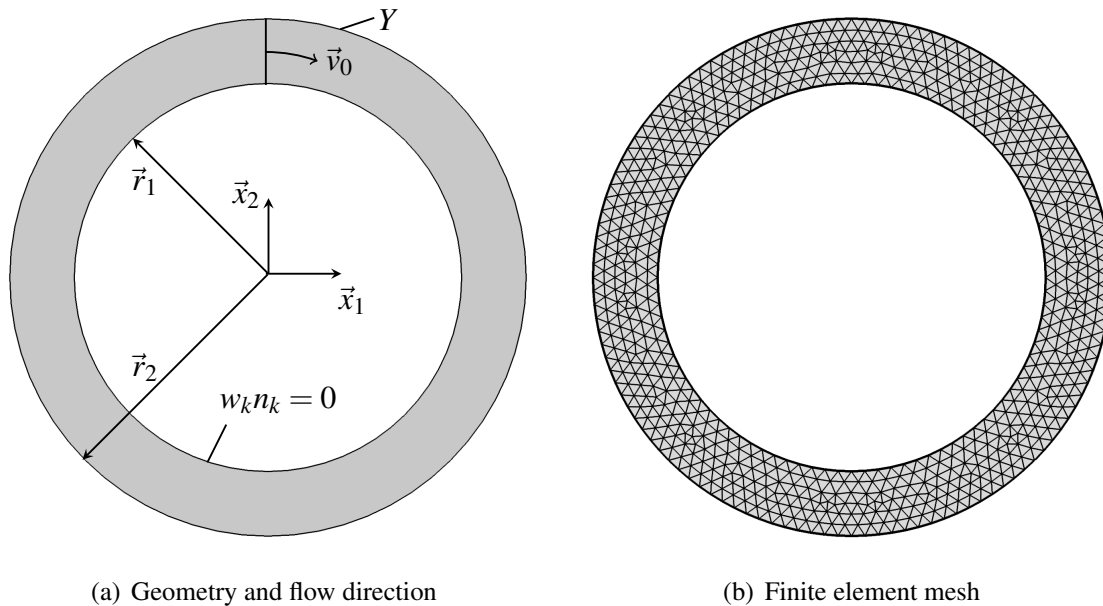
Figure 7: Annulus model, see Publication B

mesh. With respect to a cylindrical coordinate system, the inner ring at $\vec{r} = \vec{r}_1$ possesses a hard wall boundary condition, where on the outer ring at $\vec{r} = \vec{r}_2$ an admittance can be applied. This

model is studied in more detail in Publication B, where, similar to the duct case, a numerical modal analysis has been conducted to investigate the eigenvalues and eigenvectors of the swirling flow configuration and how the modes can be characterized.

A simple elastic disk

Figure 8 depicts the general geometry of the simple disk with the basic dimensions, namely the diameters d_i, $i = 1, 2, 3$ and the thickness t. Note that the area defined by d_2 and d_3 serves as a surface definition, where boundary conditions are applied that recast the built-in situation, Here, a fixed-fixed boundary condition is assumed, i.e. all degrees of freedom are set to zero. In addition, in this chapter the basis tuple $(\vec{e}_1, \vec{e}_2, \vec{e}_3)$ is equivalent to $(\mathsf{X}, \mathsf{Y}, \mathsf{Z})$. Overall, more information can be found in Publication C. The dimensions are chosen such that the disk corresponds to a version of a simplified saw blade commonly used in the industry. For investigating the dynamic behavior,

(a) Isoparametric view   (b) XY-Plane
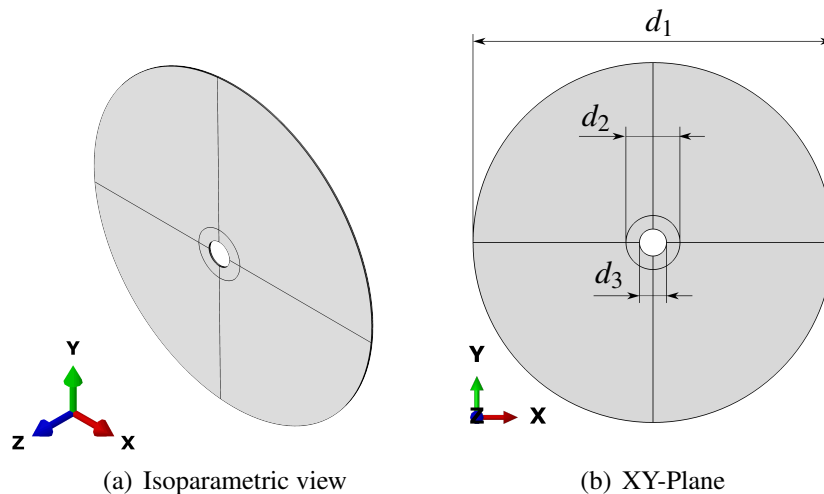
Figure 8: Disk model; $d_1 = 800\,\text{mm}$, $d_2 = 120\,\text{mm}$, $d_3 = 60\,\text{mm}$, uniform disc thickness $t = 3.5\,\text{mm}$

a suitable FEM model is required. Figure 9 shows a finite element mesh that has been utilized for a convergence study in order to identify whether converged results are achieved and to which extent the mesh can be coarsened for reducing the computational cost. As can be seen, the mesh is constructed in such a way that two quadratic elements are used to resolve the plate's thickness, which is in agreement with the recommendations of Langer et al. [115]. A global mesh seeding size of $h = 5\,\text{mm}$ was used, which results in 36,208 elements. In addition, a reduced model was used to reduce the computational time while accepting an appropriate error of the results. This model is shown in Figure 10 and has been generated by using a global seeding size of $h = 20\,\text{mm}$, which results in a number of elements of 2,268. As can be seen, the two radial lines represent roll
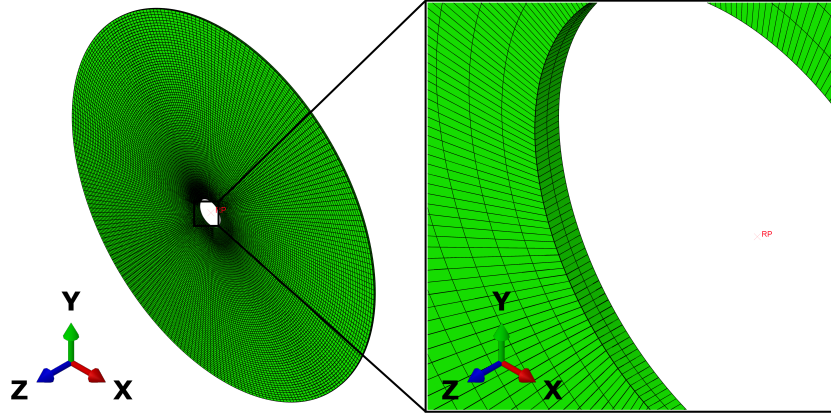
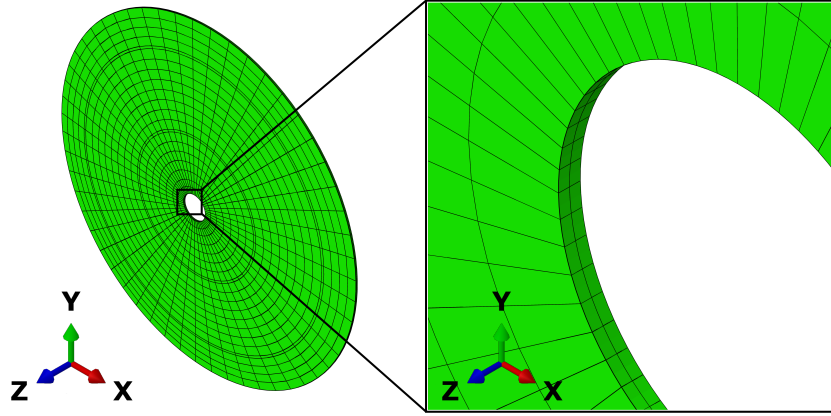Figure 9: Fine mesh configuration of simple disk model

Figure 10: Coarse mesh of simple disk model

tensioning lines that are applied to the reference model in Publication D.

After discretization, the system of equations can be formulated as

$$\left(-\omega^2[M] - \mathrm{j}\omega\Omega_{rot}[G] - \mathrm{j}\omega[D] + \left([C] + [C]_{res} + \Omega_{rot}^2[C]_{rot}\right)\right)[w] = 0 \tag{3.3}$$

in the frequency domain. Here, the skew symmetric gyroscopic matrix $[G]$ contains contributions that are linked with the rotational speed of the disk structure. Furthermore, the matrix $[C]_{res}$ contains residual stiffness contributions that can arise from plastic pre-deformation, which is the case when roll tensioning is applied, and $[C]_{rot}$ are the stiffness contributions due to centrifugal effects. Solving this system of equations is not a straightforward task due to the skew symmetric nature of $[G]$ and the damping matrix not necessarily being symmetric. However, by transforming equation (3.3) into state-space, linear solvers can be utilized to compute the eigenvalue problem,

see [64, 75, 141, 174] for deeper insight.

In order to investigate the sound radiation of the simple disk, various methods have been utilized and the results are compared to each other in terms of accuracy and computational cost. It must be noted that the global sound power is taken as a useful quantity for comparison. Three distinct numerical models have been generated, namely using BEM and FEM, where, for the former, the disk is regarded as a baffled radiator emitting sound into a half space, where the fluid is considered being at rest. This model is adequately reproduced using FEM, where the half space domain is modelled with a hemisphere and the physics of the actual unbounded domain is mapped onto the spherical surfaces using infinite finite elements [174]. In addition, a full space domain is created in a similar fashion to investigate the assumption of a baffled radiator. It is worth noting that both the model using BEM and the model using FEM together with the infinite finite elements result in system matrices that are frequency-dependent. Therefore, it is not possible to apply model reduction techniques based on modal decomposition and modal superposition strategies. Without taking further measures, this leads to the cumbersome computation of inverting the full system matrix for each single frequency of interest in order to derive harmonic solutions. For a large number of degrees of freedom as well as for fine frequency resolutions, the resulting computational cost can easily exceed justifiable values. Therefore, the results obtained by the domain discretization schemes are also compared to simplified sound power predictions using ERP and LPM for which the aforementioned model reduction techniques can be utilized. In the following, these models are further discussed.
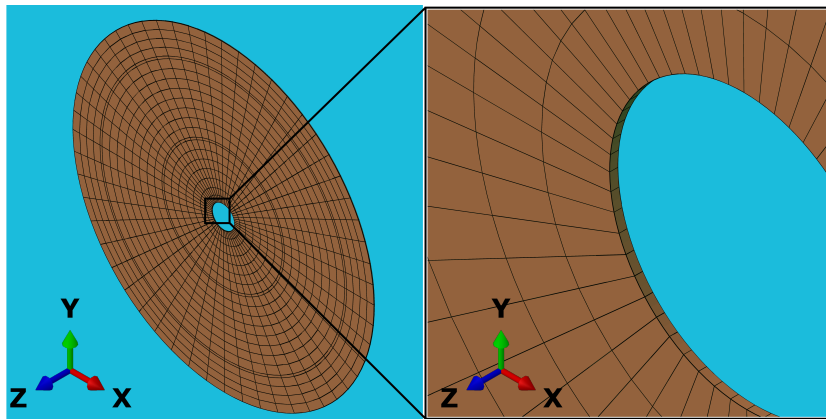

Figure 11: Coarse mesh of BEM model of simple disk

An appropriate BEM model is derived by taking the surfaces of the three-dimensional FEM model as new elements for the equivalent boundary element model as shown in Figure 11. Note that only the surface elements in the positive Z-plane have been taken into account since for that purpose
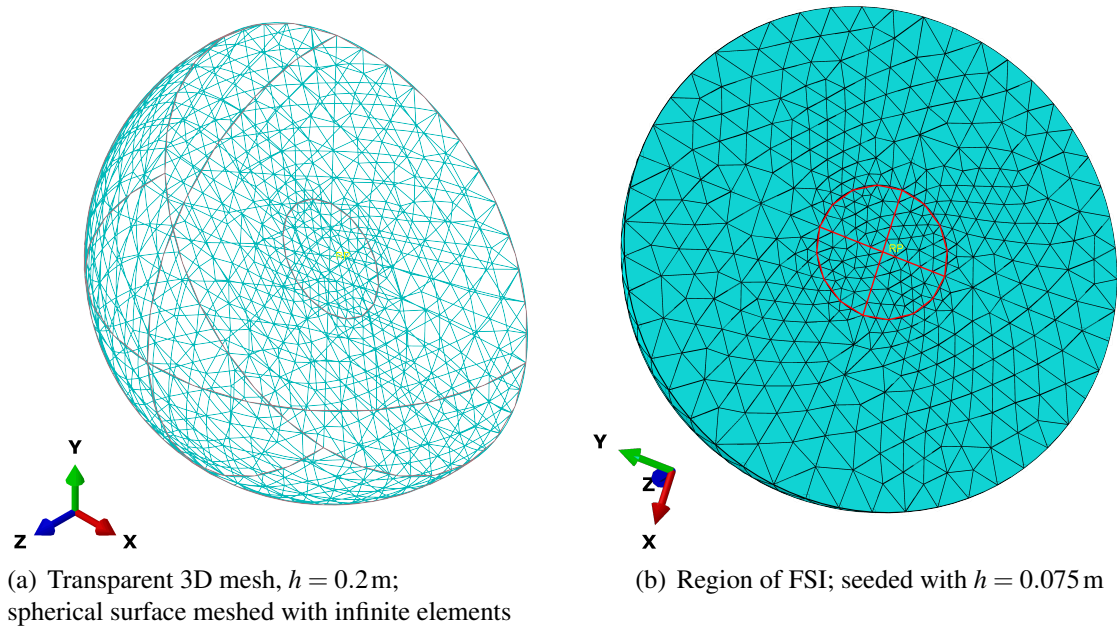
(a) Transparent 3D mesh, $h = 0.2\,\mathrm{m}$;
spherical surface meshed with infinite elements

(b) Region of FSI; seeded with $h = 0.075\,\mathrm{m}$

Figure 12: Volumetric mesh of the acoustic half space; hemisphere radius $r = 1.5\,\mathrm{m}$

the disk is considered as a baffled radiator emitting sound only in the positive half space. The baffled surface is indicated in light blue color, whereas the boundary elements are colored brown. For additional information, see the outlines in Publication C and references [128, 129]. As can be seen, a conforming mesh is utilized for simplicity. If non-conforming meshes need to be connected, usually a master-slave contact algorithm is applied [174], for which so-called mortar elements are also applicable, see [104, 128].

At this point, Figure 12 as well as Figure 13 have been recalled from Publication C for the discussion on both FEM models. In Figure 12, the equivalent FEM model with respect to the BEM model, as discussed above, is shown. In this model, the hemispherical domain is discretized with an unstructured mesh using second order tetrahedral elements. As mentioned above, the spherical surface is meshed with infinite finite elements of 10-th order [174] to map the properties of the actually unbounded domain. The baffled characteristic is realized by setting the fluid particle velocity on the circular area to zero. Only in the region where the disk is connected, see the red circle in Figure 12(b), a fluid structure interaction is realized in the form that the fluid particle velocity is connected via tie constraints to the structural velocity [174].

In the full acoustic radiation model, the hemisphere is duplicated to form a spherical domain around the rotating disc, where, again, tie constraints have been used to realize the fluid structure interaction between the disk and the acoustic fluid. This model allows to investigate to what extent the assumption of a baffled radiator is justified and where acoustic short circuits between one side of
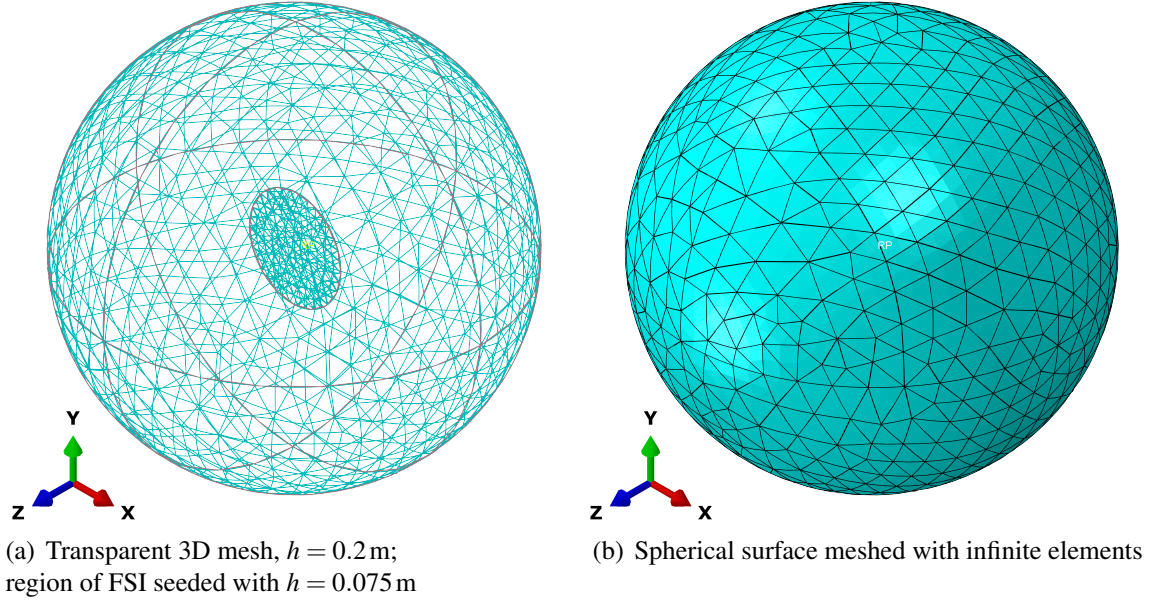
(a) Transparent 3D mesh, $h = 0.2\,\text{m}$; region of FSI seeded with $h = 0.075\,\text{m}$

(b) Spherical surface meshed with infinite elements

Figure 13: Volumetric mesh of the acoustic full space; sphere radius $r = 1.5\,\text{m}$

the plate and the other might appear.

Finally, the simplified sound power approximation schemes are discussed, which do not require the discretization of the acoustic domain. For the baffled radiator, the ERP calculation reads

$$P_{ERP} = \frac{1}{2}\rho_0 c_0 \sum_{\mu=1}^{N_e} A_\mu v_{n_\mu} v_{n_\mu}^*, \tag{3.4}$$

where the sum is taken over all radiating elements μ of the baffled structure. Note that the complex conjugated quantity is marked with the $*$ superscript and v_{n_μ} represents the surface element averaged normal velocity applied to the centroid of the surface with the associated element surface area A_μ. The assumption that a single normal velocity acts across the whole element, in this case, can be understood as a single uncorrelated piston with respect to neighboring elements. With this rather crude simplification, the existence of acoustic short circuits is excluded. In contrast, the LPM approach allows for these acoustic phenomena and reads

$$P_{LPM} = -\frac{1}{2}k\rho_0 c_0 \sum_{\mu=1}^{N_e} \sum_{\nu=1}^{N_e} A_\mu A_\nu \Im\left\{G_{\mu\nu}\right\} \Re\left\{v_{n_\mu} v_{n_\nu}^*\right\} \tag{3.5}$$

$$\text{with} \quad \Im\left\{G_{\mu\nu}\right\} = -\frac{\sin(k|x_\mu - x_\nu|)}{2\pi|x_\mu - x_\nu|}.$$

Here, the interaction between radiating elements is taken into account by considering the spatial

distance $|x_\mu - x_\nu|$ between the centroids of element μ and element ν and $\Re\left\{v_{n_\mu} v_{n_\nu}^*\right\}$ where $\Re\left\{\right\}$ denotes the real part of a complex quantity. Therefore, the phase difference between v_{n_μ} and $v_{n_\nu}^*$ is accounted for. For further details, see Publication C and references [58, 59, 111].

The improved disk

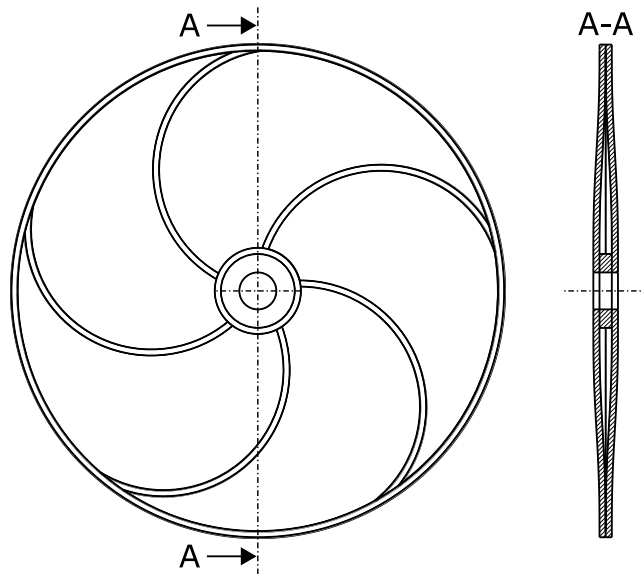Figure 14 provides a drawing of the general geometry of the improved disk. The key factor is

Figure 14: Principle sketch of the improved disk geometry

that the final disk consists of two separated sub-plates that are combined together through a small spacer disk in the middle. In the production process, the two sub-plates are connected together at the outer radius so that a closed cavity is formed. Various materials can be filled into this cavity to improve or to influence the dynamic behavior. For simplicity, a vacuum is assumed at this point. In addition, spiral lines on both main surfaces of the sub-plates indicate the region where pre-stresses due to plastic deformation are introduced. The indentation depth is comparable to standard roll tensioning procedures [86, 87].

The simulation that to some extent reassembles the main steps of a possible production process of the final disk is straightforward. It is assumed that the two sub-plates are connected through the spacer disk, where the rotational axis of all three sub-structures are aligned and pre-deformation as well as pre-loads are zero, i.e. the sub-plates have a flat surface where the curvature along the radius is zero. Therefore, in the initial status, both sub-plates are separated from each other along the common radial direction. Note that the simulation procedure from the undeformed initial

49

configuration to the one shown in Figure 14 must be part of the overall simulation process in order to adequately account for elastic pre-stresses and residual stresses due to plastic deformation. The step-by-step simulation procedure reads as follows.

1. Apply pre-deformation of spiral lines and compute plastic deformation.

2. Release pre-deformation so residual stresses remain.

3. Deform the outer rim of both sub-plates towards each other until contact is established.

4. Apply zero pressure on the surface inside the formed cavity and ambient pressure to the exterior surface of the disk.

5. Simulate deformation due to pressure gradient between interior cavity and exterior domain.

6. Tie all surfaces in contact.

This pre-deformation procedure is only conducted once for the prediction of accurate pre-stress distribution. In the subsequent simulation, this pre-deformation state serves as a starting point for

(a) Isoparametric view

(b) Cut with magnification of spacer and double disk
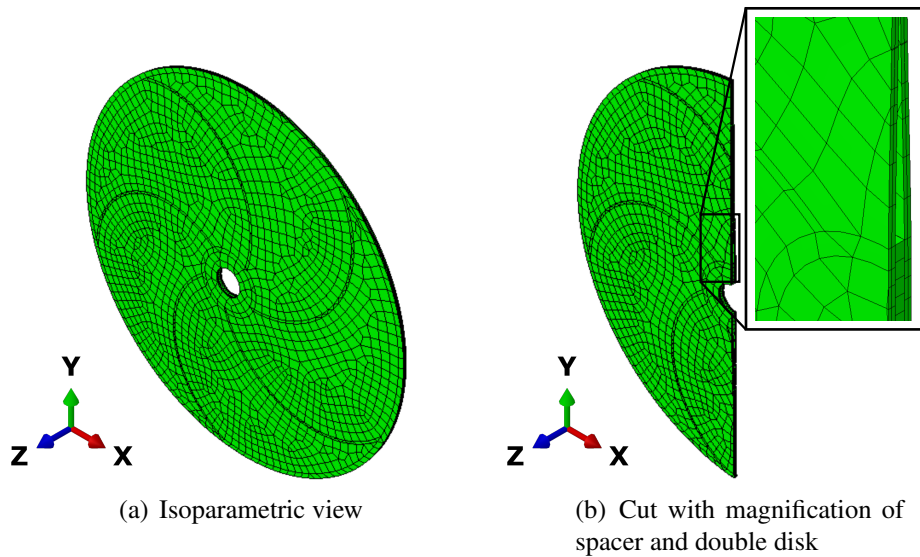
Figure 15: FE mesh of improved disk

the application of rotational loads and the following investigation of complex modes within the framework of a numerical modal analysis [174]. Figure 15 displays the mesh configuration of the improved disk configuration. As can be seen in the magnification of Figure 15(b), a closed cavity is formed between the two sub-plates.

In Publication D, a comparison is conducted with respect to a conventional disk, as shown in Figure 10, to indicate the improved performance of the new disk design. Please note that the

overall geometry of the reference disk and the new design are very similar, except for the spacer disk in the middle, which alters the overall weight of the new design to some negligible extent. However, in terms of effective cutting depth when used as a saw blade, the new design provides very similar parameters.

3.2 Material models

In order to conduct the numerical simulations, appropriate material models must be specified. For solid material, a linear elastic stress-strain relation well-known as Hooke's law applies. In addition, a yield stress σ_y is specified to distinguish between elastic and plastic deformation. The latter one is specified by an isotropic hardening, see Wu [188] for deeper insight. For a simplified uniaxial stress state, Figure 16 shows the stress-strain relation. In the elastic region where $\varepsilon \leq \varepsilon_{el}$, the material behavior is defined by the Young's modulus and the Poisson's ratio. In the region where isotropic hardening exists, i.e. $\varepsilon_{el} < \varepsilon$, the material behavior is determined by the slope defined by the plastic strain, i.e. $\varepsilon_{pl} = \varepsilon_{tot} - \varepsilon_{el}$, and an associated plastic stress σ_p. With this model for solid
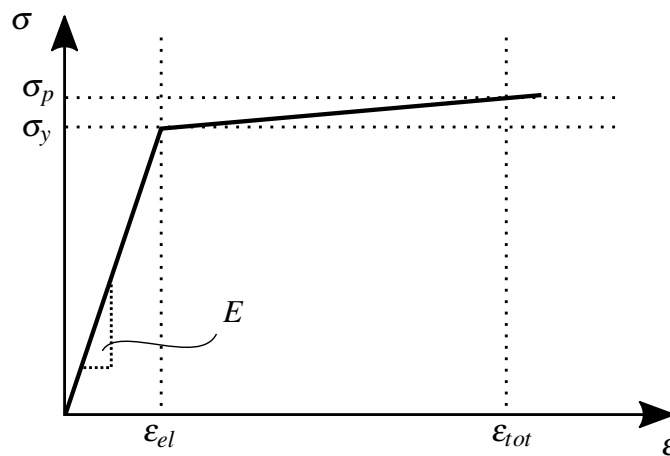

Figure 16: Stress-strain relation of material model for solid structures

material, the elastic deformation of a structure can be computed and residual stresses due to plastic deformation can be accounted for.

Fluids, as considered in this work, are adequately described by Newton's law, fulfill adiabatic assumptions of thermodynamics and are seen as inviscid. Therefore, it is convenient to specify the material parameters such as fluid density, the bulk modulus, and the speed of sound with respect to the fluid at rest.

All relevant material parameters are listed in Table 3. Note that the plastic stress σ_p was arbitrarily chosen in order to realize a small but finite slope of the stress-strain relation for improved numerical stability. The associated material properties for steel are based on the specifications in the available literature, see [86, 87, 120, 121].

Material	Symbol	Description	Value	Unit
Steel	E	Young's modulus	210	GPa
	ν	Poisson's ratio	0.3	–
	ρ_s	Density	7800	kg/m^3
	$\alpha^{(d)}$	Rayleigh parameter	0.1826	s^{-1}
	$\beta^{(d)}$	Rayleigh parameter	$5.0125 \cdot 10^{-6}$	s
	σ_y	Yield stress	1.262	GPa
	σ_p	Plastic stress	1.280	GPa
	ε_{pl}	Plastic strain	0.5	–
Air	K	Bulk modulus	$1.42 \cdot 10^{-4}$	GPa
	ρ_0	Density	1.225	kg/m^3
	c_0	Speed of sound	340	$m\,s^{-1}$

Table 3: Material properties

In conclusion, in this chapter all numerical models as well as material models with the associated material properties have been presented and discussed.

Chapter 4

Summary of Appended Publications

The key results and short summaries of the appended publications are included in this section. The contribution of this work can be divided into two parts, the first part being devoted to Galbrun's equation as a formulation of aeroacoustics utilizing a mixed frame and the second part to the dynamics of an elastic rotating disk as a specific topic of rotor dynamics.

Figure 17 presents an overview of the appended publications with regard to the individual contributions to the scientific field of aeroacoustics and rotor dynamics.
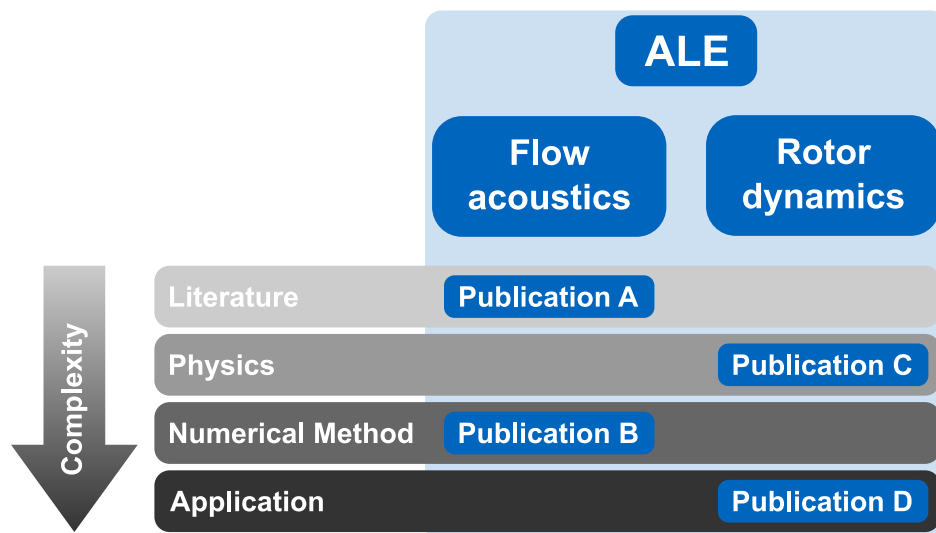
Figure 17: Overview of contributions

As can be seen, each publication contributes to a different subfield of research, i.e. Publication A provides a basic overview of the available literature concerning Galbrun's equation and its classification with respect to other aeroacoustic methods, Publication B improves the methodology

with respect to numerical methods for solving Galbrun's equation, Publication C discusses the basic understanding of the physics of sound radiation from rotating disks, and last but not least, Publication D provides an improved version of an application of a rotating disk. In addition, the increasing complexity is highlighted.

The key results of each publication are stated as follows.

Galbrun's equation:

- Publication A summarizes for the first time research contributions that are directly or indirectly related to Galbrun's equation and offers an integration into the scientific field of aeroacoustics with respect to other approaches and methods. Within the scope of the publication, the fundamentals for further developing Galbrun's equation with regard to non-linear effects and sound propagation in moving fluid, including viscous and heat conduction effects, are presented. Furthermore, a general relationship between pressure and density variations has been recalled in order to support appropriate experiments investigating constitutive relations of flow acoustics.

- Publication B presents the application of a discontinuous Galerkin finite element method for solving the pure displacement based Galbrun's equation in the context of a numerical modal analysis. A convergence study convinces the reader of the numerical stability and applicability. Utilizing this approach, spurious modes are clearly separated from physical modes and thus can be excluded when reconstructing the acoustic field using a modal superposition strategy. In addition, an estimation has been presented to identify acoustic modes. This procedure can be used to filter the solution space from vorticity and spurious modes. In order to consider absorbing boundary conditions, an adequate formulation based on the well-known Robin boundary condition was developed. The new formulation can be simplified to already known boundary conditions for the Galbrun equation utilizing suitable assumptions.

Rotating disk:

- Publication C discusses the far-field sound radiation of a rotating elastic disk, utilizing the sound power as a global measure for the comparison between different numerical methods. The applied lumped parameter model agrees well with state-of-the-art methods such as BEM or FEM. Significant reduction in computational cost was achieved due to the LPM's applicability in the frame of a harmonic analysis using modal superposition. Furthermore, it has been discovered that acoustic short circuits disappear at high rotational speeds and that mode splitting is audible but not along the rotational axis.

- Publication D offers a new design for rotating disks. The combination of the specific geometry and the spiral shape of the rolling lines improves stability by 33 % in terms of rotational speed compared to conventional versions. If the kinetic energy is used as a measure of productivity, this leads to an increase of 75 %.

4.1 Publication A

90 years of Galbrun's equation: An unusual formulation for aeroacoustics and hydroacoustics in terms of the Lagrangian displacement

Submission status: Currently, this publication is accepted in the *Journal of Theoretical and Computational Acoustic* after having resubmitted a revised version.

Novelty and key results: Since Galbrun published his work in 1931 [73], a number of researchers have worked on this form of describing aeroacoustics, i.e. in a mixed Lagrangian-Eulerian framework. However, after about 90 years of research on this topic, no review paper has been published. This publication is intended to give an overview of the vast number of contributions available in the literature which are related to Galbrun's equation. In addition, a classification of different sounds and an overview of existing methods of aeroacoustics are presented. Furthermore, an overview of the transition from Lagrangian to Eulerian to the mixed frame is offered, which was translated from a French publication into English. Rather than presenting a collection of publications along a historical line, this publications offers a subdivision into different categories such as "general derivation", "numerical analysis", "fluid structure interaction", and "far field approximation". This way, it is believed that access to the theoretically challenging topic is facilitated. Furthermore, the importance of the precise definition of the Cauchy stress tensor and the divergence operator acting on it were emphasized and stressed in order to avoid confusion when reading literature with different definitions. Based on general concepts of thermodynamics, a universal formalism is presented to support experimental scientists and engineers in measuring material properties in combination with flow acoustics. Finally, the possibility of defining Lagrangian densities for the derivation of Galbrun's equation from Hamiltonian principles as well as an energy concept for wave propagation are recalled. Such approaches are usually not available for standard wave propagation formulations within a Euler frame.

Specific contribution to the publication: Maeder proposed the concept of the manuscript and reviewed the literature related to Galbrun's equation and compiled an overview of the existing methods and terminologies. Maeder also wrote the original draft of the manuscript and coordinated all author contributions.

4.2 Publication B

Solving Galbrun's Equation with a discontinuous Galerkin Finite Element Method

Novelty and key results: In the field of aeroacoustics, a rather unknown approach utilizing a mixed Lagrangian-Eulerian framework, was first formulated by Galbrun in 1931 [73]. Besides the interesting advantage that only the Lagrangian displacement perturbation is considered as the main unknown for the description of aeroacoustic phenomena, the disadvantage exists that numerical instabilities occur, also called spurious modes, which can pollute the final solution. To overcome this drawback, the use of a discontinuous Galerkin finite element method seems to be a promising remedy for the above mentioned problem.

A weak formulation of Galbrun's equation was established, which is suitable for the application of a discontinuous Galerkin finite element method. This formulation was subsequently implemented in Comsol Multiphysics®. A corresponding convergence analysis highlighted the numerical performance and stability. Furthermore, an advanced boundary condition formulation in the frequency domain was introduced to take absorbing boundaries into account. By comparing the results of an eigenvalue analysis with standard methods such as the linearized Euler equation and the linearized Navier-Stokes equation, the essential advantage of the postulated approach has been revealed. The results showed that by applying the proposed method, vortical and spurious modes are well separated from acoustic modes within the complex plane. A crucial parameter is the constant within the applied Lax-Friedrich flux. Therefore, a detailed parameter analysis provides information about this parameter with which converged results were obtained. Essentially, two cases have been studied. The first one being a duct with laminar flow configuration and the second one being an annulus with a rotating shear flow. By computing the rotation and the divergence of the solution field for both acoustic modes and vortical modes, a criterion is offered that allows the user to estimate to what extent individual modes are primarily acoustic modes or vortical modes, respectively. The latter show a proportional dependency on the Mach number. The presentation of a filter technique for the identification and exclusion of vortical modes finalized the contribution.

Specific contribution to the publication: Maeder proposed the basic concept and realized the essential implementation in the software Comsol Multiphysics®. After setting up appropriate numerical models, Maeder was responsible for carrying out the simulations as well as the analysis and validation of the results. Furthermore, Maeder wrote the original draft of the manuscript and coordinated all author contributions.

4.3 Publication C

Numerical analysis of sound radiation from rotating discs

Novelty and key results: To analyze rotating elastic structures such as saw blades, it is important to consider gyroscopic effects and centrifugal forces. These effects also play an important role when the sound radiation of such structures is of interest, because these effects lead to forward and backward traveling wave propagation known as the so-called mode splitting. Since mode splitting is particularly associated with mode shapes that develop radial node lines, the sound radiation of these modes is of particular interest. The publication aims to answer the question whether a lump parameter model is an adequate sound power estimation for rotating disks instead of using wave-based methods and whether mode splitting is audible as part of a deeper physical understanding of such problems.

This study deals with the far field sound radiation of a rotating disk under consideration of gyroscopic effects as well as centrifugal forces utilizing numerical methods such as FEM/BEM in the frequency domain. Starting with a full three-dimensional model, the problem is reduced towards a baffled sound radiator theory. With this simplification, a lumped parameter model is utilized as an appropriate sound power estimate. The simulations show that the model is capable of taking acoustic short circuits into account and that the results are in very good agreement with state-of-the-art methods. As a side effect, the comparison with the so-called equivalent radiated power enables one to determine whether acoustic short circuits exist, which, from an engineering point of view, is not straightforward for complex configurations and models involving rotation. This helps to understand the underlying physics in more detail. As a major benefit, it was possible to utilize a state space formulation in order to conduct a harmonic analysis, which is hard to realize when using standard BEM or standard infinite finite elements due to the frequency dependent system matrices. Compared to standard FEM simulations, the proposed method achieved a saving in terms of computational costs by a factor of 30. Surprisingly, the analysis showed that deflection shapes, which form acoustic short circuits at low rotational speeds, contribute to sound radiation at high speeds. Last but not least, a detailed analysis of the far field sound radiation revealed that mode splitting is audible away from the rotational axis.

Specific contribution to the publication: Maeder set up appropriate numerical models and he improved an existing LMP script in python in order to account for acoustic short circuits. In addition, Maeder implemented an interface between Abaqus and Akusta (in-house BEM code) and conducted all of the simulations, data visualization and interpretation. Furthermore, Maeder wrote the original draft of the manuscript and coordinated all author contributions.

4.4 Publication D

Double cutting disc with curved deformation lines (WP 2018/234547 A1)

Novelty and key results: The stability of rotating disks such as saw blades is defined by the so-called critical rotational speed, see Schajer [167]. This situation occurs when the associated rotational frequency coincides with a natural frequency of an out-of-plane vibration. It must be noted that only deflection shapes with radial nodal lines show the mentioned behavior. As seen from a stationary observer, this leads to a quasi stationary deflection while the disk is still rotating. Various methods have been identified to improve the stability of such disks, in particular by applying residual stresses due to plastic deformation or geometric optimization.

The presented publication offers a new design in terms of geometry and a new configuration of deformation lines for the application of residual stresses. The main characteristics such as mass and cutting depth remain almost constant compared to state-of-the-art saw blades that have comparable dimensions. The emerging improvement results from a combination of different effects. First, two sub-plates separated by a spacer are subjected to pre-deformation forming the final geometry. This leads to a non-linear stiffening effect, as this deformation is beyond the small deformation theory which improves the susceptibility to buckling. In addition, a closed cavity is formed between the two sub-plates. This cavity can be filled with any material, allowing to improve the damping behavior since the relevant shear stresses have a maximum value at the symmetry plane of the disk for the case of out-of-plane deformations. Therefore, any viscous material located between the sub-plates has a major impact on energy dissipation. Second, instead of applying circular pre-tensioning lines, spiral lines, i.e. lines that are a function of radius and angle, improve the performance of the disk. As a side effect, the spiral shape of the pre-tensioning lines prevent the sub-plates from early buckling. Third, only the combination of the pre-deformed geometry together with the spiral pre-tensioning lines improves the critical rotational speed up to 33 % with respect to a conventional disk. In terms of kinetic energy which can be a measure for productivity, this increase in rotational speed results in an improvement of 75 %. Currently, the patent is in the phase of nationalization and regionalization in the European Union, the United States of America and the Republic of China.

Specific contribution to the publication: Maeder is the inventor of the disk. Furthermore, Maeder was in charge of setting up appropriate numerical models in order to conduct an optimization process and to highlight the final improved performance. In addition, Maeder comprehensibly presented the results to the Technical University of Munich and at a number of international conferences and highlighted the improved performance of the new design.

Chapter 5

Discussion of Results

In this chapter, the main achievements of this work are critically discussed with regard to currently available publications from the literature, where the main idea of understanding and analyzing sound and vibration in a mixed frame serves as the central theme. As indicated in chapter 4, this discussion is outlined following the concept presented in Figure 17, where the contributions of this work are considered with respect to the general "Literature", "Physics", which is understood as the general understanding of physical relations, followed by the discussion towards the applied "Numerical Method", and finally a last part that considers the "Application".

As a scholar, when getting involved with a new research field of interest, publications that review the available literature towards that topic are essentially a reasonable starting point for getting involved with the subject matter. The main advantage of such reviewing publications, as understood by the author, is that in the majority of cases such publications give a good overview and more or less highlight open research questions. In fact, the latter possibly facilitates the scholar's creativity and ambition to contribute to the research field. In this sense, Publication A reviews the literature of the past 90 years that can be linked to the derivation and use of Galbrun's equation, which describes sound propagation and generation in moving media, utilizing a mixed or ALE framework, respectively. This topic belongs to the research field of aeroacoustics, if the fluid is considered to be a gas. However, within the publication, ways for applying Galbrun's equation to hydroacoustics are pointed out, too. To the author's best knowledge, Publication A is the first attempt to summarize and review this specific research topic. Of course, utilizing Galbrun's equation to solve aeroacoustic problems is only one possible way – special in the sense that an ALE framework is applied. Several other methods have been developed that are usually described in a Eulerian frame. Since this framework is commonly used by engineers working in the field of fluid dynamics, these methods are generally more recognized in the scientific community than the method proposed by

Galbrun. Just to mention a few, the well-known acoustic analogies of Lighthill have been strongly developed since the 1950s and critically reviewed by Doak [51]. But there also have been other analogies, such as Howe's analogy [47], and Goldstein's analogy [82], see Musafir [139] for a review on these analogies. Other approaches that utilize a linearization of the set of balance equations, such as LEE and APE are reviewed in Schoder and Kaltenbacher [170] as well as for the LNSE in Guz' [83]. As can be seen, Publication A is intended to join the series of review publications among the various methods that have been developed for solving aeroacoustic problems. This contribution facilitates interested researchers to get access to the research topic linked to Galbrun's equation. In addition, Publication A provides a way for further developing Galbrun's equation towards the application to problems involving viscothermal losses and presents a framework for identifying source terms of Galbrun's equation, which are rarely discussed in the literature, cf. Gabard et al. [67].

In terms of understanding the physical relations, this work contributes in a number of ways. First of all, the deductive approach, by recalling general expressions of the ALE framework and further by applying these concepts to the field of aeroacoustics as well as rotor dynamics, serves as a promising way of eventually deriving a unified theory with which very complex problems can be solved. As a thought experiment, such problems could include rotating elastic/plastic deforming bodies, where a relatively non-stationary moving fluid flow generates and propagates sound waves from the moving body. Even viscothermal losses could be included in such computations. The proposed approach enables a straightforward interaction between various domains with adequate boundary conditions. In this sense, a generalized version of the Robin boundary condition for Galbrun's equation has been proposed in Publication B, which simplifies under appropriate assumptions to the version presented by Dietzsch et al. [50]. Furthermore, as an example, when conducting a complex modal analysis of both cases, i.e. the circulating flow in the annulus discussed in Publication B as well as the rotating elastic plate in Publication C, a mode splitting is recognizable of modes that develop radial nodal lines. This circumstance, which sometimes is referred to forward and backward traveling waves, is in agreement with Dietzsch et al. [50] when speaking about Galbrun's equation in aeroacoustics and Weidauer and Willner [186], Vila et al. [184], Fayos et al. [60], and Schajer and Mote [168] for rotor dynamics. As can be seen, with a unified approach it is possible to find similar arguments when explaining circulating modes in aeroacoustics as well as rotor dynamics whenever a rotating reference field is present. However, this relation is to some extent not surprising since both applications – even quite different in their application – can be derived from a common set of balance equations viewed in an ALE framework. Keeping this in mind, it is straightforward to assume that once rotating elastic structures and rotating flows are present in one problem, mode coupling could occur, possibly leading to excessive sound radiation. Therefore,

it seems to be a reasonable approach to investigate such cases with a unified approach; see for example research with respect to fan noise in Sutliff [178], tire dynamics with contact in Ziefle and Nackenhorst [190], and tire acoustic radiation in Brinkmeier et al. [39]. Furthermore, investigating the sound radiation of an elastic rotating disk, see Publication C, highlighted that when conducting a harmonic analysis, the so-called mode splitting is audible, but disappears once the receiver is placed on the axis of rotation. This phenomenon can be easily explained by having a sound radiating monopole source circling around an axis of rotation. If the receiver is placed on the axis of rotation, the distance between the source and the receiver remains constant. Therefore, no convective contribution is recognized. This circumstance changes, once the receiver is placed away from the axis of rotation. In time domain, these convective terms lead to frequency modulation known as Doppler effect, see Poletti and Teal [157]. However, this effect can not be captured by standard harmonic analysis procedures and more investigations are needed with respect to the generalization towards rotating elastic sound radiating bodies. Some research has been conducted towards this topic [118, 127].

Concerning "Numerical Methods", the presented work utilized a DG-FEM scheme to solve the aeroacoustic problems involving Galbrun's equation. Utilizing DG-FEM in fluid dynamics has been widely studied and is a powerful numerical method when convective terms and fluxes across element boundaries are present, see [16, 43–45, 88, 95, 104, 177]. However, when it comes to the application of the DG-FEM to solve Galbrun's equation, no publication could be identified so far, to the author's best knowledge, to deal with this topic. Bonnet-Ben Dhia et al. [35] utilized a DG-FEM scheme to solve the convective equation associated to the regularization of Galbrun's equation, but the actual equation was solved with standard FEM scheme. This regularization is necessary, since numerical instabilities can occur when using standard Lagrange finite elements. However, if a mixed formulation is applied, where the Lagrangian displacement and the Lagrangian pressure perturbations are the degrees of freedom, the numerical scheme provides uncorrupted results [50, 67, 72, 183]. Unfortunately, this comes with cost of the additional degrees of freedom, namely the pressure perturbations, for which adequate boundary conditions must be formulated. As discussed in Publication B, utilizing the DG-FEM scheme offers the possibility to use the pure displacement based formulation of Galbrun's equation and still achieve stable results. An additional benefit of this approach is that only the displacement field is the sought solution from which modes, as results of a numerical modal analysis, can be analyzed by computing the divergence and the curl of the solution field. With these results, a deeper insight is facilitated, whether modes have either vortical or acoustical characteristics. With this knowledge, a filtering technique is proposed so that unwanted modes are directly excluded by the numerical scheme. Note that the applicability of this filtering technique must be carefully identified. A slightly less crude approach

was published by Bonnet-Ben Dhia et al. [32]. The application of DG-FEM on this regularized form of Galbrun's equation remains an open task. In terms of acoustic radiation from rotating disks, see Publication C, it was possible to show that when using an ALE framework for computing the effective displacement felt by the surrounding fluid, simplified radiation models, known as ERP and LPM, can be utilized to estimate the radiated sound power. This becomes especially interesting when model reduction procedures can significantly reduce the computational costs. In such cases the ERP and LPM are still applicable, which is not the case involving numerical schemes where the system matrices are frequency dependent. As described by Brinkmeier et al. [39], using Astley-Leis infinite finite elements results in frequency independent system matrices. However, the additional discretization of the fluid domain, though acknowledging mass loading effects of the surrounding fluid, comes with the burden of higher computational costs. This circumstance is also discussed in Publication C to highlight the limits of the applied sound power approximation methods. Interestingly, mode shapes that develop acoustic short circuits and have radial nodal lines are inefficient sound radiators at low rotational speeds, but can contribute significantly at higher speeds, which is in agreement with Lee and Singh [118]. A possible explanation could be that at a certain rotational speed the characteristic time scale of the physical process that develops the acoustic short circuit is longer than the resulting characteristic time scale of the structural dynamics of the rotating disk. This way, even low order modes can become efficient sound radiators at high rotational speeds. This circumstance should be addressed in future studies for clarification. However, since the ERP does not account for acoustic short circuits, as the LPM does, comparing the results of both approximation methods gives an indication at which frequencies acoustic short circuits are present. This rather crude but efficient type of approach might be attractive to engineers who are interested in whether acoustic short circuits exist or not. Note that this kind of investigation holds also for non-rotating structures as long as the assumption holds for applying ERP and LPM.

Finally, with the understanding and the knowledge of the aforementioned concepts, an improved disk design was developed, which can be seen as a possible "Application" for circular saws blades. Since Publication D is an international patent, the design is original and only in its main properties comparable to standard disk designs commonly used as saw blades. Furthermore, the improved stability is characterized by a combination of (i) membrane stresses within the two sub-plates instead of shear stresses when transverse deformation (plate bending motion) occurs, (ii) elastic pre-deformation which results in a pre-tensioning of both sub-plates, and (iii) a number of spiral roll-tensioning lines that result in residual stresses after plastic deformation. Only this combination has led to an increase in the critical speed of 33 % with respect to a standard state-of-the-art disk model, as presented in Publication D. As part of the development and patenting process, meticu-

lous care has been taken to ensure that the design is scalable to very different radii. To give the reader an impression of how complex the process of roll-tensioning is, the following references can be considered [86, 87, 120, 121, 151, 167, 168]. Note that the design offers a number of further developments. As an example, in a simple thought experiment in which any viscous solid material could fill the cavity, it is obvious that any bending of the disk leading to a small out-of-plane deformation would result in a relative high value of shear-stress in the vicinity of areas where the radial stresses σ_{rr} vanish. Therefore and straightforward, placing an energy-dissipating material in the disks' cavity can reduce resonances of out-of-plane deformations. Note that with respect to future developments of the disk, uncertainty and sensitivity analysis should be conducted. Since this topic is beyond this work, the reader is referred to the literature [114, 116].

Summarizing this result discussion, it was shown that the work at hand contributes to four distinct fields of research as understood by the author, namely "Literature", "Physics", "Numerical Method", and finally "Application", where the application of an ALE framework to the field of aeroacoustics and rotor dynamics is a superordinate theme. This way, it is possible to gain a fundamental understanding of the basic equations, how to derive a unified theory, and finally to be able to identify common aspects, even though the field of aeroacoustics and rotor dynamics are quite different with respect to applications and engineering problems.

Chapter 6

Conclusion

By concluding this work, on the one hand the main results are summarized and on the other hand the implication to the scientific field as well as open questions for future research are discussed as follows.

When developing new products or prototypes, the research that is associated to this development is based on knowing the state-of-the-art literature, the theoretical understanding of physical processes as well as their mathematical formulations, which then can be solved by means of numerical methods. Utilizing computer aided engineering, virtual prototypes are developed and analyzed without having the necessity to produce a large number of test objects, to verify performance variations with respect to design changes. This kind of development process gets increasingly accepted in the industry, due to the cost savings associated with virtual prototyping. In this sense, this work presented a way to unify two research fields, first appearing being very different from each other, namely aeroacoustics and rotor dynamics. Since this unification is not straightforward when approaching via an inductive research strategy, the abstraction level has been raised to the application of an ALE framework to the balance equations of continuum mechanics, which in turn can be seen as a deductive way of pursuing these two topics. As a result, both applications can be described by such a general theory, which allows one to find common similarities, e.g. when rotation is present. In order to give the reader access to the higher abstraction level, four main fields have been identified, namely "Literature", "Physics", "Numerical Method" and finally "Application", where this work contributes. These contributions, with respect to aeroacoustics and rotor dynamics, can be summarized as follows.

The main achievement towards to the research field of aeroacoustics, described by Galbrun's equation as sort of an ALE formulation of sound generation and propagation in moving fluids, are the following:

- A first attempt has been realized to review the available literature, linked to Galbrun's equations, of the past 90 years.

- Based on the Robin boundary condition for time harmonic problems, a generalized boundary condition for Galbrun's equation has been proposed.

- In the context of analyzing aeroacoustic problems with a numerical modal analysis, a numerical scheme utilizing DG-FEM has been successfully applied to the original Galbrun's equation.

- A filtering technique was proposed to analyze the modes associated with an eigenvalue problem, which enables one to identify the main characteristics of the modes. This filtering technique can be applied on a weak formulation level in order to reduce the solution space.

With respect to rotor dynamics and more precisely the dynamics of a thin rotating disk and its sound radiation, where the ALE framework has been applied for the rotating domain, the following main contributions can be identified:

- The LPM, which takes acoustic short circuits into account, is a suitable sound power estimate that can be used in conjunction with model reduction techniques to save computational cost.

- A comparison between ERP, LPM, BEM and infinite FEM highlighted the restrictions of the sound power approximation methods as well as the computational cost.

- Comparing results computed by using ERP and LPM enables one to identify whether acoustic short circuits develop as part of the fluid structure interaction.

- It was identified that in a harmonic analysis, mode splitting is audible, but only away from the rotational axis.

- An original disk design has been proposed that involves a significant increase in the critical speed with respect to common disk shapes, as an application for saw blades.

As pointed out before, the application of an ALE framework as a higher abstraction level enables a better understanding of phenomena linked to aeroacoustics and rotor dynamics and potentially gives rise to formulate a unified theory in future research investigations. This unified theory appears to be helpful when effects that are present in both cases, e.g. the occurrence of the so-called mode splitting, can possibly couple, such as in turbofan engineering. But also the sound radiation of wind turbines would be an interesting application to see, whether such an approach as

presented could lead to a better understanding of the complex physical processes. In addition, developing Galbrun's equation towards considering viscothermal losses offers a wide range of new applications, especially for cases where fluid structure interaction plays a significant role. Possible applications could be hearing aids or elastoacoustic meta-materials, insofar as for the latter acoustic materials are assumed where the fluid structure interaction takes a strong coupling between the two domains.

As a direct consequence of the presented work, a few aspects are recalled that could be part of future developments. First, the proposed form of providing sources of Galbrun's equation should be further analyzed and tested against other methods of hybrid flow/acoustic analysis, such as LEE, LNSE, or APE. Second, the generalized form of the Robin boundary condition for Galbrun's equation should be analyzed on inflow and outflow boundaries. Third, the proposed mode filtering strategy for distinguishing acoustic, physical or even spurious modes from each other, as part of an eigenvalue analysis in aeroacoustics, represents a rather crude approach. In cases where modes have vortical as well as acoustic characteristics, better methods are needed. One possibility of achieving that could be to apply the DG-FEM scheme to the augmented Galbrun equation as presented by Bonnet-Ben Dhia et al. [35].

Equivalently, with respect to rotor dynamics, future works could include the investigation of the audible mode splitting in further detail. Here, it would be interesting to see whether the frequency modulation that results from a rotating monopole, which can not be adequately covered by an harmonic analysis, turns into an amplitude modulation once the number of rotating sources is increased and matches the sound radiation of the rotating elastic deforming disc as analyzed in this work. Furthermore, the proposed design of the improved disk has not undergone any structured optimization process. Therefore, it is assumed that an even better performance can be realized. Fortunately, the application of the LPM provides an effective method for optimization procedures where the minimization of the radiated sound power could be part of the objective function.

In terms of a unified theory, the use of generalized functions such as the Heaviside function would be interesting to apply, which could be a virtual switch between different neighboring domains. Furthermore, the DG-FEM seems to be a capable numerical method for solving such a unified theory, where fluxes across boundaries can adequately be considered.

It is evident that with a fundamental understanding of the underlying framework, numerous applications are conceivable and it is only a matter of creativity, from which further developments could arise moving forward.

Bibliography

[1] H. Altenbach. *Kontinuumsmechanik*. Springer, Berlin, Heidelberg, 2018.

[2] H. Altenbach and A. Öchsner, editors. *Encyclopedia of Continuum Mechanics*. Springer, Berlin, Heidelberg, 2020.

[3] R. J. Astley. Numerical methods for noise propagation in moving flows, with application to turbofan engines. *Acoustical Science and Technology*, 30(4):227–239, 2009.

[4] R. J. Astley and W. Eversman. A finite element formulation of the eigenvalue problem in lined ducts with flow. *Journal of Sound and Vibration*, 65(1):61–74, 1979.

[5] R. J. Astley, G. J. Macaulay, and J. P. Coyette. Mapped wave envelope elements for acoustical radiation and scattering. *Journal of Sound and Vibration*, 170(1):97–118, 1994.

[6] R. J. Astley, R. Sugimoto, I. M. Achunche, M. F. Kewin, P. Mustafi, and E. P. Deane. Reprint of: A review of CAA for fan duct propagation and radiation, with application to liner optimisation. *Procedia IUTAM*, 1:143–152, 2010.

[7] R. J. Astley, R. Sugimoto, and P. Mustafi. Computational aero-acoustics for fan duct propagation and radiation. Current status and application to turbofan liner optimisation. *Journal of Sound and Vibration*, 330(16):3832–3845, 2011.

[8] R. Baccouche, M. Ben Tahar, and S. Moreau. Perfectly matched layer for Galbrun's aeroacoustic equation in a cylindrical coordinates system with an axial and a swirling steady mean flow. *Journal of Sound and Vibration*, 378:124–143, 2016.

[9] R. Baccouche, S. Moreau, and M. Ben Tahar. Test of single degree of freedom acoustic treatment impedance models for multimodal acoustic propagation in duct with flow. *The Journal of the Acoustical Society of America*, 141(6):4168–4178, 2017.

[10] C. Bailly and D. Juvé. Numerical solution of acoustic propagation problems using linearized Euler equations. *AIAA Journal*, 38(1):22–29, 2000.

[11] E. Barz. Vergleichende Untersuchungen über das Spannen von Kreissägeblättern mit Maschinen und mit Richthämmern. *Holz als Roh- und Werkstoff*, 21(4):135–144, 1963.

[12] K.-J. Bathe. *Finite Element Procedures*. Klaus-Jürgen Bathe, Watertown, 2nd edition, 2014.

[13] K.-J. Bathe, C. Nitikitpaiboon, and X. Wang. A mixed displacement-based finite element formulation for acoustic fluid-structure interaction. *Computers & Structures*, 56(2):225–237, 1995.

[14] Y. Bazilevs, K. Takizawa, and T. E. Tezduyar. *Computational fluid-structure interaction: Methods and applications*. Wiley series in computational mechanics. John Wiley & Sons Ltd., Chichester, 2013.

[15] E. Bècache, A.-S. Bonnet-Ben Dhia, and G. Legendre. Perfectly matched layers for time-harmonic acoustics in the presence of a uniform flow. *SIAM Journal on Numerical Analysis*, 44(3):1191–1217, 2006.

[16] A. Beck, T. Bolemann, D. Flad, H. Frank, N. Krais, K. Kukuschkin, M. Sonntag, and C.-D. Munz. Application and development of the high order discontinuous Galerkin spectral element method for compressible multiscale flows. In W. E. Nagel, D. H. Kröner, and M. M. Resch, editors, *High Performance Computing in Science and Engineering'17*, pages 387–407. Springer International Publishing, Cham, 2018.

[17] T. Belytschko, L. W. Kam, B. Moran, and K. Elkhodary. *Nonlinear Finite Elements for Continua and Structures*. John Wiley & Sons Inc, New York, 2nd edition, 2013.

[18] M. Ben Tahar and X. Feng. PML absorbing boundary condtitions for the aeroacoustic Galbrun equation in the time domain. *19th International Congress on Sound and Vibration 2012, ICSV 2012*, 1:589–596, 2012.

[19] F. K. Benra, H. J. Dohmen, J. Pei, S. Schuster, and B. Wan. A comparison of one-way and two-way coupling methods for numerical analysis of fluid-structure interactions. *Journal of applied mathematics*, 2011, 2011.

[20] A. Bensalah, P. Joly, and J.-F. Mercier. Well-posedness of a generalized time-harmonic transport equation for acoustics in flow. *Mathematical Methods in the Applied Sciences*, 41(8):3117–3137, 2018.

[21] H. Bériot. *Eléments finis d'ordre élevé pour Galbrun en régime harmonique: High-order FEM method for the Galbrun equation in the frequency domain.* Presses Académiques Francophones, Saarbrücken, 1st edition, 2014.

[22] H. Bériot, F. Treyssede, and M. Ben Tahar. Ducted propagation in the presence of vortical flow using an Eulerian-Lagrangian description. In *13th AIAA/CEAS Aeroacoustics Conference (28th AIAA Aeroacoustics Conference)*. American Institute of Aeronautics and Astronautics, 2007.

[23] A. Bermúdez, L. Hervella-Nieto, A. Prieto, and R. Rodríguez. Perfectly matched layers for time-harmonic second order elliptic problems. *Archives of Computational Methods in Engineering*, 17(1):77–107, 2010.

[24] K. Berriri. *Approche analytique et numérique pour l'aéroacoustique en régime transitoire par le modèle de Galbrun.* PhD thesis, ENSTA ParisTech, Paris, 2006.

[25] K. Berriri, A.-S. Bonnet-Ben Dhia, and P. Joly. Numerical analysis of time-dependent Galbrun equation in an infinite duct. *arXiv Mathematics e-prints*, page math/0603546, 2006.

[26] C. W. Bert and T. L. C. Chen. On vibration of a thick flexible ring rotating at high speed. *Journal of Sound and Vibration*, 61(4):517–530, 1978.

[27] W. B. Bickford and E. S. Reddy. On the in-plane vibrations of rotating rings. *Journal of Sound and Vibration*, 101(1):13–22, 1985.

[28] C. Bogey, C. Bailly, and D. Juvé. Computation of flow noise using source terms in linearized Euler's equations. *AIAA Journal*, 40(2):235–243, 2002.

[29] C. Bogey, S. Barré, D. Juvé, and C. Bailly. Simulation of a hot coaxial jet: Direct noise prediction and flow-acoustics correlations. *Physics of Fluids*, 21(3):035105, 2009.

[30] A.-S. Bonnet-Ben Dhia, E.-M. Duclairoir, G. Legendre, and J.-F. Mercier. Time-harmonic acoustic propagation in the presence of a shear flow. *Journal of Computational and Applied Mathematics*, 204(2):428–439, 2007.

[31] A.-S. Bonnet-Ben Dhia, E.-M. Duclairoir, and J.-F. Mercier. Acoustic propagation in a flow: numerical simulation of the time-harmonic regime. In G. Caloz and M. Daug, editors, *CANUM 2006 – Congrès National d'Analyse Numérique*, volume 22, pages 1–14, 2008.

[32] A.-S. Bonnet-Ben Dhia, G. Legendre, and E. Lunéville. Analyse mathématique de l'équation de Galbrun en écoulement uniforme. *Comptes Rendus de l'Académie des Sciences Paris*, 329:601–606, 2001.

[33] A.-S. Bonnet-Ben Dhia, G. Legendre, and E. Lunéville. Regularization of the time-harmonic Galbrun's equations. In G. C. Cohen, P. Joly, E. Heikkola, and P. G. Neittaan-mäki, editors, *Mathematical and Numerical Aspects of Wave Propagation WAVES 2003*, pages 78–83, 2003.

[34] A.-S. Bonnet-Ben Dhia, J.-F. Mercier, F. Millot, S. Pernet, and E. Peynaud. Galbrun based numerical scheme to compute time-harmonic scattering in an arbitrary mean flow. In *17th AIAA/CEAS Aeroacoustics Conference (32nd AIAA Aeroacoustics Conference)*. American Institute of Aeronautics and Astronautics, 2011.

[35] A.-S. Bonnet-Ben Dhia, J.-F. Mercier, F. Millot, S. Pernet, and E. Peynaud. Time-harmonic acoustic scattering in a complex flow: A full coupling between acoustics and hydrodynamics. *Communications in Computational Physics*, 11:555–572, 2012.

[36] D. Bowdler. Amplitude modulation of wind turbine noise: a review of the evidence. *Institute of Acoustics Bulletin*, 33(4):31–41, 2008.

[37] J.-Ph. Brazier. Eulerian-Lagrangian description of acoustic propagation in a nozzle flow. In *7th AIAA/CEAS Aeroacoustics Conference and Exhibit*. American Institute of Aeronautics and Astronautics, 2001.

[38] J.-Ph. Brazier. Derivation of an exact energy balance for Galbrun equation in linear acoustics. *Journal of Sound and Vibration*, 330:2848–2868, 2011.

[39] M. Brinkmeier, U. Nackenhorst, S. Petersen, and O. von Estorff. A finite element approach for the simulation of tire rolling noise. *Journal of Sound and Vibration*, 309(1):20–39, 2008.

[40] H.-J. Bungartz, M. Mehl, and M. Schäfer. *Fluid Structure Interaction II*, volume 73. Springer, Berlin, Heidelberg, 2010.

[41] J. Chabassier and M. Durufle. Solving time-harmonic Galbrun's equation with an arbitrary flow. Application to helioseismology. Research Report RR-9192, INRIA Bordeaux, 2018.

[42] R. C. Chanaud. Experimental study of aerodynamic sound from a rotating disk. *The Journal of the Acoustical Society of America*, 45(2):392–397, 1969.

[43] B. Cockburn, G. E. Karniadakis, and C.-W. Shu. *Discontinuous Galerkin Methods*. Springer, Berlin, Heidelberg, 2000.

[44] B. Cockburn, S.-Y. Lin, and C.-W. Shu. TVB Runge-Kutta local projection discontinuous Galerkin finite element method for conservation laws III: One-dimensional systems. *Journal of Computational Physics*, 84(1):90–113, 1989.

[45] G. C. Cohen and S. Pernet. *Finite Element and Discontinuous Galerkin Methods for Transient Wave Equations*. Springer, Dordrecht, 2017.

[46] L. Cremer, M. Heckl, and B. A. T. Petersson. *Structure-Borne Sound*. Springer, Berlin, Heidelberg, 2005.

[47] D. G. Crighton, A. P. Dowling, J. E. Ffowcs Williams, M. Heckl, and F. G. Leppington. *Modern Methods in Analytical Acoustics*. Springer, London, 1992.

[48] N. Curle and M. J. Lighthill. The influence of solid boundaries upon aerodynamic sound. *Proceedings of the Royal Society of London. Series A. Mathematical and Physical Sciences*, 231(1187):505–514, 1955.

[49] G. D. C. Dhondt. *The finite element method for three-dimensional thermomechanical applications*. Wiley, Hoboken, 2010.

[50] F. Dietzsch, L. Hervella-Nieto, S. Marburg, R. Rodríguez, and H. Weisbecker. Physical and spurious modes in mixed finite element formulation for the Galbrun equation. *Acta Acustica united with Acustica*, 100:493–512, 2014.

[51] P. E. Doak. Analysis of internally generated sound in continuous materials: 2. A critical review of the conceptual adequacy and physical scope of existing theories of aerodynamic noise, with special reference to supersonic jet noise. *Journal of Sound and Vibration*, 25(2):263–335, 1972.

[52] J. Donea and T. Belytschko. Advances in computational mechanics. *Nuclear Engineering and Design*, 134(1):1–22, 1992.

[53] J. Donea and A. Huerta. *Finite Element Methods for Flow Problems*. John Wiley & Sons, Chichester, 2003.

[54] J. Donea, A. Huerta, J.-Ph. Ponthot, and A. Rodríguez-Ferran. Arbitrary Lagrangian-Eulerian methods. In E. Stein, R. Borst, and T. J. R. Hughes, editors, *Encyclopedia of Computational Mechanics*, pages 1–23. American Cancer Society, 2nd edition, 2017.

[55] W. Eversman and R. O. Dodson Jr. Free vibration of a centrally clamped spinning circular disk. *AIAA journal*, 7(10):2010–2012, 1969.

[56] R. Ewert and W. Schröder. Acoustic perturbation equations based on flow decomposition via source filtering. *Journal of Computational Physics*, 188(2):365–398, 2003.

[57] R. Ewert and W. Schröder. On the simulation of trailing edge noise with a hybrid LES/APE method. *Journal of Sound Vibration*, 270:509–524, 2004.

[58] J. B. Fahnline and G. H. Koopmann. A lumped parameter model for the acoustic power output from a vibrating structure. *The Journal of the Acoustical Society of America*, 100(6):3539–3547, 1996.

[59] J. B. Fahnline and G. H. Koopmann. Numerical implementation of the lumped parameter model for the acoustic power output of a vibrating structure. *The Journal of the Acoustical Society of America*, 102(1):179–192, 1997.

[60] J. Fayos, L. Baeza, F. D. Denia, and J. E. Tarancón. An Eulerian coordinate-based method for analysing the structural vibrations of a solid of revolution rotating about its main axis. *Journal of Sound and Vibration*, 306(3):618–635, 2007.

[61] X. Feng, M. Ben Tahar, and R. Baccouche. The aero-acoustic Galbrun equation in the time domain with perfectly matched layer boundary conditions. *The Journal of Acoustical Society of America*, 139:320–331, 2016.

[62] A. Fidlin, O. Drozdetskaya, and B. Waltersberger. On the minimal model for the low frequency wobbling instability of friction discs. *European Journal of Mechanics – A/Solids*, 30(5):665–672, 2011.

[63] J. B. Freund. A simple method for computing far-field sound in aeroacoustic computations. *Journal of Computational Physics*, 157(2):796–800, 2000.

[64] M. I. Friswell, J. E. T. Penny, S. D. Garvey, and A. W. Lees. *Dynamics of Rotating Machines*. Cambridge Aerospace Series. Cambridge University Press, Cambridge, New York, Melbourne, Madrid, Cape, Town, Singapore, São Paulo, Delhi, Dubai, Tokyo, 2010.

[65] D. Fritze, S. Marburg, and H.-J. Hardtke. Reducing radiated sound power of plates and shallow shells by local modification of geometry. *Acta Acustica united with Acustica*, 89(1):53–60, 2003.

[66] D. Fritze, S. Marburg, and H.-J. Hardtke. Estimation of radiated sound power: A case study on common approximation methods. *Acta Acustica united with Acustica*, 95(5):833–842, 2009.

[67] G. Gabard. *Méthodes numériques et modèles de sources aéroacoustiques fondés sur l'equation de Galbrun*. PhD thesis, Université de Technologie de Compiègne, Compiègne, 2003.

[68] G. Gabard, R. J. Astley, and M. Ben Tahar. Stability and accuracy of finite element methods for flow acoustics. I: General theory and application to one-dimensional propagation. *International Journal for Numerical Methods in Engineering*, 63:947–973, 2005.

[69] G. Gabard, R. J. Astley, and M. Ben Tahar. Stability and accuracy of finite element methods for flow acoustics. II: Two-dimensional effects. *International Journal for Numerical Methods in Engineering*, 63:974–987, 2005.

[70] G. Gabard, H. Bériot, A. G. Prinn, and K. Kucukcoskun. Adaptive, high-order finite-element method for convected acoustics. *AIAA Journal*, 56(8):3179–3191, 2018.

[71] G. Gabard, E. Lefrançois, and M. Ben Tahar. Aeroacoustic noise source simulations based on Galbrun's equation. In *10th AIAA/CEAS Aeroacoustics Conference*. American Institute of Aeronautics and Astronautics, 2004.

[72] G. Gabard, F. Treyssède, and M. Ben Tahar. A numerical method for vibro-acoustic problems with sheared mean flows. *Journal of Sound and Vibration*, 272:991–1011, 2004.

[73] H. Galbrun. *Propagation d'une onde sonore dans l'atmosphère terrestre et théorie des zones de silence*. Gauthier-Villars, Paris, 1931.

[74] D. Gély and G. J. Bennett. Aeroacoustics research in europe: The CEAS-ASC report on 2018 highlights. *Journal of Sound and Vibration*, 463:114950, 2019.

[75] G. Genta. *Dynamics of Rotating Systems*. Springer, New York, 2005.

[76] G. Genta and A. Tonoli. A harmonic finite element for the analysis of flexural, torsional and axial rotordynamic behaviour of discs. *Journal of Sound and Vibration*, 196(1):19–43, 1996.

[77] Y. Giga and A. Novotný. *Handbook of Mathematical Analysis in Mechanics of Viscous Fluids*. Springer International Publishing, Cham, 2018.

[78] D. Givoli. Computational absorbing boundaries. In S. Marburg and B. Nolte, editors, *Computational Acoustics of Noise Propagation in Fluids – Finite and Boundary Element Methods*, pages 145–166. Springer, Berlin, Heidelberg, 2008.

[79] D. Givoli, T. Hagstrom, and I. Patlashenko. Finite element formulation with high-order absorbing boundary conditions for time-dependent waves. *Computer Methods in Applied Mechanics and Engineering*, 195(29):3666–3690, 2006.

[80] D. Givoli and J. B. Keller. A finite element method for large domains. *Computer Methods in Applied Mechanics and Engineering*, 76(1):41–66, 1989.

[81] S. Glegg and W. Devenport. *Aeroacoustics of Low Mach Number Flows*. Academic Press, 1st edition, 2017.

[82] M. E. Goldstein. A generalized acoustic analogy. *Journal of Fluid Mechanics*, 488:315–333, 2003.

[83] A. N. Guz'. Compressible, viscous fluid dynamics (review). Part 1. *International Applied Mechanics*, 36(1):14–39, 2000.

[84] M. A. Hamdi, Y. Ousset, and G. Verchery. A displacement method for the analysis of vibrations of coupled fluid-structure systems. *International Journal for Numerical Methods in Engineering*, 13:139–150, 1978.

[85] J. C. Hardin and D. S. Pope. An acoustic/viscous splitting technique for computational aeroacoustics. *Theoretical and Computational Fluid Dynamics*, 6(5):323–340, 1994.

[86] U. Heisel, T. Stehle, and H. Ghassemi. A simulation model for analysis of roll tensioning of circular saw blade. In *Advanced Materials Research*, volume 1018, pages 57–66. Trans Tech Publications Ltd., 2014.

[87] U. Heisel, T. Stehle, and H. Ghassemi. Experimental investigation into parameters influencing roll tensioning of circular saw blades. *Journal of Machine Engineering*, 9(12):98–111, 2015.

[88] J. S. Hesthaven and T. Warburton. *Nodal Discontinuous Galerkin Methods*. Springer, New York, 2008.

[89] H. Hetzler. On moving continua with contacts and sliding friction: Modeling, general properties and examples. *International Journal of Solids and Structures*, 46(13):2556–2570, 2009.

[90] V. Hodor, D. Birle, L. Nascutiu, and I. Deac. Aeroacoustics – Noise prediction by using "LES" for signal processing. *Energy Procedia*, 112:322–329, 2017.

[91] G. Hou, J. Wang, and A. Layton. Numerical methods for fluid-structure interaction – a review. *Communications in Computational Physics*, 12(2):337–377, 2012.

[92] M. S. Howe. *Acoustics of Fluid-Structure Interactions*. Cambridge Monographs on Mechanics. Cambridge University Press, Cambridge, 1998.

[93] M. S. Howe. *Theory of vortex sound*. Cambridge texts in applied mathematics. Cambridge University Press, Cambridge, New York, 2003.

[94] F. Q. Hu. Development of PML absorbing boundary conditions for computational aeroacoustics: A progress review. *Computers & Fluids*, 37(4):336–348, 2008.

[95] F. Q. Hu, M. Y. Hussaini, and P. Rasetarinera. An analysis of the discontinuous Galerkin method for wave propagation problems. *Journal of Computational Physics*, 151(2):921–946, 1999.

[96] S. C. Huang and W. Soedel. Effects of coriolis acceleration on the free and forced inplane vibrations of rotating rings on elastic foundation. *Journal of sound and vibration*, 115(2):253–274, 1987.

[97] A. Huerta and F. Casadei. New ALE applications in non-linear fast-transient solid dynamics. *Engineering Computations*, 11(4):317–345, 1994.

[98] A. Hüppe and M. Kaltenbacher. Spectral finite elements for computational aeroacoustics using acoustic perturbation equations. *Journal of Computational Acoustics*, 20(02):1240005, 2012.

[99] C. R. S. Ilário, M. Azarpeyvand, V. Rosa, R. H. Self, and J. R. Meneghini. Prediction of jet mixing noise with Lighthill's acoustic analogy and geometrical acoustics. *The Journal of the Acoustical Society of America*, 141(2):1203–1213, 2017.

[100] F. B. Jensen, W. A. Kuperman, M. B. Porter, and H. Schmidt. *Computational Ocean Acoustics*. Springer, New York, 2011.

[101] S. V. Joubert, M. Y. Shatalov, and C. E. Coetzee. Using fourier series to analyse mass imperfections in vibratory gyroscopes. *Journal of Symbolic Computation*, 61–62:116–127, 2014.

[102] S. V. Joubert, M. Y. Shatalov, and T. H. Fay. Rotating structures and Bryan's effect. *American Journal of Physics*, 77(6):520–525, 2009.

[103] B. Kaltenbacher, M. Kaltenbacher, and I. Sim. A modified and stable version of a perfectly matched layer technique for the 3-d second order wave equation in time domain with an application to aeroacoustics. *Journal of Computational Physics*, 235:407–422, 2013.

[104] M. Kaltenbacher. *Computational Acoustics*. Springer International Publishing, Cham, 2018.

[105] M. Kaltenbacher, M. Escobar, S. Becker, and I. Ali. Computational aeroacoustics based on Lighthill's acoustic analogy. In S. Marburg and B. Nolte, editors, *Computational Acoustics of Noise Propagation in Fluids – Finite and Boundary Element Methods*, pages 115–142. Springer, Berlin, Heidelberg, 2008.

[106] S. A. Karabasov, M. Z. Afsar, T. P. Hynes, A. P. Dowling, W. A. McMullan, C. D. Pokora, G. J. Page, and J. J. McGuirk. Jet noise: Acoustic analogy informed by large eddy simulation. *AIAA Journal*, 48(7):1312–1325, 2010.

[107] A. Kierkegaard, S. Allam, G. Efraimsson, and M. Åbom. Simulations of whistling and the whistling potentiality of an in-duct orifice with linear aeroacoustics. *Journal of Sound and Vibration*, 331(5):1084–1096, 2012.

[108] T. Kiesel. *Flexible multi-body simulation of a complex rotor system using 3D solid finite elements*. PhD thesis, Technical University of Munich, Munich, 2017.

[109] T. Kiesel and S. Marburg. Simulation of mode-locking phenomena in a complex nonlinear rotor system using 3D solid finite elements. *Proceedings of the Institution of Mechanical Engineers, Part C: Journal of Mechanical Engineering Science*, 230(6):959–973, 2016.

[110] B. Kirchgäßner. Finite elements in rotordynamics. *Procedia Engineering*, 144:736–750, 2016.

[111] M. Klaerner, M. Wuehrl, L. Kroll, and S. Marburg. FEA-based methods for optimising structure-borne sound radiation. *Mechanical Systems and Signal Processing*, 89:37–47, 2017.

[112] D. W. Kurtz and J. E. Marte. A review of aerodynamic noise from propellers, rotors, and lift fans. Technical Report NASA-CR-107568; JPL-TR-32-1462, Jet Propulsion Lab., California Institute of Technology, 1970.

[113] H. Lamb and R. V. Southwell. The vibrations of a spinning disk. *Proceedings of the Royal Society of London. Series A*, 99(699):272–280, 1921.

[114] P. Langer, A. Hoppe, C. Guist, and S. Marburg. From theory to three-dimensional finite element models: An innovative method for validation. In *SAE Technical Paper*. SAE International, 2018.

[115] P. Langer, M. Maeder, C. Guist, M. Krause, and S. Marburg. More than six elements per wavelength: The practical use of structural finite element models and their accuracy in comparison with experimental results. *Journal of Computational Acoustics*, 25(04):1750025, 2017.

[116] P. Langer, K. Sepahvand, C. Guist, J. Bär, A. Peplow, and S. Marburg. Matching experimental and three dimensional numerical models for structural vibration problems with uncertainties. *Journal of Sound and Vibration*, 417:294–305, 2018.

[117] H. Lee and R. Singh. Acoustic radiation from out-of-plane modes of an annular disk using thin and thick plate theories. *Journal of Sound and Vibration*, 282(1):313–339, 2005.

[118] M. R. Lee and R. Singh. Analytical formulations for annular disk sound radiation using structural modes. *The Journal of the Acoustical Society of America*, 95(6):3311–3323, 1994.

[119] G. Legendre. *Rayonnement acoustique dans un fluide en écoulement: analyse mathématique et numérique de l'équation de Galbrun*. PhD thesis, Université Pierre et Marie Curie, Paris, 2003.

[120] B. Li and Z. Zhang. Research on the effect of yield strength of circular saw blade on roll tensioning process. *Journal of Wood Science*, 63(2):140–146, 2017.

[121] B. Li and Z. Zhang. Tensioning effect modeling of circular saw blade after multi-spot pressure tensioning process. *Advances in Mechanical Engineering*, 9(12):1687814017740476, 2017.

[122] X. Li, M. Jiang, J. Gao, D. Lin, L. Liu, and X. Li. Recent advances of computational aeroacoustics. *Applied Mathematics and Mechanics*, 36(1):131–140, 2015.

[123] M. J. Lighthill. On sound generated aerodynamically I. General theory. *Proceedings of the Royal Society of London. Series A*, 211(1107):564–587, 1952.

[124] M. J. Lighthill. On sound generated aerodynamically II. Turbulence as a source of sound. *Proceedings of the Royal Society of London. Series A*, 222(1148):1–32, 1954.

[125] W. Y. Liu. A review on wind turbine noise mechanism and de-noising techniques. *Renewable Energy*, 108:311–320, 2017.

[126] I. Lopez, R. E. A. Blom, N. B. Roozen, and H. Nijmeijer. Modelling vibrations on deformed rolling tyres – a modal approach. *Journal of Sound and Vibration*, 307(3):481–494, 2007.

[127] Y. Mao, Y. Gu, D. Qi, and H. Tang. An exact frequency-domain solution of the sound radiated from the rotating dipole point source. *The Journal of the Acoustical Society of America*, 132(3):1294–1302, 2012.

[128] S. Marburg and B. Nolte. *Computational Acoustics of Noise Propagation in Fluids – Finite and Boundary Element Methods*. Springer, Berlin, Heidelberg, 2008.

[129] S. Marburg and S. Schneider. Influence of element types on numeric error for acoustic boundary elements. *Journal of Computational Acoustics*, 11(03):363–386, 2003.

[130] G. A. Maugin. *Non-Classical Continuum Mechanics*. Springer, Singapore, 2017.

[131] F. P. Mechel. *Formulas of Acoustics*. Springer-Verlag, Berlin, Heidelberg, 2nd edition, 2008.

[132] A. Minotti, J.-Ph. Brazier, and F. Simon. Extension of the Eulerian-Lagrangian description to nonlinear perturbations in an arbitrary inviscid flow. *Journal of Sound and Vibration*, 331:4537–4553, 2012.

[133] L. Moheit and S. Marburg. Normal modes and modal reduction in exterior acoustics. *Journal of Theoretical and Computational Acoustics*, 26(03):1850029, 2018.

[134] H. J.-P. Morand and R. Ohayon. *Fluid-Structure Interaction: Applied Numerical Methods*. Wiley-Masson Series Research in Applied Mathematics. Wiley, Chichester, Masson, 1995.

[135] C. D. Mote. Free vibration of initially stressed circular disks. *Journal of Engineering for Industry*, 87(2):258–264, 1965.

[136] C. D. Mote and L. T. Nieh. On the foundation of circular-saw stability theory. *Wood and Fiber Science*, 5(2):160–169, 2007.

[137] C. D. Mote and R. Szymani. A review report on principal developments in thin circular saw vibration and control research. *Holz als Roh-und Werkstoff*, 35(5):189–196, 1977.

[138] C.-D. Munz, M. Dumbser, and S. Roller. Linearized acoustic perturbation equations for low Mach number flow with variable density and temperature. *Journal of Computational Physics*, 224(1):352–364, 2007.

[139] R. E. Musafir. Predicting aerodynamic noise – which model to use and when? In *SAE Technical Paper Series*. SAE International, Warrendale, 2010.

[140] U. Nackenhorst. The ALE-formulation of bodies in rolling contact: Theoretical foundations and finite element approach. *Computer Methods in Applied Mechanics and Engineering*, 193(39):4299–4322, 2004.

[141] U. Nackenhorst and M. Brinkmeier. On the dynamics of rotating and rolling structures. *Archive of Applied Mechanics*, 78(6):477–488, 2008.

[142] M. Naď, R. Ďuriš, and T. Nánási. Prediction of modal properties of circular disc with pre-stressed fields. *MATEC Web of Conferences*, 157:02034, 2018.

[143] A. Nandi. On computation of response of a rotor in deformed configuration using three-dimensional finite elements. *Communications in Numerical Methods in Engineering*, 19(3):179–195, 2003.

[144] A. Nandi and S. Neogy. Modelling of rotors with three-dimensional solid finite elements. *The Journal of Strain Analysis for Engineering Design*, 36(4):359–371, 2001.

[145] P. B. Nelson. Sound in the classroom: Why children need quiet. *ASHRAE journal*, 45(2):22, 2003.

[146] B. Nennig, M. Ben Tahar, and E. Perrey-Debain. A displacement-pressure finite element formulation for analyzing the sound transmission in ducted shear flows with finite poroelastic lining. *The Journal of the Acoustical Society of America*, 130(1):42–51, 2011.

[147] B. Nennig, J.-D. Chazot, E. Perrey-Debain, and M. Ben Tahar. Influence of solid phase elasticity in poroelastic liners submitted to grazing flows. *The Journal of the Acoustical Society of America*, 123(5):3571–3571, 2008.

[148] N. Nicoletti, E. Aubry, D. Fendeleur, and M. Renner. A finite element model for the analysis of roll burnishing. *Holz als Roh-und Werkstoff*, 55(2–4):183–187, 1997.

[149] G. L. Nigh and M. D. Olson. Finite element analysis of rotating disks. *Journal of Sound and Vibration*, 77(1):61–78, 1981.

[150] H. Ouyang, W. Nack, Y. Yuan, and F. Chen. Numerical analysis of automotive disc brake squeal: a review. *International Journal of Vehicle Noise and Vibration*, 1(3–4):207–231, 2005.

[151] R. G. Parker and C. D. Mote. Asymmetric tensioning of circular saws. *Holz als Roh- und Werkstoff*, 47(4):143–151, 1989.

[152] S. E. Perez Bergliaffa, K. Hibberd, M. Stone, and M. Visser. Wave equation for sound in fluids with vorticity. *Physica D: Nonlinear Phenomena*, 191(1):121–136, 2004.

[153] C. J. Peyret. Acoustic propagation in the presence of an arbitrary flow. *The Journal of the Acoustical Society of America*, 103(5):2840–2840, 1998.

[154] A. D. Pierce. Wave equation for sound in fluids with unsteady inhomogeneous flow. *The Journal of the Acoustical Society of America*, 87(6):2292–2299, 1990.

[155] A. D. Pierce. *Acoustics*. Springer International Publishing, Cham, 3rd edition, 2019.

[156] B. Poirée. Les équations de l'acoustique linéaire et non-linéaire dans un écoulement de fluide parfait. *Acta Acustica united with Acustica*, 57:5–25, 1985.

[157] M. A. Poletti and P. D. Teal. Comparison of methods for calculating the sound field due to a rotating monopole. *The Journal of the Acoustical Society of America*, 129(6):3513–3520, 2011.

[158] A. Pont, O. Guasch, J. Baiges, R. Codina, and A. van Hirtum. Computational aeroacoustics to identify sound sources in the generation of sibilant /s/. *International Journal for Numerical Methods in Biomedical Engineering*, 35(1):e3153, 2019.

[159] D. C. Pridmore-Brown. Sound propagation in a fluid flowing through an attenuating duct. *Journal of Fluid Mechanics*, 4(4):393–406, 1958.

[160] M. S. Qatu, M. K. Abdelhamid, J. Pang, and G. Sheng. Overview of automotive noise and vibration. *International Journal of Vehicle Noise and Vibration*, 5(1–2):1–35, 2009.

[161] S. Retka. *Numerische Umsetzung der Galbrun-Gleichung zur Modalanalyse strömender Medien in Außenraumproblemen unter Einsatz finiter und infiniter Elemente*. PhD thesis, Technische Universität Dresden, Dresden, 2012.

[162] S. Retka, L. Hervella-Nieto, and S. Marburg. Comparison of pressure and displacement formulations for finite elements in linear time-harmonic acoustics. *Computers & Structures*, 151:49–57, 2015.

[163] S. Retka and S. Marburg. An infinite element for the solution of Galbrun equation. *ZAMM – Journal of Applied Mathematics and Mechanics*, 93:154–162, 2013.

[164] R. Rodríguez and D. Santamarina. Galbrun's equation solved by a first order characteristics method. In *Numerical Mathematics and Advanced Applications*, pages 1212–1219. Springer, Berlin, Heidelberg, 2006.

[165] T. D. Rossing. *Springer Handbook of Acoustics*. Springer, New York, 2014.

[166] J. Salençon. *Handbook of Continuum Mechanics*. Springer-Verlag, Berlin, Heidelberg, 2001.

[167] G. S. Schajer. Understanding saw tensioning. *Holz als Roh- und Werkstoff*, 42(11):425–430, 1984.

[168] G. S. Schajer and C. D. Mote. Analysis of roll tensioning and its influence on circular saw stability. *Wood Science and Technology*, 17(4):287–302, 1983.

[169] J. H. Schmidt and M. Klokker. Health effects related to wind turbine noise exposure: A systematic review. *PloS one*, 9(12):e114183, 2014.

[170] S. Schoder and M. Kaltenbacher. Hybrid aeroacoustic computations: State of art and new achievements. *Journal of Theoretical and Computational Acoustics*, 27(04):1950020, 2019.

[171] C. Schram. A boundary element extension of Curle's analogy for non-compact geometries at low-Mach numbers. *Journal of Sound and Vibration*, 322(1):264–281, 2009.

[172] T. K. Sengupta and Y. G. Bhumkar. *Computational Aerodynamics and Aeroacoustics*. Springer, Singapore, 2020.

[173] J.-H. Seo and Y. J. Moon. Perturbed compressible equations for aeroacoustic noise prediction at low Mach numbers. *AIAA Journal*, 43(8):1716–1724, 2005.

[174] M. Smith. *ABAQUS/Standard User's Manual, Version 6.14*. Dassault Systèmes Simulia Corp., Providence, 2017.

[175] A. Sommerfeld. *Partial Differential Equations in Physics*. Pure and Applied Mathematics. Academic Press Inc., New York, 1949.

[176] M. Stache, M. Guettler, and S. Marburg. A precise non-destructive damage identification technique of long and slender structures based on modal data. *Journal of Sound and Vibration*, 365:89–101, 2016.

[177] Z. Sun, J. A. Carrillo, and C.-W. Shu. A discontinuous Galerkin method for nonlinear parabolic equations and gradient flow problems with interaction potentials. *Journal of Computational Physics*, 352:76–104, 2018.

[178] D. L. Sutliff. Advanced noise control fan: A 20-year retrospective of contributions to aeroacoustics research. Technical Report NASA/SP-2019-643, E-19643, GRC-E-DAA-TN64107, NASA Glenn Research Center, Cleveland, 2019.

[179] C. K. W. Tam. Computational aeroacoustics: Issues and methods. *AIAA Journal*, 33(10):1788–1796, 1995.

[180] D. J. Thompson and C. J. C. Jones. A review of the modelling of wheel/rail noise generation. *Journal of Sound and Vibration*, 231(3):519–536, 2000.

[181] I. Tolstoy. The theory of waves in stratified fluids including the effects of gravity and rotation. *Reviews of Modern Physics*, 35:207–230, 1963.

[182] F. Treyssède and M. Ben Tahar. Jump conditions for unsteady small perturbations at fluid-solid interfaces in the presence of initial flow and prestress. *Wave Motion*, 46:155–167, 2009.

[183] F. Treyssède, G. Gabard, and M. Ben Tahar. A mixed finite element method for acoustic wave propagation in moving fluids based on an Eulerian-Lagrangian description. *The Journal of Acoustical Society of America*, 113:705–716, 2003.

[184] P. Vila, A. Rovira, J. Fayos, and L. Baeza. Dynamic model of a railway wheelset for corrugation problem analysis. *Noise & Vibration Worldwide*, 40(11):10–17, 2009.

[185] X. Wang and K.-J. Bathe. Displacement/pressure based mixed finite element formulations for acoustic fluid-structure interaction problems. *International Journal for Numerical Methods in Engineering*, 40:2001–2017, 1997.

[186] T. Weidauer and K. Willner. Model reduction of gyroscopic systems in ALE formulation with and without non-linearities. *PAMM*, 18(1):e201800216, 2018.

[187] T. Weidauer and K. Willner. Reduced order modelling for non-linear rotating systems in ALE formulation with contact. In G. Kerschen, editor, *Nonlinear Dynamics, Volume 1*, pages 287–302. Springer International Publishing, Cham, 2019.

[188] H.-C. Wu. *Continuum, mechanics, and plasticity*, volume 3 of *CRC series : modern mechanics and mathematics*. Chapman & Hall/CRC, Boca Raton, London, New York, Washington D. C., 2005.

[189] Q. Zhang and T. Hisada. Studies of the strong coupling and weak coupling methods in FSI analysis. *International Journal for Numerical Methods in Engineering*, 60(12):2013–2029, 2004.

[190] M. Ziefle and U. Nackenhorst. A new update procedure for internal variables in an ALE-description of rolling contact. *PAMM*, 5(1):71–74, 2005.

[191] O. C. Zienkiewicz and P. Bettess. Fluid-structure dynamic interaction and wave forces. An introduction to numerical treatment. *International Journal for Numerical Methods in Engineering*, 13(1):1–16, 1978.

[192] O. C. Zienkiewicz, R. L. Taylor, and P. Nithiarasu. *The finite element method for fluid dynamics*. Butterworth-Heinemann, Oxford, Waltham, 7th edition, 2014.

[193] S. Zörner, P. Šidlof, A. Hüppe, and M. Kaltenbacher. Flow and acoustic effects in the larynx for varying geometries. *Acta Acustica united with Acustica*, 102(2):257–267, 2016.

Part II

Appended Publications

The appended publication was accepted in the international Journal of Theoretical and Computational Acoustics on May 24, 2020 and can be found using the following citation:

M. Maeder, G. Gabard and S. Marburg. 90 Years of Galbrun's Equation: An Unusual Formulation for Aeroacoustics and Hydroacoustics in Terms of the Lagrangian Displacement. *Journal of Theoretical and Computational Acoustics*, 28(4):2050017, 2020, DOI:10.1142/S2591728520500176.

Solving Galbrun's Equation with a Discontinuous Galerkin Finite Element Method

Marcus Maeder[1], Andrew Peplow[2], Maximilian Meindl[1], Steffen Marburg[1]

[1] Technical University of Munich, Munich, Germany. Marcus.Maeder@tum.de
[2] Zayed University, Abu Dhabi Campus, Abu Dhabi

Colour Figures: Figures in colour are given in the online version

Summary

Over many years, scientists and engineers have developed a broad variety of mathematical formulations to investigate the propagation and interactions with flow of flow-induced noise in early-stage of product design and development. Beside established theories such as the linearized Euler equations (LEE), the linearized Navier–Stokes equations (LNSE) and the acoustic perturbation equations (APE) which are described in an Eulerian framework, Galbrun utilized a mixed Lagrange–Eulerian framework to reduce the number of unknowns by representing perturbations by means of particle displacement only. Despite the advantages of fewer degrees of freedom and the reduced effort to solve the system equations, a computational approach using standard continuous finite element methods (FEM) suffers from instabilities called spurious modes that pollute the solution.

In this work, the authors employ a discontinuous Galerkin approach to overcome the difficulties related to spurious modes while solving Galbrun's equation in a mixed and pure displacement based formulation. The results achieved with the proposed approach are compared with results from previous attempts to solve Galbrun's equation. The numerical determination of acoustic modes and the identification of vortical modes is discussed. Furthermore, case studies for a lined-duct and an annulus supporting a rotating shear-flow are investigated.

PACS no. 43.28.Bj

1. Introduction

Acoustic noise reduction, which is a wide matter of concern in industry, calls for a better understanding of the complex phenomena that occur when an acoustic wave propagates in a mean flow. A majority of research performed in aeroacoustics and computer aided engineering (CAE) has been aimed at the aircraft noise community, arguably starting by the work of Lighthill, [25]. Commonly, aircraft noise research traditionally focusses on high Mach number and high Reynolds number free-field jet flows. In high-speed jets, noise generation is considered to be of quadrupole type, caused by unsteady nonlinear mechanisms. The methodologies developed in CAE have rejected this, in their focus on time-domain solutions of the non-linear Navier–Stokes equations, either as Direct Numerical Simulations (DNS) where no turbulence models are included, to turbulence models such as Reynolds-Averaged Navier-Stokes (RANS) and Large Eddy Simulation (LES) codes. In wall-bound and internal flows at low Mach numbers, the sound generating mechanisms are however governed by fundamentally different physics than that of free-field jet noise. When an air flow is obstructed by a change of geometry, such as a sharp corner or a bifurcation, flow instabilities and vortices are generated. As

these vortices impinge on boundaries, sound impulses are generated.

A less explored field of aeroacoustics is that of pure wave propagation in inhomogeneous media with arbitrary mean flows, as this is disconnected from the noise generation processes. The conceptual difference in the simulation of sound generation and sound propagation is large enough to justify a treatment of the two as separate topics. In regions outside of acoustic sources, the acoustic quantities are often small in comparison to the flow-field quantities. In many cases, it can be assumed that the flow-field affects the sound waves, whereas the sound waves do not induce the flow-field. Thus, the perturbations about the mean flow are often small enough to justify linearization. This enables a two-stage treatment of the acoustic wave propagation: firstly, the mean flow can be calculated without the need to consider any acoustic waves, and secondly, the sound waves can be calculated as perturbations about the mean flow-field. Also, as a consequence of the linearization, a frequency domain approach can be taken. A main benefit of a frequency-domain approach, as opposed to a time-domain approach, is the significant reduction of computational time in case of harmonic excitation. Since most research efforts have been aimed at jet noise generation, where unsteady simulations are needed, only a few studies on frequency-domain aeroacoustics are available.

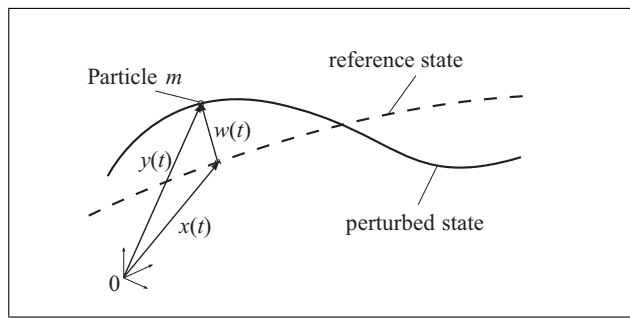Currently, different methods such as the Linearized Euler Equation (LEE) [4], the Linearized Navier–Stokes

Figure 1. Frame of reference state and perturbed state.

Equation (LNSE), see Kierkegaard et al. [27] or the Acoustic Perturbation Equation (APE), see Ewert and Schröder [15], Munz *et al.* [32], Hüppe and Kaltenbacher [22] and Zörner *et al.* [43], are utilized besides the well known acoustic analogies by Lighthill [24, 25], Curle [11] and Ffowcs William and Hawkings [16] for solving aeroacoustic tasks such as wave propagation in moving fluid as part of CAE.

Galbrun [18] proposed a displacement based description in a Lagrange–Eulerian mixed frame for analyzing the propagation of sound waves in moving fluids. Since only the displacement field is the unknown quantity, Galbrun's equation represents a potent alternative to the methods mentioned above. Among the possibility of reducing the degrees of freedom, boundary conditions can naturally be expressed, i.e. in terms of boundary displacement.

Despite the positive aspects of Galbrun's equation, socalled spurious modes exist when extracting the eigenvalues of the associated boundary value problem utilizing a standard, unstabilized finite element method. The same holds for the LNSE and LEE formulation. These spurious modes possibly pollute the solution when using the standard continuous Galerkin discretization [20, 13]. Various attempts have been published in the literature for handling the problems associated with spurious modes, cf. [5, 35, 41, 42]. The work presented in this paper aims as a step to the development of a simulation methodology for alternative strategies for flow acoustics.

Bécache *et al.* [2] and Bonnet *et al.* [6, 5] have demonstrated that the direct displacement-based formulation associated with Galbrun's equation may produce erroneous or spurious solutions if the finite element method is based on simple continuous finite elements. In particular, it is proposed in [5] that a regularized reformulation of the variational equation for uniform and shear flows can produce robust solutions by damping them out. Other authors, such as Dietzsch *et al.* [12], have used finite element functions which can shift, but not remove, the location of spurious solutions to higher frequencies and higher damping values. In this paper, a formulation based on the displacement variables is presented which minimizes the appearance of spurious solutions without the need of a regularized reformulation.

The paper is organized as follows: Section 2 sets up the Galbrun equations from basic principles which leads to Section 3 a description of the numerical scheme. The authors utilize a discontinuous Galerkin (DG) method, cf. [9, 10, 1, 39], for discretizing Galbrun's equation for which a time-harmonic behavior is assumed. To account for inter-element fluxes, a local Lax–Friedrichs flux, cf. [21], is used and discussed. In order to highlight the benefits of the proposed method, solutions are compared to the state of the art methods such as LNSE and LEE as case studies in Section 3 which includes a discussion on the influence of an appropriate flux factor. Further, a filtering (Lagrange multiplier) technique is applied to exclude non relevant modes from the solution space. Finally, in Section 4 examples including a lined duct and a circulating flow within an annulus are investigated.

2. Theory and Numerical Method

In this section, the fundamental principles for deriving Galbrun's equation are outlined. For additional insight, the reader is referred to the literature [18, 41, 33, 6, 12, 19, 20, 23, 34]. In order to give a comprehensive description, some mathematical fundamentals are required. Hereafter, a Cartesian coordinate system defined by the orthonormal directions '1' and '2' is used, such that a two-dimensional space is considered. Further, a vector component description together with Einstein's summation convention is assumed to indicate component summation for repeated indices. Hereafter, the domain of interest is $\Omega_F \subset \mathbb{R}^2$ which is bounded by a closed surface, Γ_F.

2.1. Lagrange-Eulerian frame

For deriving Galbrun's equation, one has to be familiar with the concept of a mixed Lagrange-Eulerian frame in the view of continuum mechanics and the associated appropriate balance equations. Despite the fact that the theory to derive Galbrun's equation is well published in the literature, the authors present the basic principles for better readability.

Two distinguished states are considered. In the first state namely the perturbed state, any given particle is defined by its spatial coordinate position $\boldsymbol{y}(t)$ where in the second state or the unperturbed state or reference state, the same particle takes the position $\boldsymbol{x}(t)$, cf. Figure 1. The vector components of the Lagrangian displacement $\boldsymbol{w}(t)$ are defined as the difference of these two states, i.e.

$$w_l(t) = y_l(t) - x_l(t). \tag{1}$$

Further, any given field quantity Φ takes the form

$$\Phi(y_l, t) = \Phi_0(y_l) + \Phi'(y_l, t) \tag{2}$$

in the Eulerian frame with the Eulerian perturbation $\Phi'(y_l, t)$ and

$$\Phi(y_l, t) = \Phi_0(x_l) + \tilde{\Phi}(x_l, t) \tag{3}$$

in the Lagrangian frame with the corresponding Lagrangian perturbation $\tilde{\Phi}(x_l, t)$, cf. Poirée [33]. Since the

application of Galbrun's equation is basically a linear perturbation procedure, the mean flow quantities, Φ_0, can be calculated from an adequate preceding stationary boundary value problem. It must be noted that these mean flow quantities Φ_0 are described specifically in Eulerian coordinates, cf. Brazier [7]. Combining equations (1)–(3) while assuming that the mean values Φ_0 are slowly varying, i.e. associated gradients in time and space are integrable continuous functions. Together with a Taylor expansion up to the linear terms, one identifies the relation between Eulerian and Lagrangian perturbations

$$\Phi'(y_l, t) = \tilde{\Phi}(x_l, t) - w_j\big(\Phi_0(x_l, t)\big)_{,j}, \tag{4}$$

where $()_{,j} = \nabla() = \frac{\partial()}{\partial x_j}$ represents the Nabla-Operator with the corresponding spatial derivative in the j-direction. From equation (4), it is apparent that if the spatial gradient of the mean values vanishes, the Eulerian and the Lagrangian perturbations are equal, see [31].

2.2. Galbrun's equation formulation

The acoustic radiation of a source produces a small perturbation of the physical quantities such as pressure and density. The propagation of that small perturbation is governed by the Galbrun equation which is a linear equation whose unknown $\mathbf{w}$ is the perturbation of displacement. The well known conservation equations of fluid dynamics, namely the mass, momentum and energy balance equations in an Eulerian frame are used to derive Galbrun's equation. Assuming small perturbations, the displacement based expression is formulated. Further, it is assumed that the fluid of interest is a perfect inviscid gas with adiabatic thermodynamic properties (i.e. isentropic material behavior). Under these assumptions, Galbrun's equation is stated, cf. the references [18, 41, 7, 31].

$$\rho_0 \frac{\mathrm{D}^2 w_k}{\mathrm{D}t^2} - p_{0,l} w_{l,k} + p_{0,k} w_{l,l} - \big(c_0^2 \rho_0 w_{l,l}\big)_{,k} = 0, \tag{5}$$
$$k, l = 1, 2, 3, \quad \text{in} \quad \Omega_F,$$

and

$$w_j n_j = 0, \quad \text{on} \quad \Gamma_F. \tag{6}$$

In addition, appropriate initial boundary for $w_j(t = 0)$ and $\mathrm{D}(w_j)/\mathrm{D}t(t = 0)$ in Ω_F and on Γ_F must be stated that fulfill the boundary conditions on Γ_F.

Further,

$$\frac{\mathrm{D}()}{\mathrm{D}t} = \frac{\partial()}{\partial t} + v_{0k}()_{,k} \quad \text{and} \tag{7}$$
$$\frac{\mathrm{D}^2()}{\mathrm{D}t^2} = \frac{\partial^2()}{\partial t^2} + \frac{\partial(v_{0k})}{\partial t}()_{,k} + 2v_{0k}\frac{\partial}{\partial t}()_{,k} + v_{0k}v_{0l}()_{,lk},$$

where ρ_0 represents the mean flow mass density, p_0 the mean flow pressure, c_0 the speed of sound and v_{0k} the mean flow velocity in the k-direction, respectively. The surface normal vector $\mathbf{n}$ on Γ_F is pointing outward of the domain Ω_F.

Following the arguments considered in the works by Gabard *et al.* [17], Treyssède et. al [41, 40] and Wang *et al.* [42], a mixed formulation can be achieved by introducing a Lagrangian pressure perturbation

$$\tilde{p} = -c_0^2 \rho_0 w_{l,l}. \tag{8}$$

Following this, combining equations (5) and equation (8) yields

$$\rho_0 \frac{\mathrm{D}^2 w_k}{\mathrm{D}t^2} - p_{0,l} w_{k,l} + p_{0,k} w_{l,l} + \tilde{p}_{,k} = 0_k \quad \text{in} \quad \Omega_F, \tag{9}$$

$$\tilde{p} + c_0^2 \rho_0 w_{l,l} = 0. \quad \text{in} \quad \Omega_F \tag{10}$$

To revert the displacement field back to the well known acoustic pressure p' in the associated Eulerian frame, Expressions (4) and (8) are required. Note that the assumptions of slowly varying mean flow quantities such as ρ_0, p_0 and v_{0k} must still hold.

Further, a time harmonic dependency is assumed to convert the Galbrun equation from the time to the frequency domain, i.e. any given quantity takes the form $\phi(x, t) = \Re\big(\hat{\phi}(x)e^{-\mathrm{j}\omega t}\big)$, while j depicts the imaginary unit, $\omega = 2\pi f$ represents the angular frequency and $\hat{\phi}(x)$ the complex amplitude. Hereafter, the hat symbol is omitted to improve readability. It is thought that all quantities and fields are in a time harmonic regime. Furthermore, the operator of the material time derivative reduces to

$$\frac{\mathrm{D}()}{\mathrm{D}t} = -\mathrm{j}\omega() + v_{0k}()_{,k}.$$

In equation (6), rigid boundary conditions representing hard walls have been introduced. To account for more complicated boundary conditions, we present an admittance boundary condition for the displacement based Galbrun equation, see [30, 29],

$$v'_f - v'_s = Y p', \tag{11}$$

expressed in Eulerian quantities, where v'_f is the normal component of the Eulerian fluid velocity perturbation, v'_s the normal component of the Eulerian structure velocity perturbation, $\bar{Y} = Y/(\rho_0 c_0)$ the boundary admittance and its normalized part $\bar{Y}$ and p' the Eulerian acoustic pressure perturbation. Applying these and assuming zero structural velocity $v'_s = 0$, the equivalent admittance boundary condition for Galbrun's equation may be derived. Making use of equation (4), this leaves a relation between admittance and displacement

$$\big(-\mathrm{j}\omega w_l + v_{0k} w_{l,k} - w_k v_{0l,k}\big)n_l \tag{12}$$
$$= Y\big(-c_0^2 \rho_0 w_{l,l} - w_l p_{0,l}\big).$$

Note that $\tilde{v}_k = \mathrm{D}(w_k)/\mathrm{D}t$ has been used for the relation between the Lagrangian velocity perturbation $\tilde{v}_k$, when applying equation (4), and the Lagrangian displacement. If the mean pressure p_0 is constant and the flow velocity v_{0k} is constant and orthogonal to the surface normal vector n_l, equation (12) reduces to a familiar form for boundary admittance

$$\mathrm{j}\omega w_l n_l = Y c_0^2 \rho_0 w_{l,l}, \tag{13}$$

which is in agreement with Dietzsch *et al.* [12].

2.3. Numerical method

Discontinuous Galerkin finite element methods (DG-FEM) combine favourable features of finite element methods (FEM) and finite volume methods (FVM) with strong mathematical foundation. DG-FEM possess a number of favourable properties especially in hydrodynamic, uniform and non-uniform flow problems. They are robust and high-order accurate and are able to capture physical phenomena common to mixed finite element problems other methods cannot reach. For this problem we make use of DG-FEM to overcome an inherent issue.

Generally, DG-FEM combines the flexibility of introducing high-order FEM schemes with the flexibility of FVM to formulate numerical schemes locally, which can reflect flow, for example. However, finite volume methods are often too inaccurate and diffusive when applied, especially, to wave propagation problems. The basic FVM is a form of the lowest-order DG-FEM. So, it makes sense to increase accuracy but keep the conservation part by developing DG-FEM further.

Considering Figure 2, it is clear that the global approximation $u(x)$ is not well-defined at the boundaries of each element. As Figure 2 demonstrates, at each node x, two solutions exist belonging to the respective adjacent elements so that both, a left element D_k and a right element D_{k+1} evaluate the approximation $u(x)$. Since we do not enforce continuity over the boundaries of the elements as in standard finite element methods, we are not guaranteed that $u_{il}(x) = u_{ir}(x)$, and thus, it appears $u(x)$ is not uniquely defined. To establish a connection between elements, we introduce a flux condition. For this study, a Lax-Friedrich scheme, which blends between central and upwind flux, is chosen. This defines the DG-FEM formulation. For a detailed description of the numerical scheme and possible stabilization techniques, the authors refer to the literature [1, 10, 9, 39].

In this section, the finite element method utilized to solve Galbrun's equation is described. To do this, we first construct the weak form of Galbrun's equation with appropriate test functions that exist in a suitable mathematical space. We define the inner product as

$$(u, v)_{\Omega_F} = \int_{\Omega_F} u v \, d\Omega_F \qquad (14)$$

in the space of functions denoted by $L^2(\Omega_F)$ where all functions are square integrable over the domain Ω_F. In the weak formulation, this inner product is used to define a local inner product and norm such that

$$(u, v)_{D_F^k} = \int_{D_F^k} u v \, dD_F^k \quad \text{and} \quad \|u\|^2_{D_F^k} = (u, u)_{D_F^k} \qquad (15)$$

with

$$\Omega_F \simeq \Omega_h = \bigcup_{k=1}^{K} D_F^k, \qquad (16)$$

where Ω_h represents the approximated domain due to the discretization procedure.
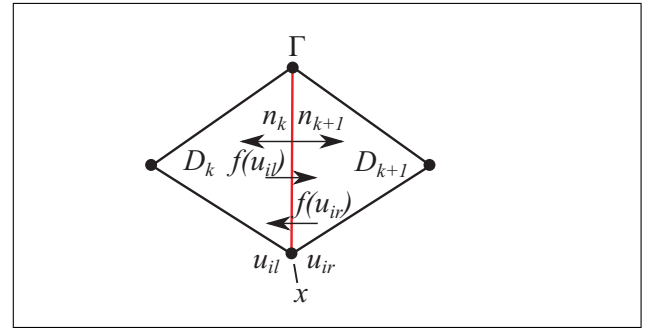
Figure 2. A Lax–Friedrichs flux is defined across a shared element boundary, shown as a red line Γ between the two elements D_k and D_{k+1}. Displacement across this boundary can be discontinuous, i.e. $u_{il} \neq u_{ir}$.

This allows the local unknowns to be discontinuous from one element D^k to the other.

$$f_{LF}(u_{il}, u_{ir}) = \frac{f(u_{il}) + f(u_{ir})}{2} + \frac{\alpha}{2} n \cdot (u_{il} - u_{ir}) \qquad (17)$$

To account for inter element fluxes, the Lax-Friedrichs-Flux, cf. Equation (17), is chosen, where the scaling factor α needs to be defined. For Galbrun's equation, the flux term scales with c_0^2. Therefore, in accordance to Hesthaven and Warburton [21], the flux constant α is set to $\alpha = 10^6$, see Section 3.4.

Figure 2 illustrates the definition of the Lax-Friedrichs-flux between two elements D_k and D_{k+1}, respectively. The flux in element D_k across the boundary Γ is denoted by $f(u_{il})$ and *vice versa* from element D_{k+1} across Γ with $f(u_{ir})$ where at the boundary the unknowns can take the value u_{il} in element D_k and u_{ir} in element D_{k+1}. The corresponding outward normal vectors are n_k and n_{k+1}.

Applying all the forgoing principles, the weak form of Galbrun's equation for each element domain Ω_h^e with boundaries Γ_h^e reads as

$$\int_{\Omega_h^e} \left(\rho_0 \frac{D^2 w_k}{Dt^2} - p_{0,l} w_{k,l} + p_{0,k} w_{l,l} \right. \qquad (18)$$
$$\left. - \left(c_0^2 \rho_0 w_{l,l} \right)_{,k} \right) \bar{w}_k^* \, d\Omega_h^e = 0,$$

with the piecewise discontinuous complex conjugated test functions $\bar{w}_k^*$. Expanding the material time derivative using equation (7) and simplifying $\partial(v_{0k})/\partial t = 0$, $\rho_{0,l} = 0$ and $p_{0,l} = 0$ results in

$$\int_{\Omega_h^e} \left(-\omega^2 w_k - 2j\omega v_{0l} w_{k,l} + v_{0j} v_{0l,j} w_{k,l} \right. \qquad (19)$$
$$\left. + v_{0j} v_{0l} w_{k,lj} - \left(c_0^2 w_{l,l} \right)_{,k} \right) \bar{w}_k^* \, d\Omega_h^e = 0.$$

After integrating by parts and utilizing Green's identity, the weak form can be rearranged as

$$\int_{\Omega_h^e} -\omega^2 w_k \bar{w}_k^* + 2j\omega (v_{0l} \bar{w}_k^*)_{,l} w_k$$
$$- (v_{0j} v_{0l,j} \bar{w}_k^*)_{,l} w_k - (v_{0j} v_{0l} \bar{w}_k^*)_{,j} w_{k,l}$$
$$+ c_0^2 w_{l,l} \bar{w}_{k,k}^* \, d\Omega_h^e \quad \ldots \qquad (20)$$

$$+ \int_{\Gamma_h^e} \Big(-(2j\omega v_{0l} - v_{0j}v_{0l,j})w_k\bar{w}_k^* \tag{21}$$

$$+ v_{0j}v_{0l}w_{k,j}\bar{w}_k^* - c_0^2 w_{k,k}\bar{w}_l^* \Big) n_l \, d\Gamma_h^e = 0.$$

In order to apply the discontinuous Galerkin method, the boundary integral in equation (20) does not vanish and accounts for inter-elemental fluxes. At this stage, any constraint condition such as the restriction to the rotational field of w, e.g. $\nabla \times w = 0$, can be easily integrated using a Lagrange multiplier λ_h in the form of

$$\int_{\Omega_h^e} \lambda_h^e (\nabla \times w)_h \bar{w}^* \, d\Omega_h^e = 0$$

$$\text{or} \quad \int_{\Omega_h^e} \lambda_h^e (e_{kmn} w_{m,n}) \bar{w}_k^* \, d\Omega_h^e = 0,$$

where e_{kmn} is known as the permutation tensor. For the remainder of this paper the Lagrange multiplier is discretized using piecewise discontinuous linear basis functions.

To demonstrate how the inter-elemental fluxes are set up, as an example, the last part of the boundary integral in equation (20) is reformulated according to the notation highlighted in Figure 2.

$$\int_{\Gamma_h^e} c_0^2 w_{k,k}\bar{w}_l^* n_l d\Gamma_h^e =$$

$$\int_{\Gamma_h^e} \Big(\frac{1}{2}c_0^2 \big((w_{1,1}+w_{2,2})_{il} + (w_{1,1}+w_{2,2})_{ir} \big) n_1$$

$$+ \frac{\alpha}{2}\big(w_{1il}-w_{1ir} \big) \Big) \big(\bar{w}_{1il}^* - \bar{w}_{1ir}^* \big) \tag{22}$$

$$\Big(\frac{1}{2}c_0^2 \big((w_{1,1}+w_{2,2})_{il} + (w_{1,1}+w_{2,2})_{ir} \big) n_2$$

$$\frac{\alpha}{2}\big(w_{2il}-w_{2ir} \big) \Big) \big(\bar{w}_{2il}^* - \bar{w}_{2ir}^* \big) d\Gamma_h^e.$$

Utilizing the well known approach of partial integration and discretizing the unknowns as well as the test functions according to Galerkin, a matrix formulation in the form of

$$\Big(-\omega^2 \big[M\big] + j\omega \big[D\big] + \big[C\big] \Big) \big[w\big] = 0 \tag{23}$$

can be achieved. $\big[M\big]$ represents the mass matrix and $\big[D\big]$, $\big[C\big]$ the damping and stiffness matrices, respectively. The system of equations is analyzed in terms of eigenvalues and eigenvectors using a Krylov subspace method where the size of the subspace is set to be twice as large as the number of eigenvalues of interest, cf. [8, 14, 37].

For this purpose, the software tool Comsol Multiphysics together with Matlab is used to set up the model as well as the system of equations and finally solve for eigenvalues and eigenvectors.

3. Finite element model

In this section, we present a parameter study to investigate the performance of applying a discontinuous Galerkin
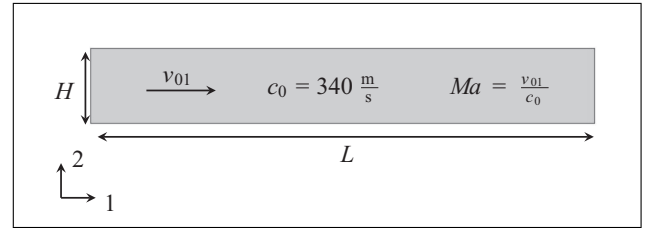
Figure 3. Model geometry for verification example, a bounded rectangular domain with hard-walls.

discretization method with different boundary conditions and approaches for filtering Galbrun's equation. The test is conducted on an purely academic test case where the results are compared to the conventional continuous Galerkin discretization method applied to the mixed and pure displacement based formulation of Galbruns' equation as well as the linearized Navier-Stokes equation and linearized Euler equation. Reference values are provided by the solution of the convected Helmholtz equation.

The no-flow case for Galbrun's equation was first studied in the 1970s [20] and was proved to exhibit spurious circulation or rotational modes. In the case spurious modes were solutions of the source-free problem associated with non-zero real-valued frequencies. Determined numerically, these modes could be shifted to higher frequencies by refining the mesh or by enforcing the numerical method to avoid these solutions [12]. It was not until Wang and Bathe [42] showed a mixed pressure–displacement formulation, using a certain type of finite element, could lead to numerical solutions without spurious modes.

For the no-flow case, a pure displacement formulation can make use of edge elements which are also known as Raviart–Thomas elements [3]. It was shown in [36] that they are of similar efficiency as Lagrangian elements when used for the pure pressure formulation. However, with mean-flow, a mixed formulation of Galbrun's equation can develop numerical spurious modes due to the inherent mathematical nature of the problem [17].

3.1. Finite duct with uniform mean flow

Since this article focuses on the finite element method used to compute a solution of the Galbrun equation, we consider the artificial case set in a bounded domain, since analytical results are available. Figure 3 illustrates a rectangular duct configuration in two dimensions with height $H = 0.5\,\text{m}$ and length $L = 3.4\,\text{m}$. The air filled duct is bounded by acoustically hard walls, i.e. the surface normal particle velocity is set to zero. In terms of particle displacement within Galbrun's equation, the following expression is equivalent to the hard walled boundary condition:

$$w_j n_j = 0 \quad \text{on} \quad \Gamma_F. \tag{24}$$

For this test case, the Mach number is defined by the ratio of the homogeneous constant mean flow velocity v_{01} and the constant speed of sound $c_0 = 340$ m/s. The flow velocity is varied so that the Mach number takes values from 0 to 0.3.

Table I. Analysis configuration: unknowns are density ρ, flow velocity v and displacement w. Order: 1 - linear and 2 - quadratic elements. DOF: degrees of freedom per node.

Abbreviation	Method	Order	DOF
LNSE $\rho 1 v 2$	CG	1 & 2	3
LEE $\rho 1 v 2$	CG	1 & 2	3
GAL $w 2 p 1$	CG	1 & 2	3
GAL $w 1$ CG	CG	1	2
GAL $w 2$ CG	CG	2	2
GAL $w 1$ DG	DG	1	2
GAL $w 2$ DG	DG	2	2

Figure 4 illustrates the finite element mesh consisting of 930 triangular elements.

Table I lists all investigated model configurations for the parameter analysis. As an example, the abbreviation "LNSE $\rho 1 v 2$" is understood as the linearized Navier–Stokes equation where a conventional continuous Galerkin discretization method is used and the basis functions are of 1st-order (or linear) for the density ρ and of 2nd-order (or quadratic) for the velocity v. The temperature field within the LNSE and the pressure field within the LEE are omitted since all processes are considered adiabatic. Further, no stabilization scheme is applied. The mixed formulations are solved numerically using Taylor-Hood elements, see [12], which are commonly adopted as basis functions for mixed-formulations.

In order to compare the results of the eigenvalue extraction, analytical solutions of the convected Helmholtz equation are taken as references. For the duct case with plane wave propagation, the eigenfrequencies of the acoustic modes are calculated as follows (cf. Dietzsch *et al.* [12]).

$$f_n = \frac{c_0 n}{2l} \left(1 - Ma^2\right) \quad \text{with} \quad n = 0, 1, 2 \dots N. (25)$$

Eigenvalue calculations are limited to the set up to the frequency $f \leq 100\,\text{Hz}$. It can be seen that for the test case, one expects three solutions at $f_0 = 0\,\text{Hz}$, $f_1 = 50\,\text{Hz}$ and $f_2 = 100\,\text{Hz}$ for a vanishing mean flow velocity. Further, the eigenfrequencies decrease with $(1 - Ma^2)$ for increasing flow velocity.

3.2. Convergence study

For a convergence study the duct geometry from the previous numerical model, Section 3.1, was adopted to investigate the numerical scheme. On applying a discontinuous Galerkin method to the displacement based form of Galbrun's equation, Figure 5 illustrates two structured mesh configurations, i.e. a first and a second level of mesh refinement. In total seven mesh refinements, from eight triangular meshes, have been conducted.

The relative error for each mesh refinement can be computed since the exact solution is easily derived. Relative errors, ε are measured in discrete L_2 norms and $h := min(H_x, h_y) > 0$ is the size of a triangle element length. To illustrate how the numerical schemes improve
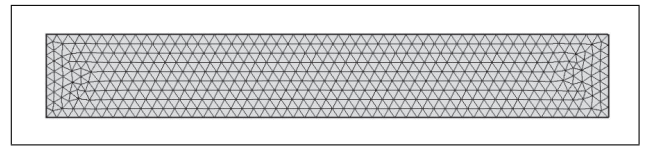
Figure 4. Finite element mesh for domain, cf. Figure 3 with 930 triangular elements
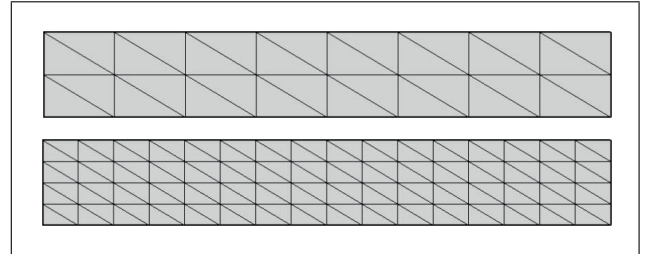
Figure 5. Two sample mesh configurations, the first and second examples taken from eight variations in the h–convergence study. Top: 1st level of refinement, bottom: 2nd level of refinement.

with mesh-refinement, as $h \rightarrow 0$, experimental convergence rates are illustrated in Figure 6. It is clear that solutions follow an asymptotic convergence rate which suggests numerical stability. The outliers in Figure 6 for the first mesh refinements are thought to be a result of a spatial undersampling of the associated eigenvectors and can thus be ignored. To the authors' knowledge, it is not clear why the convergence rate remains linear when using quadratic elements. Nevertheless due to computational costs, the authors use linear and quadratic elements hereafter since the relative errors are sufficient.

3.3. Comparison of theoretical and numerical formulations

First a comparison between different mixed-formulation methods is presented, to give a reference and also to illustrate an improvement due to a suggested approach. In the subsequent figures, the eigenfrequencies are plotted within the complex plane where the real part $\Re\{f\}$ is associated with the corresponding physical eigenfrequency of the corresponding harmonic oscillation.

Figures 7 and 8 show the results for three mixed-formulations, namely solving the test case with LNSE, cf. Figure 7a, with LEE, cf. Figure 7b, and the mixed formulation of Galbrun's equation, cf. Figure 8. From Figure 7a and 7b, it is not possible to clearly identify the acoustic eigenfrequencies at $f_1 = 50\,\text{Hz}$ and $f_2 = 100\,\text{Hz}$ at $Ma = 0$ for both methods using LNSE and LEE. Moreover, the imaginary parts of the eigenvalues have small values leading to a possible pollution of the results when a subsequent modal superposition procedure is applied in order to restore the system response in the frame of a harmonic analysis. In contrast, the mixed formulation of Galbrun's equation shows a more stable behavior since the imaginary parts of all acoustically not relevant eigenvalues (i.e. convective and spurious modes) increase their value with increasing Mach number.
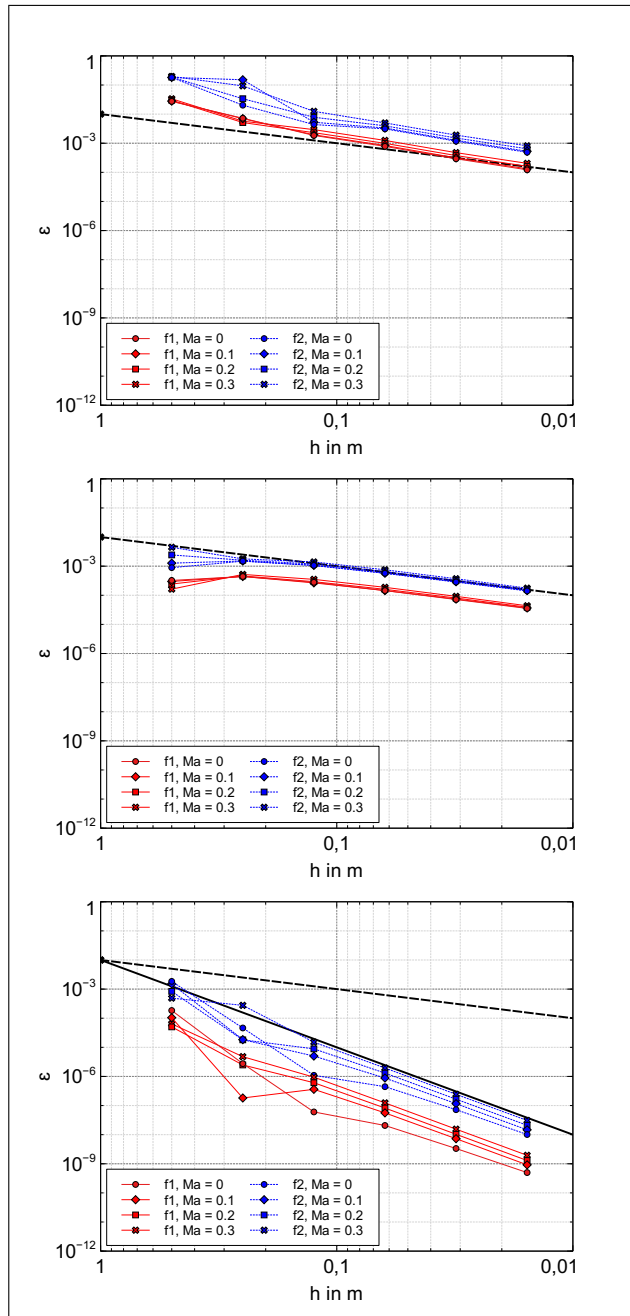
Figure 6. Numerical *h*-convergence rates for linear, quadratic and cubic elements for the displacement-based Galbrun duct problem, cf. Section 3.1, of the first two modes f1 and f2 for different Mach numbers. The black doted line indicates an $\mathcal{O}(h)$-convergence, the black solid line indicates an $\mathcal{O}(h^3)$-convergence. (a) Linear basis function, (b) Quadratic basis function, (c) Cubic basis function.

As mentioned before, the authors propose the use of a discontinuous Galerkin discretization method to determine solutions to Galbrun's equation in a displacement-based formulation, rather than solving the mixed formulation with the use of continuous Galerkin discretization.

For this purpose, the two different discretization schemes are compared in Figure 9 and Figure 10 specifically to highlight the benefits of the DG method. In Figure 9a and 9b, the computed eigenvalues are plotted in the complex plane when using a continuous discretiza-
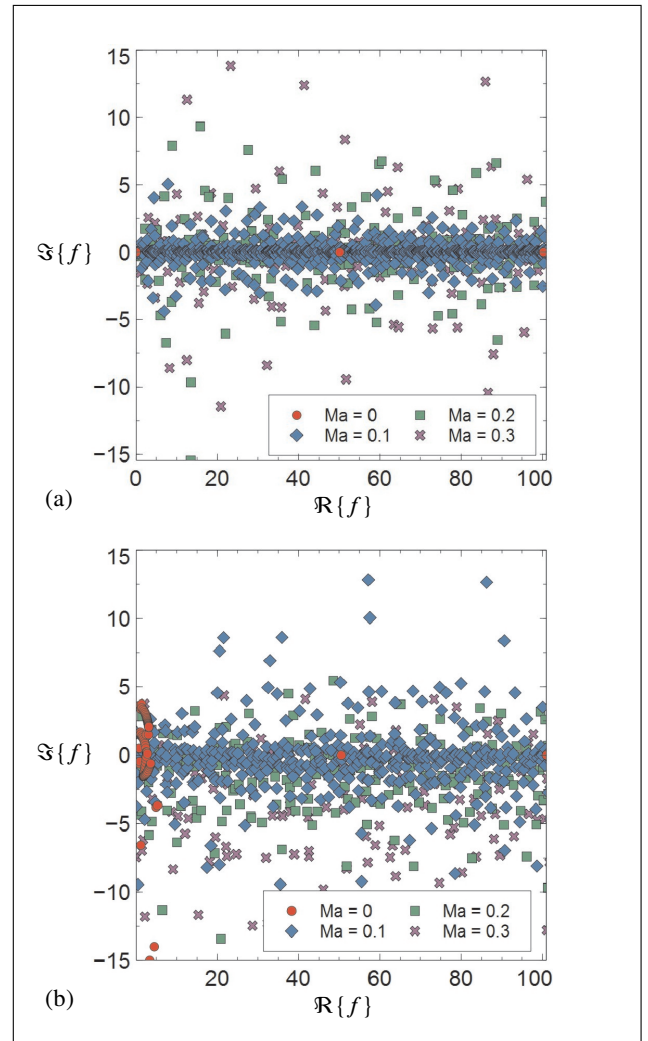
Figure 7. Comparison of eigenfrequencies from LNSE and LEE formulation solutions of the duct problem using continuous Galerkin methods, cf. Section 3.1. (a) LNSE $\rho 1 v 2$, (b) LEE $\rho 1 v 2$.

tion scheme while utilizing linear and quadratic basis functions, respectively. It is observed that the eigenvalues are widely spread across the complex plane and the acoustic modes of interest at $f_1 = 50\,\mathrm{Hz}$ and $f_2 = 100\,\mathrm{Hz}$ are not distinguishable from the others.

In contrast, cf. Figure 10a and 10b, the use of a discontinuous Galerkin discretization method enables a clear separation of the relevant acoustic eigenfrequencies from the others.

Comparing the solution of the acoustic eigenfrequencies from the numerical examples of "GAL *w*1 DG" (linear elements) and "GAL *w*2 DG" (quadratic elements), cf. Figure 10a and 10b, with the analytical values according to equation (25), we find good agreement. These values are listed in Table II where the relative error is calculated in accordance to

$$\varepsilon = \frac{|f - \tilde{f}|}{f} \cdot 100\%,\qquad(26)$$

where f denotes the analytic result and $\tilde{f}$ the numerical approximation.
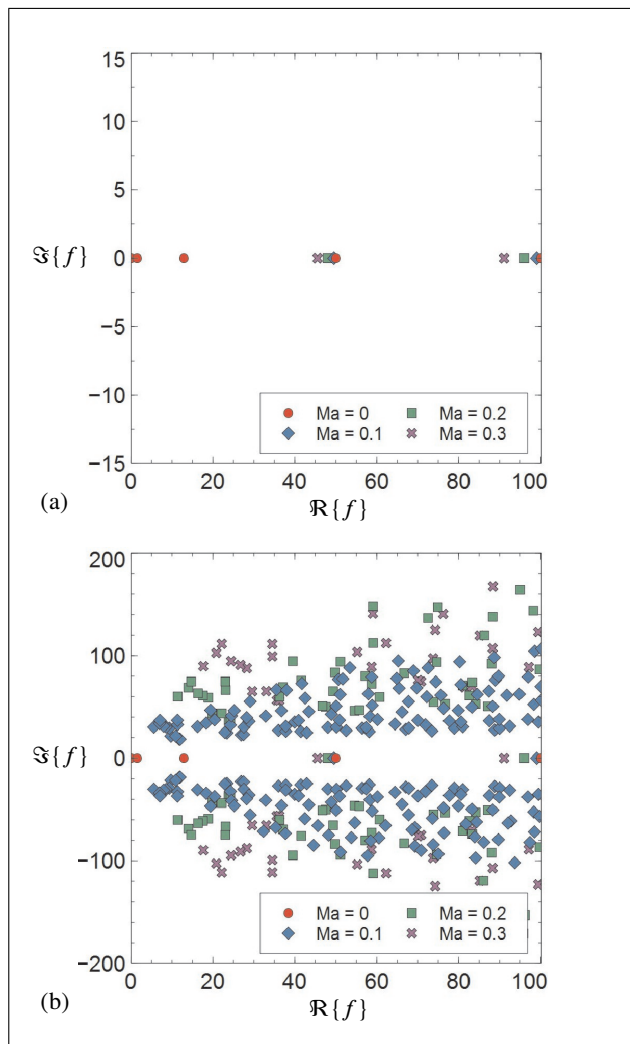
Figure 8. Comparison of eigenfrequencies from LNSE and LEE formulation solutions of the duct problem using continuous Galerkin methods, cf. Section 3.1. (a) GAL w2p1, (b) GAL w2p1 extended scale.
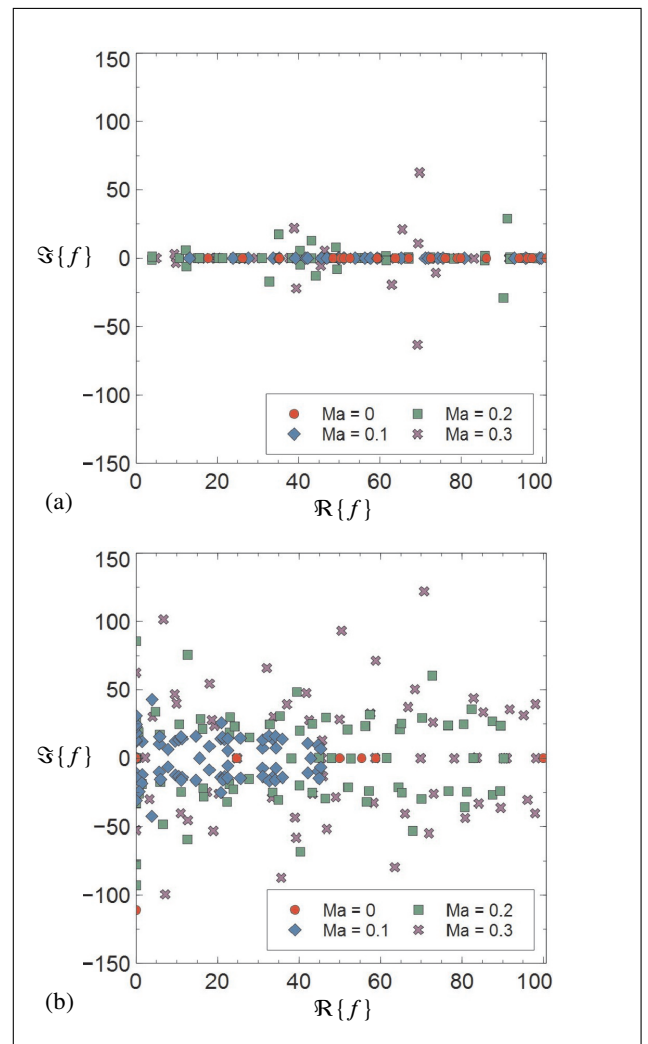
Figure 9. Results of standard continuous discretization method for solving the displacement based Galbrun equation. (a) GAL *w*1 CG; linear elements, (b) GAL *w*2 CG; quadratic elements.

Table II. Comparison of acoustic eigenvalues to analytical results at $Ma = 0.3$; Mesh used as shown in Figure 4.

	Analytical	GAL *w*1 DG	GAL *w*2 DG
f_1	$45,500\,\text{Hz}$	$45,522\,\text{Hz};$ $\varepsilon = 0.05\%$	$45,496\,\text{Hz};$ $\varepsilon = 0.009\%$
f_2	$91,000\,\text{Hz}$	$91,179\,\text{Hz};$ $\varepsilon = 0.12\%$	$90,967\,\text{Hz};$ $\varepsilon = 0.036\%$

3.4. Flux constant

As mentioned in the previous section, an appropriate value for α within the Lax-Friedrichs-Flux needs to be chosen in order to adjust for a correct flux representation across each finite element. For this purpose, the influence of the parameter α with respect to the results is investigated for the filtered Galbrun equation, i.e. a Lagrange multiplier λ_h is used to enforce $\nabla \times \boldsymbol{w} = 0$.

By varying the parameter α for a constant Mach number, it is observed that for sufficiently accurate results, α should

be larger than 10^6, cf. Figure 11 and Figure 12, independent of flow velocity and order of basis function. The authors identified that α scales with $(c_0 + v_0)^2$. These results are in close agreement to reported conclusions, see [13].

3.5. Vortical and spurious modes

The originality of Galbrun's equation is that the mixed pressure–displacement formulation given by Treyssède [41] is not changed by the presence of flow and is generally identical to the no-flow case. Except the presence of flow complicates the analysis to the existence of modal solutions due to the convective terms present. Even for an irrotational source term, the displacement field is not generally *curl-free* for shear-flow problems. Nevertheless, it has not yet been proven whether Discontinuous Galerkin methods satisfy the *inf-sup* condition. Vortical modes are non-acoustic perturbations convected with the mean flow, i.e. propagate with the flow. If the mean-flow is uniform, acoustic and vortical modes are decoupled but when the mean flow is rotational, the two types of modes couple.
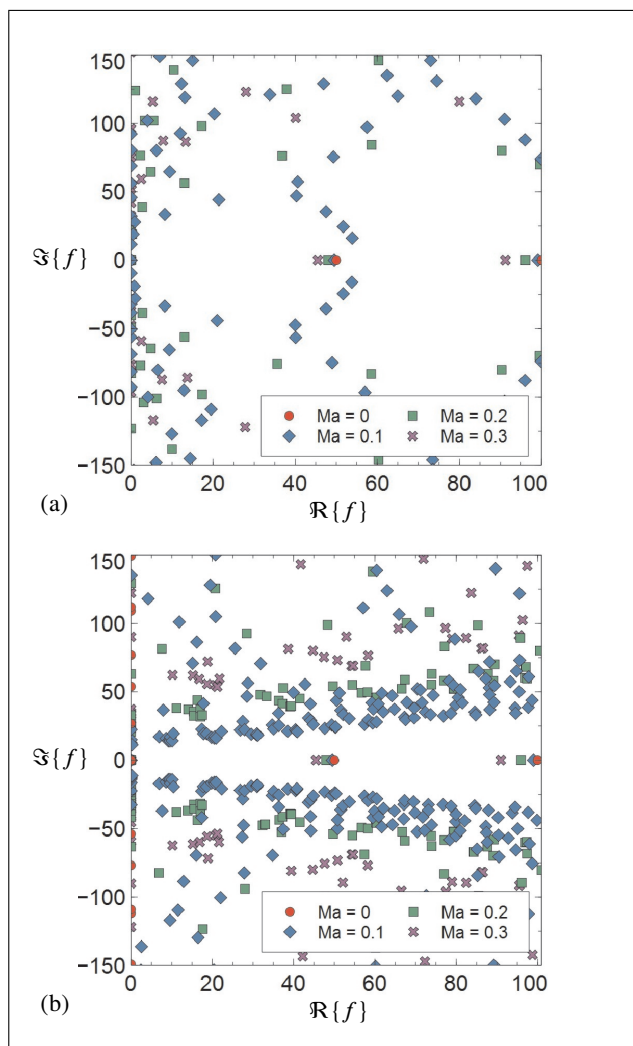
Figure 10. Results of discontinuous discretization methods for solving the displacement based Galbrun equation; flux parameter $\alpha = 10^6$, cf. Equation (17). (a) GAL $w1$ DG; linear elements, (b) GAL $w2$ DG; quadratic elments.
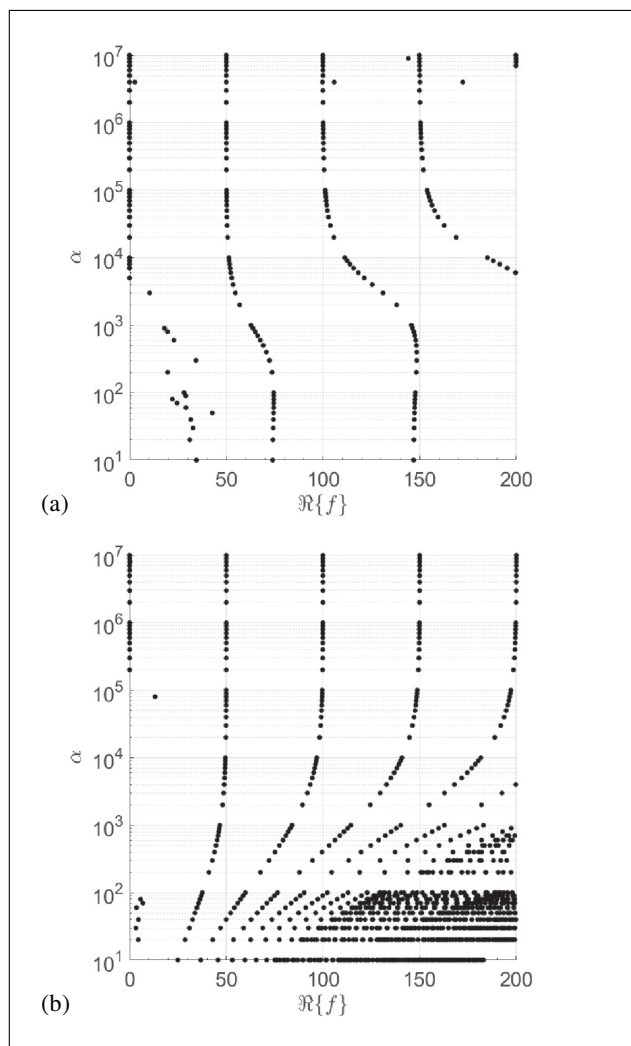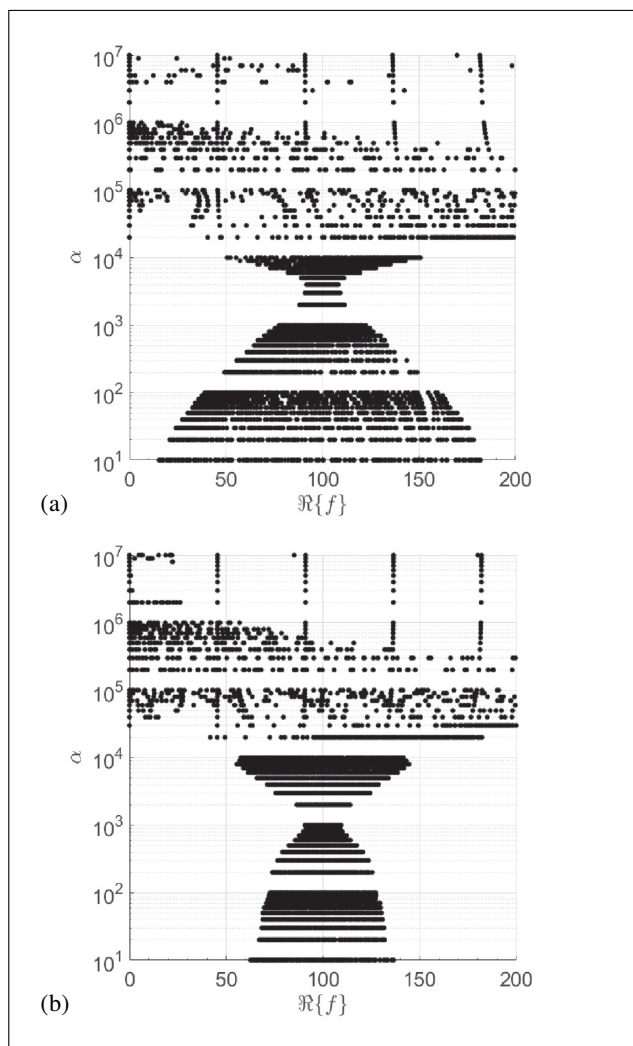

Figure 11. Dependency of results due to varying the flux parameter α for the $(\nabla \times \boldsymbol{w})$-filtered Galbrun equation, cf. equation (20), for $Ma = 0$. (a) GAL $w1$ DG, (b) GAL $w2$ DG.

Hence it is possible to identify these modes from numerical artefacts, the spurious modes.

Further, especially for uniform mean-flow, it is clear that while the location of acoustic eigenfrequencies decrease with increasing Mach number, some other (non-acoustic) eigenfrequencies show a clear proportional dependency on the Mach number while others seem to be randomly distributed across the complex plane.

Now, Figure 13 displays a similar version of Figure 10b. In Figure 13, the Mach number was sampled in 100 steps between $Ma = 0$ and $Ma = 0.3$, where each color code represents a different Mach number sample. This way, it is possible to follow the development of the eigenvalues with increasing Mach number. Figure 13 displays all the results where associated eigenvectors (colored boxes represent rectangular domain of duct, while the arrows point to the eigenvalue at the certain Mach number sample) for a chosen Mach number dependent eigenvalue are displayed. The plotted eigenvectors show the rotation of the displacement field. It is clear that despite the increasing Mach

number, the eigenvector remains stable. The authors understand "stable" in the sense that the eigenvalue depends on the Mach number and is following a certain characteristic where the associated eigenvector remains unchanged in its appearance. The mentioned characteristics are frequency as well as mesh size dependent. Until today it remains an open question how these characteristics can be described and whether their nature is either physical or numerical? Notably, slightly altering the finite element mesh structure changes these Mach-number-dependent eigenvectors entirely.

To investigate this behavior further more, Figure 14 shows the eigenvectors of the two acoustic modes and two other modes that follow a certain characteristic $\Theta_3(f_3) = const.$ and $\Theta_4(f_4) = const.$, cf. Figure 14a. Since the acoustic pressure is proportional to the divergence of the displacement field, see equation (8), we present the divergence $(\nabla \cdot \boldsymbol{w})$ and the rotation $(\nabla \times \boldsymbol{w})$ of the displacement field in Figures 14b to 14i. It can be seen that for the acoustic modes, the rotation of the displacement field is two orders of magnitude lower compared to the divergence of

(a)

(b)

Figure 12. Dependency of results due to varying the flux parameter α for the $(\nabla \times \boldsymbol{w})$-filtered Galbrun equation, cf. equation (20), for $Ma = 0.3$. (a) GAL $w1$ DG, (b) GAL $w2$ DG.

the displacement field. In contrast, for non-acoustic modes the rotation is two orders of magnitude higher. This comparison is valid since the data to calculate the divergence and the rotation of the displacement field is relative to the mode.

3.6. Filtering Galbrun's equation

Bearing in mind results from the previous section, a filtering of Galbrun's equation is conducted to exclude the vorticity related eigenvalues from the solution space. Keeping this in mind, the Lagrange multiplier λ_h formulation introduced, introduced in an earlier section, to enforce the rotation of the displacement field to be zero within the domain. The results are shown in Figure 15 and Figure 16.

It can be seen that by filtering Galbrun's equation, vorticity related eigenvalues are suppressed leaving only for acoustics relevant modes. Figures 15(b) and Figure 16(b) display an extended area of the complex plane. For larger imaginary values some eigenvalues persist. Since these eigenvalues are unlikely to be related to vorticity modes
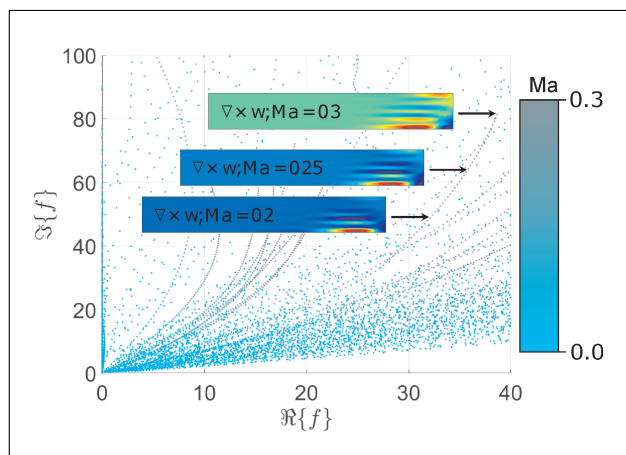
Figure 13. Numerical solutions of the displacement-based Galbrun equation by the Discontinuous Galerkin method, GAL $w2$ DG; The dots represent all computed eigenfrequencies in the complex quarter plane for distinct uniform-flow eigenvalue problems, $Ma = 0 : 0.05 : 0.3$. Linear-interpolation in increasing darker-shade color coding for dots is assumed: from $Ma = 0$ to $Ma = 0.3$. The inserts illustrate eigenvectors of rotation-modes for the displacement field at non-zero Mach numbers.

(a)

(h) $f_1: \nabla \cdot \boldsymbol{w} \sim \mathcal{O}(10^{-5})$

(i) $f_2: \nabla \cdot \boldsymbol{w} \sim \mathcal{O}(10^{-5})$

(d) $f_1: \nabla \times \boldsymbol{w} \sim \mathcal{O}(10^{-7})$

(e) $f_2: \nabla \times \boldsymbol{w} \sim \mathcal{O}(10^{-7})$

(f) $f_3: \nabla \cdot \boldsymbol{w} \sim \mathcal{O}(10^{-5})$

(i) $f_4: \nabla \cdot \boldsymbol{w} \sim \mathcal{O}(10^{-5})$

(h) $f_3: \nabla \times \boldsymbol{w} \sim \mathcal{O}(10^{-3})$

(i) $f_4: \nabla \times \boldsymbol{w} \sim \mathcal{O}(10^{-3})$
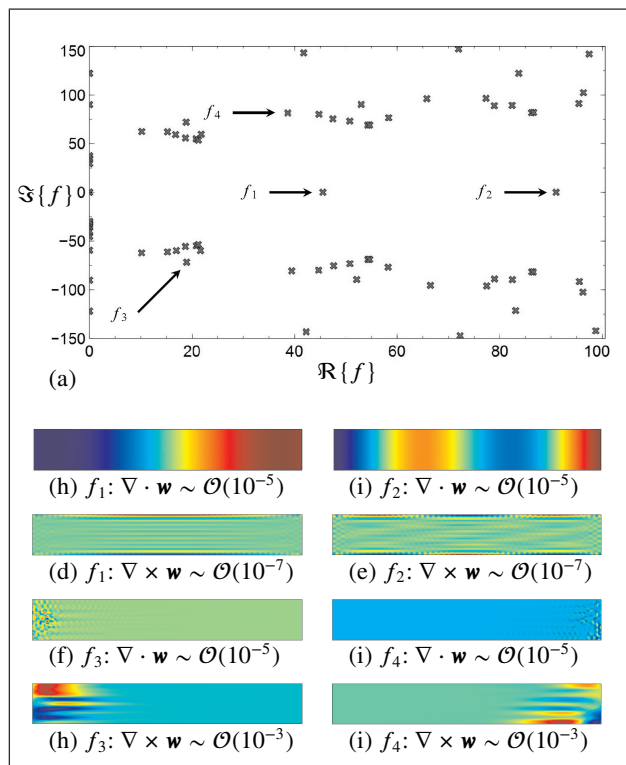
Figure 14. Eigenvectors corresponding to four eigenvalues for the solution of the displacement-based Galbrun equation using continuous finite element basis functions, GAL $w2$ CG at $Ma = 0.3$

and in addition they are well separated from any acoustic mode, the authors understand them as spurious modes.

4. Examples

In this section the capabilities of the numerical method to solve more realistic problems are illustrated. The first ex-
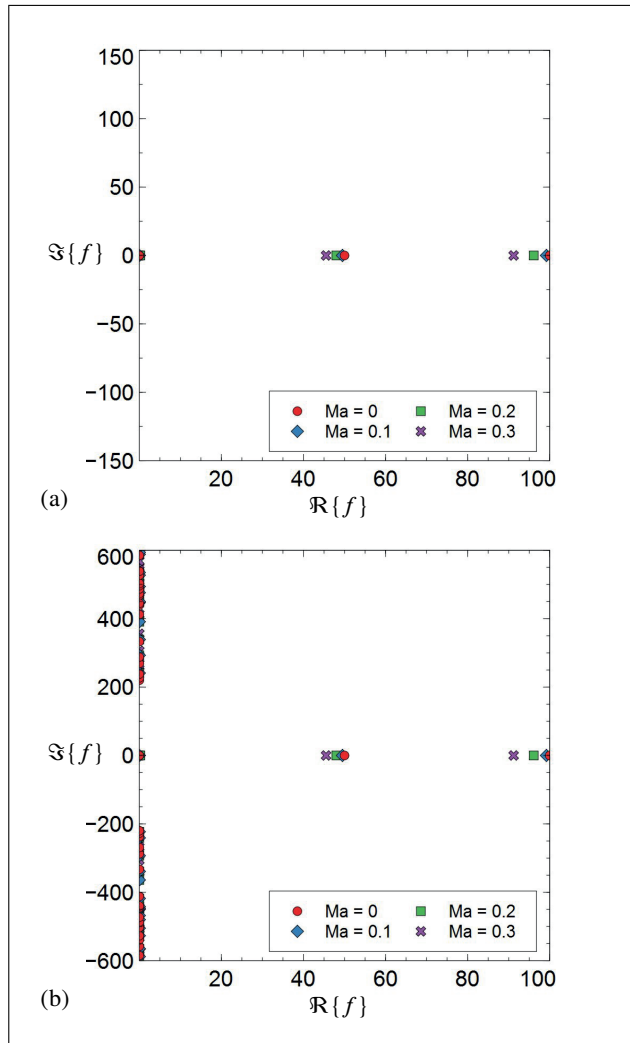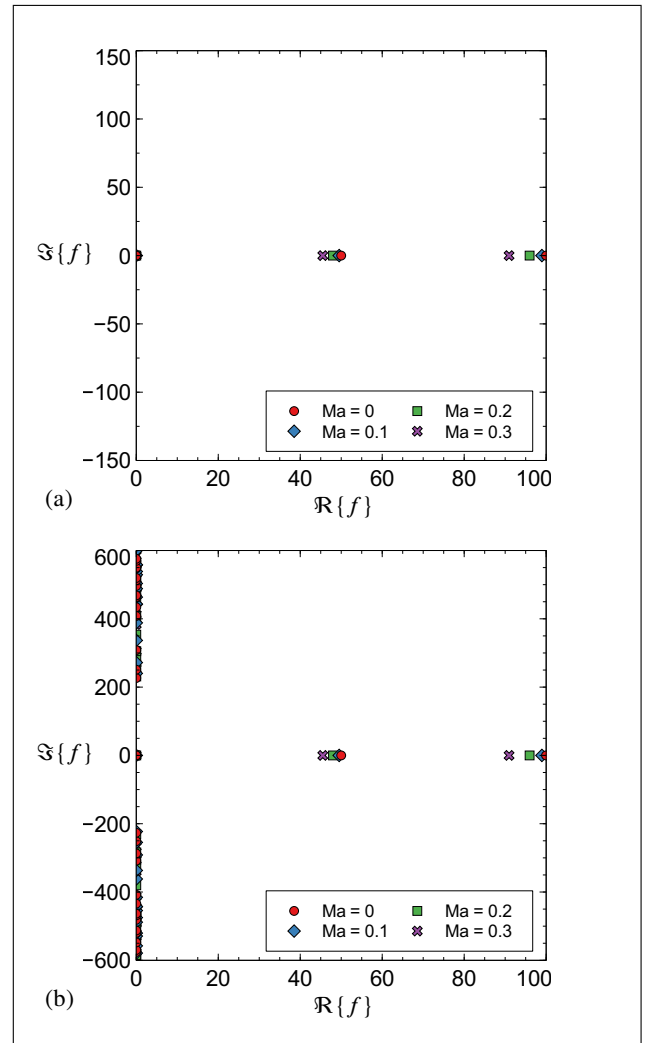
Figure 15. Eigenfrequencies corresponding to solutions of the $(\nabla \times \boldsymbol{w})$-filtered Galbrun equation using linear elements; $\alpha = 10^6$, cf. Equation (17). (a) GAL $w1$ DG, (b) GAL $w1$ DG; extended scale.

Figure 16. Eigenfrequencies corresponding to solutions of the $(\nabla \times \boldsymbol{w})$-filtered Galbrun equation using quadratic elements; $\alpha = 10^6$, cf. Equation (17). (a) GAL $w1$ DG, (b) GAL $w1$ DG; extended scale.

ample represents a duct with uniform flow such as in Section 3 is considered. An admittance boundary condition is applied at the outlet of the duct. The remaining boundaries are considered as acoustically hard walls, i.e. the associated eigenvectors to the solution of Galbrun's equation have zero displacement on these boundaries.

The second example can be seen as a cross section of a swirling flow represented by an annulus with a shear flow in circumferential direction. A boundary admittance is considered on the outer ring.

4.1. Finite duct with an absorbing end-condition

To extend our verification of the non-mixed Galbrun formulation, we present solutions for an equivalent boundary condition for Galbrun's equation in comparison to the Robin boundary condition when considering the Helmholtz equation. Figure 18 displays the model under consideration with the corresponding results. In this step the Mach number is set to zero in order to compare the results of the proposed method for solving Galbrun's

equation with the standard Galerkin (CG) discretization of the Helmholtz equation using quadratic elements for the pressure unknowns. The mesh is chosen as illustrated in Figure 4.

As can be seen, the results are in very good agreement. Since the duct configuration is such that only plane wave propagation is possible below a cut on frequency of $f = 340$ Hz, there is no propagating mode below this frequency, which correlates with the results pictured above. For the acoustic eigenvalues inside a duct below the cut-on frequency, Marburg [28] presented comparable results. In addition considering the dispersion relation, the same results, i.e. $f = 340$ Hz can be found.

When the flow velocity is increased, the eigenvalues spread into the complex plane, see Figure 19(a). Again, only for acoustics relevant eigenvalues decrease with increasing Mach number. Figures 19(b) to 19(e) show the eigenvectors of the first propagating mode that depend on the Mach number. It can be seen that with increasing Mach
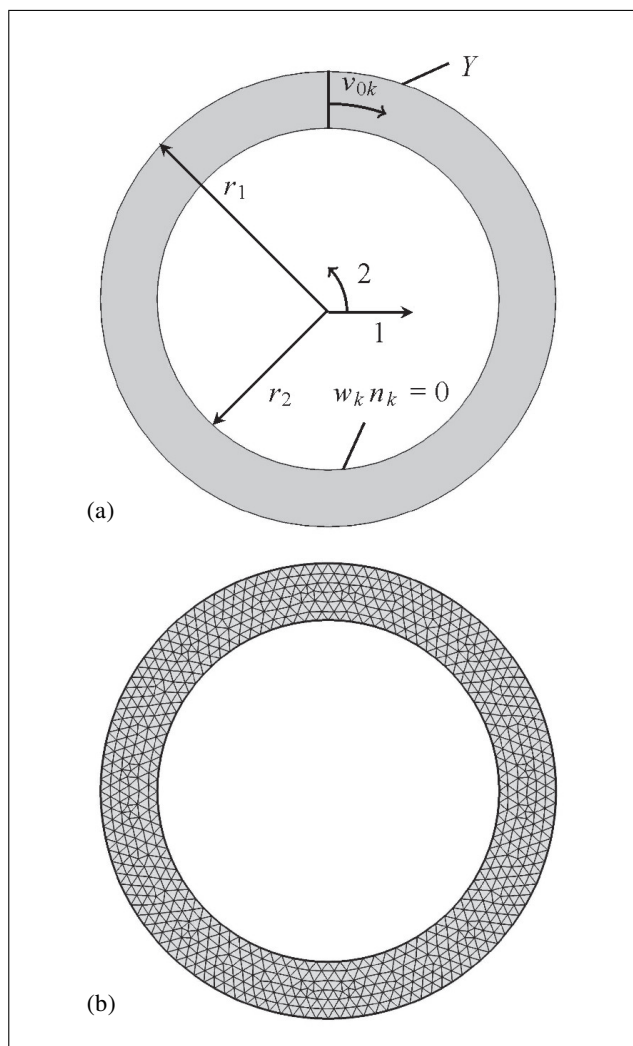
Figure 17. Annulus geometry with corresponding finite element mesh. (a) Geometry and flow direction, (b) Finite element mesh.

number the convectional effect on the mode shape is increasing, too.

4.2. An annulus supporting a rotating shear flow

To investigate the capabilities of the proposed method on a more realistic problem, an annulus with circulating flow is analyzed.

Figure 17 shows the configuration of the test case model. An annulus with an inner radius $r_1 = 0.75$ m and an outer radius of $r_2 = 1$ m is chosen, which is equivalent to the model investigated in Dietzsch *et al.* [12].

The mean flow velocity is defined as

$$v_{0k} = \begin{bmatrix} v_{01} \\ v_{02} \end{bmatrix} = \begin{bmatrix} 0 \\ -Ma\, c_0\, \frac{1}{r_2-r_1}\, (2r - (r_1 + r_2)) \end{bmatrix} \quad (27)$$

where r denotes the radial or "1"-direction. For simplicity the mean flow mass density is $\rho_0 = 1$ kg/m^3 and the mean pressure is set to $p_0 = 0$. For the case of $Ma = 0.3$ the mean flow would circulate clockwise at $r = r_2$ and counterclockwise at $r = r_1$ the tangential component of the mean flow velocity at $r = r_2$ would be $|v_{02}| = 102$ m/s.

The radial component remains zero at all the time. Again, the eigenvalues at four different flow velocities are investigated.

As a first case the boundary condition on the outer surface takes $\bar{Y} = 0$ which corresponds to an acoustically hard wall or $w_k n_k = 0$, respectively. In this case, the acoustically relevant modes can be identified with respect to their vanishing imaginary part.

Figure 20 displays the results of the eigenvalues for the annulus configuration with acoustically hard walls. It is noticeable that all acoustic eigenvalues have a negligible imaginary part and can easily be separated. In addition, for $Ma = 0$, the eigenvalue at $\Re(f) = 124.098$ is a double mode due to the double symmetry of the geometry. As the mean flow velocity increases, the modes separate into a forward and a backward traveling wave where one eigenvalue increases and the other one decreases. The same behavior can be found when investigating tyre cavities under rotation, see Lopez *et al.* [26].

In a second example, $\bar{Y} = 1$ and the $(\nabla \times \mathbf{w})$-filtered Galbrun equation is used. Figure 21 shows the results for eigenvalue computation. It can be seen that when increasing $\bar{Y}$, the eigenvalue distribution is shifted to lower imaginary values and is not symmetric with respect to the real axis. Further depending on the Mach number, characteristic lines are identifiable where eigenvalues group along. Investigating this further more, the authors identify acoustically relevant eigenvalues between these characteristic lines for a given Mach number. Additionally, for the acoustically relevant eigenvalues, a behavior where $(\nabla \cdot \mathbf{w}) \gg (\nabla \times \mathbf{w})$ was noticed. For all other eigenvalues the divergence of the displacement field is in the same order of magnitude as the curl of the displacement field, i.e. $(\nabla \cdot \mathbf{w}) \approx (\nabla \times \mathbf{w})$. This behavior can be used to separate acoustically relevant eigenvalues from others. At this point it must be noted that with a pure displacement based formulation of Galbrun's equation such a determination is easily possible. So any scaling of the eigenvectors would result in a scaling of the divergence and the curl of the displacement field.

5. Conclusions

When solving Galbrun's equation in its pure displacement based formulation, the authors propose the use of a discontinuous Galerkin method for discretizing Galbrun's equation. Due to discontinuity between neighboring elements it is shown that a Lax-Friedrichs condition with a flux factor $\alpha \geq 10^6$ gives sufficiently accurate results. In order to exclude vorticity modes from the modal space, a $(\nabla \times \mathbf{w})$-filtering with the aid of a Lagrange multiplier is successfully applied and illustrating by various examples. Since the pressure distribution is related to the divergence of the displacement field, the presented studies show the separation between acoustic modes from vorticity modes or numerical spurious modes. It is shown that the vorticity modes follow a certain characteristic which are frequency
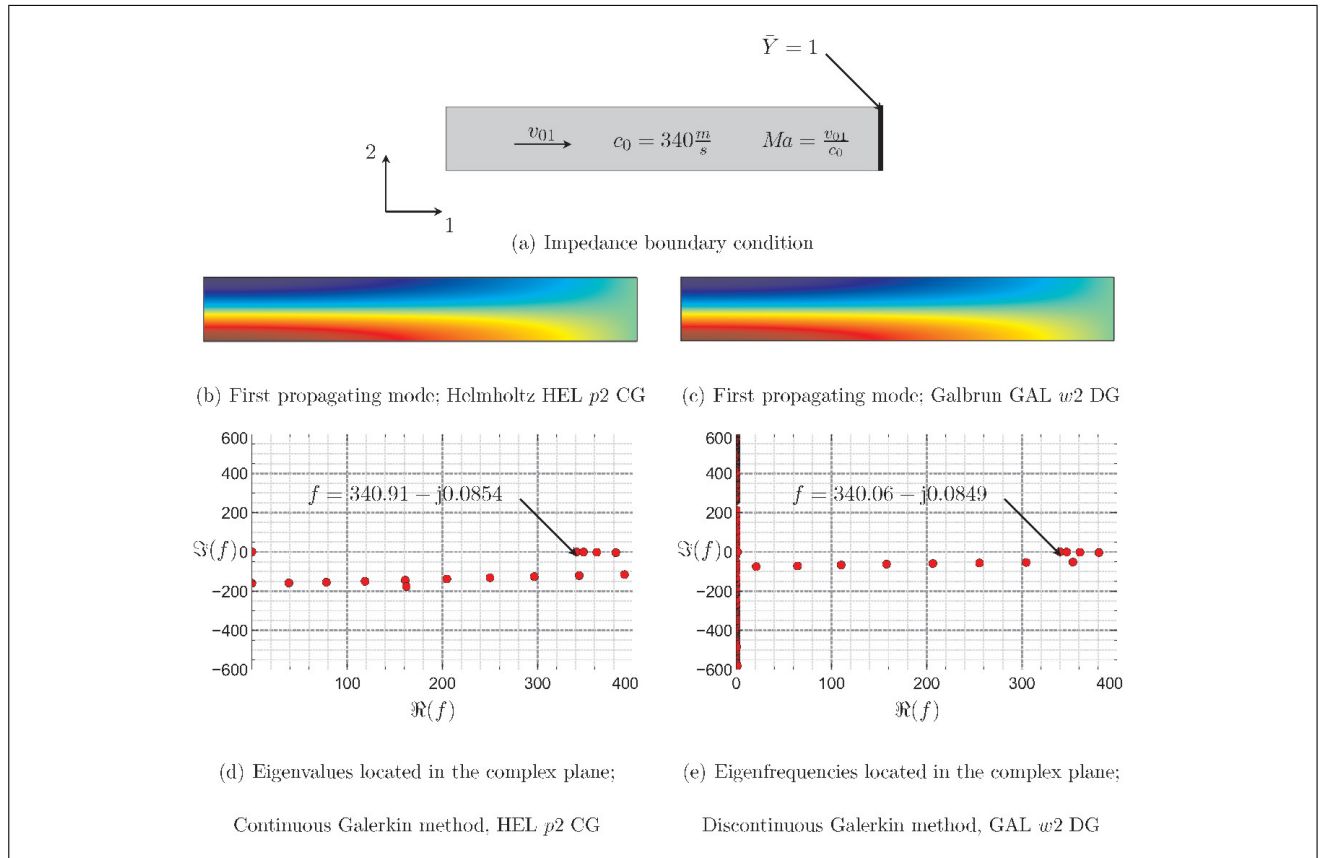
Figure 18. Comparison of numerical solutions for the the scalar Helmholtz equation against displacement based Galbrun equation with $\bar{Y} = 1$ at the outlet and $Ma = 0$.
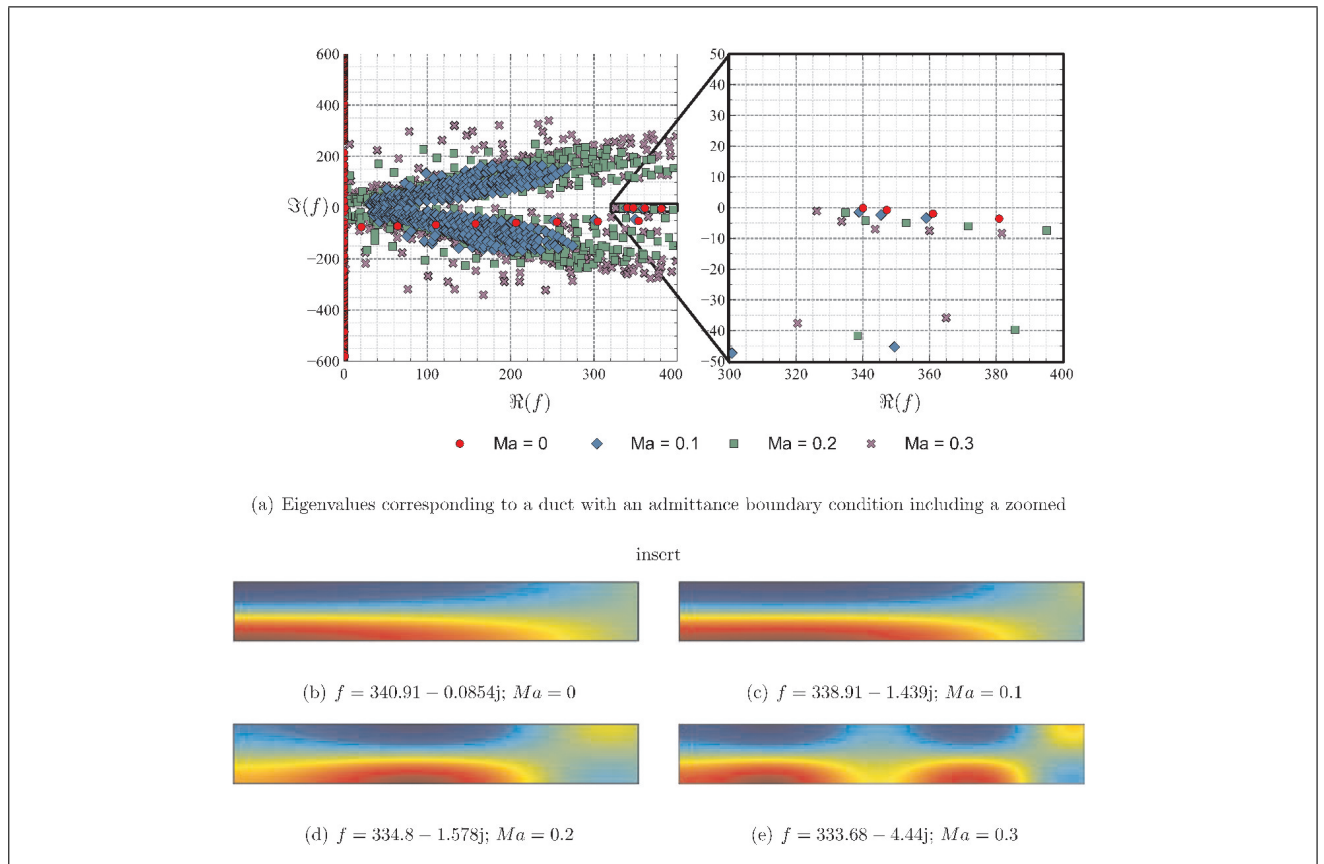

Figure 19. Eigenfrequencies located in the complex plane with corresponding eigenvectors of the first propagating mode for four Mach flow speeds; numerical solution Galbrun $w2$ DG.
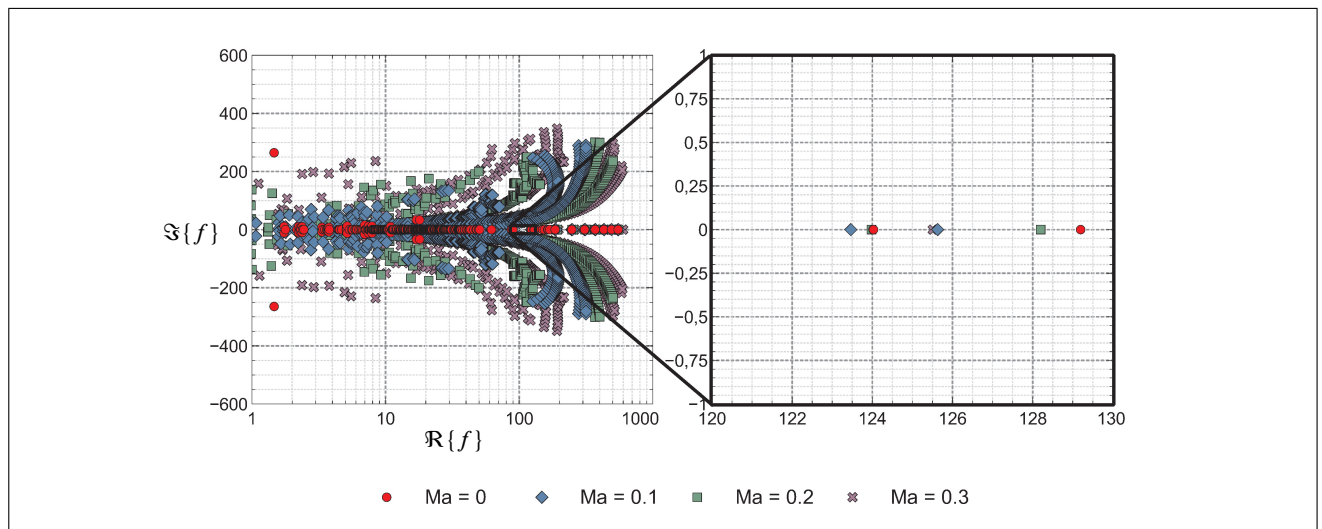
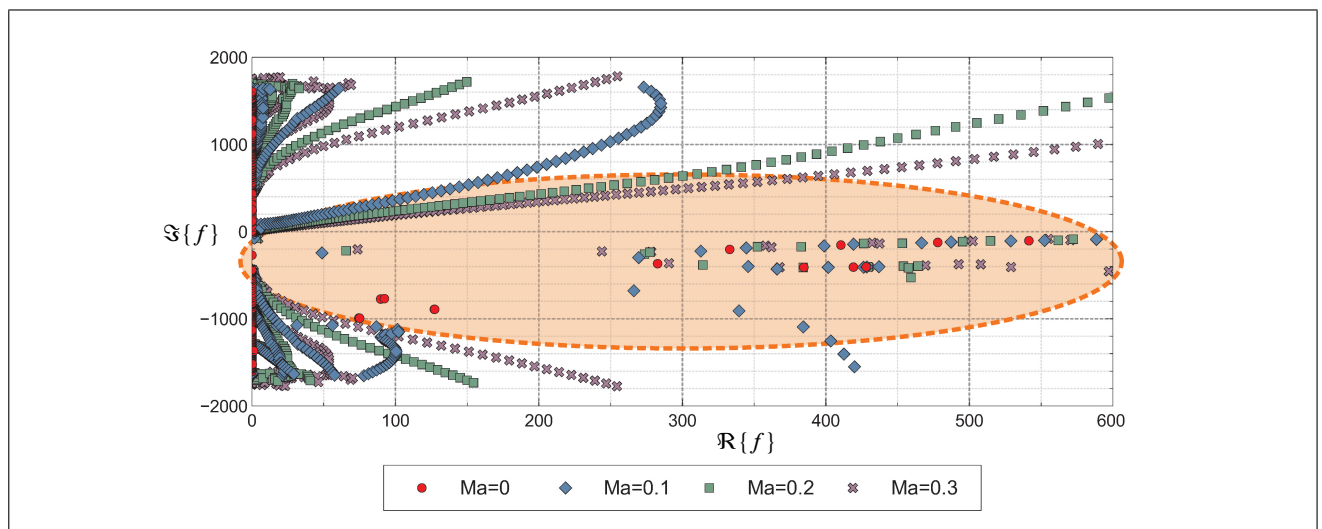Figure 20. Eigenfrequencies related to the rigid-walled annulus problem with four Mach flow speeds.

Figure 21. Eigenfrequencies related to the absorbing-lined annulus problem for four Mach flow speeds. Acoustic relevant frequencies are highlighted in the red zone.

and mesh size dependent. To account for admittance conditions on domain boundaries, an adequate boundary formulation is presented.

Future research will be dedicated towards formulating appropriate boundary conditions for solving general exterior problems and duct problems by robust reformulations provided by Bonnet-Benn Dhia *et al.* [5], for example, using discontinuous Galerkin numerical solutions.

References

[1] A. Avdonin, M. Meindl, W. Polifke: Thermoacoustic Analysis of a Laminar Premixed Flame Using a Linearized Reactive Flow Solver. Proceedings of the Combustion Institute (2018)

[2] E. Bécache, A. S. Bonnet-Ben Dhia, G. Legendre: Perfectly Matched Layers for Time-Harmonic Acoustics in the Presence of a Uniform Flow. SIAM Journal on Numerical Analysis **44**(3) (2006) 1191–1217.

[3] A. Bermúdez, L. Hervella-Nieto, R. Rodríguez: Finite element computation of three-dimensional elastoacoustic vibrations. Journal of Sound and Vibration **219** (1999) 279–306.

[4] C. Bogey, C. Bailly, D. Juvé: Computation of flow noise using source terms in linearized Euler's equations. AIAA Journal **40** (2002) 235–243.

[5] A.-S. Bonnet-Ben Dhia, È.-M. Duclairoir, G. Legendre, J.-F. Mercier: Time-harmonic acoustic propagation in the presence of a shear flow. Journal of Computational and Applied Mathematics **204** (2007) Nr. 2, 428–439.

[6] A.-S. Bonnet-Ben Dhia, G. Legendre, E. Lunéville: Analyse mathématique de l'équation de Galbrun en écoulement uniforme. Comptes Rendus de l'Académie des Sciences Paris **329** (2001) 601–606.

[7] J.-Ph. Brazier: Derivation of an exact energy balance for Galbrun equation in linear acoustics. Journal of Sound and Vibration **330** (2011) 2848–2868.

[8] P. N. Brown, A. C. Hindmarsh, L. R. Petzold: Using Krylov Methods in the Solution of Large-Scale Differential-Algebraic Systems. SIAM Journal on Scientific Computing **15** (1994) 2848–2868.

[9] B. Cockburn, S.-Y. Lin, C.-W. Shu: TVB Runge-Kutta Local Projection Discontinuous Galerkin Finite Element Method for Conservation Laws III: One-Dimensional Systems. Journal of Computational Physics **84** (1988) 90–113.

[10] B. Cockburn, G. E. Karniadakis, C.-W. Shu: Discontinuous Galerkin Methods. Springer, Berlin Heidelberg, 2000.

[11] N. Curle: The influence of solid boundaries upon aerodynamic sound. Proceedings of the Royal Society of London **231** (1955) 505–514.

[12] F. Dietzsch, L. Hervella-Nieto, S. Marburg, R. Rodríguez, H. Weisbecker: Physical and spurious modes in mixed finite element formulation for the Galbrun equation. Acta Acustica united with Acustica **100** (2014) 493–512.

[13] J. Donéa, A. Huerta: Finite Element Methods for Flow Problems. Wiley, Chichester, Hoboken, NJ: 2003. ISBN 978–0–471–49666–3.

[14] H. C. Elman, O. G. Ernst, D. P. O'Leary: A multigrid method enhanced by Krylov subspace iteration for discrete Helmholtz equations. SIAM Journal on Scientific Computing **23** (2001), Nr. 4, 1291–1315.

[15] R. Ewert, W. Schröder: Acoustic perturbation equations based on flow decomposition via source filtering. Journal of Computational Physics **188** (2003) 365–398.

[16] J. E. Ffowcs Williams, D. L. Hawkings: Sound generation by turbulence and surfaces in arbitrary motion. Philosophical Transactions of the Royal Society of London. Series A, Mathematical and Physical Sciences **264** (1969) 321–342.

[17] G. Gabard, R. J. Astley, M. Ben Tahar: Stability and accuracy of finite element methods for flow acoustics. I: General theory and application to one-dimensional propagation. International Journal for Numerical Methods in Engineering **63** (2005) 947–973.

[18] H. Galbrun: Propagation d'une onde sonore dans l'Atmosphère terrestre et Théorie des Zones de Silence. Paris, Gauthier-Villars, phdthesis, 1931.

[19] O. A. Godin: Reciprocity and energy theorems for waves in a compressible inhomogeneous moving fluid. Wave Motion **25** (1997) 143–167.

[20] M. A. Hamdi, Y. Ousset, G. Verchery: A displacement method for the analysis of vibrations of coupled fluid-structure systems. International Journal for Numerical Methods in Engineering **13** (1978) 139–150.

[21] J. S. Hesthaven, T. Warburton: Nodal discontinuous Galerkin methods. Springer, New York, 2008

[22] A. Hüppe, M. Kaltenbacher: Spectral finite elements for computational aeroacoustics using acoustic perturbation equations. Journal of Computational Acoustics **20** (2012) 1240005-1–1240005-13.

[23] G. Legendre: Rayonnement acoustique dans un fluide en écoulement: analyse mathématique et numérique de l'équation de Galbrun, Université Pierre et Marie Curie, Diss., 2003.

[24] M. J. Lighthill: On sound generated aerodynamically I. General theory. The Royal Society **211** (1952) Nr. 1107, 564–587.

[25] M. J. Lighthill: On sound generated aerodynamically. II. Turbulence as a source of sound. The Royal Society **222** (1954) 1–32.

[26] I. Lopez, R. E. A. Blom, N. B. Roozen, H. Hijmeijer: Modelling vibrations on deformed rolling tyres - a modal approach. Journal of Sound and Vibration **307** (2007) 481–494.

[27] A. Kierkegaard, S. Allam, G. Efraimsson, M. Åbom: Simulations of whistling and the whistling potentiality of an in-duct orifice with linear aeroacoustics. Journal of Sound and Vibration **331** (2012) 1084–1096.

[28] S. Marburg: Normal modes in external acoustics. Part I: Investigation of the one-dimensional duct problem. Acta Acustica united with Acustica **91** (2005) 1063–1078.

[29] S. Marburg, R. Anderssohn: Fluid structure interaction and admittance boundary conditions: setup of an analytical example. Journal of Computational Acoustics **19** (2011) 63–74.

[30] S. Marburg, H.-J. Hardtke: A study on the acoustic boundary admittance. Determination, results and consequences. Engineering Analysis with Boundary Elements **23** (1999) 737–744.

[31] A. Minotti, J.-Ph. Brazier, F. Simon: Extension of the Eulerian-Lagrangian description to nonlinear perturbations in an arbitrary inviscid flow. Journal of Sound and Vibration **331** (2012) 4537–4553.

[32] C. D. Munz, M. Dumbser, S. Roller: Linearized acoustic perturbation equations for low Mach number flow with variable density and temperature. Journal of Computational Physics **224** (2007) 352–364.

[33] B. Poirée: Les équations de l'acoustique linéaire et non-linéaire dans un écoulement de fluide parfait. Acta Acustica united with Acustica **57** (1985) 5–25.

[34] S. Retka: Numerische Umsetzung der Galbrun-Gleichung zur Modalanalyse strömender Medien in Außenraumproblemen unter Einsatz finiter und infiniter Elemente, Technische Universität Dresden, Diss., 2012.

[35] S. Retka, S. Marburg: An infinite element for the solution of Galbrun equation. ZAMM - Journal of Applied Mathematics and Mechanics **93** (2012) 154–162.

[36] S. Retka, L. Hervella-Nieto, S. Marburg: Comparison of pressure and displacement formulations for finite elements in linear time-harmonic acoustics. Computers & Structures **151** (2015) 49–57.

[37] Y. Saad: Krylov subspace methods for solving large unsymmetric linear systems. Mathematics of Computation **37** (1981) 105–126.

[38] S. Sack, M. Åbom, G. Efraimsson: On Acoustic Multi-Port Characterisation Including Higher Order Modes. Acta Acustica united with Acustica **115** (2016) 834–850.

[39] Z. Sun, J. A. Carrillo, C.-W. Shu: A discontinuous Galerkin method for nonlinear parabolic equations and gradient flow problems with interaction potentials. Journal of Computational Physics **352** (2018) 76–104.

[40] F. Treyssède, M. Ben Tahar: Comparison of a finite element model with a multiple- scales solution for sound propagation in varying ducts with swirling flows. The Journal of Acoustical Society of America **115** (2004) 2716–2730.

[41] F. Treyssède, G. Gabard, M. Ben Tahar: A mixed finite element method for acoustic wave propagation in moving fluids based on an Eulerian-Lagrangian description. The Journal of Acoustical Society of America **113** (2003) 705–716.

[42] X. Wang, K. J. Bathe: Displacement/Pressure based mixed finite element formulations for acoustic fluid-structure interaction problems. International Journal for Numerical Methods in Engineering **40** (1997) 2001–2017.

[43] S. Zörner, P. Šidlof, A. Hüppe, M. Kaltenbacher: Flow and acoustic effects in the Larynx for Varying Geometries. Acta Acustica united with Acustics **102** (2016) 257–267.

Numerical analysis of sound radiation from rotating discs

M. Maeder [a,*], R. D'Auria [a,b], E. Grasso [a,b], G. Petrone [b], S. De Rosa [b], M. Klaerner [c], L. Kroll [c], S. Marburg [a]

[a] *Technical University of Munich, Munich, Germany*
[b] *Università degli Studi di Napoli "Federico II", Napoli, Italy*
[c] *Chemnitz University of Technology, Chemnitz, Germany*

ARTICLE INFO

ABSTRACT

The analysis of sound radiation from rotating elastic discs, e.g. saw blades, is an interesting research topic. Especially for people who work in the vicinity of such machines, health related issues with respect to noise exposure levels gain more and more awareness. Therefore, the industry is faced with the challenge of developing quieter products in order to improve the working environment and to extend the time a worker can use these tools before a harmful situation arises. Moreover, less noise emission means less energy consumption and therefore a higher productivity. In this paper, the authors investigate the sound radiation from a rotating disc where the sound power is used as a global measure for the acoustic performance. Different methods for calculating the sound power of a spinning saw blade are compared. These are a fully coupled finite element approach, a hybrid finite element/boundary element approach, a simplified form of the RAYLEIGH integral known as the lumped parameter model, and the equivalent radiated sound power. The results show good agreement between the costly full models and those utilizing approximation methods which can save remarkable computational costs. The proposed frame can be used in optimization procedures for developing quieter saw blades and other rotating discs. Furthermore, the paper discusses mode splitting which is a well-known phenomenon for rotating machinery. For this, the results of sound radiation are investigated with respect to the question whether mode splitting is actually audible.

1. Introduction

Circular spinning discs are extensively used in many fields of engineering industry, e.g. computer hard drive discs, mechanical rotors, tools, and aerospace engine components. Owing to a variety of effects associated with rotation, e.g. gyroscopic effects, the dynamic behavior of such mechanical systems is still an interesting and challenging research field. The major concern of engineers when dealing with rotating structures consists in the possibility of unstable dynamic behavior which can lead to excessive deflections and thus, may cause mechanical failure or even dangerous situations for workers in the vicinity of these machines. An unstable situation, considered by the authors, arises when the excitation frequency of a spinning blade approaches the frequencies of natural modes. In this case, the force excitation gets into resonance with the mechanical system and therefore,

---

can lead to excessive deformation if the system is weakly damped. Usually, this case becomes relevant for spinning blades made of metal or similar monolithic materials [1].

If no rotation is present, the natural modes are constant with respect to frequency as long as the mass, damping and stiffness properties remain unchanged. If rotation is considered, several effects influence the mechanical behavior [2]. On the one hand, centrifugal forces induce in-plane stresses causing additional stiffness contributions. Therefore, natural frequencies tend to rise with increasing rotation [3–5]. On the other hand, gyroscopic effects that result from a change of the radial distance of any given material particle with respect to the axis of rotation due to structural vibration, result in an unsymmetrical contribution to the mechanical behavior. As seen from a stationary observer, this effect leads to traveling waves in and against the direction of rotation. These two waves are known as forward and backward traveling waves [1]. In terms of natural modes, this effect is known as mode splitting, where the associated eigenfrequency of the backward traveling wave decreases and the eigenfrequency of the forward traveling wave increases with increasing rotational speed. Bearing this in mind, it is obvious that a critical rotational speed exists where the frequency of the backward traveling wave tends to zero. In this case, as seen from a stationary observer, the deformation is quasi static while the disc is still spinning [1,6]. In order to improve the stability of rotating discs, pretensioning or prestresses can be applied through plastic deformation [7–12].

It must be noted that the acoustic radiation of discs and plates have been discussed in literature for rotating structures [1,13–16] and for cases without rotation [14,17–21], where it is possible to derive analytical formulations [16,19,21]. The research associated with understanding noise radiation of rotating structures is often concerned with noise exposure measures that are linked to health issues of workers in the vicinity of such rotors.

In the frame of product development, computer aided engineering (CAE) is a common tool for analyzing designs in an early stage of the development process. There, the finite element method (FEM), the boundary element method (BEM) and others have proved to be suitable and reliable tools [12,14,18,22–27] for vibroacoustic analysis. In order to include sound radiation analysis in the CAE frame, efficient numerical tools need to be developed and validated. Especially in cases for which an optimization procedure is part of the development process, fast and reliable methods are necessary [24,25].

The analysis of sound radiation from vibrating structures requires to couple structure and fluid. Usually, one of two coupling strategies is applied. The first one assumes structural vibrations in vacuo which are used as boundary conditions for the fluid, see for example [17,24–26]. Hence, the structure excites the fluid but there is no feedback from the fluid to the structure. In what follows, this approach will be referred to as the one-way fluid structure interaction (FSI) approach. In literature, this approach is often called *weak coupling* or even uncoupled. The second category includes the feedback from the fluid to the structure [22,28–30]. This will be referred to as a two-way FSI approach. Synonyms will be *strong coupling* or fully coupled FSI. The proper choice of the FSI approach depends on the particular problem and needs to be chosen carefully [31,32]. Furthermore, implementing stable algorithms is not straightforward and can lead to various difficulties [33,34].

Another aspect of wave propagation is concerned with the so-called far field approximation, when dealing with exterior acoustic domains [27]. Since computing wave propagation to infinity is neither reasonable nor even possible, the computational domain must be truncated. This artificial boundary must resolve the far field conditions in order to model the physical behavior of the real system. One possible solution beside using perfectly matched layers (PML) [35–37] or absorbing boundary conditions (ABC) [38,39] consists in the use of infinite finite elements [40,41]. The boundary element method does not require a truncation of the domain since only the radiating surface appears in the simulation model [27,42].

With these methods, it is possible to compute the radiated sound power of the structure. However, the radiated sound power accounts for a global measure for assessment of the acoustic performance [43]. Therefore and owing to the costly frequency sweep, solution of the fully coupled problem for large-scale applications still requires enormous computational resources, not to speak of uncertainty quantification and optimization and even though there is a large body of scientific work on this. For this reason, approximation methods have been developed to reduce the computational costs while conserving an appropriate accuracy of the numerical results. A very simple approximation technique assumes a unit radiation efficiency, see for example [26]. The resulting radiated sound power approximation is known as Equivalent Radiated Power (ERP) which is a very simple approach usually overestimating the actual value. It can be understood as a postprocessing of a structural analysis. Another common approximation is based on a TAILOR expansion of the free field GREEN's function of the RAYLEIGH integral. It is known as the lumped parameter model (LPM) allowing to estimate the radiated sound power based just on structural analysis, too. Other than ERP, LPM is able to capture acoustic short circuit effects. For further details, the authors refer to the literature [24,26,44–46].

In this paper, the authors investigate the sound radiation from rotating discs. Results for the radiated sound power show that under certain valid simplifications, it is possible to reduce the numerical effort significantly. As an approximation, the LPM shows good agreement with respect to full finite and boundary element models. Further, the paper will compare results of one-way and fully coupled FSI.

With respect to physics, the sound radiation of mode splitting will be discussed. While the mode splitting is a well-known and well-studied effect for spinning discs, the authors have not found any clear indication in literature about whether or not the mode splitting is indeed audible. Since mode splitting is only visible for a stationary global observer, but not for the observer traveling on the rotating disk, the authors try to illuminate this problem. Indeed, the former one is more of practical interest, since a co-rotating listener is not meaningful in this sense.

The paper at hand is structured as follows: Section 2 presents a brief overview of the basic theory. Aspects such as the general model, numerical methods as well as ERP and LPM are explained. In Section 3, the simulation models and simulations are discussed. The results follow in Section 4. Some conclusions will be provided in Section 5.
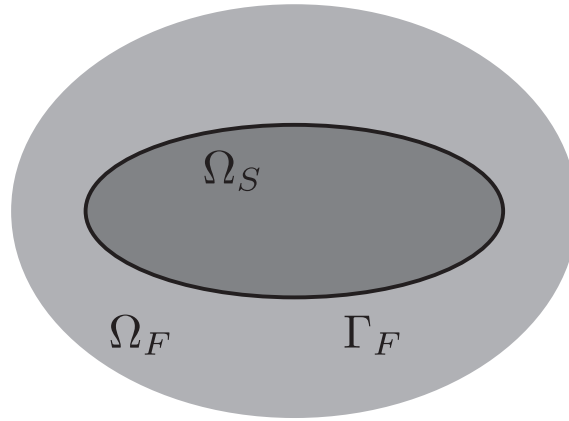
Fig. 1. Description of domain with the solid domain Ω_S and its boundary Γ_F which is surrounded by a fluid Ω_F.

2. Theoretical background

For a general description, the authors consider a three dimensional Euclidean space in $\Omega_S \subset \mathbb{R}^3$ which is bounded by a closed surface $\Gamma_F \subset \mathbb{R}^2$ that serves as a common boundary to the surrounding fluid $\Omega_F \subset \mathbb{R}^3$ which is assumed to be unbounded, cf. Fig. 1.

2.1. Numerical methods

Following the principles of the finite element method for structural dynamic problems, one can state the system of discrete equations for the structural component as [47–49]

$$\mathbf{M}\ddot{\mathbf{u}} + \mathbf{D}\dot{\mathbf{u}} + \Omega\mathbf{G}\dot{\mathbf{u}} + \mathbf{K}\mathbf{u} = \mathbf{f} \tag{1}$$

with **M**, **D**, and **K** as mass, damping, and stiffness matrices, respectively. The vector of unknowns is $\mathbf{u}(x, t)$, i.e. the nodal displacements, while the components of external nodal forces are accommodated in $\mathbf{f}(x, t)$. Further, Ω denotes the angular velocity about the axis of rotation which introduces centrifugal and gyroscopic forces that are considered by the gyroscopic matrix **G**. Typically, the gyroscopic matrix is skew symmetric if a single axis of rotation is considered only. For the remainder of this paper, a harmonic time dependence is assumed for all unknowns and excitation forces.

Equation (1) is transformed such that

$$\left[\mathbf{K} - \mathrm{j}\omega\mathbf{D} - \mathrm{j}\omega\Omega\mathbf{G} - \omega^2\mathbf{M}\right]\mathbf{U} = \mathbf{A}_s\mathbf{U} = \mathbf{F}, \tag{2}$$

where ω denotes the angular frequency and $\mathbf{A}_s$ will be referred to as dynamic stiffness matrix of the structure.

A similar approach is conducted for deriving the system matrices of the surrounding inviscid fluid. This system is given by Refs. [27,43]

$$\mathbf{A}_f(\omega)\mathbf{P}(\omega) = \mathbf{F}_f(\omega) = \mathbf{B}\mathbf{V}_f(\omega) \tag{3}$$

where $\mathbf{A}_f$ denotes the fluid system matrix and **P** the column matrix of unknown sound pressure. $\mathbf{F}_f$ contains the external forces acting on the fluid. The latter can be expressed by a matrix **B** and the fluid particle velocity $\mathbf{V}_f$. This form of formulation is achieved for both, the FEM and the BEM. For further details, the authors refer to Refs. [27,43].

2.2. Fluid structure interaction

Over the last decades, numerous methods have been developed to solve problems with fluid structure interaction, cf. [22,28,33]. For a deeper insight, the authors refer to the literature [27,34,43,50–52].

As already discussed in the introduction, two ways of coupling are considered. The first one is named one-way interaction, meaning that the continuity of the particle velocity is enforced and the second one is named two-way or full interaction, for which continuity of the particle velocity and the force equilibrium are enforced.

The first one assumes structural analysis in vacuo and its results are applied as boundary conditions to the fluid domain. The second coupling takes the full interaction of both domains into account which includes the feedback of the fluid to the structure.

Looking at the resulting system of equations

$$\begin{bmatrix} \mathbf{A}_s & \mathbf{C}_{sf} \\ \mathbf{C}_{fs} & \mathbf{A}_f \end{bmatrix} \begin{bmatrix} \mathbf{U} \\ \mathbf{P} \end{bmatrix} = \begin{bmatrix} \mathbf{F} \\ \mathbf{B}\mathbf{V}_f \end{bmatrix}, \tag{4}$$

one can identify the previously presented system of equations for the structural and the fluid domain, which are linked by the coupling matrices $\mathbf{C}_{sf}$ and $\mathbf{C}_{fs}$.

In case of one-way coupling, matrix $\mathbf{C}_{sf} = \mathbf{0}$. Then, NEUMANN boundary conditions for the fluid apply, i.e.

$$\mathbf{V}_f - \mathbf{V}_s = 0, \tag{5}$$

where $\mathbf{V}_s$ is the structural surface normal velocity, which results from an adequate structural dynamic simulation.

2.3. Simplified sound power evaluation

For most practical cases, it is necessary to solve a boundary value problem for accurate sound power evaluation even in case of a one-way coupling. Both, the FEM and the BEM are computationally expensive, in particular if frequency sweeps are considered [43]. Analytical solutions are available for a limited number of cases only, cf. [17,18,42]. To efficiently estimate the radiated sound power based on finite element analysis (FEA) simulations of the structure only, two formulations are utilized. These are the equivalent radiated power (ERP) and the lumped parameter model (LPM), respectively. Both techniques have been successfully applied for harmonic FEA, cf. [24,26].

The equivalent radiated sound power P_{ERP} is calculated as [24,26]

$$P_{ERP} = \frac{1}{2} \rho_f \, c_f \int_{\Gamma_F} |\boldsymbol{v}_n|^2 \mathrm{d}\Gamma_F. \tag{6}$$

The integral is computed over the structural surface Γ_F with the fluid mass density ρ_f, the speed of sound c_f and the normal component of the structural particle velocity $v_n = \vec{v} \cdot \vec{n}$. For the discretized finite element model, the integral is computed as the sum over N_e surface elements with the corresponding area A_μ

$$P_{ERP} = \frac{1}{2} \rho_f \, c_f \sum_{\mu=1}^{N_e} A_\mu v_{n_\mu} v_{n_\mu}^* \tag{7}$$

where the superscript $*$ represents the complex conjugated. The particle velocity on the elements is assumed to be constant which is a reasonable simplification since the structural meshes in use will be rather fine. The equivalent radiated sound power is based on the assumption of a unit radiation efficiency, i.e. $\sigma = 1$. Local effects such as acoustic short circuits between sources are neglected. Therefore, P_{ERP} is usually overestimating the radiated sound power, especially in the low frequency range.

Often, more accurate results are possible using the LPM [26]. The LPM is based on discretizing the RAYLEIGH-Integral with a TAYLOR series of the GREEN's function and constant particle velocity on the elements [15,44,45]. This formulation can be written as a double sum over all surface elements as

$$P_{LPM} = -\frac{1}{2} k \, \rho_f \, c_f \sum_{\mu=1}^{N_e} \sum_{\nu=1}^{N_e} A_\mu A_\nu \, \mathfrak{I}\left\{G_{\mu\nu}\right\} \mathfrak{R}\left\{v_{n_\mu} v_{n_\nu}^*\right\} \tag{8}$$

$$\text{with} \qquad \mathfrak{I}\left\{G_{\mu\nu}\right\} = -\frac{\sin(k|x_\mu - x_\nu|)}{2\pi |x_\mu - x_\nu|},$$

where k denotes the wave number and $\mathfrak{R}\{\}$ and $\mathfrak{I}\{\}$ are the real and the imaginary parts of a complex value, respectively. Since the imaginary part of the GREEN's function accounts for the interaction between sources, the use of the LPM is often a very good approximation in the low and mid frequency range, even in (some) cases for which the assumptions of a planar radiator are violated [26].

All computed results of the sound power are converted into sound power levels using common standards where $L_W = 0$ dB has a reference sound power of $P_0 = 10^{-12}$ W. For the post-processing algorithms, user defined scripts have been developed in Python language using NumPy and SciPy routines [48,53,54].

3. Simulation

Starting with the definition of the general geometry, the numerical models are presented. They have been created using Abaqus 6.14–2 CAE and calculated by the Abaqus standard solver [48]. Two different structural models are considered. The first one is a fine resolution model to verify the implemented ERP and LPM routine. The second model is a coarse model that is utilized to create solutions when rotation is applied to the structure. The reason for this approach is to keep the computational costs at a reasonable level while the effects under investigation are still recognizable. In order to verify the acoustic sound power estimates by the ERP and LPM, an adequate acoustic volume mesh and an equivalent boundary element model were created, respectively. A closer insight will be given in the dedicated sections hereafter.
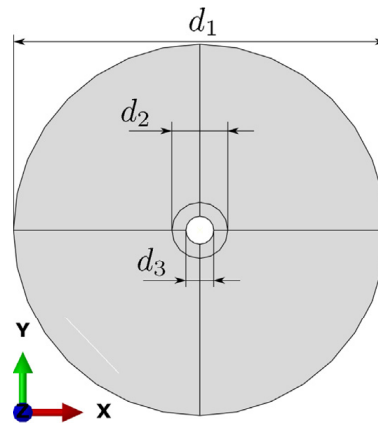
Fig. 2. Disc geometry; $d_1 = 800$ mm, $d_2 = 120$ mm, $d_3 = 60$ mm, disc thickness $t = 3.5$ mm.

Table 1
List of material properties.

Material	Property	Symbol	Value	Unit
Steel	Density	ρ_S	7800	kgm^{-3}
	E-Modulus	E	$2.1 \cdot 10^5$	MPa
	Poisson ratio	ν	0.3	–
	Damping factors	α	0.1826	s^{-1}
		β	$5.0125 \cdot 10^{-6}$	s
Air	Density	ρ_F	1.225	kgm^{-3}
	Bulk-Modulus	K	$1.42 \cdot 10^5$	Pa
	Speed of sound	c	340	m/s

3.1. Geometry and material properties

The geometry of interest - named as disc hereafter - consists of a plate structure depicted in Fig. 2, where the outer diameter d_1 and the inner diameter d_3 together with the disc thickness t define its geometrical shape. The additional diameter d_2 defines the area where a fixed-fixed boundary condition will be applied during the studies. The disc itself will be enclosed by air at rest. The disc is made of steel where HOOKE's law is considered as the linear elastic behavior for the material model. Furthermore, RAYLEIGH damping is assumed with the associated damping factors α and β. These values are set such that the critical damping ratios η_1 and η_2 of the first and second eigenfrequencies ω_1 and ω_2 take the values $\eta_1 = 1 \cdot 10^{-3}$ and $\eta_2 = 2 \cdot 10^{-3}$. Table 1 lists all the material properties.

3.2. Numerical models

Based on the created geometry, the Abaqus 6.14–2 CAE mesher is used to generate the finite element (FE) meshes. These meshes will serve as a basis for the associated boundary element models that will be analyzed with the in house BEM code *Akusta* [27,55]. In order to make the mesh data created by Abaqus available to the *Akusta* solver, a python interface routine was created.

Table 2 shows a comprehensive collection of the finite and boundary elements that where used during the simulations. Further details will be given in the subsequent sections. For a more detailed description of the Abaqus elements, the authors refer to the Abaqus documentation [48]. Constant boundary elements and their performance have been discussed in the literature [27,43].

Table 2
List of mesh properties; NoN: Number of nodes per element; Hex: 3D Hexahedral element; Tet: 3D Tetrahedral element; Quad: 2D quadrilateral element; Tri: 2D Triangular element.

Method	Domain	Software	Element type	Basis order	NoN
FEM	3D Structure	Abaqus	Hex C3D20R	quadratic	20
	3D Fluid	Abaqus	Tet AC3D10	quadratic	10
	2D Fluid	Abaqus	Tri ACIN3D6	quadratic	6
BEM	2D Fluid	Akusta	Quad	constant	1

3.2.1. Structural mesh

In order to verify the implemented ERP and LPM routines, a fine mesh resolution is chosen. Fig. 3 shows the finite element mesh for the reference model. To create this mesh, a global seeding size of 5 mm was applied. This results in a mesh of $n_{el} = 36208$ elements or with respect to the highest mode computed, approximately 40 quadratic elements per wave length of the associated mode shape. The reason for choosing such a fine mesh is due to the fact that no distorted elements are present with respect to the default aspect ratio criteria defined by the Abaqus software. For more details, the authors refer to the Abaqus documentation [48] and to Langer et al. [56]. We will present results of a brief mesh study in the subsequent section to show the applicability of the used mesh.

For further studies, it is useful to run simulations on smaller models to investigate global effects such as the mode splitting due to rotation while the computational efforts remain in reasonable expenditure. Therefore, a coarse mesh is created for fast preliminary investigations. For this coarse configuration, a global mesh seed size of $h = 20$ mm is used which, after meshing, results in a number of elements of $n_{el} = 2268$. In both cases, the symmetry plane is located at $Z = 0$.

3.2.2. Acoustic mesh

In order to quantify the feedback effect of the fluid onto the structure, a fully coupled finite element model of the surrounding fluid domain in the form of a sphere with a radius of $r = 1.5$ m is generated using three dimensional ten node tetrahedral elements, cf. Fig. 4. Here, the fluid sphere has been reduced by the volume of the disc to guarantee that the surface of the disc is shared by the structure and the fluid and no elements are overlapping or interfering with each other. Two different seeding sizes have been used for meshing. For the shared surface, the seeding size of the fluid domain was chosen as $h = 0.075$ m and on the outer boundary as $h = 0.2$ m to ensure a smooth transition from a fine mesh at the contact area between fluid and structure and a coarser mesh further away from the center of the fluid domain.
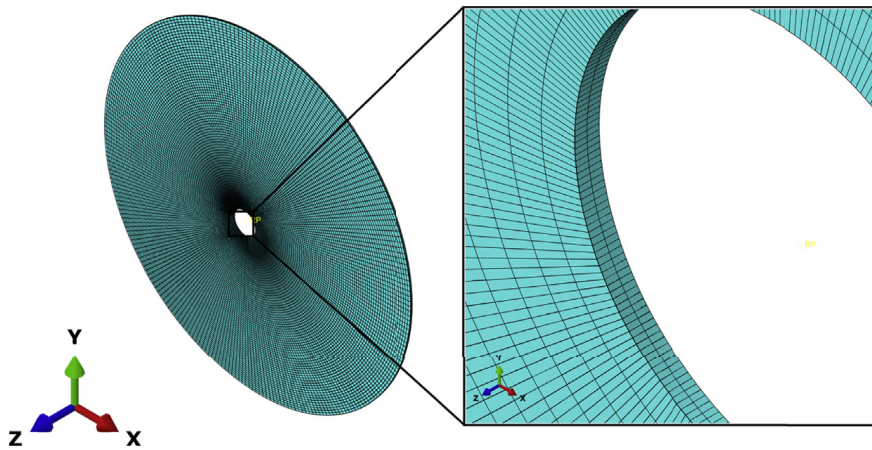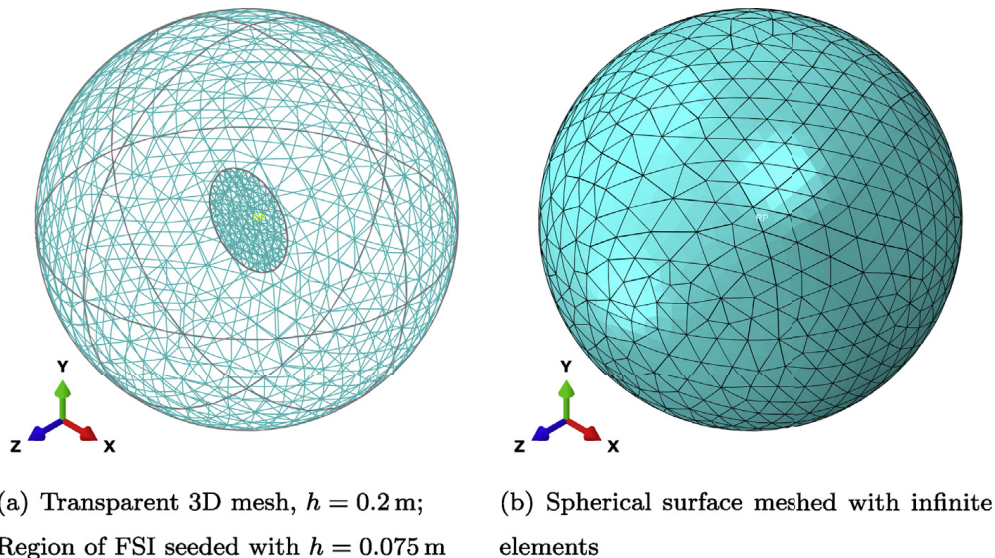

Fig. 3. Fine volumetric mesh of disc; global seeding size $h = 5$ mm, number of elements $N_e = 36208$.

(a) Transparent 3D mesh, $h = 0.2$ m; Region of FSI seeded with $h = 0.075$ m

(b) Spherical surface meshed with infinite elements

Fig. 4. Volumetric mesh of the acoustic full space; sphere radius $r = 1.5$ m.

(a) Transparent 3D mesh, $h = 0.2\,\text{m}$; sphere surface meshed with infinite elements

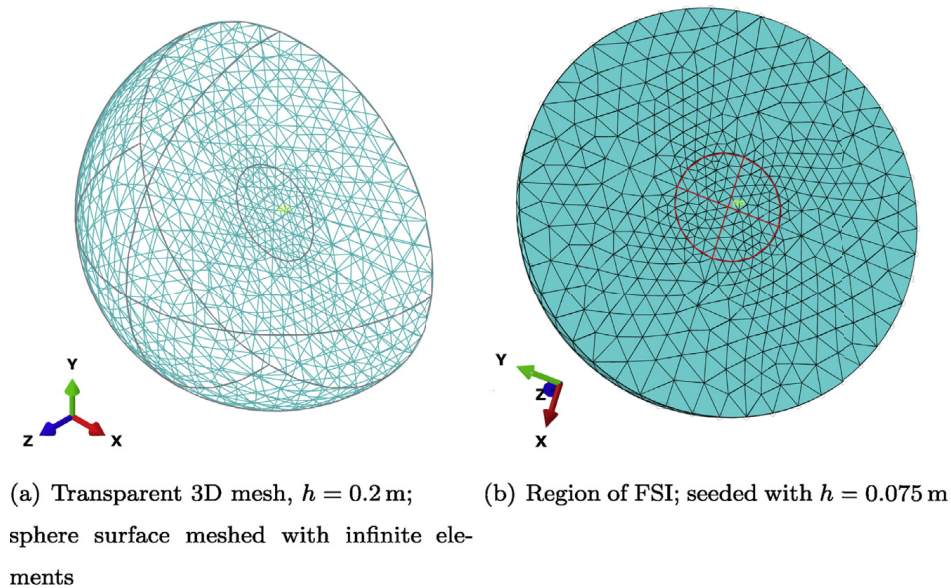(b) Region of FSI; seeded with $h = 0.075\,\text{m}$

Fig. 5. Volumetric mesh of the acoustic half space; sphere radius $r = 1.5$ m.

Since the computational effort is proportional to the size of the model, the fluid domain must be truncated at some extend. To account for the far field radiation, two dimensional infinite finite elements - called infinite elements hereafter - are attached to the outer boundary of the spherical fluid domain. These elements serve as an appropriate far field approximation. A substantial drawback with respect to the computational cost is associated with the use of infinite elements as they are implemented in Abaqus 6.14–2. The drawback lies in the fact that when using infinite elements, no modal decomposition procedure is possible, i.e. when investigating the harmonic behavior, the complete system matrix must be inverted for each frequency step. This results in large computational costs and is therefore only applicable for a limited model size when using conventional workstation machines.

To reduce the computational effort, symmetry is assumed together with appropriate boundary conditions on the symmetry plane. To take this into account, a half space model is generated, cf. Fig. 5. This is equivalent of considering a baffled plate. Here, the symmetry plane at $Z = 0$ is used to cut the acoustic domain, where symmetry boundary conditions must be applied. This topic is addressed in the subsequent sections.

3.2.3. Boundary element model

Based on the structural meshes, equivalent boundary element models are created by identifying the surface element faces of the three dimensional meshes in the positive half plane, i.e. $Z \geq 0$, and converting these faces into surface elements using a scripting interface written in Python language, cf. Fig. 6. The transferred data consists of all surface element nodes with their coordinates, the element coincidence matrix and the surface normal velocities which are the result of a preceding harmonic analysis of the structure in the frequency range of interest. Since the boundary element matrices are fully populated and thus, quite large, the authors use half space models only. This approach is justified by the assumptions for using the lumped parameter model.

3.2.4. Boundary conditions

In the following, the applied boundary conditions will be discussed. In order to tie the disc in space, two areas, i.e. front and back, of the disc defined by the geometrical parameters d_2 and d_3 are used to apply fixed-fixed boundary conditions (BC), cf. Fig. 7.

In Fig. 7(b), the Abaqus specific symbols indicate that all translational and rotational degrees of freedom are fixed. The boundary conditions are applied to surfaces. In the case of the half space radiation problem, symmetry boundary conditions are fulfilled if the velocity normal to the symmetry plane vanishes. This automatically applies to all free edges or surfaces. Therefore, no special care of the symmetry plane must be taken.

The boundary conditions for the fluid models stem from a preceding harmonic analysis of the structure. For each element which is shared by the structure and the fluid, the surface normal velocity is calculated. This information serves as the input data for the fluid model assuming a sound hard boundary conditions.

3.2.5. Excitation

For analyzing the structural behavior in frequency domain, a harmonic force excitation is considered, cf. Fig. 8. For all dynamic analysis hereafter, this force is set to $F(X = 0.4\,\text{m}, Y = 0\,\text{m}, Z = 0\,\text{m}) = 1$ N for all frequencies of interest and is acting in
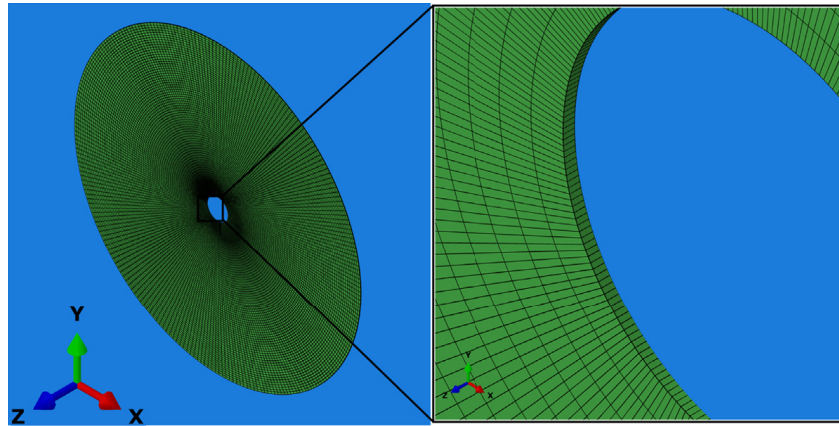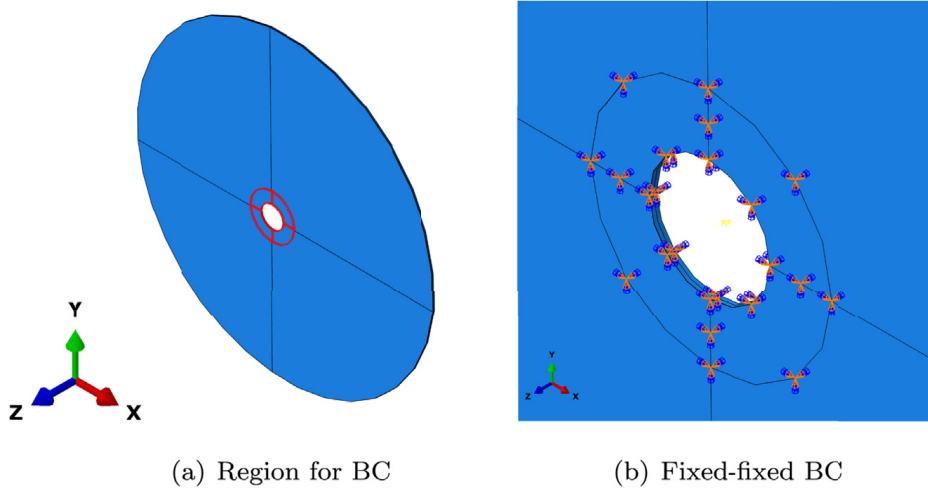
(a) Fine BEM mesh
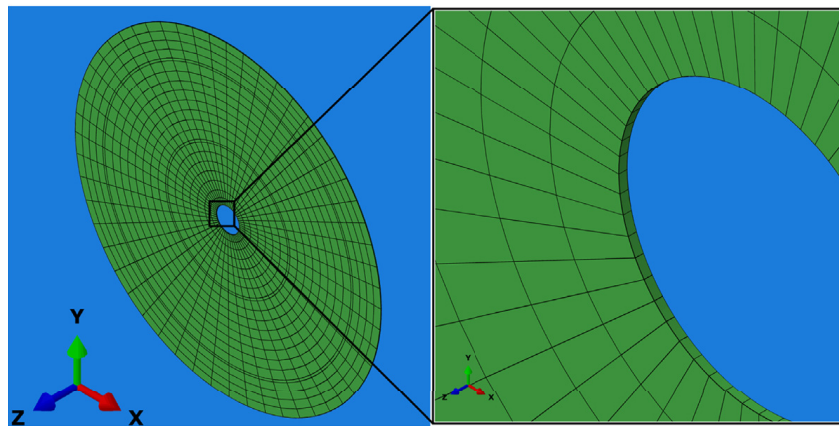
(b) Coarse BEM mesh

Fig. 6. Boundary elements in green and symmetry plane in blue color. (For interpretation of the references to color in this figure legend, the reader is referred to the Web version of this article.)

(a) Region for BC   (b) Fixed-fixed BC

Fig. 7. Application of boundary conditions.

Z-direction, i.e. normal to the main discs' surface. This kind of unit force excitation is idealized and the subsequent results can be understood as transfer functions.

This force excitation has been selected to excite the out-of-plane modes of the structure since they contribute to the main sound radiation. It must be noted that for the real case, two additional forces, one in radial and one in tangential directions,
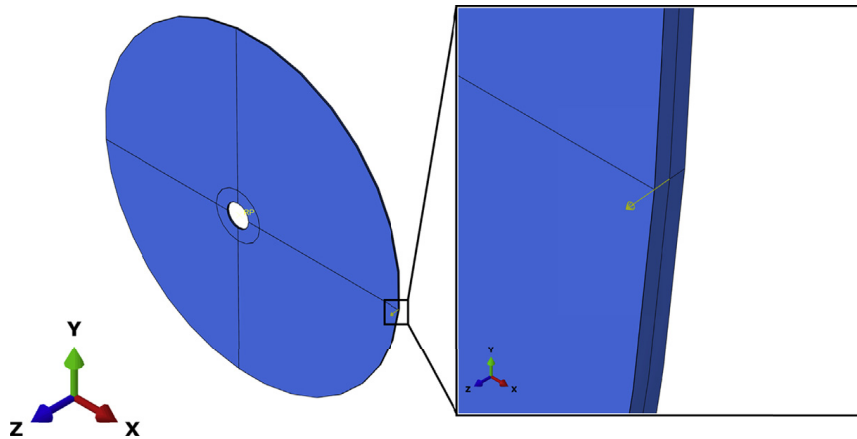
Fig. 8. Structural excitation of disc.
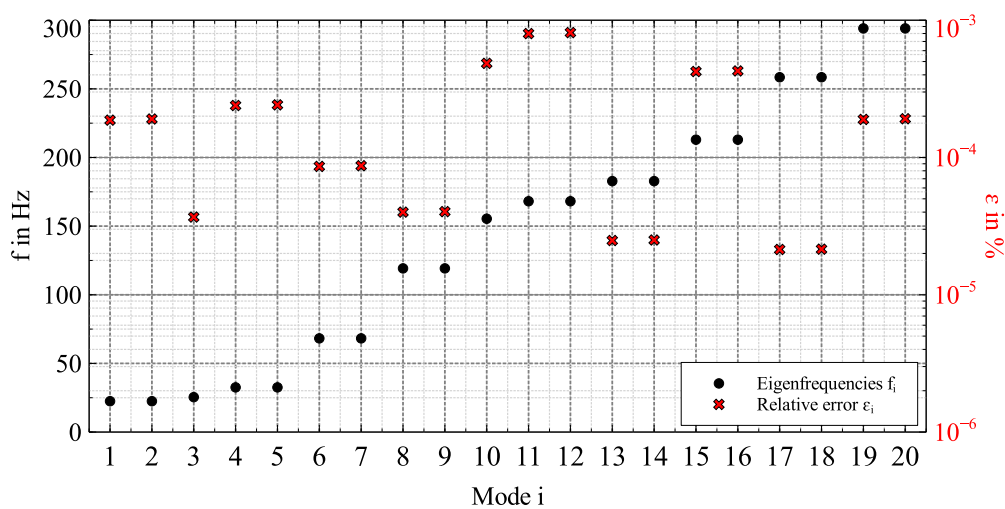
Fig. 9. Results of modal analysis and relative errors.

would act on the structure with possible excitation of in-plane modes. These modes can interact with the out-of-plane modes if the associated frequencies are close to each other. In this case, a mode coupling is possible. Preliminary studies have shown that these modes appear at frequencies above 500 Hz, which are much higher than the scope of this work and are therefore omitted. In addition, the three dimensional elastic behavior of the structure, related to the Poisson's ratio, results in an out-of-plane movement whenever an in-plane deformation is excited. Since the plate can be seen as a thin-walled structure, these out-of-plane deformations are negligible. Further, having a closer look at a realistic application such as a saw blade, it is clear that the saw teeth are not symmetrically aligned with the main geometry. Therefore, any radial or tangential force will furnish a contribution to the excitation of the out-of-plane modes. Thus, it is justified to focus on the normal plane excitation.

4. Results

In the subsequent section, the numerical results are presented and discussed. It will be shown that the numerical analysis using LPM as the acoustic radiation model is capable to correctly estimate the radiated sound power of a spinning disc while using modal superposition for harmonic analysis. All computations have been carried out on a 64 bit-Windows machine with six Intel® Xeon® CPUs E5-1650 v3 @ 3.5 GBHz cores and 64 GB B-RAM.

4.1. Modal analysis of disc

As a first step, the mesh quality is investigated comparing the results of a numerical modal analysis. For this purpose, the first 20 eigenvalues of the fine mesh configuration, cf. Fig. 3, are calculated. Taking into account the fixed-fixed boundary condition, this model results in approximately 1.8×10^6 degrees of freedom. The number of elements is 36208 and none of them is distorted when using a seeding size of $h = 5$ mm. The resulting eigenfrequencies are plotted in Fig. 9. To evaluate the accuracy of the calculations, the results of the coarse model are compared. In this model, the global seeding size was set to $h = 20$ mm, which results in 2268 elements and 26082° of freedom. 1404 elements, i.e. 61.9%, where considered as distorted in this case,
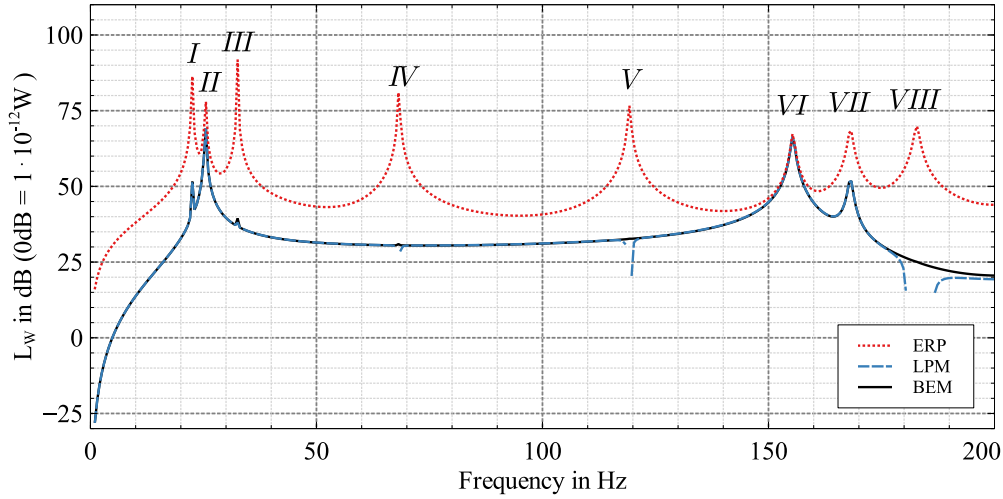
(a) Sound power level
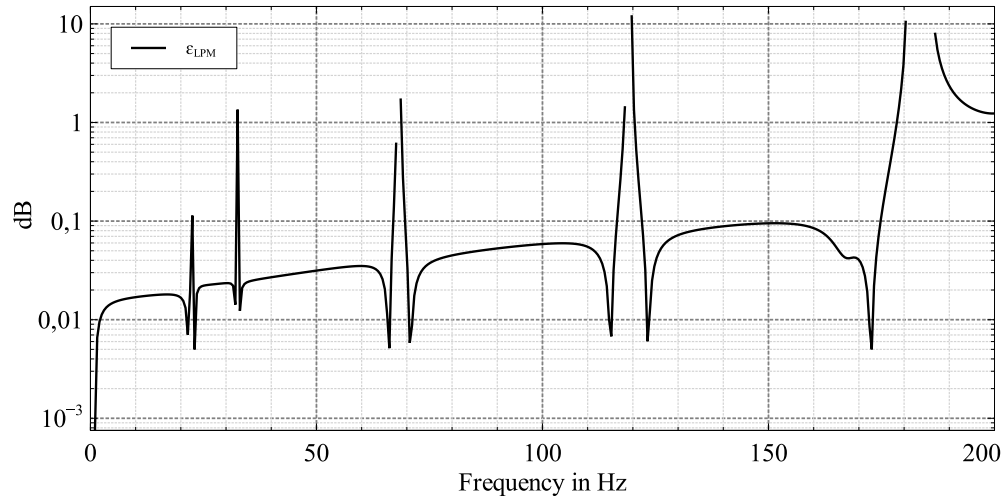
(b) Error plot between BEM and LPM results

Fig. 10. Comparison of ERP, LPM and BEM solutions; $\Omega = 0\,\mathrm{s}^{-1}$.

which may result in inaccurate results. An error measure was calculated as follows.

$$\varepsilon_i = \frac{\left(f_{i\ fine} - f_{i\ coarse}\right)^2}{f_{i\ fine}^2}, \tag{9}$$

where *$f_{i fine}$* is the i-th eigenfrequency of the fine meshed model and *$f_{i coarse}$* is the i-th eigenfrequency of the coarse meshed model.

It can be seen that the error values of all 20 eigenfrequencies remain below 10^{-3}. Therefore, the fine mesh model is considered as converged, cf. Langer et al. [56] for a similar discussion, and can be utilized to generate reference solutions.

4.2. Reference solutions

In this section, the fine mesh model, cf. Fig. 3, is utilized to verify the implemented routine for calculating ERP and LPM results for the non rotating case. From the theory it is known that the LPM gives exact results if the element size becomes infinitesimal small while the vibrating surface radiates sound into an acoustic half space domain under the assumption of an acoustic hard wall boundary condition on the structural surface.

To compute ERP and LPM results, the following steps were executed:

1. Compute the harmonic vibration using the fine finite element model of the structure without the acoustic domain, i.e. in vacuo.
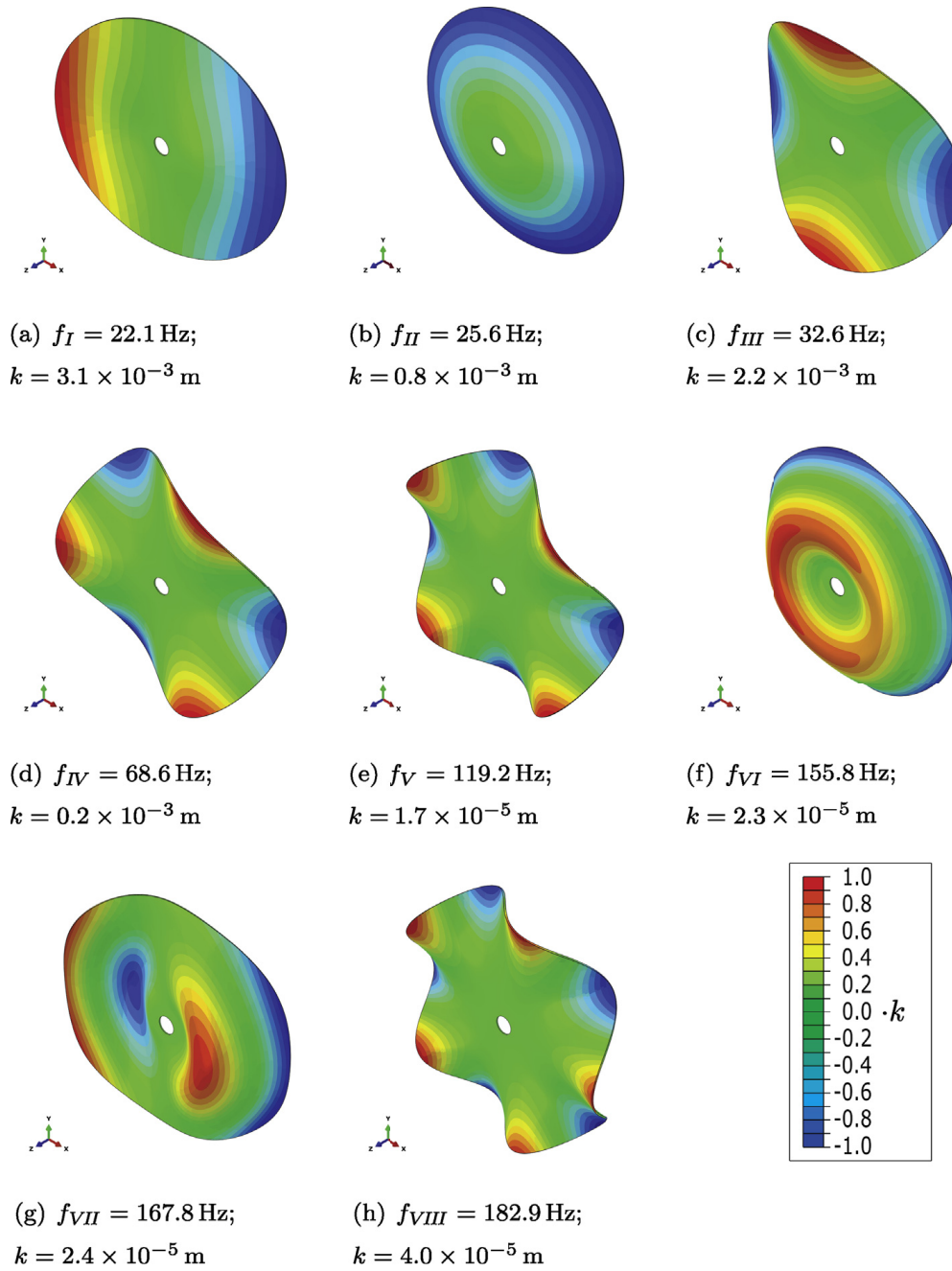
(a) $f_I = 22.1\,\text{Hz}$;
$k = 3.1 \times 10^{-3}\,\text{m}$

(b) $f_{II} = 25.6\,\text{Hz}$;
$k = 0.8 \times 10^{-3}\,\text{m}$

(c) $f_{III} = 32.6\,\text{Hz}$;
$k = 2.2 \times 10^{-3}\,\text{m}$

(d) $f_{IV} = 68.6\,\text{Hz}$;
$k = 0.2 \times 10^{-3}\,\text{m}$

(e) $f_V = 119.2\,\text{Hz}$;
$k = 1.7 \times 10^{-5}\,\text{m}$

(f) $f_{VI} = 155.8\,\text{Hz}$;
$k = 2.3 \times 10^{-5}\,\text{m}$

(g) $f_{VII} = 167.8\,\text{Hz}$;
$k = 2.4 \times 10^{-5}\,\text{m}$

(h) $f_{VIII} = 182.9\,\text{Hz}$;
$k = 4.0 \times 10^{-5}\,\text{m}$

Fig. 11. Deflection shapes at resonances, cf. Fig. 10; u_z component of deformation plotted.

2. Compute ERP and LPM results based on normal particle velocities on the structure's surface.

Similar steps are necessary to compute the reference solutions with the use of the BEM model:

1. Compute the harmonic vibration using the fine finite element model of the structure without the acoustic domain, i.e. in vacuo.
2. Transfer the surface normal velocities of the finite element model as boundary conditions into the boundary element model.
3. Calculate surface sound pressure values based on surface velocities.
4. Evaluate the sound power by integration over the whole boundary element mesh.

The results of BEM, LPM and ERP are compared in Fig. 10. Fig. 10(a) shows the sound power level whereas in Fig. 10(b), the difference between the sound power levels calculated with BEM ($L_{W_{BEM}}$) and with LPM ($L_{W_{LPM}}$), i.e.

$$\varepsilon_{LPM} = |L_{W_{BEM}} - L_{W_{LPM}}| \tag{10}$$
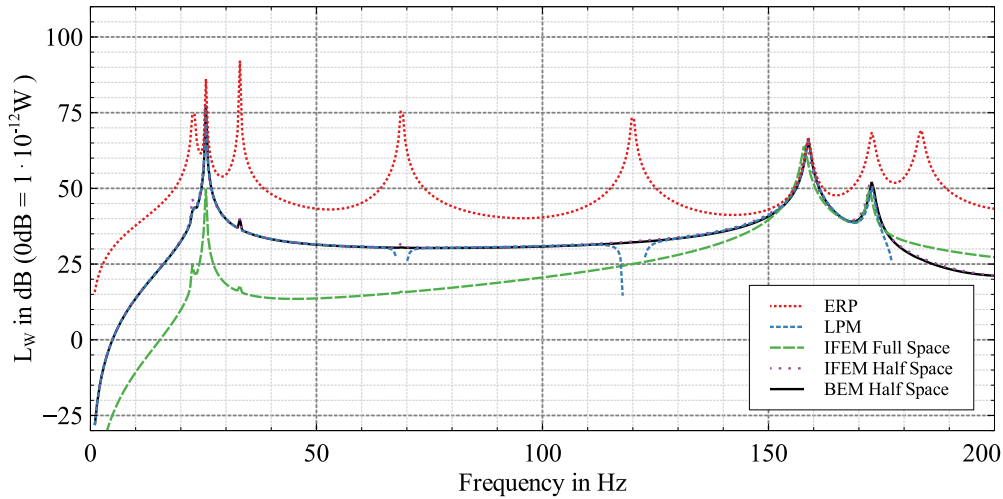
(a) $\Omega = 0\,\mathrm{s}^{-1}$
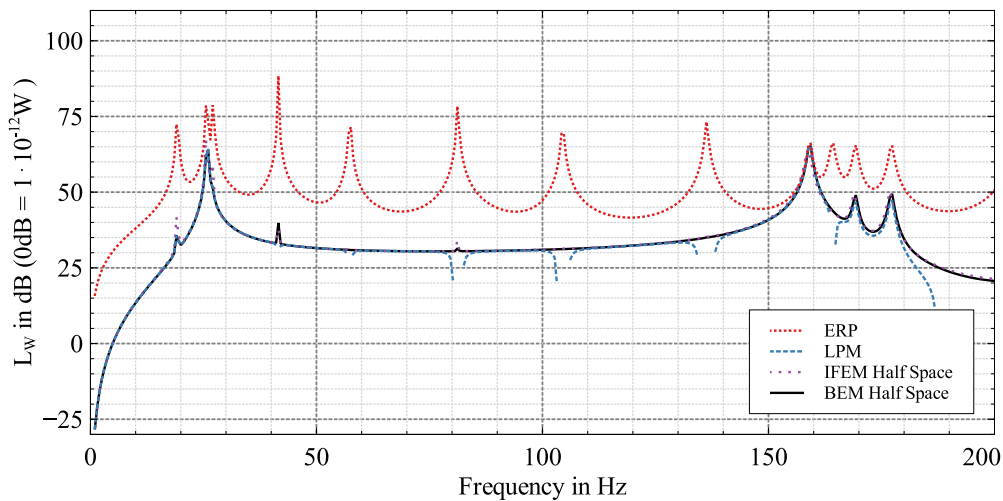
(b) $\Omega = 25\,\mathrm{s}^{-1}$

Fig. 12. Comparison of ERP, LPM, FEM and BEM solutions for coarse structural mesh.

is plotted. It can be seen that the sound power level calculated as ERP clearly overestimates the radiated sound power resulting from the boundary element model and the LPM.

Since the ERP does not consider acoustic short circuits, it is a good measure to identify structural resonances of the disc. These resonances are marked with the roman letters *I* to *VIII*, cf. Fig. 10(a). Note that such perfect acoustic short circuits require perfect symmetry. Since the kinetic energy is quite high at these resonances and technical realization of perfect symmetry quite challenging, ERP indicates at which frequencies unexpected additional resonance peaks could be observed by far-field radiation.

Further, it can be seen that the differences between the BEM and LPM results are of low level except in the vicinity of resonances where acoustic short circuits occur. The authors assume that this behavior is due to numerical errors that arise when differences of approximated values of the same size are computed as it happens for noise cancellation of acoustic short circuits. Apart from the resonances with acoustic short circuits, the LPM results match the BEM results very well. In terms of time efficiency, the wall clock times to compute the LPM and BEM results have been noted. A factor of 40–50 was identified, making the LPM computation computational more efficient. Even though the authors do not want to present an extensive computational timing analysis, the benefit in terms of saving computational resources is obvious. The reader should note that none of the in-house codes are optimized.

In Fig. 11, the u_z-component of the deflection shapes are presented. It can be seen that the sound radiation of the deflection shapes *II* and *VI* are not subjected to acoustic short circuits. *I* and *VII* produce peaks since the active vibration bulges cover large areas and are further away from each other than those of the other deflection shapes. For the remainder of this work, the numerical models are reduced in order to minimize the computational costs. It will be seen that the interesting effects are still prominent and thus can be analyzed in a more effective way.
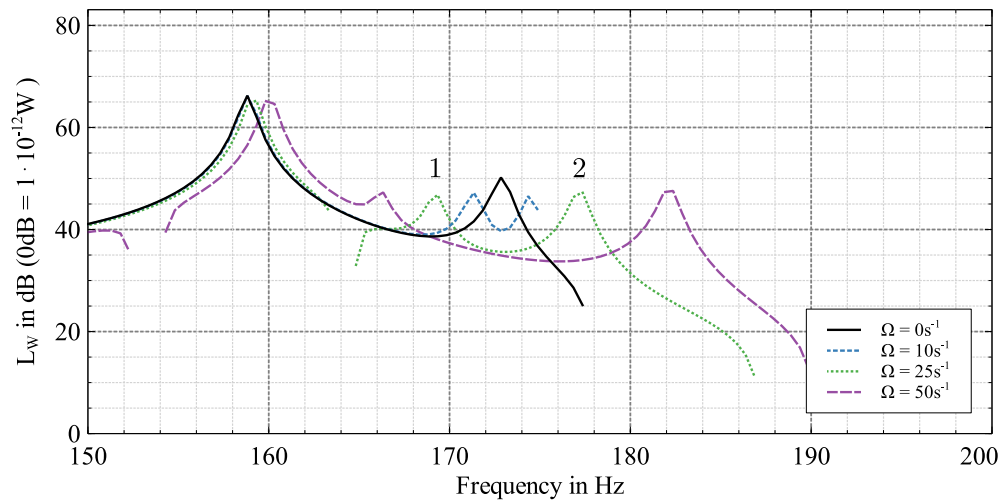
(a) Mode splitting phenomena due to an increase in rotational speed
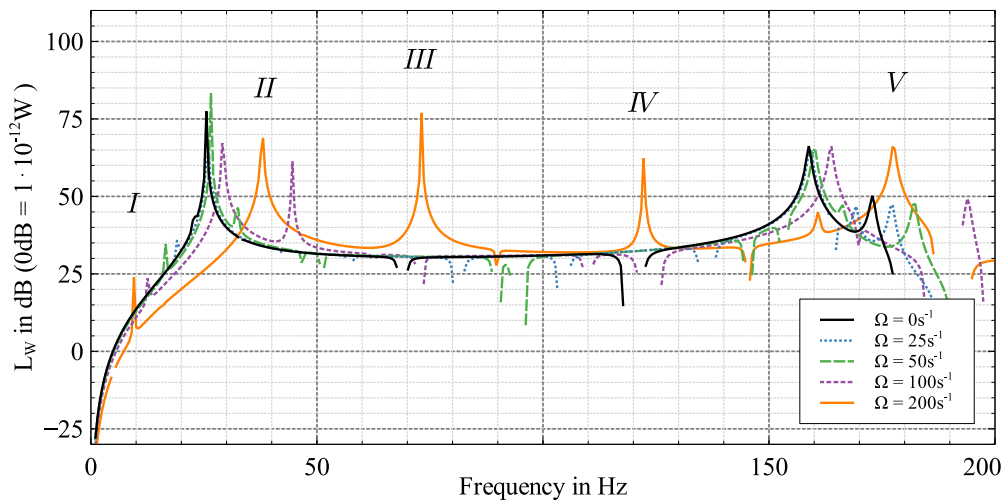
(b) Additional peaks for high rotational speeds

Fig. 13. Comparison of LPM results for different rotational speeds.

4.3. Comparing methods

In this section, the authors discuss the results computed by using different methods, namely ERP and LPM as well as the boundary element model of the half space domain, which is considered as a one-way coupled problem.

In order to study the effects of a fully coupled structure fluid interaction, two additional models are considered. The first model is a fully coupled three dimensional full space finite element model, cf. Fig. 4, and the second one is a half space approximation, cf. Fig. 5. The two fully coupled models are named "IFEM Full Space" or "IFEM Half Space", respectively, in order to indicate that infinite elements are used as a far field approximation and the full space or half space around the disc are considered. Fig. 12 presents the results for the non-rotating case and for a rotational speed of $\Omega = 25$ s^{-1} (or 239 rpm). Comparing the wall clock times, we can estimate a relation of timing for the non-rotating case as (t_{LPM}: t_{BEM}: $t_{FEMHalf}$: $t_{FEMFull}$) to (1: 2.5: 30: 62). Since we compare the full simulation, i.e. the time consumption of the structural dynamic analysis is included, the time relation between LPM and BEM differs with respect to the results presented in the previous section. It can be seen that the results of LPM, BEM and IFEM Half Space are in close agreement. If the full space is considered, the results show some deviations in the low frequency range where not only acoustic short circuits exist on one side of the disc but also from the front side to the backside. In addition, a slight shift of resonance peaks to lower frequencies can be noticed due to the significant mass load of the surrounding fluid. Nevertheless, it can be noted that the full space finite element model retains the same characteristics as the simplified models. Therefore, the proposed approach of simplifying the problem is assumed to be valid.

It must be noted that the proposed method is a simplification with respect to sources radiating into an acoustic half space domain. Therefore, analyzing the full space problem will not be pursued for the reminder of this paper. The readers' attention is called when full space problems need to be analyzed.
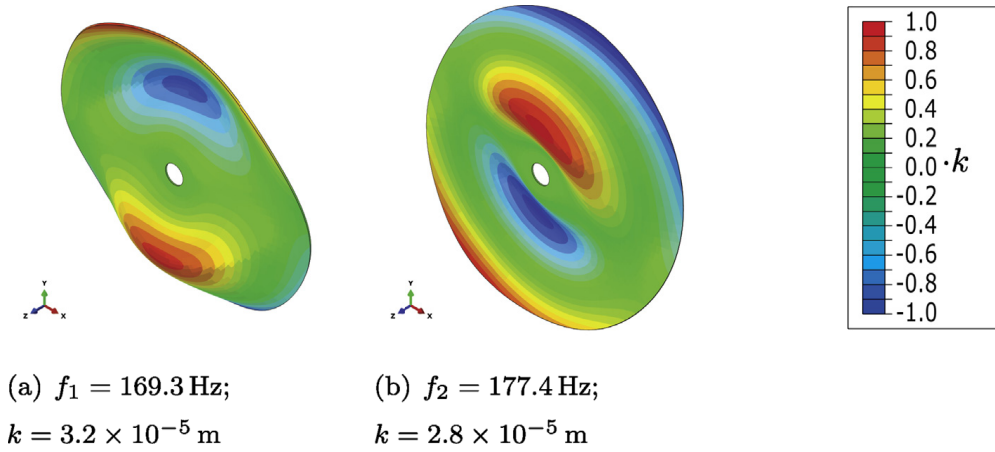
(a) $f_1 = 169.3\,\text{Hz}$;   (b) $f_2 = 177.4\,\text{Hz}$;

$k = 3.2 \times 10^{-5}\,\text{m}$ $k = 2.8 \times 10^{-5}\,\text{m}$

Fig. 14. Deflection shapes of resonances f_1 and f_2, cf. Fig. 13(a), for rotational speed $\Omega = 25\,\text{s}^{-1}$; u_z component of deformation plotted; $\phi = 0°$.
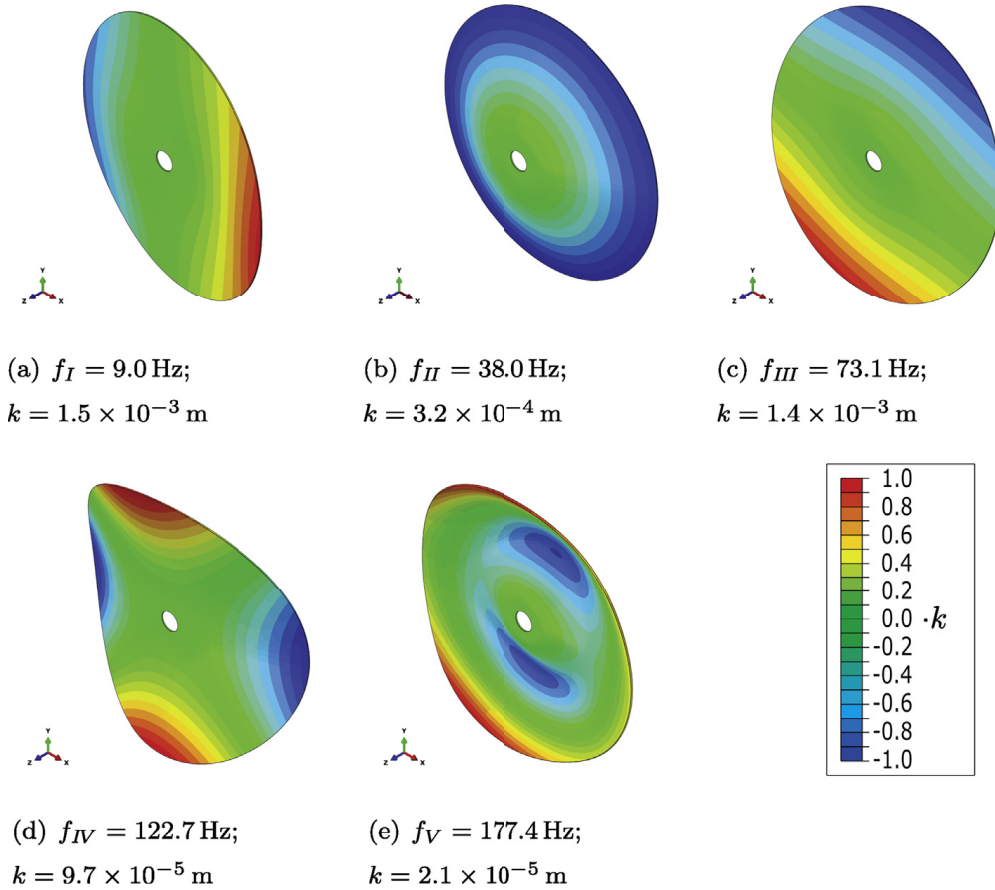

(a) $f_I = 9.0\,\text{Hz}$;   (b) $f_{II} = 38.0\,\text{Hz}$;   (c) $f_{III} = 73.1\,\text{Hz}$;

$k = 1.5 \times 10^{-3}\,\text{m}$ $k = 3.2 \times 10^{-4}\,\text{m}$ $k = 1.4 \times 10^{-3}\,\text{m}$

(d) $f_{IV} = 122.7\,\text{Hz}$;   (e) $f_V = 177.4\,\text{Hz}$;

$k = 9.7 \times 10^{-5}\,\text{m}$ $k = 2.1 \times 10^{-5}\,\text{m}$

Fig. 15. Deflection shapes at resonances, cf. Fig. 13(b) with $\Omega = 200\,\text{s}^{-1}$; u_z component of deformation plotted; phase angle $\phi = 0°$.

When considering rotation of the disc, the ERP results exhibit a clear mode splitting, cf. Fig. 12(b), where, for instance, the resonance close to $f = 70\,\text{Hz}$ in the non-rotating case, cf. Fig. 12(a), splits up into resonances at $f = 58\,\text{Hz}$ and $f = 81\,\text{Hz}$ for the rotating case. This effect is due to superimposition of the rotational frequency and the vibrational frequency of the disc. From the outside perspective this results in a forward and backward traveling wave with respect to the rotation. Again, comparing the results of the LPM, BEM and IFEM Half Space calculations, it can be seen that all three methods give very similar results and that, in the low frequency range, acoustic short circuits can occur. Then, no resonant sound radiation is expected. Only at higher frequencies where acoustic short circuits are less pronounced due to the higher radiation efficiency, the mode splitting leads to resonant sound radiation. As a final remark, it can be stated that the LPM method can be used as a suitable numerical tool for investigating the sound radiation of rotating discs. This will be discussed in more detail in the subsequent section.

4.4. Analysis of different rotational speeds

To investigate the sound radiation from the spinning disc, different rotational speeds are considered. Fig. 13 shows results for various angular velocities Ω. It was already mentioned that for higher frequencies, acoustic short circuits are less pronounced and mode splitting can be noticed in the LPM results. Fig. 13(a) shows a zoomed window of the mentioned frequency range between $f = 150$ Hz and $f = 200$ Hz. The calculated data is plotted for $\Omega = 0\,\mathrm{s}^{-1}$, $\Omega = 10\,\mathrm{s}^{-1}$, $\Omega = 25\,\mathrm{s}^{-1}$ and $\Omega = 50\,\mathrm{s}^{-1}$. It can be clearly seen that once the rotational speed increases, the resonance peaks start to split where the resonance associated with the backward traveling wave decreases in frequency and the resonance associated with the forward traveling wave increases. This effect is not symmetric with respect to the resonance frequency of the non-rotating disc since centrifugal forces lead to an increase in stiffness of the whole system. It is clearly identified for the resonance at $f = 159$ Hz for the non-rotating case which is then shifted up to $f = 160$ Hz for the case where the rotational speed is increased to $\Omega = 50\,\mathrm{s}^{-1}$, cf. Fig. 13(a).

Exemplarily, Fig. 14 pictures the deflections shapes of the two resonances in Fig. 13(a) marked with the numbers "1" and "2" for the rotational speed of $\Omega = 25\,\mathrm{s}^{-1}$.

It can be seen that the form of the deflection shape is similar and that, at first glance, only the associated frequencies differ. The second difference that the authors want to point out is that the deflections shapes have a complex form, i.e. that the radial nodal lines of the deflection shape do not remain at their initial position but rather rotate in the opposite direction of the rotation for the backward traveling wave and rotate with the direction of the rotation for the forward traveling wave. This will be discussed in more detail later in this section.

For a wide range of rotational speeds, i.e. up to $\Omega = 50\,\mathrm{s}^{-1}$, no identifiable resonances occur between $f = 50$ Hz and $f = 150$ Hz. In contrast, when the rotational speed is increased up to $\Omega = 200\,\mathrm{s}^{-1}$, suddenly resonances occur. This is somehow surprising since the associated deflection shapes of deflection *III* and *IV*, cf. Fig. 15(c) and (d), respectively, tend to form acoustic short circuits. A possible explanation, proposed by the authors, can be related to the fact that for the rotating case, stationary nodal lines of the deflection shapes are not pronounced anymore. They rather consist of stationary and traveling wave components. Due to the traveling wave characteristics, acoustic short circuits are less likely to occur and thus resulting in additional peaks in the far field radiation spectrum. Similar discussions have been conducted in Unruh at al. [57] and Liu et al. [58].

Further, the authors present the deformations shapes of the rotating deflection shapes associated with the rotational speed of $\Omega = 200\,\mathrm{s}^{-1}$ at the resonant frequencies of $f_I = 9.0$ Hz and $f_{III} = 73.1$ Hz, cf. Figs. 13(b) and 15. Figs. 16 and 17 show the deflection shapes of the mentioned resonances for different phase angles of the vibration. It can be seen that in Fig. 16, the nodal line stretching in radial direction rotates in the opposite direction of the rotation whereas in Fig. 17, the nodal line rotates in the direction of the discs' rotation. The latter one can be regarded as acoustically relevant as long as the vibrating frequency remains in the audible frequency range. Since the associated frequency of the backward traveling wave $f_I = 9.0$ Hz is below the audible frequency range of $f = 20.0$ Hz, it can be neglected with respect to usual acoustic problems. However, from a mechanical point of view this vibration is more crucial since there exists a critical rotational speed Ω_{crit} where the associated frequency of the vibration tends to zero. This phenomenon is similar to a tumbling rotor where it is called wobbling [59]. For the case where the vibrating frequency is zero, a fixed observer recognizes a stationary deflection of the disc while still spinning.

As a final remark, the question will be addressed whether the mode splitting is audible or not. For this reason, the sound pressure is evaluated at three different positions in the YZ-plane, cf. Fig. 18, of the half space model, namely at $\Phi = 0°$, $\Phi = 45°$ and $\Phi = 90°$ according to the definition of Φ which can be found in Fig. 18(a). Fig. 18(b) depicts the real part of the sound pressure taken from the surface of the half space model, i.e. the disc is considered as baffled, plotted in the frequency range between $f = 150$ Hz and $f = 180$ Hz where the disc is rotating with $\Omega = 25\,\mathrm{s}^{-1}$. It can be seen that if a listener is located on the axis of rotation, no mode splitting is audible. When moving away from the axis of rotation, mode splitting is audible.
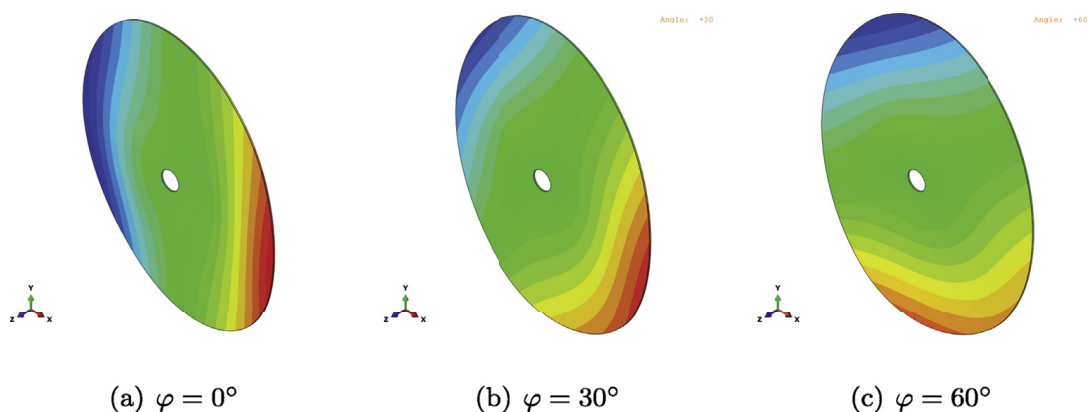

(a) $\varphi = 0°$ (b) $\varphi = 30°$ (c) $\varphi = 60°$

Fig. 16. Deflection shapes at phase angles at resonance f_I with $\Omega = 200\,\mathrm{s}^{-1}$; u_z component of deformation plotted.

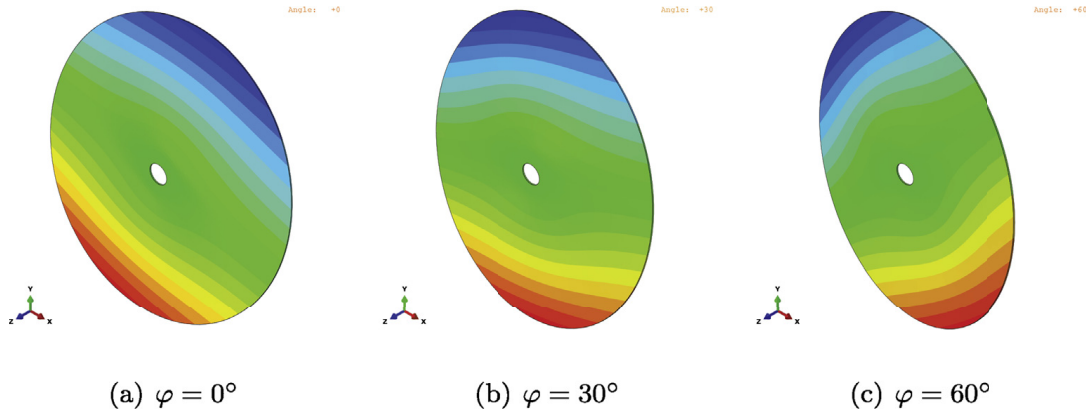(a) $\varphi = 0°$ (b) $\varphi = 30°$ (c) $\varphi = 60°$

Fig. 17. Deflection shapes at phase angles at resonance f_{III} with $\Omega = 200 \text{ s}^{-1}$; u_z component of deformation plotted.

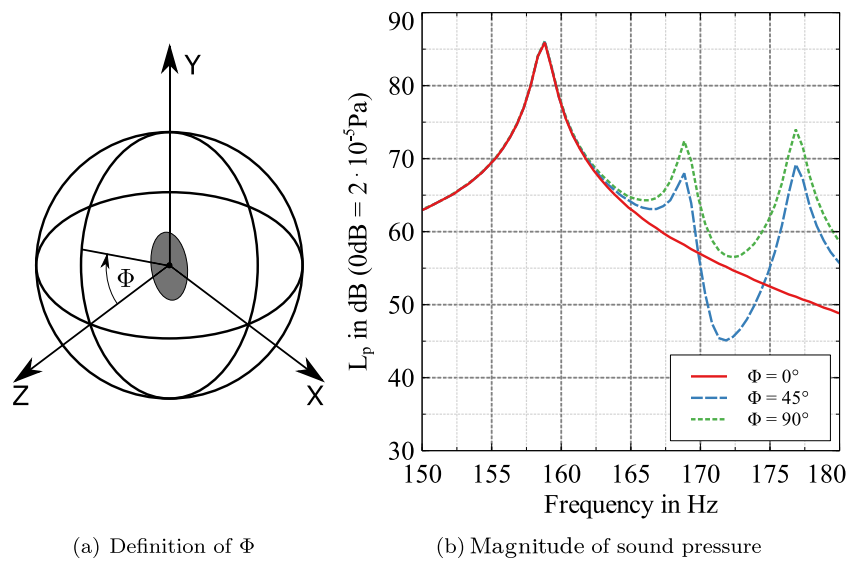(a) Definition of Φ (b) Magnitude of sound pressure

Fig. 18. Sound radiation at different polar coordinates for $\Omega = 25 \text{ s}^{-1}$.

5. Conclusions

In conclusion, the authors want to point out the following statements. At first, the fully coupled finite element model gives the most accurate results, where acoustic short circuits on the disc surface as well as between the front and the back side are considered. Further, the mass loading of the full space model is recognizable by means of shifts in the resonance frequencies. Second, ERP and LPM are suitable approaches for computing sound power values of rotating structures. It must be noted that the LPM assumes a baffled sound radiator. In addition, it is a valid approach to simplify the structural normal surface velocity across a finite element if the element size is adequate. Comparing results of LPM and ERP enables the user to identify acoustic short circuits. For the cases where acoustic short circuits are present, one should choose LPM over ERP. Third, utilizing LPM reduces the computational efforts by a factor of 50 compared to an equivalent BEM simulation and a factor of 60 compared to the full FEM simulation where FEA is included within the LPM timing. Fourth, for high rotational speeds, additional resonances occur. It is expected that cancellation effects due to acoustic short circuits are not present anymore. Last but not least, the authors identified that mode splitting is audible but not along the axis of rotation.

Based on these conclusions, the authors see the LPM as a useful tool to integrate sound power estimations to the frame of acoustic optimization problems of rotating structures.

Author contribution statement

Maeder, Marcus: Conceptualization, Methodology, Software, Validation, Formal analysis, Investigation, Data Curation, Writing - Original Draft, Writing - Review & Editing, Visualization, Project administration. **D' Auria, Roberto**: Methodology, Software, Investigation, Writing - Original Draft, Writing - Review & Editing. **Grasso, Ettore**: Conceptualization, Methodology, Software,

Investigation, Writing - Original Draft, Writing - Review & Editing. **Petrone, Giuseppe**: Writing - Review & Editing. **De Rosa, Sergio**: Writing - Review & Editing, Supervision. **Klaerner, Matthias**: Software, Writing - Review & Editing. **Kroll, Lothar**: Supervision. **Marburg, Steffen**: Resources, Writing - Review & Editing, Supervision.

References

[1] C.D. Mote, R. Szymani, A review report on principal developments in thin circular saw vibration and control research, Holz Roh Werkst. 35 (5) (1977) 189–196.

[2] H. Lamb, R.V. Southwell, The Vibration of a Spinning Disk, The Royal Society Publishing.

[3] W. Eversman, J.R.O. Dodson, Free vibration of a centrally clamped spinning circular disk, AIAA J. 7 (10) (1969) 2010–2012.

[4] T. Kiesel, S. Marburg, Simulation of mode-locking phenomena in a complex nonlinear rotor system using 3d solid finite elements, Proceed. Inst. Mech. Eng., Part C: J. Mech. Eng. Sci. 230 (6) (2016) 959–973, https://doi.org/10.1177/0954406215617196.

[5] S. Huang, W. Soedel, Effects of coriolis acceleration on the free and forced in-plane vibrations of rotating rings on elastic foundation, J. Sound Vib. 115 (2) (1987) 253–274.

[6] M.A. Prohl, A general method for calculating critical speeds of flexible rotors, Trans. ASME 67 (1945) A142.

[7] W. Prager, Recent developments in the mathematical theory of plasticity, J. Appl. Phys. 20 (3) (1949) 235–241.

[8] G.S. Schajer, C.D. Mote, Analysis of roll tensioning and its influence on circular saw stability, Wood Sci. Technol. 17 (4) (1983) 287–302.

[9] U. Heisel, T. Stehle, H. Ghassemi, Experimental investigation into parameters influencing roll tensioning of circular saw blades, J. Mach. Eng. 15 (2015).

[10] M. Na, R. uri, T. Nnsi, Prediction of modal properties of circular disc with pre-stressed fields, MATEC Web Conf. 157 (2018) 02034, https://doi.org/10.1051/matecconf/201815702034.

[11] M. Na, Structural dynamic modification of vibrating systems, Appl. Comput. Mech. 1 (2007) 203–214.

[12] N. Nicoletti, E. Aubry, D. Fendeleur, M. Renner, A finite element model for the analysis of roll burnishing, Holz Roh Werkst. 55 (24) (1997) 183–187.

[13] R. Chanaud, Experimental study of aerodynamic sound from a rotating disk, J. Acoust. Soc. Am. 45 (2) (1969) 392–397.

[14] L. Chen, D. Schweikert, Sound radiation from an arbitrary body, J. Acoust. Soc. Am. 35 (10) (1963) 1626–1632.

[15] G.H. Koopmann, J.B. Fahnline, Active Control of Radiated Acoustic Power, Designing Quiet Structures, Academic Press, London, 1997, pp. 179–200.

[16] M. Lee, R. Singh, Analytical formulations for annular disk sound radiation using structural modes, J. Acoust. Soc. Am. 95 (6) (1994) 3311–3323, https://doi.org/10.1121/1.409993.

[17] O. Tger, M. Dannemann, W.A. Hufenbach, Analytical study of the structural-dynamics and sound radiation of anisotropic multilayered fibre-reinforced composites, J. Sound Vib. 342 (2015) 57–74.

[18] L. Cremer, M. Heckl, B. Petersson, Structure-Borne Sound, Springer Berlin Heidelberg, 2005.

[19] H. Lee, R. Singh, Acoustic radiation from out-of-plane modes of an annular disk using thin and thick plate theories, J. Sound Vib. 282 (1) (2005) 313–339, https://doi.org/10.1016/j.jsv.2004.02.059.

[20] F. Gao, Y. Yan, F.F. Yap, Study on idle noise characteristics of hard disk drives based on a multibody dynamic formulation, Mech. Based Des. Struct. Mach. 33 (2) (2005) 215–241, https://doi.org/10.1081/SME-200067068.

[21] A. Chatterjee, V. Ranjan, M.S. Azam, M. Rao, Theoretical and numerical estimation of vibroacoustic behavior of clamped free parabolic tapered annular circular plate with different arrangement of stiffener patches, Appl. Sci. 8 (12) (2018), https://doi.org/10.3390/app8122542.

[22] H. Lee, M.C. Song, J.C. Suh, B.J. Chang, Hydro-elastic analysis of marine propellers based on a bem-fem coupled fsi algorithm, Int. J. Nav. Architect. Ocean Eng. 6 (3) (2014) 562–577.

[23] I. Harari, K. Grosh, T.J.R. Hughes, M. Malhotra, P.M. Pinsky, J.R. Stewart, L.L. Thompson, Recent developments in finite element methods for structural acoustics, Arch. Comput. Methods Eng. 3 (2) (1996) 131–309, https://doi.org/10.1007/BF03041209.

[24] M. Klaerner, M. Wuehrl, L. Kroll, S. Marburg, Fea-based methods for optimising structure-borne sound radiation, Mech. Syst. Signal Process. 89 (2017) 37–47, https://doi.org/10.1016/j.ymssp.2016.07.019.

[25] D. Fritze, S. Marburg, H. Hardtke, Reducing radiated sound power of plates and shallow shells by local modification of geometry, Acta Acustica United Acustica 89 (1) (2003) 53–60.

[26] D. Fritze, S. Marburg, H.-J. Hardtke, Estimation of radiated sound power: a case study on common approximation methods, Acta Acustica United Acustica 95 (5) (2009) 833–842.

[27] S. Marburg, B. Nolte (Eds.), Computational Acoustics of Noise Propagation in Fluids - Finite and Boundary Element Methods, Springer-Verlag, Berlin, Heidelberg, 2008.

[28] Y. Cheng, H. Zhang, Immersed boundary method and lattice Boltzmann method coupled fsi simulation of mitral leaflet flow, Comput. Fluid 39 (5) (2010) 871–881.

[29] H.G. Matthies, R. Niekamp, J. Steindorf, Algorithms for strong coupling procedures, Comput. Methods Appl. Mech. Eng. 195 (1718) (2006) 2028–2049.

[30] M. Mnsch, M. Breuer, Numerical simulation of fluidstructure interaction using eddyresolving schemes, in: Fluid Structure Interaction II, Springer, 2011, pp. 221–253.

[31] F. Benra, H. Dohmen, J. Pei, S. Schuster, B. Wan, A comparison of one-way and two-way coupling methods for numerical analysis of fluid-structure interactions, J. Appl. Math. 2011 (6) (2011) 1–16, https://doi.org/10.1155/2011/853560.

[32] Q. Zhang, T. Hisada, Studies of the strong coupling and weak coupling methods in fsi analysis, Int. J. Numer. Methods Eng. 60 (12) (2004) 2013–2029.

[33] J. Degroote, P. Bruggeman, R. Haelterman, J. Vierendeels, Stability of a coupling technique for partitioned solvers in fsi applications, Comput. Struct. 86 (2324) (2008) 2224–2234.

[34] G. Hou, J. Wang, A. Layton, Numerical methods for fluid-structure interaction - a review, Commun. Comput. Phys. 12 (2) (2012) 337–377.

[35] A. Bermdez, L. Hervella-Nieto, A. Prieto, R. Rodrguez, Perfectly matched layers for time-harmonic second order elliptic problems, Arch. Comput. Methods Eng. 17 (1) (2010) 77–107, https://doi.org/10.1007/s11831-010-9041-6.

[36] B. Kaltenbacher, M. Kaltenbacher, I. Sim, A modified and stable version of a perfectly matched layer technique for the 3-d second order wave equation in time domain with an application to aeroacoustics, J. Comput. Phys. 235 (2013) 407–422, https://doi.org/10.1016/j.jcp.2012.10.016.

[37] A. Hppe, M. Kaltenbacher, Stable matched layer for the acoustic conservation equations in the time domain, J. Comput. Acoust. 20 (01) (2012) 1250004, https://doi.org/10.1142/S0218396X11004511.

[38] D. Givoli, Computational absorbing boundaries, in: S. Marburg, B. Nolte (Eds.), Computational Acoustics of Noise Propagation in Fluids - Finite and Boundary Element Methods, Springer Berlin Heidelberg, Berlin, Heidelberg, 2008, pp. 145–166, https://doi.org/10.1007/978-3-540-77448-8_6.

[39] D. Givoli, T. Hagstrom, I. Patlashenko, Finite element formulation with high-order absorbing boundary conditions for time-dependent waves, Comput. Methods Appl. Mech. Eng. 195 (29) (2006) 3666–3690, https://doi.org/10.1016/j.cma.2005.01.021 absorbing Boundary Conditions.

[40] L. Moheit, S. Marburg, Normal modes and modal reduction in exterior acoustics, J. Theor. Comput. Acoust. 26 (03) (2018) 1850029, https://doi.org/10.1142/S2591728518500299.

[41] R. Astley, G. Macaulay, J. Coyette, Mapped wave envelope elements for acoustical radiation and scattering, J. Sound Vib. 170 (1) (1994) 97–118, https://doi.org/10.1006/jsvi.1994.1048.

[42] F.P. Mechel (Ed.), Formulas of Acoustics, second ed., Springer-Verlag, Berlin, Heidelberg, 2008.

[43] S. Marburg, Developments in structural-acoustic optimization for passive noise control, Arch. Comput. Methods Eng. 9 (4) (2002) 291–370, https://doi.org/10.1007/BF03041465.

[44] J.B. Fahnline, G.H. Koopmann, A lumped parameter model for the acoustic power output from a vibrating structure, J. Acoust. Soc. Am. 100 (6) (1996) 3539–3547.
[45] J.B. Fahnline, G.H. Koopmann, Numerical implementation of the lumped parameter model for the acoustic power output of a vibrating structure, J. Acoust. Soc. Am. 102 (1) (1997) 179–192.
[46] G.H. Koopmann, J.B. Fahnline, Designing Quiet Structures, Academic Press, London, 1997.
[47] G. Genta, Dynamics of Rotating Systems, Mechanical Engineering Series, Springer ScienceBusiness Media, Inc, New York, NY, 2005.
[48] Dassault Systmes, ABAQUS Product Documentation, Release Abaqus 6.14-2, Providence, RI, USA: Dassault Systmes 2014, 2017.
[49] Y. Liu, Y. Zhao, Z.-Q. Lang, J. Li, X. Yan, S. Zhao, Weighted contribution rate of nonlinear output frequency response functions and its application to rotor system fault diagnosis, J. Sound Vib. 460 (2019) 114882, https://doi.org/10.1016/j.jsv.2019.114882.
[50] M.S. Howe, Acoustics of Fluid-Structure Interactions, Cambridge Monographs on Mechanics, Cambridge University Press, 1998, https://doi.org/10.1017/CBO9780511662898.
[51] Y. Bazilevs, K. Takizawa, T.E. Tezduyar, Computational Fluid-Structure Interaction: Methods and Applications, Wiley Series in Computational Mechanics, Wiley, 2013. Chichester, West Sussex, United Kingdom.
[52] O.C. Zienkiewicz, R.L. Taylor, P. Nithiarasu, The Finite Element Method for Fluid Dynamics, seventh ed., Butterworth-Heinemann, Oxford and Waltham, Mass., 2014.
[53] T.E. Oliphant, A Guide to NumPy, vol. 1, Trelgol Publishing USA, 2006.
[54] T.E. Oliphant, Python for scientific computing, Comput. Sci. Eng. 9 (3) (2007) 10–20, https://doi.org/10.1109/MCSE.2007.58.
[55] S. Marburg, S. Schneider, Influence of element types on numeric error for acoustic boundary elements, J. Comput. Acoust. 11 (03) (2003) 363–386, https://doi.org/10.1142/S0218396X03001985.
[56] P. Langer, M. Maeder, C. Guist, M. Krause, S. Marburg, More than six elements per wavelength: the practical use of structural finite element models and their accuracy in comparison with experimental results, J. Comput. Acoust. 25 (04) (2017) 1750025, https://doi.org/10.1142/S0218396X17500254.
[57] O. Unruh, M. Sinapius, H.P. Monner, Sound radiation properties of complex modes in rectangular plates: a numerical study, Acta Acustica United Acustica 101 (1) (2015) 62–72, https://doi.org/10.3813/AAA.918805.
[58] D. Liu, S. Marburg, C. Geweth, N. Kessissoglou, Non-negative intensity for structures with inhomogeneous damping, J. Theor. Comput. Acoust. 27 (01) (2019) 1850050, https://doi.org/10.1142/S2591728518500500.
[59] A. Fidlin, O. Drozdetskaya, B. Waltersberger, On the minimal model for the low frequency wobbling instability of friction discs, Eur. J. Mech. A Solid. 30 (5) (2011) 665–672, https://doi.org/10.1016/j.euromechsol.2011.03.009.

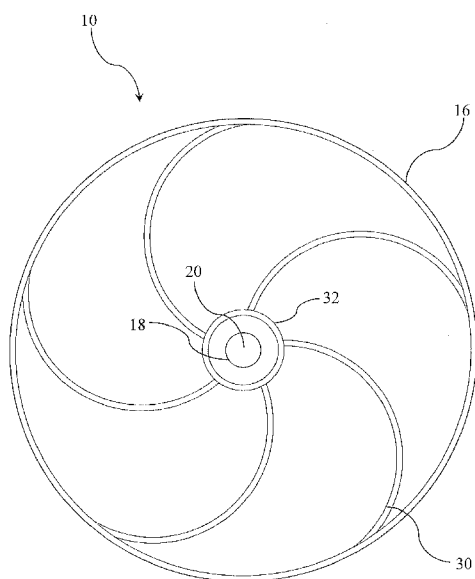(54) Title: DOUBLE CUTTING DISC WITH CURVED DEFORMATION LINES

Fig. 2

(57) Abstract: A rotary cutting disc (10) comprising two coaxial mutually opposed disc-shaped elements (12a, 12b) each having a circumferential edge, wherein circumferential edges (14a, 14b) of the disc-shaped elements (12a, 12b) are joined together forming a cutting edge (16) of the cutting disc (10); wherein each of the disc-shaped elements (12a, 12b) comprises one or more at least partly curved elongated deformation lines (30), wherein the one or more deformation lines (30) have a radial distance from the centre (26) of the cutting disc (10) that increases along at least a part of the length of the deformation line (30). The rotary cutting disc (10) has an increased critical speed that allows improving the efficiency of a cutting operation with a cutting disc while maintaining acceptable levels of quality, cutting precision and safety.

Double cutting disc with curved deformation lines

FIELD OF THE INVENTION

The present invention is related to a cutting disc or diamond blade for cutting materials. More particularly, the present invention relates to a cutting disc with a novel configuration allowing for improved dynamical properties of the cutting disc in operation.

BACKGROUND OF THE INVENTION

Rotary cutting discs are widely employed in different fields of technology for cutting purposes. Cutting discs of relatively small dimensions in the submillimetric range are used for medical purposes, for example in the field of odontology. Cutting discs having diameters in a range from approximately 50 cm to as large as 2 m are used for instance in the fields of metallurgy, civil construction and wood processing for cutting a variety of materials.

In a continued effort to increase the efficiency of cutting operations by cutting tools making use of cutting discs, manufacturers of cutting discs aim at an increasingly thinner shape thereof. Thinner cutting discs generally allow cutting through objects in shorter times and with less power consumption, as less material of the object being cut needs to be removed. However, these efforts are faced with technical limitations with regard to the mechanical properties of the tool and its dynamic behaviour in operation, for the cutting disc must maintain structural integrity, dynamic stability and withstand centrifugal and transversal forces.

Rotating machinery, as any dynamical system, is exposed to vibrations and deformations depending for instance upon structural properties thereof, possible functioning faults and force imbalances. A thin rotary cutting disc rotating in a physical environment may severely deform when subjected to loss of dynamical stability and to arising resonances. This may result in a widening and a deviation of the intended cutting line, such that the final cutting line may in some instances be several times wider than the width of the cutting disc, which leads to increased material consumption, reduced cutting precision, increased wear of the cutting disc and increased power consumption. Further, this undesired stability loss may lead to fatal mechanical disruptions of the cutting disc itself or the surrounding machinery as a result of increased forces transversal to the cutting line. For example, the cutting

disc may penetrate sideways into the material being cut along a direction perpendicular to the cutting line, which may cause severe damage to the cutting disc or cause the cutting disc to remain trapped and/or bent upon turning off the cutting machine.

5   It is seen in practice that there is typically a rotation frequency above which the disc of the cutting machine exhibits a large deformation, leading to an undesired increase in the width of the cut, excessive wear or even breakage of the disc upon operation. This frequency is referred to as "critical frequency" herein. Clearly, by restricting the rotational speed of the cutting disc to frequencies below this critical frequency, the
10   efficiency of the cutting tool is likewise limited. Hence, there is a strong demand in the art to provide cutting discs with an extended range of operable rotational speeds.

SUMMARY OF THE INVENTION

It is an object of the present invention to provide a rotary cutting disc for a cutting tool machine with an improved structural stability overcoming the above technical
15   disadvantages and allowing for an increased maximal feasible rotational speed of the cutting disc. This is achieved by a cutting disc according to claim 1. Preferable embodiments of the invention are captured by the dependent claims.

The dynamical stability of the cutting disc is governed by its vibrational modes. Namely, as any mechanical object with some degree of elasticity, the cutting disc will
20   exhibit certain vibrational modes in which the cutting disc can exhibit standing wave deformation vibrations at corresponding mode frequencies. These modes are usually referred to as "resonances" in the art, and the corresponding frequency is referred to as the "resonance frequency" or, from a mathematical perspective, "eigenfrequency" of the disc.

25   When the disc is at rest, i.e. not rotating, the formation of the vibrational modes is well understood, and the shape and frequency of the vibrational modes may be predicted using suitable computer simulations. However, when the disc is rotating, the situation becomes more complicated. It is seen that individual vibrational modes of the disc when at rest split up into two vibrational modes for the rotating disc, when
30   observed from the stationary reference frame, i.e. the reference frame of the object to be cut by the rotating disc. This split leads to one vibrational mode with higher and one vibrational mode with lower frequency than the mode frequency of the cutting disc at rest. The mode frequencies are found to diverge with increasing rotational speed, and it is seen that at some rotation frequency, which corresponds to the

"critical frequency" referred to in the introductory portion above, the resonance frequency of one of the "split modes" becomes zero. This means that, as observed from the stationary reference frame, the cutting blade becomes statically deformed, and in this case the cutting blade is no longer operable for obvious reasons, as it

5   would no longer "fit" into a cut of normal size. Accordingly, the aforementioned "critical frequency" indeed sets an upper limit for the rotational speed of the cutting blade in operation, and thereby an upper limit for the cutting efficiency.

An intuitive way to understand the split-up of the vibrational modes upon rotation of the disc is as follows. As the skilled person is aware, a vibrational mode is essentially

10   a standing wave, which is in turn the result of the superposition of two counter directional waves. In the case of a disc, a standing wave can be generated by circumferential deformation waves propagating in clockwise and counter clockwise directions, respectively. When the disc rotates e.g. in clockwise direction, as observed from the stationary frame of reference, the speed of the waves propagating in

15   clockwise direction is increased, while the speed of the wave propagating in counter clockwise direction is decreased, such that a split of the resonance frequencies may not come as a surprise. However, the analysis of the true behaviour is more complicated, because the rotation of the disc is an accelerated motion, and the disc itself therefore cannot serve as an inertial frame of reference. In order to understand

20   the dynamical behaviour of the rotating disc, one can therefore not simply solve the equations of motions for the vibrations of the disc at rest and then transform the resulting dynamic behaviour with a simple rotation in space. Instead, in order to properly analyse the vibrational behaviour of the rotating disc, the full continuum mechanics problem of the rotating disc has to be solved.

25   The present inventor has carried out simulations of this full continuum mechanics problem regarding the deformation of the rotating disc and was able to determine the vibrational modes, as well as the corresponding frequencies, as a function of the rotational speed. With this insight into the dynamical behaviour of the continuum mechanics of the rotating disc, the inventor was able to establish a new design for a

30   cutting disc, as set forth in claim 1 below, that permits increasing the critical frequency considerably as compared to discs of conventional design.

More particularly, a rotary cutting disc according to the invention comprises two coaxial mutually opposed disc-shaped elements each having a circumferential edge, wherein circumferential edges of the disc-shaped elements are joined together

35   forming a cutting edge of the cutting disc. Thus, the cutting disc is formed by the

4

union of the two disc-shaped elements, wherein each disc-shaped element constitutes one half of the cutting disc. The circumferential edges of the disc-shaped elements are joined together forming a common circumferential edge that constitutes the cutting edge of the cutting disc, that is, the outermost edge of the cutting disc that is rotated against the material to be cut. The cutting edge may constitute the cutting surface of the cutting disc itself or may be used for accommodating any kind of cutting blades, teeth or the like on it.

It is noteworthy that, while reference is made herein to a cutting disc comprising two coaxial mutually opposed disc-shaped elements, configurations of the invention are foreseen in which the cutting disc comprises more than two disc-shaped elements. Further, as is clear to the skilled person, the term "disc-shaped" should not be construed to be restricted to perfectly planar and circular objects, but rather to extended objects having an outermost perimeter that may deviate from a perfect circle and having a thickness that is much smaller than the aforesaid perimeter.

Each of the disc-shaped elements comprises one or more at least partly curved elongated deformation lines, wherein the one or more deformation lines have a radial distance from the centre of the cutting disc that increases along at least a part of the length of the deformation line. Herein, "curved" refers to the fact that the deformation lines do not extend straight along the radial direction of the disc-shaped elements only, but rather have a radial component and a component perpendicular thereto (i.e. angular or circumferential component). "Partly curved" refers to the fact that such curved shape may correspond to the entire length of a deformation line or only to a portion thereof. The fact that the radial distance of the deformation lines increases along at least a part of the length of the deformation line implies that deformation lines according to this invention are not formed at a constant distance of the centre of the cutting disc, i.e. not ring-shaped. In terms of polar coordinates, the radial component of the deformation line would be dependent on the azimuthal phase. The deformation lines may for instance have a spiral form, a wavy form, any combination thereof, or any other partly curved form according to the above definition.

The deformation lines may be formed as deformations of the material of which the disc-shaped elements are made. Typically, the deformation lines are formed by exerting a mechanical pressure upon the material from both sides of the disc-shaped elements of the cutting disc thereby causing a plastic deformation. The deformation lines may for example be formed by a rolling process. Herein, the term "line" shall

not be understood literally, because the rolling lines will have a certain non-vanishing width, which however is much smaller than the length of the deformation line, such as at least 10 times smaller, typically at least 20 times smaller. The formation of the deformation lines causes so-called residual stresses to be present in the material, which has a relevant influence on the dynamical properties of the cutting disc.

The inventor has realised that surprisingly the combination of the two-element design with the specific shape of the deformation lines causes an increase of the critical speed of the cutting disc in a synergistic manner, i.e. in a manner that exceeds by far the effect expected from each single design feature by itself. The increase in critical speed thanks to the cutting disc of the invention with respect to an analogous single-pieced cutting disc having the same diameter and total mass and having conventional annular deformation lines has been found to be of at least 33%, which results in a very significant increase in the cutting kinetical energy of more than 75%. This way, the efficiency of a cutting operation with a cutting disc can be improved while maintaining acceptable levels of quality, cutting precision and safety. The aforesaid conclusions are supported by simulation results that are summarised below.

The dynamic behaviour of the cutting disc is governed by the rotational inertia tensor thereof. The rotational inertia tensor, also known as angular mass tensor, of a system describes the rotational inertia of the system and the degree to which a rotation around one axis induces a rotation around another axes, as is typically known for precession phenomena. The rotational inertia tensor J_{ij} is a symmetric tensor of the form

$$J = \begin{bmatrix} J_{xx} & J_{xy} & J_{xz} \\ J_{xy} & J_{yy} & J_{yz} \\ J_{xz} & J_{yz} & J_{zz} \end{bmatrix},$$

where the diagonal terms J_{xx}, J_{yy}, and J_{zz}, characterise the rotation inertia of the corresponding system around the axis x, y, and z, respectively, and the off-diagonal terms characterise the degree to which a rotation around one axis induces a rotation around another axis. In other words, the off-diagonal terms are a measure of the "rotation rigidity" of a rotating system. The smaller an off-diagonal term $J_{\alpha\beta}$ is, the less resistance the system offers for a rotation around the direction α to induce a further rotation around the direction β, and hence the less stable the system is when rotating.

The experiments by the inventor reveal that the aforesaid combination of the two element design with the specific shape of the deformation lines may influence the deformation behaviour of the cutting disc in such a way as to result in an increase in the off-diagonal terms of the rotational inertia tensor with respect to cutting discs of conventional design in as much as four orders of magnitude. While conventional cutting discs display off-diagonal terms of the inertia tensor having a typical order of magnitude of 10^{-13} as compared to the diagonal terms, the inventor found out that the inventive design of a cutting disc can result in off-diagonal terms of the rotational inertia tensor of the cutting disc having an order of magnitude of 10^{-9} or higher as compared to the diagonal terms. This may lead to a regime in which the deformation behaviour of the cutting disc may no longer be reliably approximated by a linear planar approximation, as would correspond to a symmetric and plane cutting disc. Instead, quadratic and higher terms become significant for the calculations, which contributes to the effective increase of the critical frequency of the cutting disc.

In a preferred embodiment of the invention the two disc-shaped elements form a cavity in between that contains a vacuum. According to this embodiment, the two disc-shaped elements are not continuously in contact with each other all along their respective radial length but instead are in contact with each other at their outermost circumferential edges, which jointly form the cutting edge of the cutting disc, and possibly in a neighbouring environment thereof, while they are mutually separated along the rest of their radial extensions corresponding to those portions of the disc-shaped elements that are not joined together forming the cutting edge of the cutting disc. An interspace between the two disc-shaped elements is then formed between these portions thereof which constitutes the cavity.

The cutting edge of the cutting disc may be provided by a sealed junction or connection between the disc-shaped elements. Further, the disc-shaped elements may be confined by an innermost circumferential edge around their common axis, which may for instance be formed around an opening suitable for accommodating a shaft. A sealed junction or connection may be provided between such an opening and the cavity between the disc-shaped elements, such that the cavity is a sealed cavity suitable for containing a vacuum. When the cavity is evacuated, i.e. it contains a vacuum, a pressure gradient is created between the interior of the cutting disc and the exterior thereof, which is believed to contribute to a better dynamical stability of the cutting disc in operation.

According to other preferred embodiments of the invention, the two disc-shaped elements form a cavity in between that is filled with a fluid, preferably with a Newtonian or a non-Newtonian fluid such as a gas-like air, an inert gas or a combination thereof, or a liquid like water, an oil, a gel-like substance or a

5   combination thereof that improves the dynamic behaviour of the disc.

In other preferred embodiments of the invention, the two disc-shaped elements form a cavity in between that is filled with a damping material, preferably with a damping material with viscoelastic properties such as rubber, silicate, a gel, a synthetic or natural material with vibration attenuating properties or a combination thereof.

10   The presence of a vacuum, a fluid, or a damping material in the cavity may modify the dynamical properties of the cutting disc in an advantageous manner by increasing the damping behaviour and/or its mechanical resistance to uncontrolled deformations that may lead to deviations or irregularities of the cutting profile and contribute to the elevation of the critical rotational speed of the cutting disc.

15   In preferred embodiments of the invention, the disc-shaped elements are separated by a separating element. The separating element may contribute to a better static and dynamic stability of the cutting disc against deformations and vibrations. The separating element may be formed as an extension of the disc-shaped elements. Alternatively, the separating element may be an independent element. Further, the

20   separating element may be formed along an inner circumferential edge of the disc-shaped elements and around an opening confined by said inner circumferential edge for receiving a shaft.

In some preferred embodiments of the invention, the separating element and/or the disc-shaped elements may be configured such that the disc-shaped elements assume

25   a lens-shaped geometry, wherein the distance between the disc-shaped elements increases at least in part along the radial direction from the cutting edge towards the centre of the cutting disk. The distance between the disc-shaped elements may increase throughout their respective radial lengths or in a part thereof. The disc-shaped elements may assume the lens-shaped geometry in combination, such that

30   the geometry of the rotary cutting disc is lens-shaped in the aforesaid sense. This may be achieved by appropriately choosing the dimensions and material composition of the separating element and/or by appropriately choosing the dimensions and/or the material composition of the disc-shaped elements.

The inventor realised that the lens-shaped geometry induced by the separating element and/or by the disc-shaped elements may further contribute to the aforementioned non-linear regime of the deformation behaviour of the cutting disc and hence to the increase of the critical frequency of the cutting disc.

5   For the purpose of implementing the lens-shaped geometry of the cutting disc described above, the separating element may be made of a monolithic material, for example a metal, or a composite material, and may have a width along the axial direction, i.e. an extension between the disc-shaped elements, of between R/1000 and 2R/3, preferably between R/100 and R/2, more preferably between R/10 and
10   R/3, where R is the radius of the disc-shaped elements. Additionally or alternatively, the disc-shaped elements may be made of a monolithic material, for example a metal, or a composite material.

The distance between the disc-shaped elements may increase along the radial direction from the cutting edge towards the center of the cutting disk, throughout
15   their respective radial lengths or in a part thereof, linearly, logarithmically, exponentially, and/or according to a polynomial function, a trigonometric function and/or a rational function.

In a preferred embodiment of the invention, the one or more deformation lines formed on different disc-shaped elements are arranged in an overlaying
20   configuration in the assembled state of the cutting disc. This means that the deformation lines as formed on the individual disc-shaped elements are mirror images of one another.

In a related embodiment, the pattern of deformation lines on the individual disc-shaped elements are mirror images of one another, such that they could be arranged
25   in an overlaying configuration in the assembled state of the rotary cutting disc, but are offset with respect to each other by a predefined angle. The offset of the deformation lines may lead to an increased degree of asymmetry of the cutting disc, which may further contribute to influence the deformation behaviour of the cutting disc in such a way as to increase the critical frequency of the cutting disc, as explained
30   above.

According to an alternative embodiment of the invention, the pattern of deformation lines as formed on the individual disc-shaped elements is identical. This means that in the assembled state, where the individual disc-shaped elements are arranged back-

to-back, the location and shape of the deformation lines are mirror images of each other.

In some preferred embodiments of the invention, the one or more deformation lines are formed on an outer surface of the disc-shaped element not facing the opposed

5   disc-shaped element.

According to a preferred embodiment of the invention, the radial distance of the one or more deformation lines increases monotonically along the length of the deformation line. The radial distance refers herein to the radial coordinate that would be used for describing the path of a deformation line on a disc-shaped element in

10   polar coordinates, which would increase monotonically with increasing angle, i.e. along the length of the deformation line. This characteristic may extend to an entire deformation line or only to a portion thereof. The monotonic increase may for instance correspond to a linear increase or to a logarithmic increase, although other increase rates are possible as well.

15   In a preferred embodiment of the invention, the deformation lines extend from a first end to a second end, said first end being located at the innermost circumferential edge of the disc-shaped elements, or within a distance of said innermost edge that is less than 15%, preferably less than 10% of the diameter of the respective disc-shaped element. According to this embodiment, the disc-shaped elements may be confined

20   on one side by an innermost circumferential edge around their common axis, which may for instance be formed around an opening suitable for accommodating a shaft.

In a related embodiment of the invention, the second end of the deformation lines is located at the cutting edge, or within a distance from said cutting edge that is less than 15%, preferably less than 10% of the diameter of the respective disc-shaped

25   element.

In a preferred embodiment of the invention, the two disc-shaped elements are welded or glued together. In particular, the disc-shaped elements may be welded together by means of point welding, line welding, friction welding, soldering, or glued together using a gluing paste.

30   According to a preferred embodiment of the invention, each of the disc-shaped elements comprises at least 4 deformation lines, preferably between 6 and 20 deformation lines.

In a preferred embodiment of the invention the deformation lines, when expressed in polar coordinates, cover an angular range between 1° and 720°, preferably between 10° and 90°, along their length.

5   Herein, it is preferable if the value of the angle coordinate increases or decreases monotonically along the length of the deformation line. Additionally or alternatively, the deformation lines preferably have the shape of a section of a circle having a centre located at a radial distance from the centre of the rotary cutting disc corresponding to 35% to 65%, preferably 40% to 60% and most preferably 45% to 55% of the radius of 10   the rotary cutting disc.

BRIEF SUMMARY OF THE FIGURES

Fig. 1   shows a side sectional view of a cutting disc according to an embodiment of the invention.

15   Fig. 2   shows a front view of a cutting disc according to an embodiment of the invention.

Fig. 3   shows a monolithic prior art cutting disc having closed annular deformation lines taken as reference.

Fig. 4   shows the six lowest resonance frequencies as a function of rotational 20   speed determined from computer simulation for the monolithic reference prior art cutting disc of Fig. 3.

Fig. 5   shows the six lowest resonance frequencies as a function of rotational speed determined from computer simulation for a monolithic cutting disc comprising spiral shaped deformation lines.

25   Fig. 6   shows the six lowest resonance frequencies as a function of rotational speed determined from computer simulation for a cutting disc comprising two disc-shaped elements without deformation lines.

Fig. 7   shows the six lowest resonance frequencies as a function of rotational speed determined from computer simulation for a cutting disc comprising 30   two disc-shaped elements having closed annular deformation lines.

Fig. 8   shows the six lowest resonance frequencies as a function of rotational speed determined from computer simulation for a cutting disc according to an embodiment of the invention.

DESCRIPTION OF PREFERRED EMBODIMENTS

5   Certain embodiments of the present invention are described in detail herein below with reference to the accompanying drawings, wherein the features of the embodiments can be freely combined with each other unless otherwise described. However, it is to be expressly understood that the description of certain embodiments is given by way of example only, and that it should not be understood

10   to limit the invention.

Fig. 1 shows a side view of a rotary cutting disc 10 according to an embodiment of the invention, which comprises two coaxial mutually opposed disc-shaped elements 12a and 12b. The disc-shaped elements 12a and 12b have a respective circumferential edge 14a and 14b. The circumferential edges 14a and 14b of the disc-shaped elements

15   12a and 12b are joined together forming a cutting edge 16 of the cutting disc 10. The disc-shaped elements 12a, 12b extend between a respective innermost circumferential edge 18a, 18b of the disc-shaped elements 12a, 12b and the respective outermost circumferential edge 14a, 14b. The innermost circumferential edges 18a, 18b are arranged around their common centre 20, and form an opening 26 suitable for

20   receiving a driving shaft. The disc-shaped elements 12a and 12b are separated in a vicinity of their innermost circumferential edges 18a, 18b by a separating element 22.

The circumferential disc-shaped elements 12a and 12b are tightly joined together at the cutting edge 16 and tightly joined to the separating element 22 and the outer walls of the opening 26, thereby forming a sealed cavity 24 between the disc-shaped

25   elements 12a and 12b. In the embodiment shown, the cavity 24 contains a vacuum.

The separating element 22 and the disc-shaped elements are configured such that the disc-shaped elements 12a and 12b assume in combination a lens-shaped geometry, wherein the distance between the disc-shaped elements 12a and 12b increases along the radial direction from the cutting edge 16 towards the common centre 20,

30   according to a tangent function. The separating element 22 is made of a monolithic metal and has a width of R/5, R being the radius of the disc-shaped elements 12a and 12b. The disc-shaped elements 12a and 12b are made of a metal.

12

Fig. 2 shows a front side of the rotary cutting disc 10 of Fig. 1. The disc-shaped elements 12a and 12b each comprise five curved elongated deformation lines 30 that have a radial distance to the centre 20 of the cutting disc 10 that increases monotonically along the length of the deformation line 30. The deformation lines 30

5   of the embodiment shown are "spiral-shaped", which however shall not be construed in a strict mathematical sense. In the shown embodiment, the deformation lines 30 have the shape of a section of a circle having a centre located at a radial distance from the centre 20 of the disc-shaped element corresponding to half the radius R of the disc-shaped element. In the embodiments shown the radius R of the disc-shaped

10   elements 12a, 12b is R = 400 mm and the centre of the circular path described by the deformation lines 30 is located at a radial distance r = R/2 = 200 mm, and the deformation lines follow circular paths having a radius r = 200 mm. Please note that this shape is regarded as a "spiral-shaped" in the meaning of the present disclosure. According to this shape, when expressing the shape of the deformation line 30 in

15   polar coordinates, this means that the angle coordinate changes monotonically along the length of the deformation line 30, and thereby covers an angular range of approximately 80°. The deformation lines 30 extend between an intermediate circumferential limit 32 and the cutting edge 16, wherein the intermediate circumferential limit 32 encloses the centre of the cutting disc 10 and has a radius

20   greater than the radius 18 of the innermost circumferential edges 18a, 18b of the disc-shaped elements 12a and 12b. In the embodiment shown, the deformation lines 30 have a width of 5.4 mm.

SIMULATION EXAMPLES

In the following, it will be demonstrated that the configuration of the cutting disc

25   according to this invention allows for an increase in the critical speed based on simulation results.

Fig. 4 shows the six lowest resonance frequencies as a function of rotational speed determined from computer simulation for a reference prior art disc consisting of a monolithic cutting disc that is not made up from two coaxial mutually opposed disc-

30   shaped elements, and comprising two annular deformation lines. Such a reference prior art disc 10' is shown in Fig. 3, where elements of the disc 10' are indicated by the same reference numerals previously used for Fig. 1 and 2, wherein it is understood that those elements previously referring to the disc-shaped elements refer in Fig. 3 to the monolithic cutting disc itself . The cutting disc 10' comprises two

35   concentric annular deformation lines 30'.

As is seen in the diagram of Fig. 4, the first, third, fourth and fifth lowest resonance frequencies for the cutting disc 10 when at rest bifurcate and diverge with increasing rotational speed. The reason for this bifurcation behaviour is that these resonances or vibrational modes involve standing waves propagating counter directionally in circumferential direction. The second and sixth lowest resonance frequency do not bifurcate, as they involve standing waves propagating in radial direction only, which are not directly affected by the rotation. Accordingly, in the diagram of Fig. 4, the respective curves are approximately horizontal, indicating that the resonance frequency is indeed largely unaffected by the increase in rotational speed. However, a closer look reveals that the curves are not perfectly horizontal, but slightly increase with rotational speed. This is due to the fact that the centripetal force acting on the cutting disc upon rotation leads to a stiffening of the disc, and hence a higher resonance frequency.

Note that the computer program employed always limits the analysis to the six lowest resonance frequencies (or resonance frequency pairs, in case of bifurcating frequencies). This is why in Fig. 4 at around 150 rad/s, the frequency curve of the resonance which used to be the highest at zero rad/s stops, the reason being that at this rotation frequency another resonance frequency (not shown in the diagram), which had a higher frequency at lower rotational speeds, has dropped below it.

As can be further seen from Fig. 4, at 300 rad/s, the lower branch of the originally (i.e. at zero rad/s) third lowest frequency resonance drops to zero, meaning that this vibrational mode leads to a static deformation in the inertial reference frame of the object to be cut (or the inertial reference frame of the machine driving the cutting disc 10). Hence, this rotational speed of 300 rad/s corresponds to the critical frequency referred to above, which sets the upper limit for the operating speed of the cutting disc 10.

In order to allow for higher rotational speeds of the cutting disc 10, the aim is to push the critical frequency, i.e. the lowest rotational speed at which one of the resonance frequencies drops to zero, to higher values.

Fig. 5 shows the results of similar simulations as shown in Fig. 4, again for a monolithic cutting disc, but having 5 spiral-shaped deformation lines instead of the two annular deformation lines analogous to the pattern of deformation lines 30 shown in Fig. 2. As seen in the figures, no significant changes in the dynamical properties of the cutting disc are observed. In particular, by employing the spiral-

14

shaped deformation lines on a conventional, monolithic cutting disc, the critical rotational frequency remains at 300 rad/s and is hence not improved.

Fig. 6 shows the results of similar simulations as shown in Fig. 4, but for a cutting disc comprising two disc-shaped elements separated by a separating element and
5   having no deformation lines. The total mass of the two-part cutting disc is the same as that of the monolithic reference cutting disc of figures 3 and 5. As seen in the figures, this configuration displays an increase in the critical frequency of about 17% with respect to the reference prior art model of Fig. 4.

Fig. 7 shows the results for a cutting disc analogous to that of Fig. 6 but comprising
10   closed annular deformation lines around the centre of the cutting disc. The deformation lines on different disc-shaped elements are arrayed in an overlying configuration. No significant changes in the dynamical properties of the cutting disc as compared to that of Fig. 6 are observed which could be attributed to the closed annular deformation lines.

15   Fig. 8 shows the results of computer simulations of the six lowest resonance frequencies as a function of rotational speed determined for a cutting disc according to an embodiment of the invention. This embodiment is analogous to that of Fig. 6 and 6, but comprises curved – spiral – deformation lines analogous to those described with respect to Fig. 2, wherein the deformation lines on different disc-
20   shaped elements are arrayed in an overlying configuration. Surprisingly, the combination of the two-part structure and the curved spiral deformation lines leads to an increase in the critical frequency of about 33% over the prior art design shown in Figs. 3 and 4. The combined effect is hence much more than one would have expected from the individual effects of the two modifications over the disc of Figs. 3
25   and 4. After all, the two-part design without or with conventional annular deformation lines leads to an increase in critical frequency of only 17%, as is seen from figures 6 and 7. Moreover, as seen from Fig. 5, the spiral cutting lines by themselves, i.e. applied on a conventional monolithic cutting disc of same mass does not lead to any appreciable improvement whatsoever. However, by combining the
30   spiral shaped deformation lines with the two-part design of the cutting disc, a very significant increase in the critical frequency of about 33% with respect to the reference prior art model shown in Fig. 3 can be obtained, which clearly exceeds the sum of the individual effects of the individual features as seen by comparison with the critical frequency obtained in the cutting discs of Fig. 5, 6 and 7.

Thanks to the increase in the critical frequency realised by the invention, the cutting disc may be operated at a higher rotational speed without being disturbed by the effects of resonance, which allows higher work efficiency and safety.

The simulations with which the results shown in Fig. 4 to 8 were obtained relied on a
5   resolution of the elastic equations of motion (Lamé-Navier or Navier-Cauchy equations) by finite element computations and made use of the software tool Abaqus® by Dassault Systèmes.

It is to be understood that what is described above is what is presently considered the preferred embodiment of the present invention. However, it should be noted that the
10   description of the preferred embodiments is given by way of example only and that various modifications may be made without departing from the scope of the invention as defined in the claims.

REFERENCE SIGN LIST

10	cutting disc
12a, 12b	disc-shaped elements
14a, 14b	circumferential edges
16	cutting edge
18a, 18b	innermost circumferential edges
20	common centre
22	separating element
24	cavity
26	opening
30	deformation lines
32	intermediate circumferential limit

Claims

1.   A rotary cutting disc (10) comprising:

two coaxial mutually opposed disc-shaped elements (12a, 12b) each having a
circumferential edge, wherein circumferential edges (14a, 14b) of the disc-
shaped elements (12a, 12b) are joined together forming a cutting edge (16) of
the cutting disc (10);

wherein each of the disc-shaped elements (12a, 12b) comprises one or more at
least partly curved elongated deformation lines (30), wherein the one or more
deformation lines (30) have a radial distance from the centre (26) of the
cutting disk (10) that increases along at least a part of the length of the
deformation line (30).

2.   The rotary cutting disc (10) according to claim 1, wherein the two disc-shaped
elements (12a, 12b) form a cavity (24) in between that contains a vacuum.

3.   The rotary cutting disc (10) according to claim 1, wherein the two disc-shaped
elements (12a, 12b) form a cavity (24) in between that is filled with a fluid,
preferably with a Newtonian or a non-Newtonian fluid.

4.   The rotary cutting disc (10) according to claim 1, wherein the two disc-shaped
elements (12a, 12b) form a cavity (24) in between that is filled with a damping
material, preferably with a damping material with viscoelastic properties.

5.   The rotary cutting disc (10) according to any of the preceding claims, wherein
the disc-shaped elements (12a, 12b) are separated by a separating element
(22).

6.   The rotary cutting disc (10) according to any of the preceding claims, wherein
the separating element (22) and/or the disc-shaped elements (12a, 12b) are
configured such that the disc-shaped elements (12a, 12b) assume a lens-
shaped geometry, wherein the distance between the disc-shaped elements
(12a, 12b) increases at least in part along the radial direction from the cutting
edge (16) towards the centre (26) of the cutting disc (10).

7.   The rotary cutting disc (10) according to any of the preceding claims, wherein the one or more deformation lines (30) formed on different disc-shaped elements (12a, 12b) are arranged in an overlaying configuration.

8.   The rotary cutting disc (10) according to claim 7, wherein the pattern of deformation lines (30) on the individual disc-shaped elements (12a, 12b) are mirror images of one another, such that they could be arranged in an overlaying configuration in the assembled state of the rotary cutting disc (10), but are offset with respect to each other by a predefined angle.

9.   The rotary cutting disc (10) according to any of claims 1 to 6, wherein the pattern of deformation lines (30) as formed on the individual disc-shaped elements (12a, 12b) is identical.

10.   The rotary cutting disc (10) according to any of the preceding claims, wherein the one or more deformation lines (30) are formed on an outer surface of the disc-shaped element (12a, 12b) not facing the opposed disc-shaped element (12b, 12a)

11.   The rotary cutting disc (10) according to any of the preceding claims, wherein said radial distance of the one or more deformation lines (30) increases monotonically along the length of the deformation line (30).

12.   The rotary cutting disc (10) according to any of the preceding claims, wherein the deformation lines (30) extend from a first end to a second end, said first end being located at the innermost edge (18a, 18b) of the disc-shaped elements (12a, 12b), or within a distance from said innermost edge (18a, 18b) that is less than 15%, preferably less than 10% of the diameter of the respective disc-shaped element (12a, 12b).

13.   The rotary cutting disc (10) according to claim 12, wherein the second end of the deformation lines (30) is located at the cutting edge (16) of the cutting disc (10), or within a distance from said cutting edge (16) that is less than 15%, preferably less than 10% of the diameter of the respective disc-shaped element (12a, 12b).

14. The rotary cutting disc (10) according to any of the preceding claims, wherein the two disc-shaped elements (12a, 12b) are welded or glued together.

15. The rotary cutting disc (10) according to any of the preceding claims, wherein each of the disc-shaped elements (12a, 12b) comprises at least 4 deformation lines (30), preferably between 6 and 20 deformation lines (30).

16. The rotary cutting disc (10) according to any of the preceding claims, wherein the deformation lines (30), when expressed in polar coordinates, cover an angular range between 1° and 720°, preferably between 10° and 90°, along their length, wherein the value of the angle coordinates preferably increases or decreases monotonically along the length of the deformation line (30), and/or wherein the deformation lines (30) preferably have the shape of a section of a circle having a centre located at a radial distance from the centre of the rotary cutting disc (10) corresponding to 35% to 65%, preferably 40% to 60% and most preferably 45% to 55% of the radius of the rotary cutting disc (10).
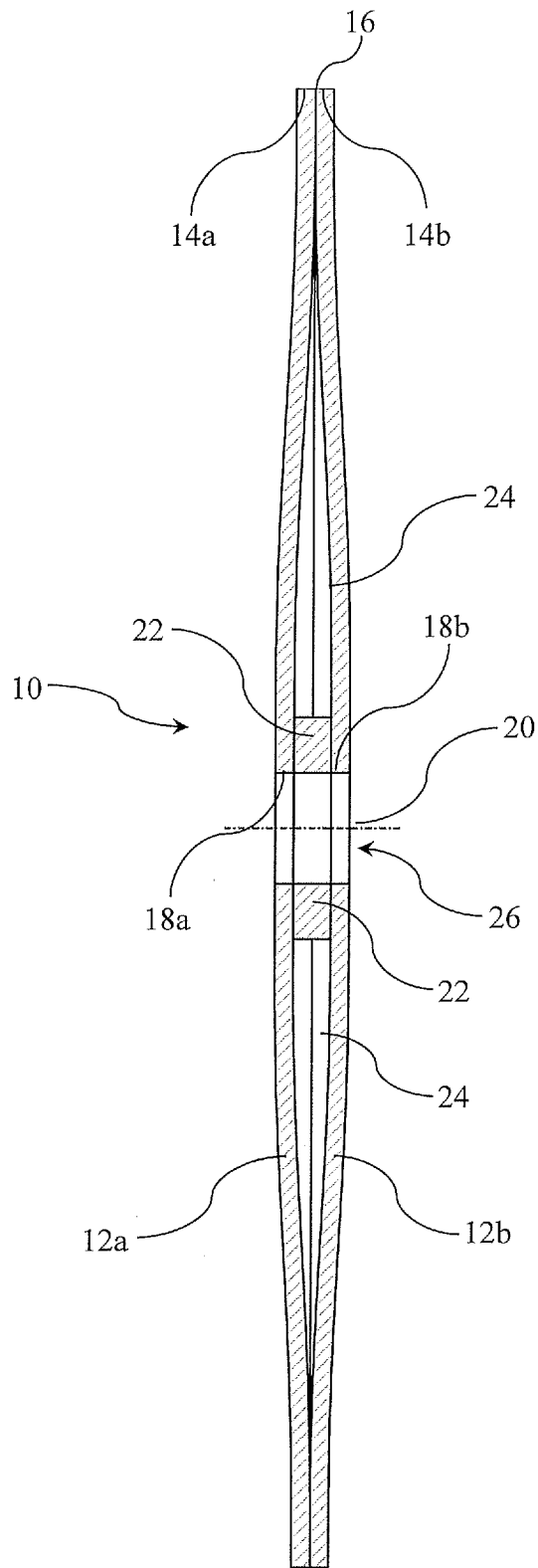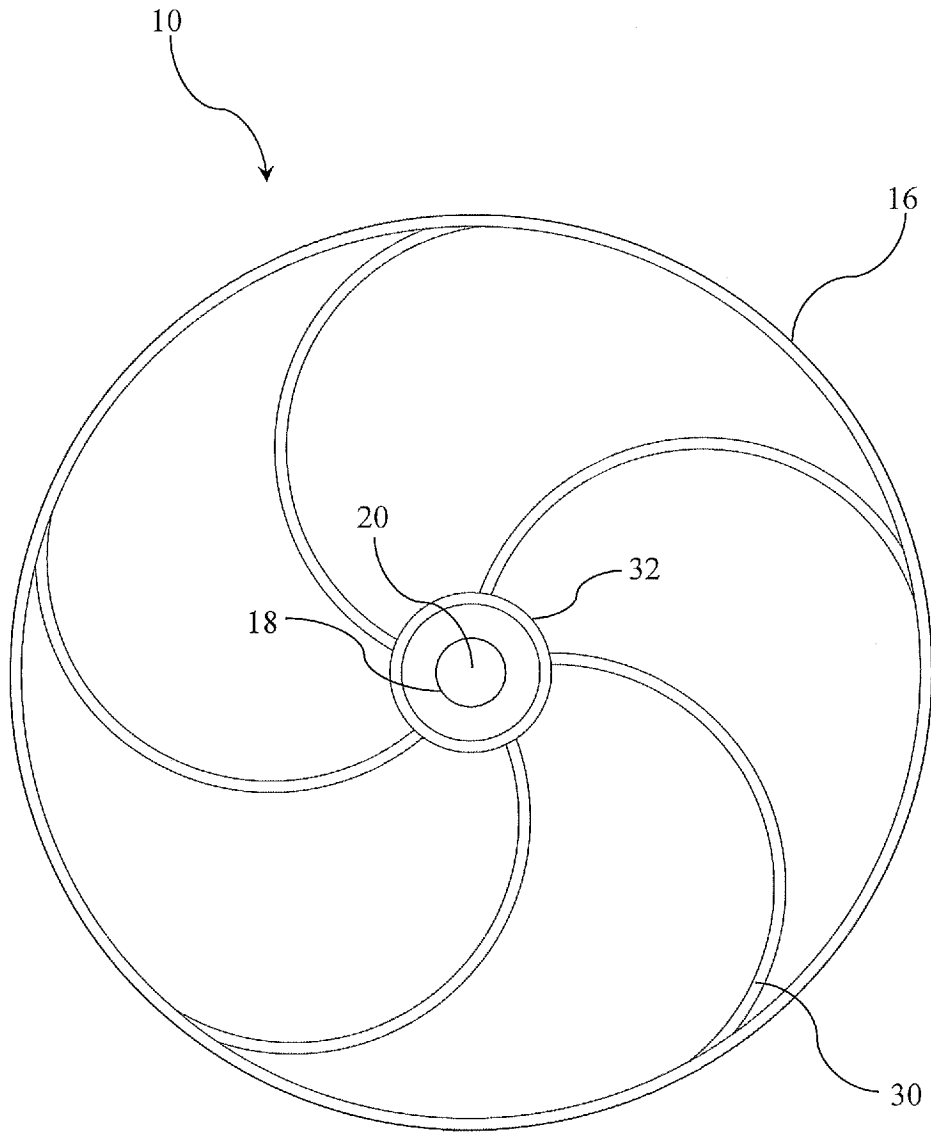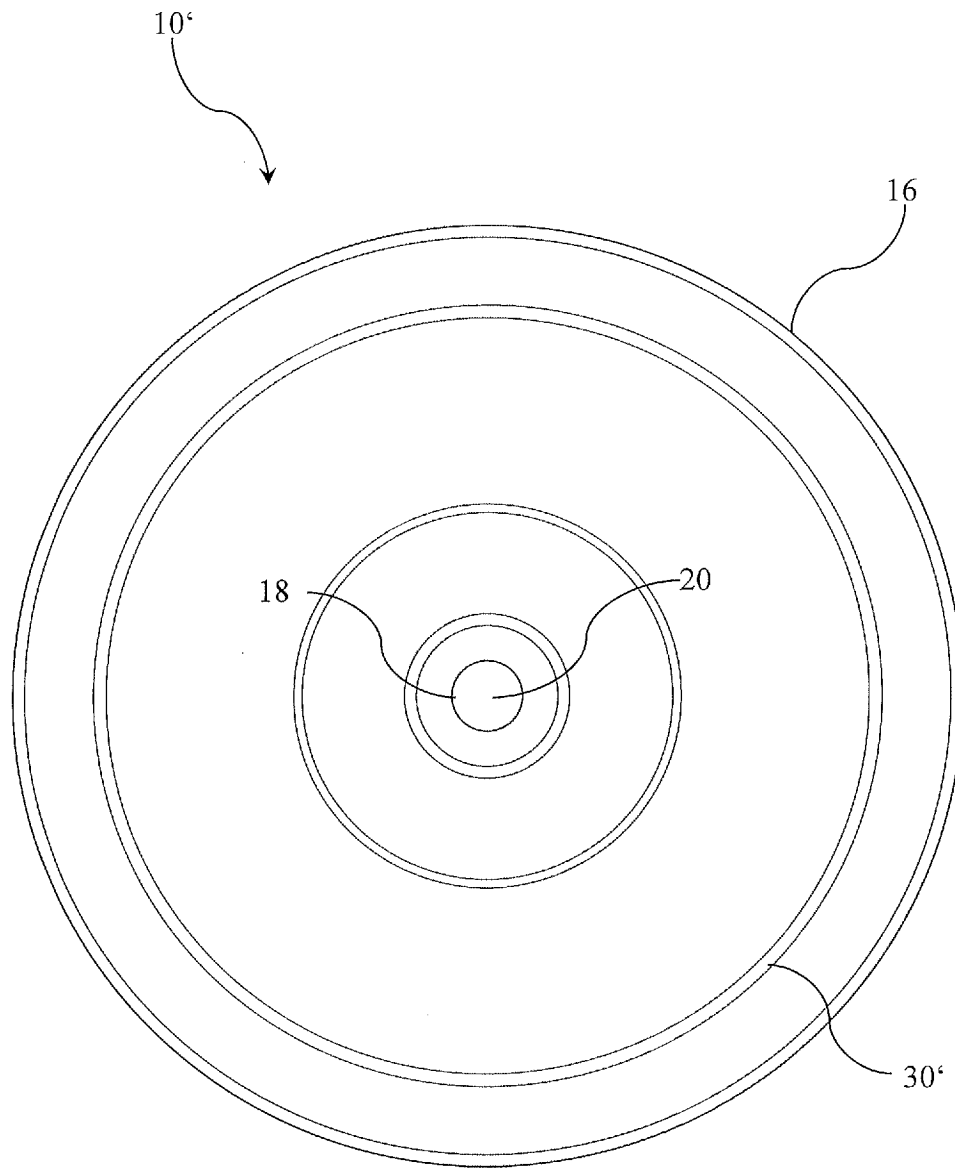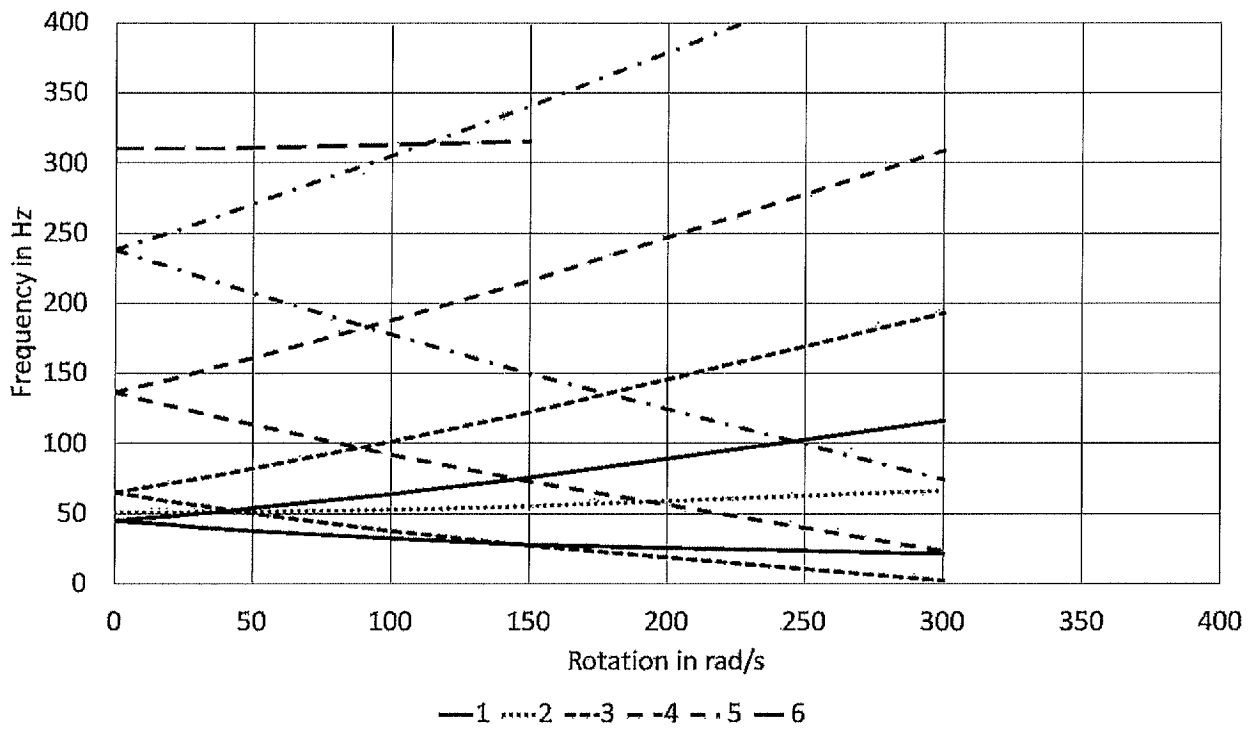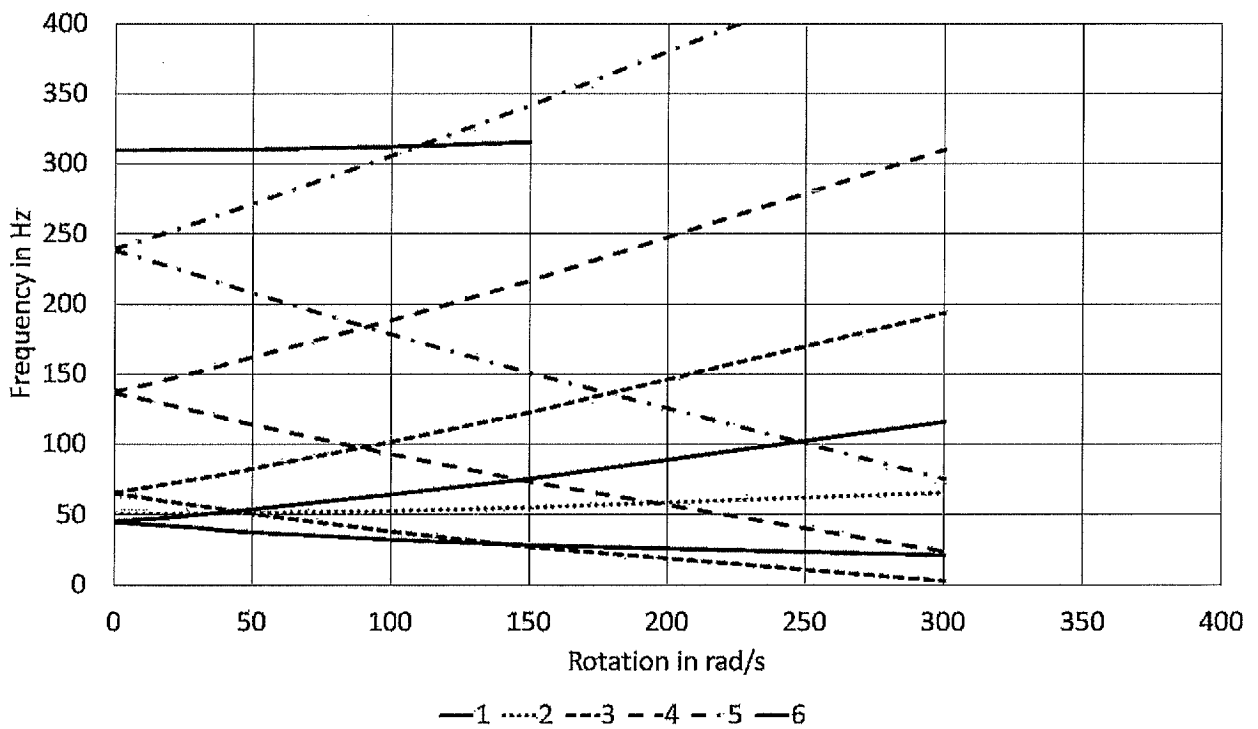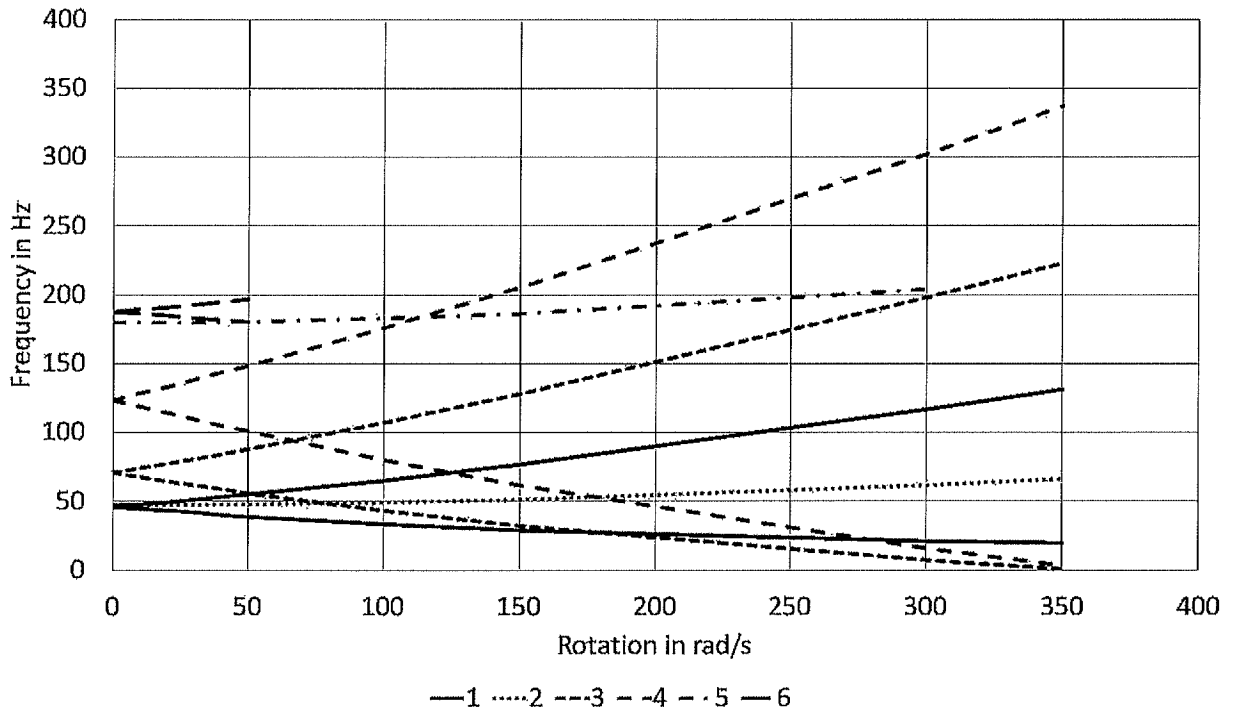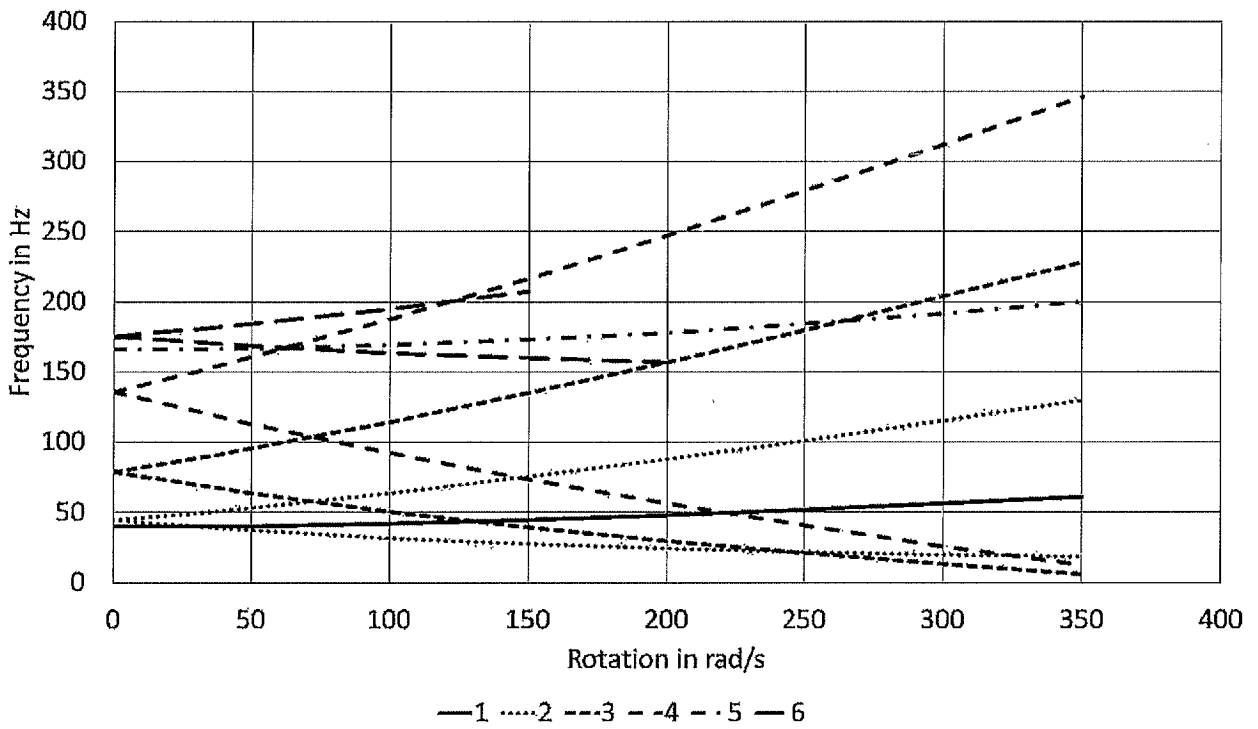
Fig. 1

Fig. 2

Fig. 3

(prior art)

Fig. 4

Fig. 5

Fig. 6

Fig. 7
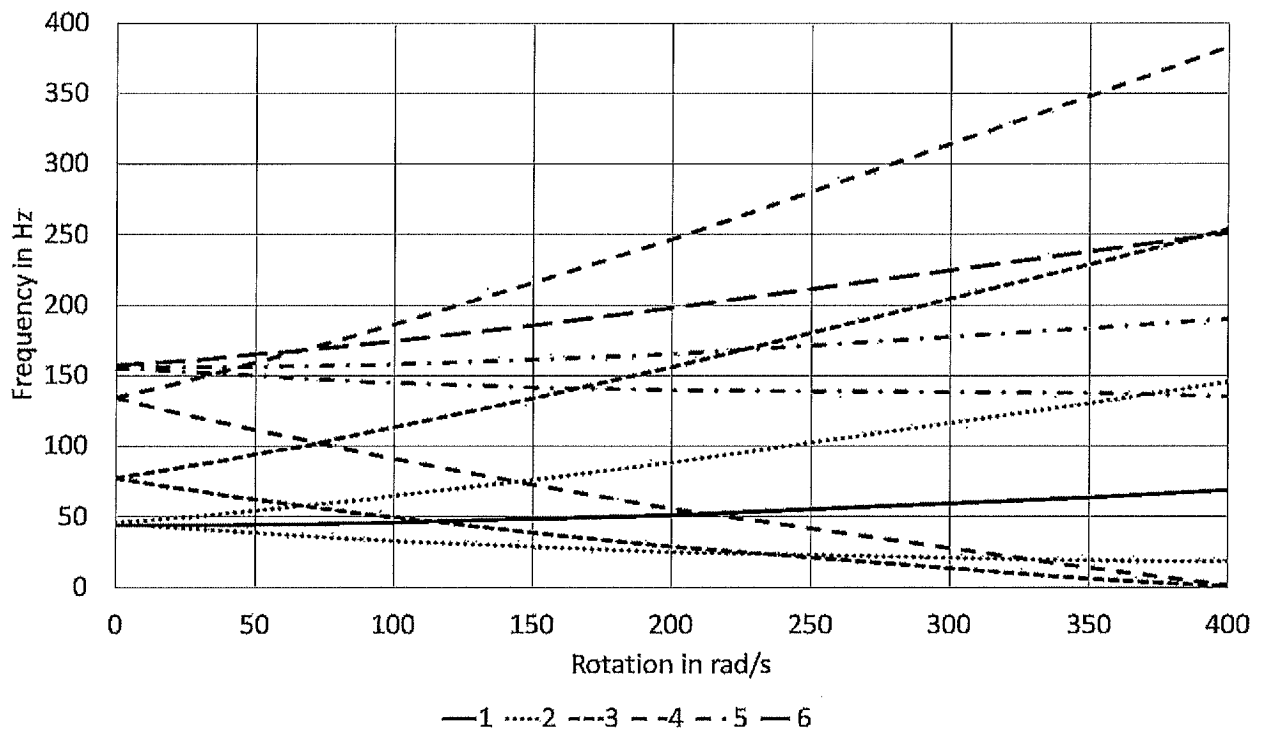
Fig. 8

INTERNATIONAL SEARCH REPORT

A. CLASSIFICATION OF SUBJECT MATTER
INV. B23D61/02
ADD.

According to International Patent Classification (IPC) or to both national classification and IPC

B. FIELDS SEARCHED

Minimum documentation searched (classification system followed by classification symbols)

B23D   B28D   B24D   B26D

Documentation searched other than minimum documentation to the extent that such documents are included in the fields searched

Electronic data base consulted during the international search (name of data base and, where practicable, search terms used)

EPO-Internal, WPI Data

C. DOCUMENTS CONSIDERED TO BE RELEVANT

Category*	Citation of document, with indication, where appropriate, of the relevant passages	Relevant to claim No.
X	JP H02 311260 A (SANKI ENG CO LTD; NIPPON KOKAN KK) 26 December 1990 (1990-12-26)	1,4,5, 7-16
A	the whole document in particular: figures 1,2	2,3,6

X	JP H06 312314 A (JIYANPU KOGYO KK) 8 November 1994 (1994-11-08)	1,4,5, 7-10, 14-16
A	paragraph [0017] - paragraph [0019] figures 3,4	2,3,6, 11-13

	-/--	

X	Further documents are listed in the continuation of Box C.		X	See patent family annex.

* Special categories of cited documents :

"A" document defining the general state of the art which is not considered to be of particular relevance

"E" earlier application or patent but published on or after the international filing date

"L" document which may throw doubts on priority claim(s) or which is cited to establish the publication date of another citation or other special reason (as specified)

"O" document referring to an oral disclosure, use, exhibition or other means

"P" document published prior to the international filing date but later than the priority date claimed

"T" later document published after the international filing date or priority date and not in conflict with the application but cited to understand the principle or theory underlying the invention

"X" document of particular relevance; the claimed invention cannot be considered novel or cannot be considered to involve an inventive step when the document is taken alone

"Y" document of particular relevance; the claimed invention cannot be considered to involve an inventive step when the document is combined with one or more other such documents, such combination being obvious to a person skilled in the art

"&" document member of the same patent family

Date of the actual completion of the international search	Date of mailing of the international search report
27 August 2018	06/09/2018

Name and mailing address of the ISA/	Authorized officer
European Patent Office, P.B. 5818 Patentlaan 2 NL - 2280 HV Rijswijk Tel. (+31-70) 340-2040, Fax: (+31-70) 340-3016	Rijks, Mark

International application No
PCT/EP2018/066767

C(Continuation). DOCUMENTS CONSIDERED TO BE RELEVANT

Category*	Citation of document, with indication, where appropriate, of the relevant passages	Relevant to claim No.
X	CN 101 518 838 A (ZL DIAMOND TOOLS CO LTD) 2 September 2009 (2009-09-02)	1,4,5, 7-10, 14-16
A	the whole document in particular: description relating to "Embodiment 4" figures 3,4 -----	2,3,6, 11-13
X	CN 201 471 006 U (ZL DIAMOND TOOLS CO LTD) 19 May 2010 (2010-05-19)	1,4,5, 7-10, 14-16
A	the whole document in particular: description relating to "Embodiment 4" figures 3,4 -----	2,3,6, 11-13
X	JP H03 104608 A (EFUPURE KK; RASA INDUSTRIES) 1 May 1991 (1991-05-01)	1,3,5-7, 9-11, 14-16
A	the whole document -----	2,4,8, 12,13
A	JP H10 180539 A (MATSUSHITA ELECTRIC WORKS LTD) 7 July 1998 (1998-07-07) abstract -----	1-6,14

2

Patent document cited in search report		Publication date	Patent family member(s)		Publication date
JP H02311260	A	26-12-1990	NONE		
JP H06312314	A	08-11-1994	JP	2519166 B2	31-07-1996
			JP	H06312314 A	08-11-1994
CN 101518838	A	02-09-2009	NONE		
CN 201471006	U	19-05-2010	NONE		
JP H03104608	A	01-05-1991	NONE		
JP H10180539	A	07-07-1998	NONE		